Characterization of the Interactions Between DNA and Oppositely Charged Species by Fluorescence

by

Christine Keyes

A thesis
presented to the University of Waterloo
in fulfillment of the
thesis requirement for the degree of
Doctor of Philosophy
in
Chemistry

Waterloo, Ontario, Canada, 2011

Author's Declaration

I hereby declare that I am the sole author of this thesis. This is a true copy of the thesis, including any required final revisions, as accepted by my examiners.

I understand that my thesis may be made electronically available to the public.

Abstract

The characterization of the interactions between DNA and oppositely charged species were characterized by fluorescence. Quantitative and insightful information on the distribution of positively charged species around the DNA helix was obtained by analyzing the fluorescence decays with an appropriate protocol. First, the interactions between DNA and divalent metal cations were studied by fluorescence using DNA – intercalated ethidium bromide (DNA-EB) as a probe. Second, the interactions between DNA and more structurally complex cations, namely positively charged gemini surfactants were studied by fluorescence. In this case, one of the two alkyl tails of the gemini surfactant was substituted with the chromophore pyrene to yield an asymmetrical gemini surfactant referred to as Py-3-12, so that the interactions between Py-3-12 and DNA could be followed by fluorescence.

The interactions between DNA-EB and metal cations in solution were studied by following the fluorescence quenching of DNA-EB by divalent metal cations randomly distributed around the DNA helix, a process which occurs via electron transfer (ET). The random distribution of divalent metal cations around the DNA helix led to a distribution of quenching rate constants that complicated the analysis of the fluorescence data. However, the Fluorescence Blob Model (FBM) was applied to analyze the fluorescence data and this analysis yielded quantitative information about the rate of ET and the distance over which ET took place from an excited DNA-EB to Cu^{2+}cations. For a salt concentration of 5×10^{-3} M, the size of a blob, equivalent to the average distance over which ET takes place, was determined to be 10 bp with a quenching rate constant of 4×10^{7} s^{-1} between an excited DNA-EB to Cu^{2+}cations. The effect of ionic strength on the distance over which ET occurred (d_{blob}) between an excited DNA-EB and Cu^{2+} was studied. The parameter d_{blob} was compared to the Debye screening length, κ^{-1}, and d_{blob} was found to follow κ^{-1} when the salt was present in excess over the

DNA phosphates and this result suggested that $\kappa^{-1} = d_{blob}$ represents a distance of minimal approach between divalent metal cations bound along the DNA helix.

The complexes formed between DNA and Py-3-12 were studied by fluorescence for the future purpose of relating structure with transfection efficiency. The Model Free (MF) analysis of the pyrene monomer and excimer fluorescence decays yielded quantitative information about the internal dynamics of the Py-3-12 surfactant micelles in water and bound to the DNA helix. The formation of Py-3-12 micelles in water was first characterized by fluorescence using the MF procedure. The robustness of the MF procedure was validated by determining the concentration of surfactant free in solution, $[\text{Py-3-12}]_{free}$, as a function of the overall surfactant concentration, [Py-3-12]. It was found that $[\text{Py-3-12}]_{free}$ increased linearly with increasing [Py-3-12] up to 0.22 mM, which is the CMC of the surfactant obtained by surface tension. Above this concentration, $[\text{Py-3-12}]_{free}$ remained constant and equal to 0.22 (±0.06) mM. When studying the interactions between Py-3-12 and DNA, the total concentration of Py-3-12 was held constant at a value lower than the CMC to ensure that any excimer formed was due to the binding of Py-3-12 to DNA. Near a (–/+) ratio of 1.0, all surfactants were bound to DNA and above this (–/+) ratio, the molar fractions of the pyrene species in solution remained unchanged with increasing DNA concentration. The parameter $\langle k \rangle$ for Py-3-12 bound to DNA was found to equal $50 \pm 3 \times 10^7$ s^{-1} which is smaller than $\langle k \rangle$ for Py-3-12 micelles equal to $79 \pm 2 \times 10^7$ s^{-1}. This suggests that the binding of Py-3-12 to the phosphates along the DNA backbone results in micelles that are more hindered than when no DNA is present in solution. The lifetime of the pyrene excimer of ~30 ns and 55 ns, for the poorly and properly stacked pyrene dimers, respectively, was the same as those found for the Py-3-12 micelles in water, which suggests that Py-3-12 clusters in a micellar form near the DNA helix and possibly adopts a “beads on a string” structure.

Acknowledgements

I would like to thank, first and foremost, my supervisor Professor Jean Duhamel. His intelligence, enthusiasm, guidance, and support are what made this work possible. He was extremely helpful throughout my thesis-writing period and for that he is dearly acknowledged. Dr. Jean Duhamel is a supervisor who is always available to help and encourage his students, and for that he is thanked.

I would like to thank all of my committee members: John Honek, Pu Chen, and Guy Guillemette, with a special thanks to Mario Gauthier for helpful guidance and direction regarding my work. I would also like to thank the graduate secretary of the Chemistry department, Cathy Van Esch, for her aid in troublesome administrative matters. NSERC is dearly thanked for funding.

A very special thank you to the Duhamel and Gauthier lab members who have made my time at UW fun and memorable. I am very happy that I am leaving UW with lifelong friends.

I would like to thank my mother- and father-in-law, Dilawaiz and Sulman Baig, for their continued love and respect.

I would especially like to thank my parents, Elizabeth and John Keyes, and my brother, Greg Keyes. It was a long road and you were always there to encourage me and offer your support. My parents are dearly thanked for always reminding me of the importance of an education. You were right.

And lastly, and definitely not least, I would like to thank my husband, Burhan Baig, for his love, support and patience, while I completed my PhD. You have always encouraged me to strive for success, and your faith in me was never wavering. I could not have done this without you.

Please note that Chapter 2 of this thesis has been published in the Journal of Physical Chemistry B. They do not require written permission to re-publish the work in a thesis. If the thesis is to be published in an electronic format, ACS requires a direct link to the published work. I have included a direct link to the published work at the end of Chapter 2.

Dedication

To my loving husband, Burhan.

Table of Contents

List of Figures

List of Tables

List of Schemes

List of Abbreviations

$<k>$	average rate constant of excimer formation
$<n>$	average number of quenchers per blob
$<\tau>_o/<\tau>_M$	number average fluorescence lifetime in the absence of quencher divided by the number average fluorescence lifetime in the presence of quencher
bp	base pairs
CMC	critical micelle concentration
CT DNA	calf thymus DNA
D	poorly stacked pyrene dimers
d_{blob}	the height of a cylindrical blob in Å (= N_{blob} × 3.4 Å)
DNA	deoxyribonucleic acid
DNA-EB	DNA intercalated ethidium bromide
E0	well-stacked pyrene dimers
EB	ethidium bromide
ET	electron transfer
f_{agg}	molar fraction of aggregated pyrenes in solution
FBM	Fluorescence Blob Model
f_{diff}	molar fraction of pyrenes forming excimer via diffusion in solution
f_{fast}	fraction of EBs that are quenched quasi-instantaneously by nearby metal cations
f_{free}	molar fraction of free pyrenes in solution that do not form excimer
f_{slow}	fraction of EBs that are quenched with a decay time greater than τ_{fast}
I_E/I_M	ratio of the excimer to monomer intensities
I_o/I_M	fluorescence intensity in the absence of quencher divided by the fluorescence intensity in the presence of quencher
K	binding constant
κ^{-1}	Debye screening length
k_{blob}	the quenching rate constant of an excited chromophore in a blob

$k_e[blob]$	rate constant to exchange a quencher between blobs times the blob concentration
MF	Model Free
N_{blob}	size of a blob in terms of bp
P_A	peak-to-valley ratio of the pyrene absorption at the 0-1 transition and its adjacent trough
Py	pyrene
Py-3-12	pyrene substituted gemini surfactant
Py_{agg}	aggregated pyrenes
Py_{diff}	pyrenes forming excimer via diffusion
Py_{free}	free pyrenes that do not form excimer
θ_N	number of condensed N-valent counterions per polyelectrolyte charge
sCT DNA	sonicated calf thymus DNA
SPC	Single Photon Counting
SS	Steady-State
τ_{fast}	lifetime of EBs that are quenched quasi-instantaneously by nearby metal cations
TPC	time per channel
ξ	charge density of the polyelectrolyte

Chapter 1
Literature Review

1.1 Introduction

DNA has been called the molecule of life and every scientist is familiar with its double helical structure shown in Figure 1.1. This structure was first reported by Watson and Crick in their paper in Nature in 1953.[1] As they commented on the possible implications of their discovery, Watson and Crick noted that "This structure has novel features which are of considerable biological interest". As it turns out, this sentence has been called one of science's most famous understatements, and it certainly is.

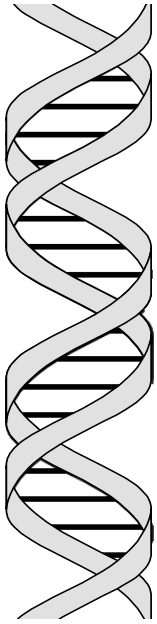

Figure 1.1: Cartoon of the molecular structure of DNA. The two ribbons symbolize the phosphate – sugar backbone and the horizontal rods represent the base pairing between adenine and thymine and/or guanine and cytosine.

The discovery of the structure of DNA has been thought of as one of the greatest scientific achievements of all times and it has enabled many key scientific developments involving DNA. Scheme 1.1 shows a timeline of the scientific milestones involving DNA that was adapted from the Nature Review Genetics article "After the double helix" which celebrates the 50th anniversary of the discovery of the structure of DNA.[2] This timeline clearly illustrates how revolutionary the discovery of the molecular structure of DNA was. All the scientific advancements shown in this timeline revolve one way or another around the helical nature of DNA. However, its unique structure confers some very interesting properties as a material, which have in fact, been realized for quite some time.

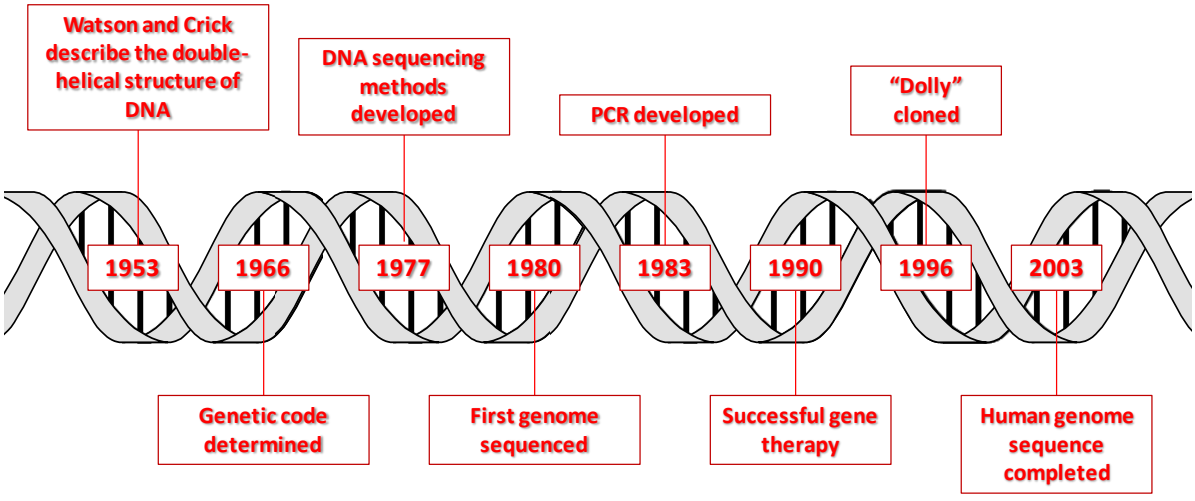

Scheme 1.1: Timeline of the scientific milestones involving DNA since the discovery of its molecular structure in 1953.[2]

In 1962, Eley and Spivery suggested that DNA is a conducting material due to the overlapping pi-orbitals of the stacked base pairs.[3] Almost 30 years later, Jacqueline Barton demonstrated that DNA could mediate the transfer of electrical charges over long distances.[4–7] In the early 1990's, Nadrian Seeman used DNA's remarkable recognition properties and its semi-rigid structure over short distances to make DNA cubes[8] and triangles.[9] Since then, DNA cages and nanotubes have also been constructed whose structures can encapsulate cargo such as gold nanoparticles or therapeutic

drugs.[10–12] Thus, it is clear that the structure of DNA does not only have "novel features which are of considerable biological interest" but also has features of considerable nanotechnological interest, that have led to the development of a new field of science called DNA nanotechnology.[13,14]

The wide range of the aforementioned applications revolving around DNA confirms the fact that the discovery of the double helical structure of DNA has revolutionized science in many ways over the last 50 years. But how did previous scientific discoveries lead to this scientific milestone occurring in 1953? The book entitled "The path to the double helix: the discovery of DNA" by Robert Cecil Olby describes the events leading up to the discovery of the DNA double helix by Watson and Crick, which unsurprisingly begins with the discovery of the macromolecule.[15]

The idea that polymers are giant molecules had been proposed since the 19th century, however, it was Hermann Staudinger's experiments that convinced the research community that high molecular weight substances were not simply aggregates of small molecules, but rather large molecules or macromolecules. He coined the term *Macromolecule* and received the Nobel Prize for his work in 1953.[15] A macromolecule is a very large molecule, such as a polymer or protein, consisting of many structural units, called monomers, linked together by covalent bonds. Therefore, DNA is simply an example of a naturally occurring polymer, whose repeating units are nucleic acids. Furthermore, DNA is special in that it is a polyelectrolyte.

1.2 Polyelectrolytes

An electrolyte, such as a salt, consists of negative and positive charges that are separated in water. A polyelectrolyte also consists of negative or positive parts, but when a polyelectrolyte dissolves in water, the positive or the negative charges remain joined together by the polyelectrolyte which is a highly charged macromolecule. The main distinction between a salt and a polyelectrolyte aqueous solution is that the salt completely ionizes or dissociates in solution whereas the polyelectrolyte does not. For example, a dilute solution of sodium acetate contains only dissociated ions whereas a

solution of polyacrylate, even highly diluted, still has a substantial fraction of counterions bound to it. This binding of counterions to a negatively charged polyelectrolyte, or polyanion, is illustrated schematically in Scheme 1.2.

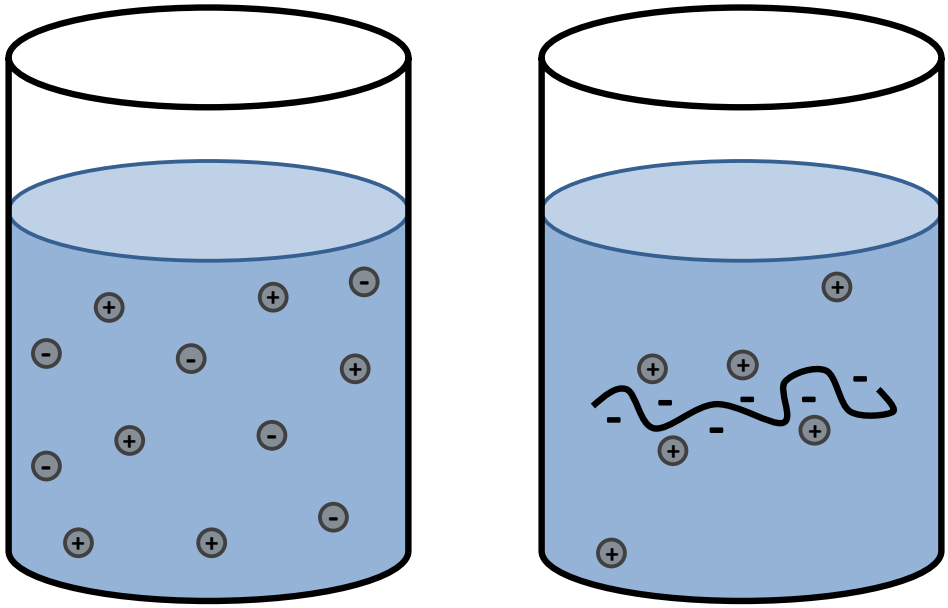

Scheme 1.2: Dissociation of a salt (left) and a polyelectrolyte (right) in water.

Counterions can be bound to polyelectrolytes in two distinct states:[16] site bound and territorially bound. Site bound counterions are classified as those counterions which are in direct contact with one or more of the charged groups of the polyelectrolyte. Site bound counterions are considered to be very tightly bound to the polyelectrolyte, with no water molecules separating the two oppositely charged species. Territorially bound counterions are fully hydrated, behaving in a manner similar to the ions constituting electrolytes like NaCl in water. Territorially bound counterions are said to be "delocalized". The hydrated counterion is drawn into the polyelectrolyte by the strong electric field exerted by the polyelectrolyte, but it is free to move along the polyelectrolyte. Univalent and multivalent ions from a salt that can also act as counterions of the polyelectrolyte can either be site bound or territorially bound when added to an aqueous polyelectrolyte solution. The fraction of

counterions that will bind or condense onto a polyelectrolyte depends on the properties of the polyelectrolyte, namely its linear charge density.

The linear charge density of a polyelectrolyte is characterized by a dimensionless parameter, ξ, given in Equation 1.1.[16] In Equation 1.1, b_B, is the Bjerrum length which is defined in Equation 1.2 and b is the average linear charge spacing of the polyelectrolyte bearing univalent charged groups taken along the contour length of the chain (for DNA, b is taken along the helical axis).[16,17]

$$\xi = \frac{b_B}{b} \tag{1.1}$$

$$b_B = \frac{q^2}{\epsilon_0 kT} \tag{1.2}$$

In Equation 1.2, q is the unit electrical charge, kT is the product of the Bolzmann constant and the absolute temperature, and ϵ_0 is the dielectric constant of pure water. b_B is equal to ~ 7.1 Å at 25 °C in water.[17] The charge fraction f of a polyelectrolyte in a solution containing counterions of one valence type is

$$f = (N\xi)^{-1} \; if \; \xi > N^{-1} \tag{1.3}$$

$$f = 1 \; if \; \xi < N^{-1}$$

where N is the counterion valence.[16] In the case where $\xi > N^{-1}$, counterions condense on the polyelectrolyte. The fraction of polyelectrolyte charge neutralized by N valent condensed counterions is

$$N\theta_N = 1 - (N\xi)^{-1} \tag{1.4}$$

where θ_N is the counterion binding fraction and represents the number of condensed N valent counterions per polyelectrolyte charge.[18]

DNA is a polyelectrolyte with a high linear charge density and counterions will condense around the DNA helix to neutralize some of its charge. The B form of DNA has a step height of 3.4 Å between base pairs or two phosphate pairs. Therefore, *b* equals 1.7 Å for DNA and ξ_{DNA} is calculated to be 4.2 using Equation 1.1. In a solution with monovalent or multivalent counterions, ξ_{DNA} is greater than N^{-1} and counterion condensation occurs. The interactions between the negatively charged DNA helix and positively charged monovalent counterions are important for a variety of applications, the simplest being the stabilization of the double helix and the determination of its overall conformation.[19] On the contrary, the binding of multivalent counterions to DNA can cause the DNA helix to condense or collapse.[20] Therefore, it is important to understand how, and to what extent, counterions bind to DNA. Other applications regarding the interactions between double-stranded DNA and oppositely charged species are described in more detail in the next section.

1.3 Interactions between DNA and Oppositely Charged Species

The interactions between DNA and oppositely charged species are found in many areas of science ranging from biochemistry to DNA nanotechnology and its applications are many and diverse. The cationic species which DNA interacts with can be as small and simple as metal cations or as large and complex as a positively charged protein. As aforementioned, the binding of metal cations to DNA is important from a biophysical standpoint, simply to understand how these cations stabilize or destabilize the structure of DNA. The binding of cations with a more complex structure, like surfactants and cationic lipids, to DNA has major applications in gene therapy as these cations cover the negatively charged DNA to provide a delivery vehicle for the gene to be carried into cells.[21] As a matter of fact, chromosomes in the cell could not be formed without binding between DNA and positively charged histone proteins. Though the interaction between DNA and oppositely charged species is the basis for a wide range of scientific applications, there is one common thread that links them all together; the electrostatic interaction between a negative and positive charge. The interactions between DNA and cationic species, and their applications, will be described in more

detail in the following sections starting with the simplest case, the binding of metal cations to DNA, followed by the binding to DNA of structurally complex cationic species, and finally the interactions between DNA and high molecular weight cationic substances.

1.3.1 DNA and Metal Cations

The interactions between DNA and metal cations have been extensively studied and these interactions have been shown to play a significant role in DNA structure. The binding of metal cations to DNA has been shown to stabilize/destabilize the helical structure,[22–26] induce B-Z – DNA transitions,[27–30] induce the formation of triplex[30–33] and quadruplex structures,[34,35] and condense DNA.[36,37]

The binding of metal cations to the phosphates of DNA stabilizes the double helical structure by partially shielding the negative charges along the backbone. The double helix can be destabilized when divalent metal cations bind to the bases of DNA as this type of binding weakens the hydrogen bonds between base pairs. Whether metal cations will stabilize or destabilize the DNA helix depends both on the type and concentration of the metal cation.

The stabilization or destabilization of the double helix by metal cations is often determined by monitoring the melting temperature of DNA, T_M, which is defined as the temperature at which half of the strands are in the double helical state and half of the strands are denatured. Divalent metal cations which stabilize the double helix result in a high T_M as was shown for the binding of a series of divalent metal cations to DNA: Mg^{2+}, Co^{2+}, Ni^{2+}, Mn^{2+}, Zn^{2+}, Cd^{2+}, and Cu^{2+}.[22] The cations on the left of the series, namely Mg^{2+}, Co^{2+}, and Ni^{2+}, were found to increase the T_M of DNA above a metal to DNA phosphate ratio of 1.0, indicating that these divalent metal cations stabilize the helix the most. At the same metal to phosphate ratio, the divalent metal cations on the right of the series, namely Mn^{2+}, Zn^{2+}, Cd^{2+}, and Cu^{2+}, destabilized the DNA helix. The difference in the stabilization potential of the series is due to their affinity for binding to the bases of the DNA. Therefore, the counterions

on the far right of the series have a higher affinity for the DNA bases, a binding that destabilizes the double helix. The binding between divalent metal cations and the bases of DNA is believed to occur between the unpaired electrons of the d-orbitals of the divalent metal cations and the aromatic bases of DNA. Ag^{+} has also been shown to destabilize the double helix by binding to the nitrogenous bases, resulting in a lower T_M.[23]

The binding of divalent metal cations to DNA has been studied by Raman spectroscopy and their affinity to the DNA bases decreases in the following order: $Hg^{2+} > Cu^{2+} > Pb^{2+} > Cd^{2+} > Zn^{2+} > Mn^{2+} > Ni^{2+} > Co^{2+} > Fe^{2+} > Ca^{2+} > Mg^{2+} > Ba^{2+}$.[24] These results compare well with the DNA base binding affinity obtained from the melting temperature studies.[22] Therefore, divalent metal cations with the strongest base affinity destabilize the B form of DNA and stabilize other structures. Conversely, divalent metal cations with a greater binding affinity to the phosphates stabilize the B form of DNA. The binding of divalent metal cations to the bases of DNA also depends on the metal to phosphate ratio. For instance, Cu^{2+} has a strong affinity for the bases of DNA, but binding of Cu^{2+} to the bases has been observed at a metal to phosphate ratio of 0.25 and higher.[39] Also, studies involving the binding of Ni^{2+} to the bases of DNA have been contradictory. The binding of Ni^{2+} to an oligonucleotide base occurred at a guanine residue in the terminal position and not a guanine residue located in the center of the helix.[40] Other studies have shown that Ni^{2+} does not bind to the DNA bases at all.[41]

The binding of metal cations to DNA is known to induce B-Z DNA transitions. The most commonly occurring DNA structure, and the most familiar one, is B-DNA. Z-DNA is a left handed double helix in which the double helix winds to the left (instead of the right like the more common B-DNA form). B-Z DNA transitions have been shown to occur when Na^{+} and Mg^{2+} are added to B-DNA at concentrations of 2.5 M and 0.7 M of the chloride salt, respectively.[28] The large concentrations of metal cations needed to induce the transition at room temperature suggested that the transition induced by the binding of these metal cations to DNA was non-specific. Another study

using vibrational circular dichroism (VCD) demonstrated that the Mn^{2+} could also induce a B-Z transition at Mn^{2+} to phosphate ratios of 8.5.[30]

Although the B-Z – DNA structure switch might be initially thought of as an effect of interesting but limited application, the Z-DNA structure might turn out to be an important biological requirement in transcription. In one study, Ho et al. studied human chromosome 22 and found that ~ 80 % of its genes have sequences that favour the Z-DNA form near the transcription start site.[29] It is also believed that Z-DNA provides torsional strain relief while DNA transcription occurs.[42]

Another form of DNA that can be stabilized by metal cations is triplex DNA. Triplex DNA forms when a DNA oligonucleotide binds to a polypurine region of DNA. These oligonucleotides bind specifically in the major groove of DNA, forming Hoogsteen or reverse Hoogsteen hydrogen bonds.[31] Hoogsteen bonds are formed when an oligonucleotide consisting of cytosine (C) and thymine (T) binds parallel to the purine rich strand of the double stranded DNA. In the case of C, it must be protonated to bind to guanine (G) in a G–C base pair, whereas T binds to adenine (A) in an A–T base pair (Figure 1.2 A). A reverse Hoogsteen bond is formed when an oligonucleotide consisting of guanine (G) and adenine (A) binds antiparallel to the purine rich strand (Figure 1.2 B).

Triplex DNA structures are dramatically stabilized in the presence of certain metal cations. Compared to alkali-earth metal cations, transition-metal ions, especially Co^{2+} and Ni^{2+}, have shown an enhanced ability in stabilizing triplex DNA.[33] On the other hand, the interaction of Ba^{2+} with DNA stabilizes the formation of duplex DNA.[33] In particular, the Mg^{2+} cation has shown large stabilizing effects on the G·G–C triplet.[32] Monovalent cations K^+ and Rb^+ inhibit the formation of DNA triplexes by interfering with the association of G-rich oligonucleotides with DNA.[43] DNA triplexes can also be formed when Ag^+ replaces the naturally hydrogen bonded base pairs by metal-mediated base pairs, a phenomenon which has found applications in molecular devices.[44]

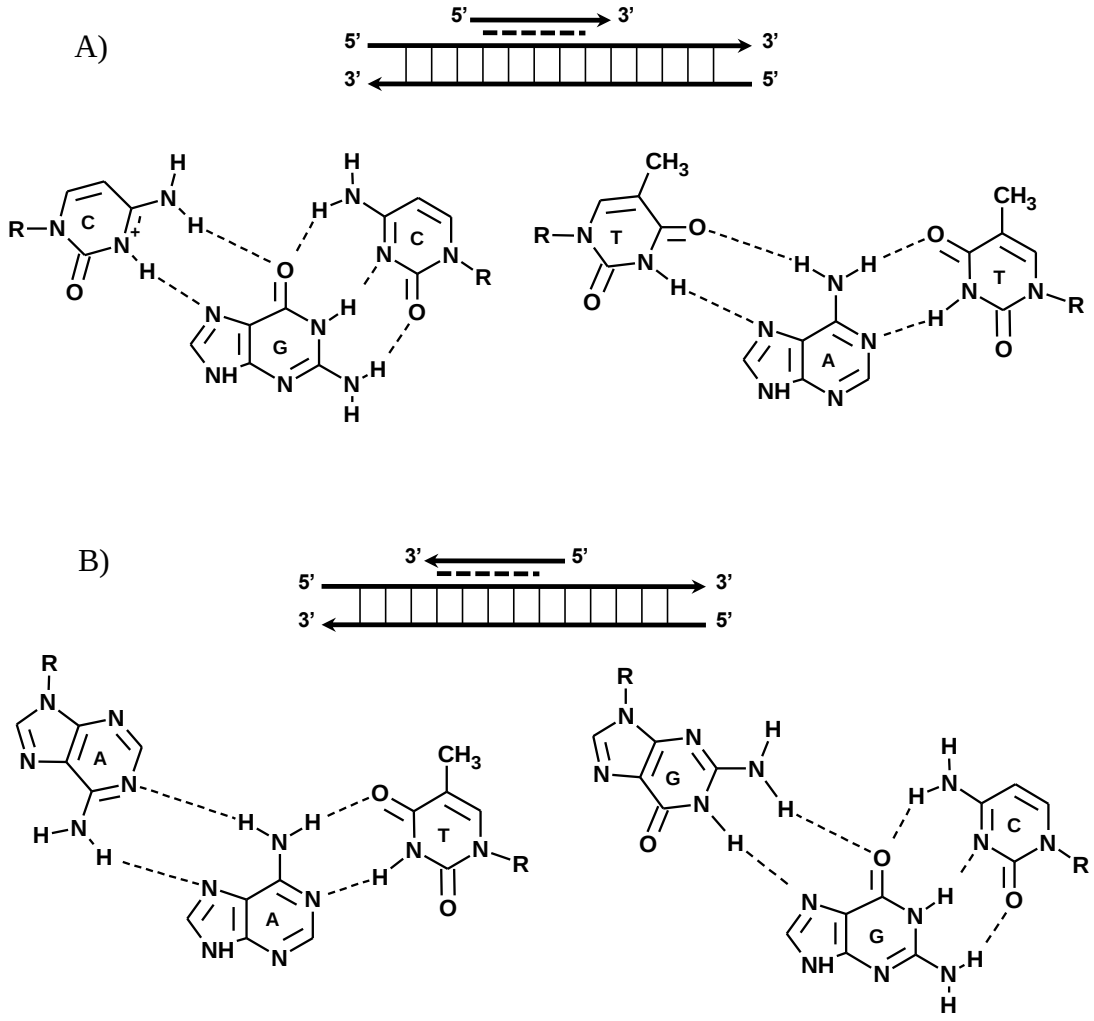

Figure 1.2: The structure of triplex DNA. A) Hoogsteen bond and B) reverse Hoogsteen bond in triplex DNA.[31] (Note: these structures do not contain the pentavalent carbon atoms which are shown in reference 31.)

Quadruplex DNA is another DNA structure which exists for nucleic acid sequences rich in guanine. These guanine-rich nucleic acid sequences form four stranded structures called G-quadruplexes, or G-tetrads, which consist of a square arrangement of the guanines stabilized by Hoogsteen hydrogen bonding and a monovalent cation in the center of the tetrad (Figure 1.3).

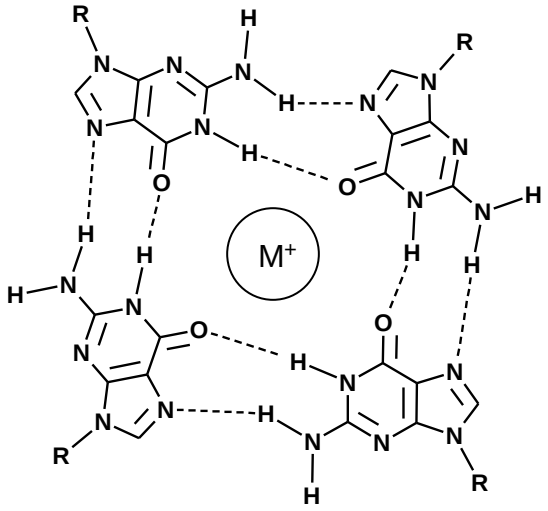

Figure 1.3: Hoogsteen hydrogen bonding in a guanine tetrad in quadruplex DNA stabilized by a metal cation.[34]

X-ray crystallography has shown that the monovalent cations Na^+ and K^+ are the most efficient at stabilizing G-quadruplexes.[34,35] It is not surprising that K^+ stabilizes DNA quadruplexes since these monovalent counterions destabilized DNA triplexes by interacting with the G residues. Other monovalent cations that stabilize G-quadruplexes are Rb^+, Cs^+, and Tl^+, as well as the divalent metal cations, Sr^{2+}, Ba^{2+}, and Pb^{2+}.[35] In general, low concentrations of these cations stabilize G-tetrads, while increasing the concentrations becomes destabilizing. Both DNA triplex and quadruplex structures are suspected to play a role in transcription.[45] Therefore, it is important to know what type of metal cations are needed to form these structures, how they bind to DNA, and at what concentrations, to better understand the role of these structures in cell transcription.

The binding of metal cations to DNA also play a role in DNA condensation. Condensing agents work by decreasing the electrostatic repulsion that takes place between DNA segments and it is known that about 90 % of the DNA charge must be neutralized for condensation to occur.[20] In aqueous solution, DNA condensation normally requires cations of a charge of 3+ or greater since the

fraction, θ_N, of DNA charges that are neutralized would be equal to or greater than 0.92 (using Equation 1.4 and $\xi_{DNA} = 4.2$). However, DNA condensation has also been reported for the divalent metal cation Mn^{2+} because the interactions between this divalent metal cation and DNA are not purely electrostatic.[36] In an interesting study, the redox state of Fe^{2+}/Fe^{3+} was used to observe DNA condensation and elongation as the valence was switched from 3+ to 2+.[37] Typically, condensing agents are not metal cations but cations with a more complex structure such as spermine and the inorganic cation, $Co(NH_3)_6^{3+}$, and the interactions between these species and DNA will be discussed in the next section.

1.3.2 DNA and Cations with a Complex Structure

DNA condensation is the most common result occurring from the interactions between DNA and small but structurally complex cations. In living cells, DNA usually exists in the condensed state. However, in aqueous solution without condensing agents, DNA chains are highly elongated and coiled because water is a good solvent for DNA. Condensing agents work by decreasing repulsions between DNA segments and by making DNA–water interactions less favourable. The most commonly studied cationic condensing agents are spermine and spermidine,[46–48] $Co(NH_3)_6^{3+}$,[49,50] cationic surfactants,[51–54] cationic gemini surfactants,[55,56] and cationic liposomes.[51,57] The structures of these condensing agents are shown in Figure 1.4.

Spermine and spermidine are found in all eukaryotic cells and are cationic under physiological pH. Light scattering studies have shown that the condensation of DNA by spermine and/or spermidine is a cooperative process where the degree of ligand binding to DNA must exceed a threshold value to induce condensation.[46,47] It was also found that the spermidine-induced condensation of DNA could be reversed by raising the salt concentration of the medium.[48] Similar trends were observed for the interactions between DNA and $Co(NH_3)_6^{3+}$.[49,50] Condensation of DNA by both of these cationic molecules results in DNA being condensed in a toroidal conformation.

However, when the length of DNA reaches values much shorter than its persistence length of ~ 500 Å, toroids were not observed but rather shapeless aggregates of condensed DNA.[46]

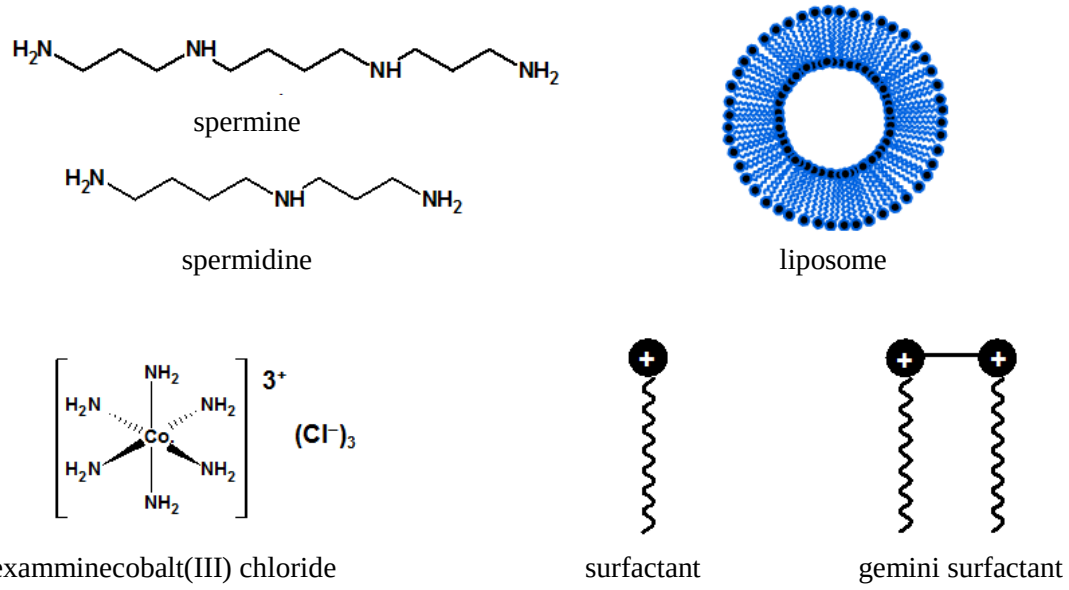

Figure 1.4: Structures of cationic DNA condensing agents.

The compaction of DNA by cationic surfactants, gemini surfactants and liposomes has widespread implications in gene therapy. Gene therapy requires a gene delivery vehicle to transport therapeutic DNA to cells. These condensing agents do not only compact DNA, but also provide a means to transport DNA into cells as they can fuse with cell membranes. The condensation of DNA by these cationic molecules results in different types of nanostructures whose characteristics depend on surfactant type and concentration, and the percentage of non-ionic surfactant added.[51–57]

An electron microscopy study showed that the condensation of long DNA molecules by cetyltrimethylammonium bromide (CTAB) results in the reproducible formation of globular aggregates of about 30 nm in size.[51] It was found that depending on the surfactant concentration,

three distinct DNA conformations existed: extended coil, coexisting coil and globule, and globule. The binding of dodecyltrimethylammonium bromide (DTAB) to DNA was studied by light scattering and high performance capillary electrophoresis (HPCE).[53] These studies revealed a two stage binding process, where in the first stage, micelle like structures bind on the DNA surface, followed by the binding of more surfactant molecules which causes DNA charge neutralization and phase separation. A study of the interactions between the double tailed didodecyldimethylammonium bromide (DDAB) and DNA by synchrotron small angle X-ray scattering showed that these complexes form a bilayered lamellar structure.[54] In this study, the binding of CTAB to DNA was also investigated and revealed a complex 2D hexagonal structure of closely packed cylinders. However, the addition of a neutral lipid to complexes of DNA and CTAB induced a structural transition from the 2D hexagonal to a multi-bilayered lamellar structure.

The complexation between gemini surfactants and DNA have gained considerable research interest due to the improved properties of the complexes over conventional surfactants, such as lower critical micelle concentrations (CMCs).[58–60] The interactions between gemini surfactants and DNA are also of particular interest due to their ability to self assemble into micelles of different shapes (spherical, rod-like) even at low surfactant concentrations.[61,62] Fluorescence microscopy (FM) was used to observe the structures formed between DNA and the gemini surfactant propanediyl-1,3-bis(dimethyldodecylammonium bromide).[55] The complex structures formed between DNA and the gemini surfactant were characterized as a "rings on a string" structure where disordered coil parts coexist with ordered compact parts with a diameter around 160 nm. Another study using atomic force microscopy (AFM) also observed a beadlike structure for the binding of hexyl-α,ω-bisdodecyldimethylammonium bromide. In fact, the so called "beads on a string" structure seems to be a common one observed between DNA and gemini surfactants.[55,56,63,64]

Cationic liposomes are studied as potential DNA carriers in gene therapy since their closed bilayer membrane mimics that of natural viruses. Interactions between cationic liposomes and DNA

lead to a variety of interesting structure like those observed with cationic surfactants and gemini surfactants. Electron Microscopy studies showed that as the liposomes DOTMA (N-[1-[2,3-bis(oleoyloxy)]propyl]-N,N,N-trimethylo ammonium chloride) or DOTMA/PE (phosphatidylethanolamine) were added to DNA, the DNA molecules became gradually covered with liposome aggregates.[51] This is in contrast to the binding of cationic surfactant to DNA which was shown to be cooperative. Studies have shown that the addition of a neutral helper lipid such as DOPE (dioleoyl phosphatidylethanolamine) to mixtures of cationic liposomes and DNA changes the structure of the complex from a lamellar phase to a columnar inverted hexagonal phase,[57] similar to the structural changes observed for surfactant-DNA complexes upon the addition of a neutral surfactant.

The interactions between DNA and cationic species with a complex structure are greatly studied for the purpose of gene delivery as these molecules coat the DNA helix and condense it into smaller packages. It is thus of no surprise that larger molecules bearing cationic charges, such as polycations, have also been studied for their ability to condense DNA and transfer it into cells. A few examples of the structures formed from the complexation of DNA with high molecular weight cationic substances will be discussed in the next section.

1.3.3 DNA and High MW Cationic Substances

The most famous example of DNA condensation by a high MW cationic substance is in the formation of chromosomes. A typical human cell is 20 μm in diameter and contains 23 pairs of chromosomes each having an average length of about 5 cm (=1.3×10^8 bp × 3.4 Å/bp).[65] Therefore, the 23 pairs of chromosomes in the 20 μm diameter cell contain more than 2 m of DNA. Thus, DNA in the cell is highly condensed and compact. This compaction of DNA begins with the binding of DNA to histones, which are positively charged arginine- or lysine-rich proteins. Histones condense DNA into a "beads on a sting" structure.[65]

The condensation of DNA by polycations has been studied for gene delivery purposes. Complexes formed between DNA and cationic polymers for use in gene delivery are called polyplexes. The cationic polymers used for gene delivery often have a high lysine content and polyplexes are studied as a function of the nitrogen to DNA phosphate ratio (N/P). The transfection efficiency of DNA complexes with polylysine was more efficient when the N/P ratio was greater than unity and when the lipoplex formed was small and positively charged.[51] Complexes between DNA and polylysine, polyarginine, and polyornithine have been found by light scattering to form uniform particles with a diameter of 80 – 120 nm which increased in size when the particles were diluted in electrolytes.[66] The transfection efficiency of these complexes was greatest for DNA complexed with polyornithine, followed by polylysine, and the weakest transfection efficiency resulted from complexes with polyarginine. However, all three polyamino acids were not as efficient as DNA/cationic lipid complexes in cell transfection. When polylysine was conjugated to transferrin, a blood plasma protein for iron delivery, and then complexed with DNA, gene delivery was very efficient in cells that had transferrin receptors.[67] Therefore, polycations have potential as gene delivery vehicles.

An interesting area of research involving the complexation of DNA and cationic polymers is in the development of DNA multilayer films. Multilayer films have been constructed by electrostatic layer-by-layer deposition of DNA and the cationic polymers, poly(dimethyldiallylammonium chloride) (PDDA)[68] and poly(allyamine).[69] These highly organized ultrathin films containing multilayers of biomolecules can be incorporated into any biomolecular devices.

1.4 Fluorescence to Study the Interactions between DNA and Oppositely Charged Species

The interactions between DNA and oppositely charged species discussed in the previous section have been studied by a variety of techniques such as absorbance, vibrational circular dichroism

(VCD), X-ray crystallography, and atomic force microscopy (AFM), to name but a few. Fluorescence spectroscopy is also a powerful tool to study the interactions between DNA and oppositely charged species. Fluorescence emission occurs on a useful time scale to monitor the interactions between DNA and cationic species. Fluorescence spectroscopy studies can also monitor events that take place between macromolecules in solution as opposed to the molecules being adsorbed onto a surface for microscopy experiments. Fluorescence Resonance Energy Transfer (FRET) can probe conformational changes and intramolecular distances over 1 – 10 nm length scales,[70,71] which are the length scales required for the study of the interactions between DNA and cationic species. The lifetime of a chromophore is often sensitive to its environment and measurement of these lifetimes by time-resolved fluorescence offers information about the microdomains formed by macromolecules. Fluorescence quenching experiments probe the dynamic processes which take place in solution inside macromolecules.[72] For all these reasons, fluorescence spectroscopy provides a useful tool to study the interactions between DNA and oppositely charged species.

The interactions between DNA and metal cations have been studied by fluorescence.[73,74] The binding and mobility of Cu^{2+}, Ni^{2+}, and Co^{2+} to DNA were probed by monitoring the fluorescence quenching of ethidium bromide (EB) intercalated in DNA (DNA-EB).[73] It was determined that fluorescence quenching is due to metal cations that are territorially bound to the DNA helix and that quenching occurs via an electron transfer mechanism. EB is often chosen as a fluorescent probe to study events involving DNA since its lifetime is dramatically increased when it is intercalated between the DNA base pairs (1.6 ns in pure water vs. 23 ns in DNA).[75] In another study, which also used DNA-EB as a probe, it was determined that the binding of aluminum to DNA was pH-dependent, and that below pH 4.5, the binding decreased with decreasing pH. This conclusion was reached from the observed decrease in the fluorescence of DNA-EB.[76]

DNA-EB is also used as a fluorescent probe to study the interactions between DNA and condensing agents such as cationic surfactants.[77] When DNA is condensed by adding increasing amounts of surfactant, EB is no longer intercalated between the base pairs of DNA and the fluorescence of EB is reduced. Pyrene is often chosen as a probe to study the interactions between DNA and gemini surfactants. Pyrene is a hydrophobic chromophore whose fluorescence is highly sensitive to its micro-environment.[78] The interactions between gemini surfactants and DNA provide a hydrophobic environment for pyrene which results from the interactions of the hydrophobic tails of the surfactant molecules. Information about the local polarity of the environment surrounding pyrene is obtained from monitoring the I_1/I_3 ratio of molecular pyrene.[78] The I_1/I_3 ratio of pyrene is lower in aqueous solutions containing complexes of DNA and gemini surfactants than in water alone, revealing that hydrophobic domains are formed between surfactant molecules along the DNA helix.[77,79]

The exclusion of EB from the interior of the DNA helix has also been used to study the formation of polyplexes between DNA and polyethylenimine (PEI) or poly(L-lysine) (PLL).[80] As more PEI or PLL was added to DNA, the contribution to the fluorescence decays of DNA-EB decreased whereas the contribution of EB in water increased, indicating complexation between DNA and the cationic polymers. This study was also able to determine that while PEI polyplexes exist in several different states, PLL complexes exist in one tightly bound state which rationalizes why PEI releases DNA more easily than PLL.

Thus fluorescence is a useful tool to study the interactions between DNA and oppositely charged species in solution and provides information on the time scale over which these events occur. Steady-state and time-resolved fluorescence spectroscopy will be used in this thesis to monitor the interactions between DNA and oppositely charged species, with a special focus on characterizing the distribution of these species around the DNA helix. As the interactions between DNA and oppositely charged species in solution take numerous aspects, this study will begin with the simplest case,

namely the interactions between DNA and metal cations, and more specifically, divalent metal cations. This investigation will be followed by a study of the interactions between DNA and more structurally complex cations, namely positively charged gemini surfactants. The reasoning behind these choices is outlined in the Goals of the Thesis.

1.5 Goals of the Thesis

The overall purpose of this thesis is to demonstrate the ability of fluorescence to characterize the interactions between DNA and oppositely charged species in solution, in particular their distribution around the DNA helix. The thesis is divided into four research chapters, two of which look into the interactions between DNA and metal cations in solution, whereas the other two investigate the interactions between DNA and gemini surfactants.

The interactions between DNA and metal cations in solution are studied in Chapters 2 and 3 by using DNA-EB as a probe whose fluorescence quenching by divalent metal cations yields information about their distribution around the DNA helix, since this quenching is due to the transfer of an electron from an excited DNA-EB to divalent metal cations randomly distributed around the DNA helix. The random distribution of divalent metal cations around the DNA helix leads to a distribution of quenching rate constants that complicates the analysis of the fluorescence data. Fortunately, the Fluorescence Blob Model (FBM) could successfully handle this distribution of rate constants and it was applied to analyze the fluorescence data. Traditionally, the FBM has been used to study the dynamics of polymers in solution randomly labeled with chromophores and quenchers [81-87] and more recently, the side chain dynamics of an alpha helix.[88,89] In the traditional FBM experiments, both the chromophore and quencher are mobile and information on long range polymer chain dynamics is obtained when the fluorescence of the chromophore is quenched, which indicates that two polymer segments bearing a chromophore and quencher have diffused in the solution and come into contact with one another. This study represents the first example in the literature where the FBM is used with a fixed chromophore (DNA-EB) and a mobile quencher, Cu^{2+}. Chapter 2 establishes the ability of the

FBM to describe quantitatively how DNA-EB is quenched by Cu^{2+} by providing the rate and distance (d_{blob}) over which an electron is transferred from an excited DNA-EB to a Cu^{2+} cation. Chapter 3 investigates the effect of ionic strength on the distance d_{blob} over which electron transfer between DNA-EB and Cu^{2+} occurs. Surprisingly, d_{blob} is found to equal the Debye screening length of the solution which decreases with increasing ionic strength. Were this result to be confirmed by others, its implications might be far-reaching as it provides a novel rational to describe the binding of metal cations to the negatively charged phosphates.

Chapters 4 and 5 study the complexes formed between DNA and gemini surfactants in solution for the future purpose of relating structure with transfection efficiency. One of the two alkyl tails of the gemini surfactant used in this study was substituted with the chromophore pyrene to yield a pyrene substituted surfactant referred to as Py-3-12. In these experiments, excimer formation is used to indicate that two surfactant molecules come in close contact with one another. Chapter 4 involves the fluorescence characterization of Py-3-12 in water alone, without DNA, with the Model Free (MF) program. The MF program globally analyzes the pyrene monomer and excimer fluorescence decays to yield quantitative information about the internal dynamics of the Py-3-12 surfactant micelles and the molar fraction of Py-3-12 species in solution, namely f_{free}, the fraction of free pyrene that does not form excimer, f_{diff}, the fraction of pyrene that forms excimer by diffusion, and f_{agg}, the fraction of aggregated pyrene. Once the validity of the MF program was established, the interactions between Py-3-12 and DNA could be studied by fluorescence as was done in Chapter 5. In these experiments, the concentration of Py-3-12 was held constant below the CMC and the concentration of DNA was increased. Therefore, any excimer formation was a result of the binding of Py-3-12 to DNA and not due to the formation of micelles in water, an experimental design that greatly simplified the analysis of the fluorescence results.

The experiments described in this thesis characterizing the interactions between DNA-EB and divalent metal cations by fluorescence are expected to provide valuable insight into electron transfer

reactions taking place between non-covalently attached, randomly distributed electron donors and acceptors and the distribution of these cations around the DNA helix. Furthermore, it is hoped that the fluorescence experiments which characterize the interactions between DNA and Py-3-12 will shed light on the nature of the complexes formed between these species. This thesis aims to demonstrate that fluorescence, especially time-resolved fluorescence, when combined with the appropriate protocol for analyzing the fluorescence decays, provides quantitative and insightful information on the interactions between DNA and oppositely charged species, which can be applied to other polyelectrolytes and their counterions.

Chapter 2

Electron Transfer Between Physically Bound Electron Donors and Acceptors: A Fluorescence Blob Model Approach

2.1 Overview

The present study reports on the applicability of the fluorescence blob model (FBM) to analyze the complex fluorescence decays obtained with DNA-intercalated ethidium bromide (EB) as it transfers an electron to copper cations bound to the DNA helix. Traditionally the information retrieved about the electron transfer process taking place between an electron donor intercalated in DNA and an electron acceptor physically and randomly bound to DNA has been limited due to the distribution of distances over which quenching can occur, which leads to a distribution of rate constants resulting in complex fluorescence decays. These complications can be overcome by analyzing the fluorescence data with a fluorescence blob model (FBM) which allows for the study of fluorescence quenching between fluorophores and quenchers randomly spaced along a polymeric backbone. The fluorescence decays obtained for EB intercalated between two DNA base pairs (bp) as it transfers an electron to copper randomly bound to the DNA were well fit with the FBM. In the FBM analysis, electron transfer is characterized by the size of a blob in term of base pairs, N_{blob}, over which electron transfer occurs, as well as the rate constant of electron transfer inside a blob, k_{blob}. The present work demonstrates that electron transfer between intercalated EB and randomly bound copper occurs over an average distance that increases with increasing duplex length up to a duplex length of 12 bp, beyond which the distance over which electron transfer occurs remains constant with duplex length and equals 10.8 ± 0.4 bp.

2.2 Introduction

Can the π-stacked array of base pairs in DNA serve as a pathway for charge transfer? This phenomenon was suggested over 40 years ago.[1] Yet the possibility of long range charge transfer facilitated by DNA goes against the notion that DNA acts as an insulator. This glaring contradiction

has led many researchers to attempt to solve the controversial question at hand.[2,3] The double helical structure of DNA discovered by Watson and Crick in 1953[4] results in a π-stacked array having an interplanar distance of 3.4 Å, close to that of other conducting stacked solids such as graphite[5] making charge transfer in DNA a promising prospective. The efficiency of charge transport in DNA has significant biological implications as radical reactions cause DNA damage.[6-9] On the other hand, the semi-rigid structure of short DNA duplexes makes it an attractive scaffold for applications in DNA biosensors[10-14] and DNA nanotechnology[15-17] where efficient charge transport enabled by DNA could be taken advantage of.

The study of photoinduced electron transfer in DNA can be divided into two cases. The first case (case #1) summarizes early research in photoinduced electron transfer and occurs with electron donors and acceptors non-covalently attached to the DNA helix.[18-26] The use of non-covalently attached electron donors and acceptors is advantageous due to the ease of sample preparation as well as the fact that electron transfer is studied in unmodified DNA. The disadvantage to dealing with electron donors and acceptors randomly distributed along the DNA helix is that the distances between the electron donors and acceptors are random and unknown. Since the rate of electron transfer depends on the distance separating each electron donor and acceptor pair,[27-38] the random distribution of electron donors and acceptors leads to a distribution of electron transfer rate constants and fluorescence data acquired under such conditions only yields qualitative information about the process of electron transfer. In the second case (case #2), the electron donor and acceptor are covalently attached to the DNA helix. Major improvements in phosphoramidite chemistry enabled the synthesis of well-defined DNA constructs bearing a pair of electron donors and acceptors separated by a known distance and electron transfer in these constructs has been well studied over the last 10 - 15 years.[27-47]

In case #2 where the distance between the electron donor and acceptor is known, the fluorescence data yield the rate of electron transfer whose magnitude can be correlated directly to the distance

spanning the electron donor and acceptor. However, sample preparation is difficult and not every lab masters the knowledge and/or techniques necessary to make such DNA constructs.[27-47] The present work attempts to combine the advantages of both cases; the ease of sample preparation of case #1 with the ability to retrieve quantitative information on electron transfer as with the well-defined DNA constructs of case #2. Demonstration that quantitative information can be retrieved on the process of electron transfer between electron donors and acceptors randomly distributed along the DNA helix is accomplished by analyzing the fluorescence decays of DNA-intercalated ethidium bromide (DNA-EB) as it transfers an electron to copper cations randomly bound to the DNA helix with the Fluorescence Blob Model (FBM).

The FBM was introduced in 1999 to account for the distribution of rate constants that is generated by the random labeling of chromophores and quenchers onto a flexible polymer backbone[48] and has been traditionally used to study the dynamics of polymers in solution[49-54] and more recently, the side chain dynamics of an alpha helix.[55,56] The FBM is based on the assumption that upon excitation, a chromophore attached onto a polymer backbone can only probe a restricted volume during its lifetime. This restricted volume is referred to as a *blob*. The blob is then used as a unit volume to partition the polymer coil into a cluster of blobs. Analogously, when dealing with DNA-EB and copper cations bound to the phosphate backbone, a copper ion can only probe a restricted volume around the DNA helix during the lifetime of EB, since its mobility is restricted by electrostatic binding to the backbone phosphates. As with a polymer chain, this restricted volume can be viewed as a *blob* and the DNA double helix can be partitioned into a string of cylindrical blobs. The FBM is described by three parameters; the average number of quenchers per blob, $<n>$, the quenching rate constant of an excited chromophore located in a blob containing a single quencher, k_{blob}, and the product $k_e[blob]$ where k_e is the rate constant to exchange a quencher between blobs and [*blob*] is the concentration of blobs along the DNA helix (Figure 2.1).

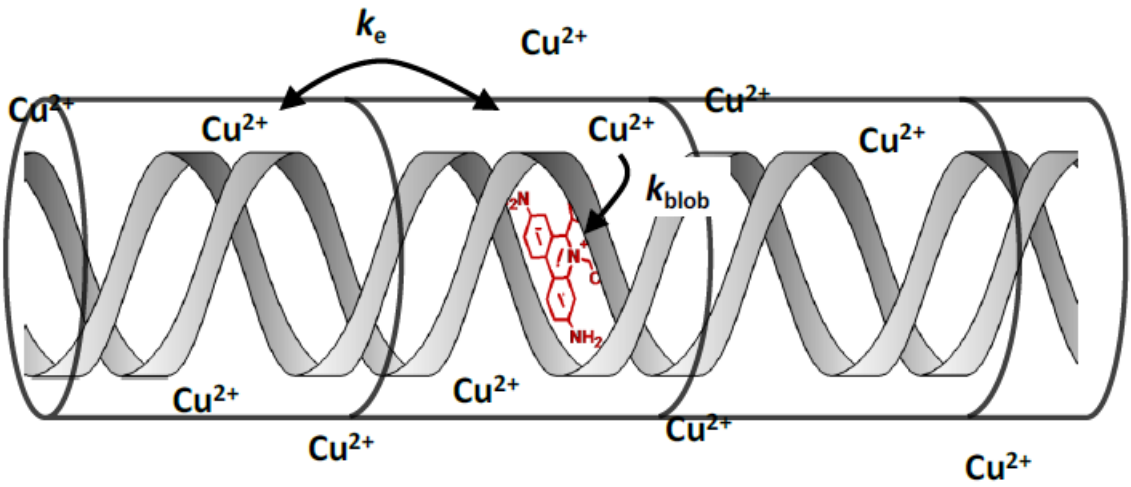

Figure 2.1: DNA double helix with ethidium bromide randomly intercalated and copper cations randomly bound. The double helix is partitioned into a string of blobs.

Over 20 years ago, Artherton and Beaumont investigated the quenching of DNA-EB by several transition metal ions and treated their data in a manner similar to that used in micelle quenching experiments.[19] This was an intriguing approach since Figure 2.1, without the DNA helix, is comparable to a linear array of surfactant micelles loaded with chromophore and quencher molecules. The double exponential behavior observed by Atherton and Beaumont was attributed to two non-interchangeable EB excited states; one that is quenched by a metal ion bound to DNA within the quenching radius contributing to the fast decaying portion of fluorescence and the other quenched by metal ions that must diffuse into the quenching sphere from other locations providing the slower decaying component. The authors fit the fluorescence decays with a biexponential function to obtain the corresponding fast and slow quenching rates and further used these rates to obtain quantitative information about the distance over which electron transfer occurs.

However, the flaw in using a biexponential fit is that the random distribution of metal ions around the DNA helix, as with quenchers in surfactant micelles, is expected to yield a multiexponential decay having a continuous range of decay components from fast to slow. Therefore the fluorescence data

should be fit with a form similar to the one commonly used to deal with micellar systems.[57-59] The FBM equation was derived by applying the same mathematical treatment used to describe micellar quenching and is thus better suited to describe quenching of EB by metal ions randomly distributed around the DNA helix.

EB was chosen as a fluorescent probe since it strongly intercalates in DNA independently of base pair composition.[60,61] Also, the fluorescence lifetime of EB is dramatically increased when it is intercalated between the DNA base pairs (1.6 ns in pure water vs. 23 ns in DNA).[62] Electron transfer was studied between EB and copper at copper-to-DNA phosphate ratios smaller than 0.20 to ensure that copper bound preferentially to the DNA phosphate groups.[63] The FBM fits the fluorescence decays, directly yielding a quantitative measure of the rate constant of electron transfer and the distance over which electron transfer occurs.

The FBM-based analysis of the fluorescence decays was successful, yielding good fits. Additional experiments were conducted, to first validate one assumption used by the FBM, second, to rationalize an observation made during this analysis, and third, to confirm that the scaling behavior expected from any blob model analysis was also observed in this study. The assumption made in the FBM analysis of the electron transfer process between EB intercalated in DNA (DNA-EB) and randomly bound copper is that the exchange of copper between blobs (i.e. DNA) and the bulk solution occurs on a time scale that is much larger than that probed by the fluorescence experiments (~ 200 ns) due to the electrostatic binding of copper cations to the phosphate backbone. Consequently, $k_e[blob]$ is assumed to represent the exchange of copper between adjacent blobs and not between the bulk solution and the blobs. The validity of this assumption was investigated by conducting a series of experiments where the solution viscosity was modified by adding sucrose and monitoring whether the 10 fold increase in bulk viscosity was reflected in a 10 fold reduction of $k_e[blob]$. The second set of experiments aimed at rationalizing the observation made during this study that a threshold copper concentration, or an onset copper concentration, needed to be reached before quenching of DNA-EB by copper cations can occur. This phenomenon was believed to be due to the

electrostatic repulsion experienced by the positively charged ethidium and Cu^{2+} cations and experiments were carried out to alter the electrostatic repulsion by increasing the EB concentration or ionic strength of the solution. Finally, any analysis relying on the use of blobs to study the behavior of macromolecules shifts the focus of the study from being a study of the entire macromolecule to the study of that section of the macromolecule found inside a blob. The implication of this postulate is that the physical phenomenon being investigated becomes independent of the overall size of the macromolecule since it occurs within a blob and the macromolecule has become an ensemble of identical blobs. Consequently, the electron transfer process probed by the FBM is expected to become independent of DNA length, as long as the DNA construct is long enough. To this end, the distance over which electron transfer occurs was monitored as a function of DNA length by using DNA constructs of length varying from a 6 bp duplex to ~ 15,000 bp (calf thymus DNA). The body of experiments presented in this report provides a self-consistent set of results which, it is hoped, demonstrates the applicability of the FBM for studying electron transfer in DNA.

2.3 Experimental

Materials. Calf Thymus DNA (CT DNA, product number D1501), custom DNA duplexes and hairpins, anhydrous copper sulfate, and ethidium bromide (EB) were purchased from Sigma-Aldrich (Milwaukee, WI). Sodium sulfate was purchased from Cambridge Isotope Laboratories, Inc. (Andover, MA). All materials were used as received except for EB. EB was recrystallized three times from methanol to ensure its fluorescence purity.[64] Doubly distilled water (deionized from Millipore Milli-RO 10 Plus and Milli-Q UF Plus (Bedford, MA)) was used in all solution preparations.

DNA Preparation. The sequences of the DNA duplexes and hairpins (Sigma) used in this study are listed in Tables 2.1 and 2.2, respectively. The sequences chosen ensured base pairing at room temperature. The DNA duplexes were made by mixing equal volumes of complementary single stranded DNA. The solutions were heated to 95 °C for 5 minutes in a water bath and were allowed to

cool slowly to room temperature to ensure that the complementary strands would anneal into the duplex. The DNA hairpins were also heated to 95 °C for 5 minutes, but were snap-cooled on ice to prevent intermolecular interactions. The sizes of the DNA duplexes and hairpins were verified via polyacrylamide gel electrophoresis and a picture of this gel is shown in Figure SI 2.1 of the Supporting Information (SI) found in the Appendix of this thesis.

Table 2.1: Duplexes Used in This Study

5′ –GGACTTCGGTCC CCTGAAGCCAGG– 5′	12-mer
5′ –CCTTCTTCCTGTTCCTGGTCTTTTGCTCACATGTTCTTTCCGG GGAAGAAGGACAAGGACCAGAAAACGAGTGTACAAGAAAGGCC– 5′	43-mer

Table 2.2: DNA Hairpins Used in This Study

6 bp	8 bp	12 bp
T C T C C–G A–T G–C G–C C–G G–C 5′	T T T C G–C C–G T–A T–A C–G A–T G–C G–C 5′	T T T C C–G C–G T–A G–C G–C C–G T–A T–A C–G A–T G–C G–C 5′

Solution Preparation. CT DNA stock solutions (0.30 wt%) were prepared by dissolution of CT DNA in water overnight containing 5×10^{-3} M sodium sulfate.[19] The absolute concentration of the DNA stock solution was obtained spectrophotometrically. An extinction coefficient per mole of bp of ε_{260} = 11,300 $M^{-1}cm^{-1}$ was determined experimentally for calf thymus DNA in 5×10^{-3} M sodium sulfate. Samples were freshly made on the day of use and all remaining CT DNA stock was discarded at the end of each day. DNA of 43 bp or smaller were prepared on the day of use from a 1.5 g/L stock solution and the remaining stock was stored at –20 °C. The concentration of the complementary single stranded DNA used to make the 43 bp and 12 bp DNA duplexes was calculated from the extinction coefficients given by Sigma which were calculated using the nearest-neighbour model.[65] The exact concentration of the 43 bp and 12 bp DNA duplexes was calculated from the mass of the single stranded stock solutions used to construct the DNA duplexes. The concentration of the hairpins was not calculated from the extinction coefficients provided by Sigma as these extinction coefficients were determined for the single stranded DNA and are larger than that of the hairpin in solution with its stem made of a base-paired duplex. Thus, the 12 bp duplex was used as a model compound to represent the double stranded DNA stem of the hairpins. An extinction coefficient per mole of bp (ε_{duplex}(per mole bp) = 13,600 $M^{-1}cm^{-1}$) was determined experimentally for the annealed 12 bp duplex. This value was used to determine the extinction coefficient of the DNA hairpins according to Equation 2.1 where ε_{loop} is the extinction coefficient of the hairpin loop which was calculated using the nearest-neighbour model.[65] The concentrations of the DNA hairpins were obtained using the extinction coefficients reported in Table 2.3.

$$\varepsilon(\textit{per mole hairpin}) = \varepsilon_{\text{duplex}}(\textit{per mole bp}) \times \textit{hairpin stem length}\ (\textit{bp}) + \varepsilon_{\text{loop}} \qquad (2.1)$$

Table 2.3: Extinction coefficient of the DNA hairpins

DNA hairpin	ε_{loop} ($M^{-1}cm^{-1}$)	Extinction coefficient per mole hairpin ($M^{-1}cm^{-1}$)
6 bp	4.5×10^4	1.3×10^5
8 bp	4.1×10^4	1.5×10^5
12 bp	4.1×10^4	2.0×10^5

Steady-State Fluorescence Spectroscopy. Steady-state fluorescence measurements were performed on a Photon Technology International (PTI) LS-100 steady-state fluorometer with an Ushio UXL-75Xe Xenon arc flash lamp and PTI 814 photomultiplier detection system. The spectra of all solutions were acquired using the right angle geometry. Samples were excited at 340 nm and the emission spectrum was collected from 450 to 650 nm. The fluorescence maximum of EB intercalated in DNA (DNA-EB) is near 590 nm and the fluorescence intensity was taken as the integral under the fluorescence spectrum from 583 nm to 603 nm.

Time-Resolved Fluorescence Spectroscopy. Fluorescence decays were acquired with an IBH Ltd. time-resolved fluorometer equipped with an IBH 340 nm NanoLED. All solutions were excited at 340 nm and the emission was collected at 605 nm. A filter was used with a cutoff of 570 nm to block potential light scattering leaking through the detection system. Fluorescence decays were acquired over 1024 channels with a 1 MHz repetition rate and a time per channel of 0.24 ns/channel using the right angle geometry. The peak maximum was 20,000 counts for the instrument response and decay curves to ensure a high signal-to-noise ratio. A Ludox solution was used to obtain the instrument response function (IRF). All decays were deconvoluted from the IRF and fitted to the desired function using a least-squares analysis.

Analysis of the Fluorescence Decays. The fluorescence decays of DNA-EB were fit with Equation 2.2 using n=2 or 3 in the absence and presence of quencher, respectively. The fluorescence decays of the solutions containing copper were also fit with the FBM equation given in Equation 2.3 which describes the time-dependence of the concentration of the excited EB as it is being quenched via

electron transfer. The resulting fits were characterized as "good" when the χ^2 parameter was smaller than 1.3 and the residuals and autocorrelation function of the residuals were randomly distributed around zero. Both a background and light scattering correction were applied to fit the fluorescence decays.

$$i(t) = \sum_{i=1}^{n} a_i e^{-t/\tau_i} \tag{2.2}$$

$$[EB^*] = [EB^*]_o \left[f_{slow} \times f(t) \times \exp\left[-A_2 t - A_3 \left(1 - \exp(-A_4 t)\right)\right] + f_{fast} \exp(-t/\tau_{fast}) \right] \tag{2.3}$$

The expression of the parameters A_2, A_3, and A_4 used in Equation 2.3 is given in Equation 2.4:

$$A_2 = \langle n \rangle \frac{k_{blob} k_e [blob]}{k_{blob} + k_e [blob]} \qquad A_3 = \langle n \rangle \frac{k_{blob}^2}{\left(k_{blob} + k_e [blob]\right)^2} \qquad A_4 = k_{blob} + k_e [blob] \tag{2.4}$$

The parameters k_{blob}, $k_e[blob]$, and $\langle n \rangle$ obtained from the fits of the fluorescence decays with the FBM equation describe the kinetics of electron transfer from EB to copper. k_{blob} is the rate constant of quenching of EB by one copper located inside the same blob, $k_e[blob]$ is the product of the rate constant (k_e) that describes the exchange of copper cations between blobs and the local blob concentration ([*blob*]), and $\langle n \rangle$ is the average number of copper cations per blob. The fraction f_{fast} represents the fraction of EBs that are quenched quasi-instantaneously by nearby copper cations with a decay time of 1 – 2 ns. The fraction f_{slow} represents the EBs that are quenched with a decay time greater than τ_{fast}. The function $f(t)$ in Equation 2.3 represents the natural decay of DNA-EB when no copper is added to the DNA. Experimentally, $f(t)$ was found to be best approximated by a biexponential whose normalized pre-exponential factors and decay times were fixed during the FBM analysis based on Equation 2.3.

Error Analysis. The error on the parameters retrieved from the analysis of the fluorescence decays with Equation 2.3 was estimated by conducting the following procedure. Using the parameters listed in Table SI 2.2f for [DNA] = 0.09 wt%, ten fluorescence decays were simulated for each copper concentration. The fluorescence decays were fitted and analysed with Equation 2.3. The parameters $<n>$, k_{blob}, and $k_e[blob]$ retrieved from this analysis were averaged and their standard deviation was determined and taken as the error. It is represented in Figures 2.5 A and B, and 2.6 to provide a feel for the errors generated by our analysis. Judging from the scatter of the experimentally obtained $<n>$, k_{blob}, and $k_e[blob]$ values, the error introduced by the analysis of the fluorescence decays appear to reflect satisfyingly the experimental errors.

Blob Size and Binding Constant. The size of a blob, N_{blob}, and the binding constant of copper to DNA, K, were found through $<n>$ which is expressed by Equation 2.5.

$$< n >= \frac{[Cu^{2+}]_{bound} - [Cu^{2+}]_o}{[blob]} \tag{2.5}$$

$[Cu^{2+}]_o$ in Equation 2.5 is the onset copper concentration representing the concentration of copper required to induce a minimum amount of quenching that can be detected through our analysis. $[Cu^{2+}]_{bound}$ represents the concentration of bound copper and is expressed in Equation 2.7 by considering the equilibrium given in Equation 2.6.

$$Cu^{2+}_{free} + DNA \underset{\longleftarrow}{\overset{K}{\longrightarrow}} Cu^{2+}_{bound} \tag{2.6}$$

$$[Cu^{2+}]_{bound} = \frac{[Cu^{2+}]_T}{\frac{1}{K[DNA]} + 1} \tag{2.7}$$

$[Cu^{2+}]_T$ in Equation 2.6 is the total Cu^{2+} concentration and is equal to $[Cu^{2+}]_{free}$ + $[Cu^{2+}]_{bound}$. The concentration [*blob*] in Equation 2.5 is obtained from the ratio [DNA]/N_{blob} where [DNA] is expressed in bp/L and N_{blob} represents the number of bp constituting a blob. Equation 2.7 is used to determine $[Cu^{2+}]_{bound}$ whose expression is combined with Equation 2.5 to yield Equation 2.8.

$$< n >= \frac{\left[Cu^{2+}\right]_T}{\frac{1}{KN_{blob}} + \frac{[DNA]}{N_{blob}}} - \frac{\left[Cu^{2+}\right]_o N_{blob}}{[DNA]} \tag{2.8}$$

Equation 2.8 predicts that a plot of <*n*> versus the total copper concentration yields a straight line with a slope that is a function of N_{blob}, *K*, and DNA concentration. The inverse of the slope is expected to increase linearly with DNA concentration as shown in Equation 2.9.

$$\frac{1}{slope} = \frac{1}{KN_{blob}} + \frac{[DNA]}{N_{blob}} \tag{2.9}$$

According to Equation 2.9, a plot of $slope^{-1}$ versus [DNA] should yield a straight line whose slope and intercept can be used to determine *K* and N_{blob}.

2.4 Results and Discussion

Electron transfer in calf thymus DNA was studied for five different DNA concentrations of 0.02, 0.03, 0.05, 0.07, and 0.09 wt%. The ratio of copper to DNA phosphate was always smaller than 0.2 to ensure that copper is bound to the DNA phosphates and not the bases.[42] A wavelength of 340 nm was used to excite EB. DNA-EB was found to absorb at 340 nm with a molar extinction coefficient of ε_{340} = 10,500 $M^{-1}cm^{-1}$. The absorption spectrum of EB free in solution and intercalated in DNA is shown in Figure SI 2.2. Excitation of DNA-EB in the near ultraviolet region has been shown to promote both short-range DNA crosslinking and long-range oxidative base damage. This effect is

more pronounced at 313 nm than at 340 nm.[44] To minimize this potential problem, solutions used for the fluorescence experiments were discarded after use.

In our hands, the fluorescence decay of DNA-EB was always biexponential and good fits could not be obtained by using a monoexponential function. This result disagrees with earlier papers reporting that DNA-EB decays as a single exponential with a lifetime of 23 ns.[19-21,62,66] In our experiments, the strongest contribution to the fluorescence decay of DNA-EB was the exponential with a 23 ns decay time, but the decays also yielded a shorter decay time around 10 – 17 ns with a pre-exponential contribution ranging from 5 to 25 % depending on the DNA construct (see Tables SI 2.1a-f, entries with $[Cu^{2+}] = 0$ M). Studies where DNA-EB was found to decay as a single exponential were conducted nearly two decades ago and older single photon counting instruments might not have been sensitive enough to resolve the shorter decay time. The existence of this second decay time has been noted in more recent publications. This shorter decay time has been attributed to EB bound electrostatically to the DNA helix.[67,68] Other intercalating agents behave in a similar manner.[69,70]

Since the calf thymus DNA purchased from Sigma might contain counterions capable of quenching DNA-EB, their presence might be responsible for the biexponential decay found for DNA-EB. To rule out this possibility, a solution of calf thymus DNA was dialyzed against 5×10^{-3} M sodium sulfate for 2 days to remove any excess metal cations that could potentially quench the fluorescence of DNA-EB. The steady-state fluorescence spectrum and time-resolved fluorescence decay of EB intercalated in the dialyzed calf thymus DNA was compared to that of EB intercalated in calf thymus DNA used as received from Sigma. The fluorescence spectra and time-resolved decays of the two samples were identical (Figure SI 2.3 and SI 2.4). Therefore calf thymus DNA purchased from Sigma was used as received.

Steady-state fluorescence spectra were obtained for DNA-EB in the absence and presence of copper cations (Figure 2.2A). The fluorescence intensity decreases as the concentration of copper

increases. This quenching of EB by Cu^{2+} is also reflected in the fluorescence decays where the fluorescence decays show stronger curvature and decay more quickly as more copper is added to the solution (Figure 2.2B).

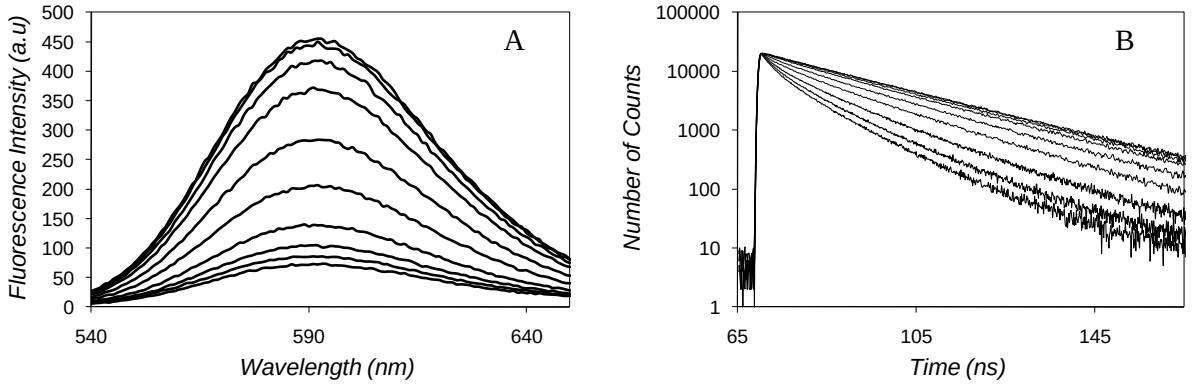

Figure 2.2: Fluorescence spectra and decays of DNA-EB quenched by copper cations. A) Fluorescence spectra and B) decays of 0.09 wt% calf thymus DNA equivalent to [bp] = 1.4×10^{-3} M, and 1×10^{-5} M ethidium bromide. The copper concentration from top to bottom is between 0 and 5.85×10^{-4} M ([Na_2SO_4] = 5×10^{-3} M, λ_{ex} = 340 nm, λ_{em} (for B) = 605 nm).

The Stern-Volmer plots were obtained from the steady-state emission spectra and the fluorescence decays. I_o/I_{Cu} and $<\tau>_o/<\tau>_{Cu}$ were plotted as a function of copper concentration in Figure 2.3 where $<\tau>_o$ and I_o are the number average fluorescence lifetime and fluorescence intensity in the absence of quencher and $<\tau>_{Cu}$ and I_{Cu} are the number average fluorescence lifetime and fluorescence intensity in the presence of quencher. The ratios I_o/I_{Cu} and $<\tau>_o/<\tau>_{Cu}$ in Figure 2.3 increase with increasing copper concentration and the plots show an upward curvature. Such an upward curvature in the Stern-Volmer plots is also observed for micellar quenching.[71] The fact that the Stern-Volmer plots in Figure 2.3 show a behavior similar to that of micellar quenching is encouraging since it suggests that quenching of EB by Cu^{2+} occurs in a restricted geometry as would

be required for the application of the FBM to the analysis of the fluorescence decays. The plots also indicate that static quenching is occurring since the ratios $<\tau>_o/<\tau>_{Cu}$ and I_o/I_{Cu} do not overlap at high Cu^{2+} concentrations.

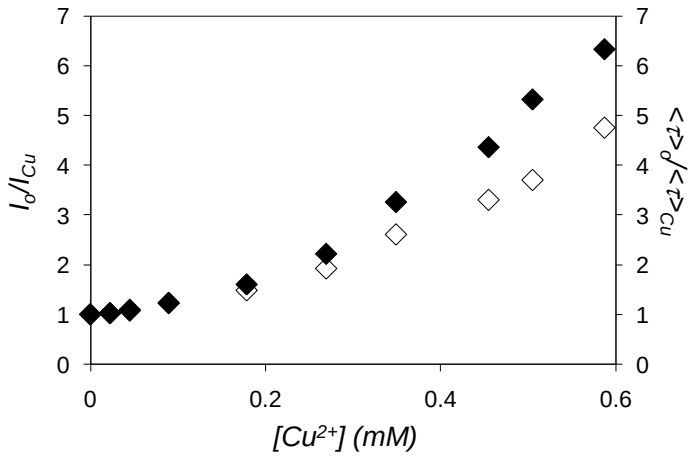

Figure 2.3: Stern-Volmer plots of DNA-EB quenched by copper cations. Stern-Volmer plot obtained from steady-state (solid diamonds) and time-resolved fluorescence (hollow diamonds) ([DNA] = 0.09 wt% equivalent to [bp] = 1.4×10^{-3} M, [EB] = 1×10^{-5} M, $[Na_2SO_4] = 5\times10^{-3}$M, λ_{ex} = 340 nm).

The fluorescence decays of DNA-EB quenched by copper cations were fit with Equation 2.3 to yield the parameters $<n>$, k_{blob}, and $k_e[blob]$. Figure 2.4 shows the fit with Equation 2.3 of a fluorescence decay of DNA-EB quenched by Cu^{2+}. All fluorescence decays acquired in this study were fit well with Equation 2.3 yielding χ^2 values smaller than 1.3. Residuals and autocorrelation of the residuals were randomly distributed around zero.

Fitting the fluorescence decays with the first part of Equation 2.3 (i.e. f_{fast} = 0) yielded poor residuals at the early times prompting the introduction of a fast decay component. The origin of this fast decay is attributed to EB-Cu^{2+} pairs where the short distance separating EB and Cu^{2+} enables efficient electron transfer resulting in a fast quenching of EB. However, since τ_{fast} was found to take a value between 1.0 and 2.0 ns, it could also reflect a relaxation process due to the emission of unbound

EB which emits with a lifetime of 1.6 ns.[41] To this end, solutions containing EB, DNA, and Cu^{2+} were filtered to remove calf thymus DNA, and hence, intercalated EB. The solution was first filtered through a membrane with a pore size of 200 nm to remove very large DNA fragments. The filtrate

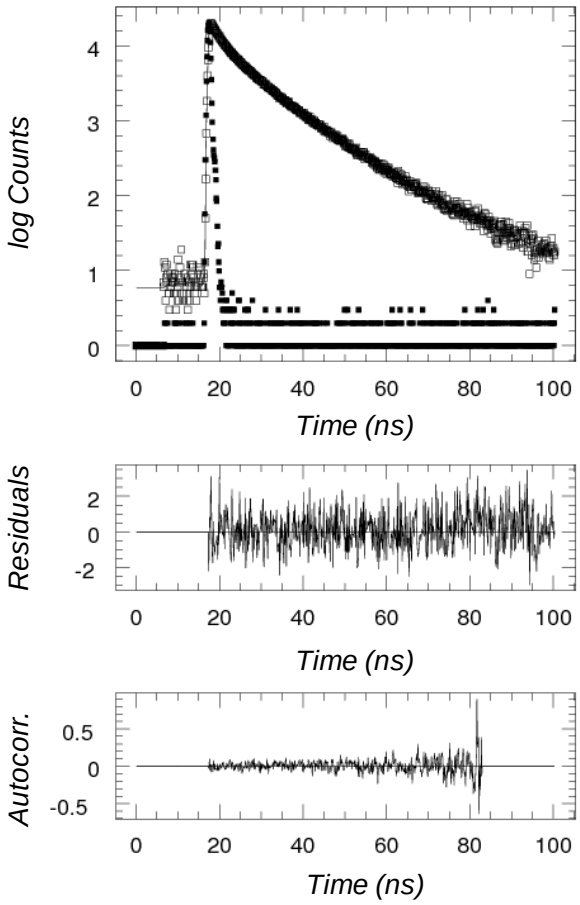

Figure 2.4: Sample time-resolved fluorescence decay fit with the FBM. Time-resolved fluorescence decay of 0.09 wt% CT DNA equivalent to [bp] = 1.4×10^{-3} M, 1×10^{-5} M EB, and 5.2×10^{-4} M Cu^{2+} fit with Equation 2.3 (λ_{ex} = 340 nm, λ_{em} = 605 nm, χ^2 = 1.15).

was then filtered a second time through a membrane with a pore size of 20 nm to remove remaining calf thymus DNA. No fluorescence signal was observed with the steady-state fluorometer once filtered through the 20 nm membrane (Figure SI 2.5). A fluorescence decay could not be acquired for the filtered solution as no signal was detected with the time-resolved fluorometer suggesting that the

fast decay time is not due to free EB in solution, but rather to pairs of DNA-EB and Cu^{2+} separated by short distances on the DNA helix. As a control, a solution of copper and EB (no DNA) was filtered through the membranes and showed EB emission. This experiment demonstrates that the decrease in fluorescence observed after filtration resulted from removal of DNA-EB from the solution and not from EB and/or copper binding to the membrane (Figure SI 2.5 inset).

2.4.1 Fluorescence Blob Model Parameters

The rate constants k_{blob} and $k_e[blob]$ were plotted as a function of the copper to phosphate ratio for each DNA concentration. Within experimental error, the quenching rate constant, k_{blob}, remained constant for each quencher and DNA concentration taking an average value around 4×10^7 s^{-1} (Figure 2.5A). This result is reasonable since an increase in copper concentration should not affect the mechanism of electron transfer, only the probability of a quenching event occurring. The exchange rate constant of copper between blobs increased slightly with increasing copper-to-phosphate ratio independently of the DNA concentration (Figure 2.5B). The scatter in the data points at lower copper-to-phosphate ratios is due to the lack of curvature in the fluorescence decays at these quencher concentrations (see Figure 2.2B) resulting in larger error on the FBM parameters.

The average number of quenchers per blob, $<n>$ was plotted as a function of copper concentration in Figure 2.6. The plots were linear with Cu^{2+} concentration after an onset copper concentration was reached for each DNA concentration as predicted by Equation 2.8. The onset copper concentration decreased with decreasing DNA concentration. Following the mathematical treatment leading to Equation 2.9, the inverse of the slope of each straight line shown in Figure 2.6 was plotted in Figure 2.7 as a function of phosphate concentration.

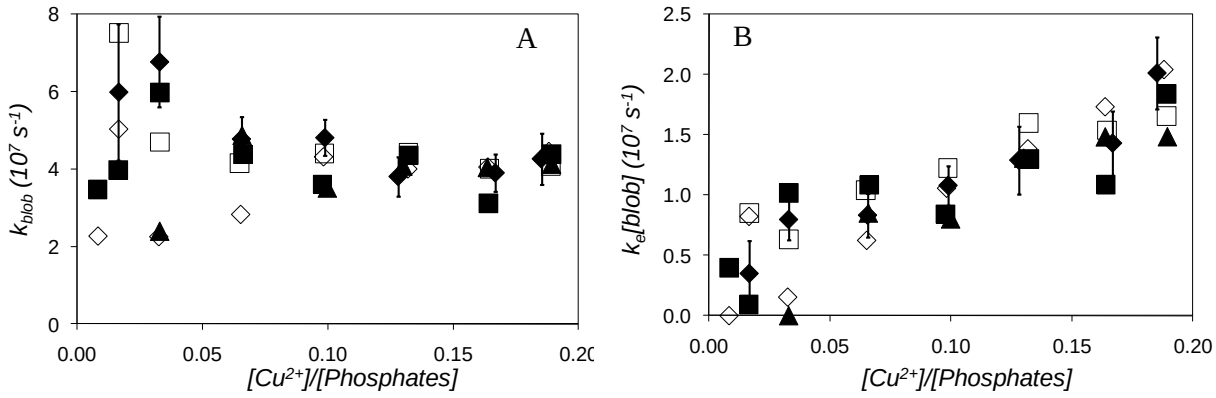

Figure 2.5: Plots of the FBM parameters k_{blob}, and k_e[blob] versus copper to phosphate ratio. A) k_{blob}, and B) k_e[blob as] plotted a function of copper to phosphate ratio. (▲) 0.02 wt% DNA or [bp] = 3.0×10^{-4} M, (□) 0.03 wt% DNA or [bp] = 4.5×10^{-4} M, (■) 0.05 wt% DNA or [bp] = 7.6×10^{-4} M, (◇) 0.07 wt% DNA or [bp] = 1.1×10^{-3} M, (◆) 0.09 wt% DNA or [bp] = 1.4×10^{-3} M. ([EB] = 1×10^{-5} M, [Na_2SO_4] = 5×10^{-3} M).

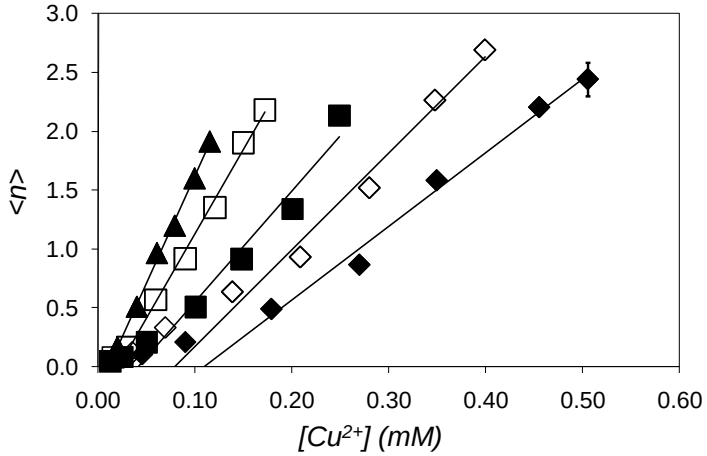

Figure 2.6: The FBM parameter <n> plotted as a function of copper concentration. (▲) 0.02 wt% DNA or [bp] = 3.0×10^{-4} M, (□) 0.03 wt% DNA or [bp] = 4.5×10^{-4} M, (■) 0.05 wt% DNA or [bp] = 7.6×10^{-4} M, (◇) 0.07 wt% DNA or [bp] = 1.1×10^{-3} M, (◆) 0.09 wt% DNA or [bp] = 1.4×10^{-3} M. ([EB] = 1×10^{-5} M, [Na_2SO_4] = 5×10^{-3} M).

A straight line was obtained as predicted by Equation 2.9 which was used to extract the parameters N_{blob} and K. The size of a blob was determined to be 11 ± 1 base pairs and the binding constant of copper to DNA was found to equal 3,500 ± 1,800 M^{-1} for a monovalent salt concentration in the solution of 5×10^{-3} M. This means that under those conditions, quenching (electron transfer) occurs over approximately 11 base pairs, with a rate constant k_{blob} of 4×10^{-7} s^{-1}. The distance over which quenching occurs is larger than the distance found by Atherton and Beaumont whose bi-exponential analysis of the fluorescence decays led to the conclusion that DNA-EB can be quenched by a copper cation positioned on any one of the six nearest phosphates, or three base pairs.[18] However, we believe our result to be more accurate as the FBM equation fits the entire decays in Figure 2.2B and the trends shown in Figure 2.5 – 2.7 are internally consistent.

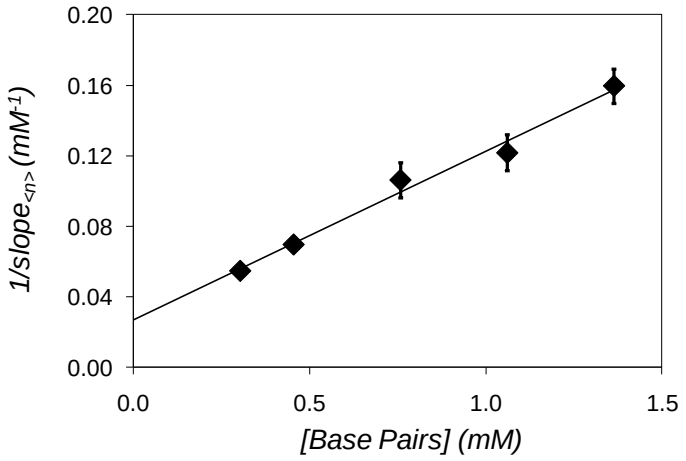

Figure 2.7: Inverse of the slope of Figure 2.6 plotted against concentration of DNA phosphates. ([EB] = 1×10^{-5} M, [Na_2SO_4] = 5×10^{-3} M).

Equation 2.3 based on the FBM was able to fit the fluorescence decays of DNA-EB quenched by copper yielding χ^2 values always smaller than 1.3. This analysis assumes that the exchange of quencher between blobs (i.e. DNA) and the bulk solution occurs on a time scale that is much larger than that probed by the fluorescence experiments (~ 140 ns). Within this framework, the FBM parameter $k_e[blob]$ represents the exchange of copper between adjacent blobs and not between the bulk solution and the blobs. To support the validity of this assumption, the viscosity of the bulk solution was increased 10-fold from 0.9 mPa·s for water to 9.6 mPa·s by adding 50% w/w sucrose. This 10-fold increase in viscosity of the bulk solution was not reflected in the $k_e[blob]$ parameter which was only decreased by 50% as shown in Figure 2.8.

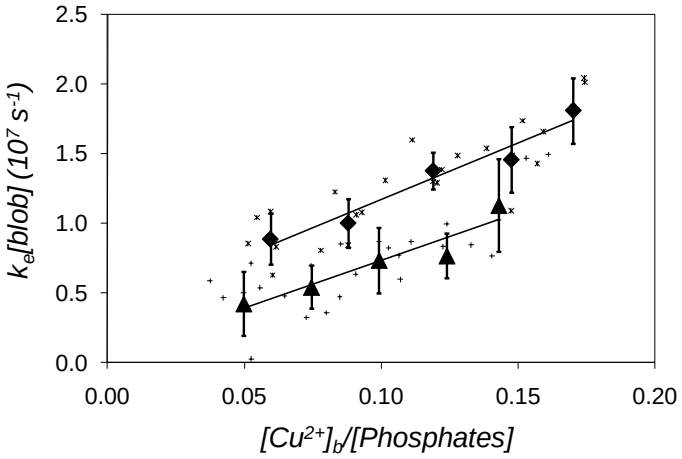

Figure 2.8: $k_e[blob]$ averaged over all DNA concentrations versus the concentration of copper bound to phosphate ratio, $[Cu^{2+}]_b/[Phosphates]$. The small data points represent $k_e[blob]$ for each DNA concentration; (◆) no sucrose (0.9 cp), (▲) 50 % w/w sucrose (9.6 cP) ([EB] = 1×10^{-5} M, $[Na_2SO_4]$ = 5×10^{-3} M).

The binding constant, however, decreased from 3,500 M^{-1} to 2,000 M^{-1} with the addition of sucrose. The binding constant was used to determine the ratio of $[Cu^{2+}]_b/[Phosphate]$ used in Figure 2.8. $k_e[blob]$ obtained for the same copper to phosphate ratio was averaged for the five DNA

concentrations studied. The averaged data points (filled diamond and triangles) and individual data points (crosses) for each DNA concentration are shown in Figure 2.8. Since the 10-fold increase in bulk viscosity was not reflected in the 2-fold decrease in $k_e[blob]$, this observation supports the claim that $k_e[blob]$ represents the exchange of copper cations between blobs along the DNA helix and not between the helix and solution.

The increase in $k_e[blob]$ with increasing copper concentration shown in Figure 2.5B and 2.8 is likely due to what we refer to as the "directional diffusion" of copper cations going from blobs having a high copper content to blobs having a low copper content. Locally, the DNA helix can be viewed as a string of blobs aligned linearly along the helix (Figure 2.1). Thus, a copper cation can only exchange between adjacent blobs. As the total concentration of copper is increased, the average number of copper cations per blob increases, and there is no longer an equal probability of copper to exchange between adjacent blobs. Copper cations will exchange with the blob containing less copper and repulsion from the blobs containing more copper increases the rate of exchange by directing the exchange process.

In the 50% w/w sucrose aqueous solution, the size of a blob, N_{blob}, was 7.2 ± 0.7 bp but k_{blob} remained unchanged when compared to k_{blob} obtained in the solution without sucrose. This result indicates that quenching is slightly less efficient as it occurs over a distance that is 30% shorter (7.2 ± 0.7 bp with 50% w/w sucrose versus 10.5 ± 1.3 bp without sucrose). Another way to approach this result is to calculate the rate constant for the quenching between an excited DNA-EB and a copper cation, k_q. By definition, k_{blob} is a pseudo-unimolecular rate constant which is expected to be the product of k_q and the local concentration of quencher equivalent to one copper in a blob which is the inverse of the volume of a blob, $1/V_{blob}$ (Equation 2.10).[48-50]

$$k_{blob} = k_q \times \frac{1}{V_{blob}} \tag{2.10}$$

The linear array of cylindrical blobs shown in Figure 2.1 suggests that V_{blob} can be assumed to be proportional to N_{blob} as the cross-section of the cylindrical blobs is the same for all identical blobs. It follows from this assumption that the product of $k_{blob} \times N_{blob}$ gives an estimate of the rate constant of quenching, k_q. Since k_{blob} remained unchanged and N_{blob} decreased by 30% with a 10-fold increase in viscosity, it implies that k_q decreases by 30% when the viscosity is increased. The 30 % decrease in k_q is much smaller than the 10-fold change in the bulk viscosity of the solution. This observation suggests that k_q describes a process that must occur at the DNA helix between excited DNA-EB and copper bound to the DNA helix. This conclusion is internally consistent with our initial assumption that the process of electron transfer described by k_{blob}, $<n>$, and $k_e[blob]$ occurs between EB and Cu^{2+} cations that are bound to the DNA helix.

2.4.2 The onset copper concentration $[Cu^{2+}]_o$

The onset copper concentration was introduced in Equation 2.5 to account for the absence of detectable quenching at low Cu^{2+} concentration. It appears that the copper concentration needs to reach a threshold ($[Cu^{2+}]_o$) before quenching of DNA-EB by Cu^{2+} can occur. What this indicates is that at low Cu^{2+} concentration, some copper cations bind to DNA but do not participate in quenching (Figure 2.6). This result might be due to electrostatic repulsion between EB and Cu^{2+}. Both ethidium and Cu^{2+} are positively charged so that, at low copper concentrations, copper cations might be repelled by the positive charge of ethidium and bind to the DNA helix further away from the intercalated chromophore. Enough copper needs to be added to induce the Cu^{2+} cations to bind to sites along the DNA helix which are close enough to EB for quenching to take place. The onset copper concentration is a result of this phenomenon. The onset copper concentration was found to decrease with decreasing DNA concentration (Figure 2.6). Two effects take place as the concentration of DNA is decreased; the EB to phosphate ratio increases, hence the average spacing between EBs decreases, and the sodium sulfate to phosphate ratio increases. To investigate which effect was likelier to induce the decrease in $[Cu^{2+}]_o$ with decreasing DNA concentration, the following

experiments were conducted. The EB-to-phosphate ratio was increased for a DNA concentration of 0.09 wt% by increasing the EB concentration from 1×10^{-5} M, to 1.8×10^{-5} M, and to 4.5×10^{-5} M, thus decreasing the average number of base pairs between two EBs from 136 bp, to 75 bp, to 30 bp, respectively. <*n*> was plotted as a function of copper concentration for these solutions (Figure SI 2.6). Within experimental error, no change was observed for the onset copper concentration when the average base pair spacing between DNA-EB was decreased from 136 bp to 75 bp to 30 bp. However the size of a blob obtained with a sodium sulfate salt concentration of 5×10^{-3} M is approximately 10 bp so that copper could still bind between EBs spaced 30 bp apart and not participate in quenching. The average spacing between EBs was not decreased further than 30 bp since energy migration can take place between two EBs separated by 10 bp or less.[72] The second effect to investigate was that of the ratio of the concentration of sodium sulfate to that of DNA phosphates in the solution. The ratio of sodium sulfate to phosphate ratio was increased by adding more salt to the solutions and <*n*> was plotted as a function of copper concentration in Figure 2.9.

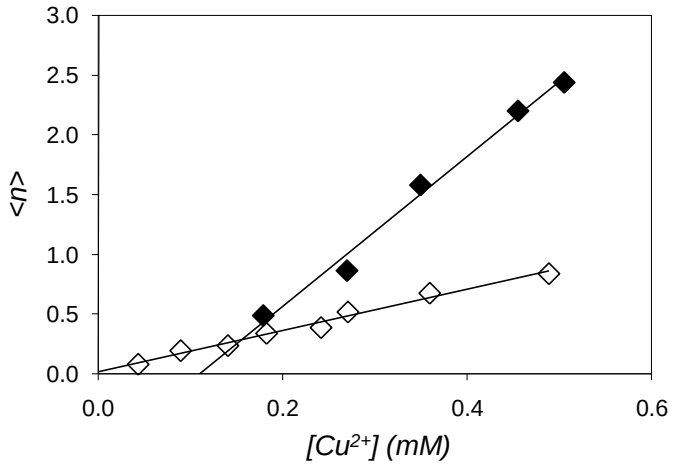

Figure 2.9: <n> as a function of copper concentration. (◆) $[Na_2SO_4] = 5\times10^{-3}$ M, (◇) $[Na_2SO_4] = 3\times10^{-2}$ M (0.09 wt% DNA equivalent to [bp] = 1.4×10^{-3} M, [EB] = 1×10^{-5} M).

An increase in sodium sulfate concentration resulted in no onset copper concentration. As the concentration of sodium sulfate is increased, repulsion between the positively charged ethidium and copper cations is reduced, the copper cations are no longer repelled by the positive charge exerted by EB, they bind randomly onto the DNA helix, and no onset copper concentration is observed. Figure 2.9 also shows that increasing the concentration of monovalent salt decreases $<n>$, the average number of quenchers per blob. Since a massive addition of salt to the solution induces the disappearance of the onset copper concentration, these experiments suggest that electrostatic repulsion between EB and copper cations are responsible for delaying the quenching of EB by Cu^{2+} at low Cu^{2+} concentration.

2.4.3 Effect of DNA length

The FBM assumes that the photophysical process of interest, namely electron transfer from an excited EB to a copper cation in this instance, occurs locally inside a blob. Consequently, the parameters retrieved from a FBM analysis of fluorescence decays are not expected to depend on the size of the macromolecule as long as the size of the macromolecule is substantially larger than a blob. To ensure that this basic requirement is obeyed, the size of DNA was decreased to investigate what happens to N_{blob} when the DNA length approaches the size of N_{blob} and becomes even smaller. N_{blob} was determined for four DNA constructs of length 43 bp, 12 bp, 8 bp, and 6 bp (Tables 2.1 and 2.2). For the 12 bp DNA length, both a duplex and hairpin were studied. This was done to investigate if the loop of the DNA hairpin had any effect on the size of a blob. When the size of DNA was decreased below N_{blob} (10 bp) a DNA hairpin had to be used to ensure that the duplex would form even at room temperature. N_{blob} was found for the four DNA lengths studied and compared to the N_{blob} obtained for calf thymus DNA (approximately 15,000 bp according to Sigma). N_{blob} was plotted as a function of DNA length in Figure 2.10. N_{blob} remained constant around 10 bp for DNA lengths of 12 bp and larger. When the DNA length was decreased below 10 bp, the size of a blob decreased to a value that was slightly smaller than the size of the DNA fragment. This result provides a good

test of the validity of the FBM since a blob cannot be larger than the DNA fragment being studied. Therefore, the size of a blob remains independent of duplex length and equal to 10.8 ± 0.4 bp for DNA longer than N_{blob} and decreases to a size slightly smaller than that of the DNA construct when the length of the DNA construct is decreased below 10 bp.

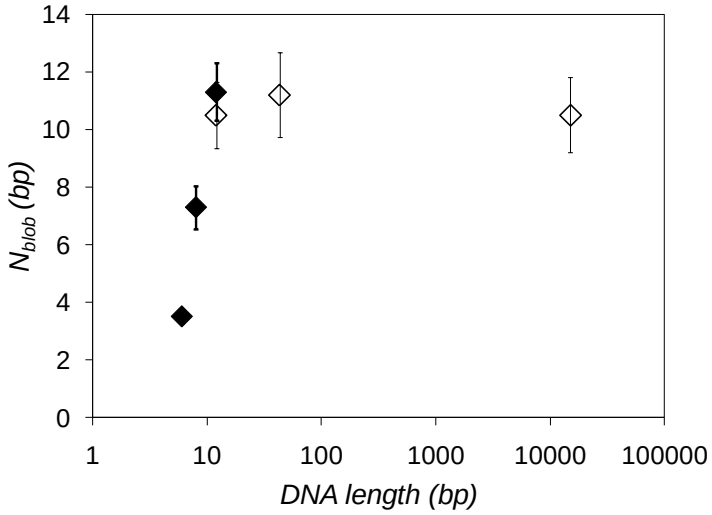

Figure 2.10: N_{blob} as a function of DNA length. (◆) DNA hairpin, (◇) DNA duplex ([EB] = 1×10^{-5} M, [Na_2SO_4] = 5×10^{-3} M).

The effect of DNA length was not the focus of previous studies of physically bound electron donors and acceptors most likely due to the fact that a quenching distance could not be obtained. Earlier studies on the effect of DNA length were purely qualitative. Baguley and coworkers studied the quenching of DNA-EB by amsacrine, which also intercalates in DNA.[22] An electron transfer mechanism was suggested by elimination of all other possible quenching mechanisms. They reported no change in the fluorescence quenching between calf thymus DNA and sheared calf thymus DNA. Since an electron transfer distance was never reported, one cannot draw any conclusions from the fact that there was no change observed between calf thymus and sheared calf thymus DNA. The longest distances reported for photoinduced electron transfer in DNA is approximately 40 Å for tethered

metallointercalators[40] which is much shorter than the fragments obtained from shearing calf thymus DNA.

The binding constant, *K*, of copper to DNA decreased with decreasing chain length although the error bars are large (Figure 2.11). If valid, such a trend would indicate that copper binds weakly to DNA when the DNA fragments become small. *K* in Figure 2.11 was omitted for the 6 bp hairpin since the error bars are greater than its value. When generating a plot similar to that in Figure 2.7 for the 6 bp hairpin, a near zero intercept was found making it impossible to retrieve an accurate value for *K* according to Equation 2.9. Fenley *et al.* have showed that as the length of DNA is decreased below 100 bp, the fraction of condensed counterions decreases as well.[73] This result also depends on the concentration of monovalent salt. The observed decrease in *K* agrees with the results obtained by Fenley *et al*. Counterion condensation theory also states that when the length of DNA is decreased to finite values, condensed counterions are more weakly bound as end effects are no longer negligible.[74]

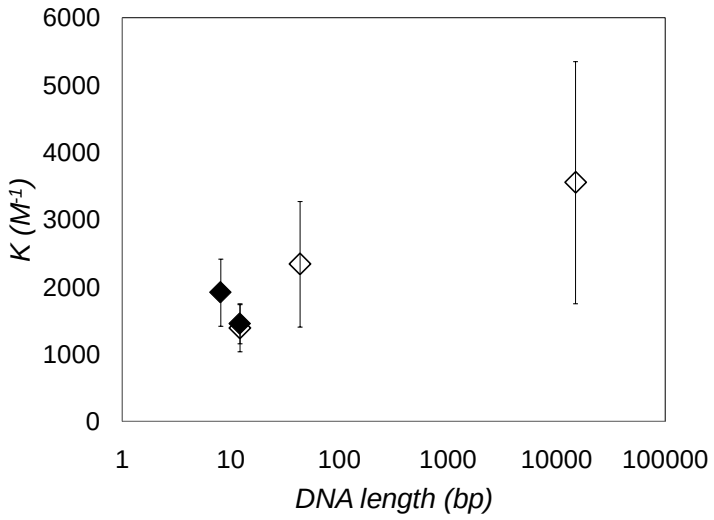

Figure 2.11: *K* as a function of DNA length. (◆) DNA hairpin, (◇) DNA duplex ([EB] = 1×10^{-5} M, [Na_2SO_4] = 5×10^{-3} M).

The quenching rate constant, k_{blob}, increased slightly with a decrease in DNA length from 4×10^7 s^{-1} for calf thymus DNA to a maximum value of 7×10^7 s^{-1} for the smallest DNA hairpin. EB and copper are forced closer together when the length of DNA is decreased below N_{blob} enabling the transfer of electrons at a faster rate. Figure 2.12 A and B show how k_{blob} varies with N_{blob} and DNA length, respectively. As the blob size is increased to 10 bp or as the length of the DNA construct is increased, the quenching rate constant within a blob decreases and reaches a minimum value. The four data points in Figure 2.12A clustered between 10 – 11 bp for N_{blob} represent DNA lengths in the plateau region of Figure 2.10. Nonetheless, both plots in Figure 2.12 show a decrease of the quenching rate constant inside a blob as the size of a blob or the length of the DNA construct is increased.

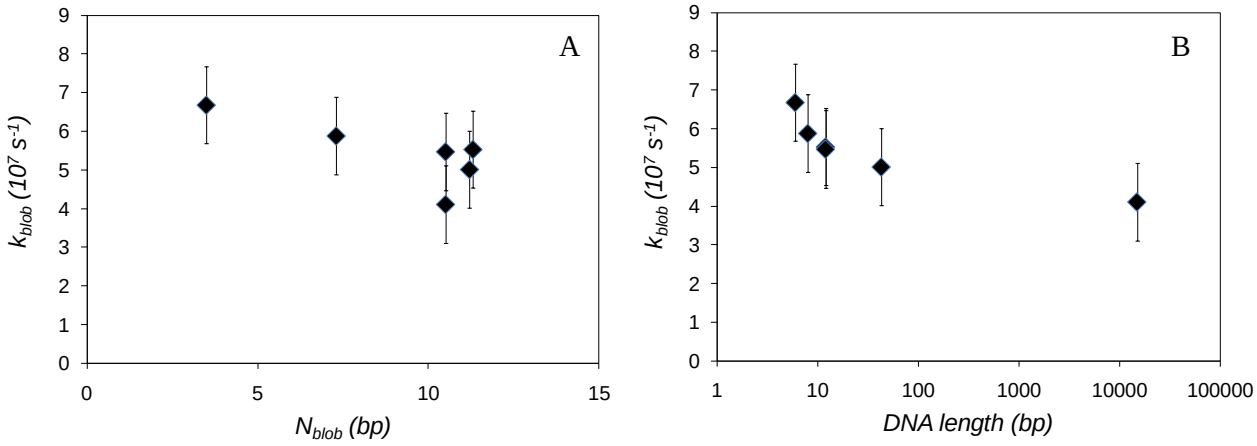

Figure 2.12: The FBM parameter k_{blob} versus N_{blob} or DNA length. A) N_{blob} and B) DNA construct length ([EB] = 1×10^{-5} M, [Na_2SO_4] = 5×10^{-3} M).

For shorter DNA constructs, N_{blob} becomes slightly smaller than the size of the DNA construct implying that the DNA constructs contain a single blob. In turn, this observation brings into question the existence of an exchange mechanism between blobs for short DNA constructs. Yet analysis of the fluorescence decays acquired with the short hairpins assuming that $k_e[blob]$ equals 0 in Equation 2.3

yielded poor fits. The existence of an exchange mechanism between blobs for the short DNA constructs can be rationalized by considering the number of phosphates found in the DNA constructs and their corresponding N_{blob} value given in Table 2.4. Since $2 \times N_{blob}$ for the smaller DNA constructs is smaller than the total number of phosphates found in the constructs, exchange into and out of the single blob must be due to copper bound to phosphate groups that are not contained in the blob.

Table 2.4: Values of the base pair length of the DNA construct and the value of the corresponding N_{blob}

DNA construct in bp length	Number of Phosphates	N_{blob} (bp)	$2 \times N_{blob}$ (phosphates)
6 (hairpin)	16	3.5 ± 0.2	7 ± 0.5
8 (hairpin)	20	7.3 ± 0.8	15 ± 2
12 (hairpin)	28	11.3 ± 1.0	22 ± 2
12 (duplex)	24	10.5 ± 1.2	21 ± 3

2.4.4 Comparison of results to other FBM studies

To this date, the FBM has been used mostly to study the dynamics in solution of polymers randomly labeled with a chromophore and quencher.[49-54,75] In this case, the chromophore and quencher are both mobile and a *blob* is defined as the volume probed by the chromophore during its lifetime. Information on long range polymer chain dynamics is obtained when the fluorescence of the chromophore is quenched, which indicates that two polymer segments have diffused in the solution and have come into contact with one another. These studies have illustrated that above a critical polymer chain length, quenching occurs inside a blob and does not depend on chain length, as expected from scaling arguments. The FBM has also been used to study energy migration and

trapping in a poly(ethylene 2,6-naphthalenedicarboxylate) (PEN) matrix.[76,77] PEN contains naphthalene dimers which can transfer energy to one another upon excitation. Co-polymerization of PEN with an appropriate quencher resulted in the trapping of the energy migrating between naphthalene dimers. In these experiments, the energy is mobile, the quencher is fixed, and a *blob* is defined as the volume where migrating energy is captured by a quencher. In the present work, the chromophore was fixed (DNA-EB), the copper quencher was mobile, and a *blob* was defined as the volume probed by the quencher (copper) during the lifetime of the chromophore. Even though the dynamics of the chromophore and/or quencher in the previous examples may differ in nature, there is one constant denominator between them: fluorescence quenching occurs locally in a volume much smaller than the overall dimension of the macromolecule of interest and despite the fact that the reactants (fluorophores and quenchers) are homogeneously distributed in the medium of interest. Thus, it appears that, when quenching occurs in a local, compartmentalized, volume due to hindered motion of the exciton and quencher, the FBM is a powerful analytical tool that describes quantitatively the quenching kinetics.

2.5 Conclusions

Electron transfer between a physically bound electron donor (DNA-EB) and acceptor (divalent copper cations) was studied using a Fluorescence Blob Model (FBM). The FBM proved successful in analyzing the complicated fluorescence decays obtained from the random distribution of the electron donors and acceptors. This analysis combined the ease of sample preparation when the electron donors and acceptors are physically bound to the DNA helix (case #1 as defined in the introduction) with the ability of retrieving quantitative information on the process of electron transfer as in case #2. The assumption that negligible exchange of copper between the bulk solution and the DNA helix takes place was supported by the observation that a 10-fold increase in bulk viscosity resulted in a 2-fold decrease in $k_e[blob]$. Also, it was shown that at a salt concentration of 5×10^{-3} M, an onset copper concentration must be reached before a minimum amount of quenching can be probed by

fluorescence. This onset copper concentration arose from the electrostatic repulsion taking place between the positively charged ethidium and copper cations. At a higher salt concentration, the onset copper concentration vanishes as the repulsion between the positively charged ethidium and copper cations is reduced. For a salt concentration of 5×10^{-3} M, the size of a blob, equivalent to the average distance over which electron transfer takes place was determined to be 10 bp with a quenching rate constant of 4×10^{7} s^{-1} for CT DNA.

The parameters retrieved from the FBM analysis of the fluorescence decays were found not to depend on the size of the DNA constructs as long as the DNA construct was substantially larger than a blob. The size of a blob was constant until the length of DNA was decreased below 10 bp at which point the size of a blob "adapted" to the smaller size of the DNA construct yielding N_{blob} values that were smaller than the size of the DNA fragment. The quenching rate constant increased to a maximum value of 7×10^{7} s^{-1} for the smallest DNA hairpin where the electron donor and acceptor are forced to occupy a smaller volume. The binding constant of copper to DNA was found to decrease with decreasing DNA length as end effects are no longer negligible. The fluorescence decays of the smaller DNA constructs could not be fit without the $k_e[blob]$ parameter, even though there was only one blob per construct. Exchange of copper can still occur into and out of a blob with the smaller DNA constructs since there are phosphate groups flanking the blob where copper can bind. The FBM was successful in obtaining quantitative information about the process of electron transfer taking place between DNA-EB and copper cations randomly and externally bound to the DNA helix. This work will be extended to investigate whether the FBM analysis can be applied to different electron donor and acceptor pairs.

Note: Chapter 2 has been published in the *Journal of Physical Chemistry B*. The original content can be found at the online link: http://pubs.acs.org/doi/abs/10.1021/jp105550r

Chapter 3

DNA as a Molecular Ruler to Determine the Limiting Length Scale Between the Distance of Electron Transfer and Screening Length

3.1 Overview

This work uses DNA as a molecular ruler to measure the average distance (d_{blob}) over which electron transfer (ET) takes place between DNA-intercalated ethidium bromide (DNA-EB) and electrostatically bound divalent metal cations and compare it to the Debye screening length (κ^{-1}). The fluorescence decays of DNA-EB quenched by Cu^{2+} and Ni^{2+} were acquired and analyzed using the Fluorescence Blob Model (FBM) for varying ionic strengths to yield d_{blob}. κ^{-1} was calculated for each ionic strength studied. d_{blob} was found to faithfully track κ^{-1} when the ions generated by the addition of salt were in excess of the DNA phosphates and to be independent of the type of divalent metal cation used as well as the lifetime of the chromophore. At the other extreme, when the DNA phosphate concentration exceeded the salt concentration, d_{blob} plateaued at 33 ± 4 Å and 33 ± 3 Å for Cu^{2+} and Ni^{2+}, respectively. This distance is expected to represent the screening distance resulting from the DNA counterions.

3.2 Introduction

By definition, a molecular ruler must be capable of measuring distances on the nanometer scale. Thus, it should be rigid and well calibrated over the length scale of interest to help measure distances at the molecular level. The structure of DNA fits these criteria. With a well-defined π–stacking distance between two base pairs of 3.4 Å[1] and a rigid structure below its persistence length of 50 nm,[2] DNA makes the perfect molecular ruler for measuring lengths in the nanometer scale. Many chemical events taking place in macromolecules and their supramolecular assemblies occur over the nanometer scale and the study of such phenomena rests on the availability of experimental techniques that can measure such distances accurately. Techniques such as Fluorescence Resonance Energy

Transfer (FRET)[3–5] or small angle neutron or X-ray scattering[6,7] have been instrumental in probing conformational changes and intramolecular distances of macromolecules in the critical 1 – 10 nm length scale regime. Recently, plasmon rulers have been constructed to monitor separations up to 70 nm.[8,9]

Electron transfer (ET) is another phenomenon that can occur over tens of nanometers, depending on the material being studied.[10] ET can be readily probed by fluorescence, but in our view, its potential at probing length scales in materials has been largely untapped mostly because of the heavy theoretical background that is usually needed to comprehend the theory of ET.[11] This complexity is exacerbated further when ET proceeds between electron donors and acceptors randomly distributed in a given matrix, as the random distribution of distances between donors and acceptors results in a random distribution of ET rate constants.[12] Interestingly, these complications appear to be satisfyingly handled if the Fluorescence Blob Model (FBM), originally introduced to study polymer chain dynamics in solution,[13] is applied to analyze the fluorescence decays of ethidium bromide (EB) intercalated between DNA base pairs (DNA-EB) as it transfers an electron to copper cations electrostatically bound to the phosphate anions lining the DNA double helix.[14]

The FBM assumes that quenching of DNA-EB by ET occurs locally inside a restricted volume referred to as a blob. A blob in this case is a cylindrical volume centered on the DNA helix as shown in Figure 3.1. The DNA helix is divided into a string of cylindrical blobs among which the copper cations distribute themselves randomly according to a Poisson distribution. The FBM analysis of the fluorescence decays of DNA-EB yields N_{blob}, the number of base pairs constituting a DNA blob, and $d_{blob} = N_{blob} \times 3.4$ Å which represents the height of a cylindrical blob. In Chapter 2, N_{blob} was found to increase with increasing size of the DNA construct, until an $N_{blob}(\infty)$ value of 11 bp was reached beyond which, any further extension of the DNA construct resulted in no further increase in N_{blob}. In essence, $N_{blob}(\infty)$ appeared to represent the maximum distance over which ET could occur under these experimental conditions.

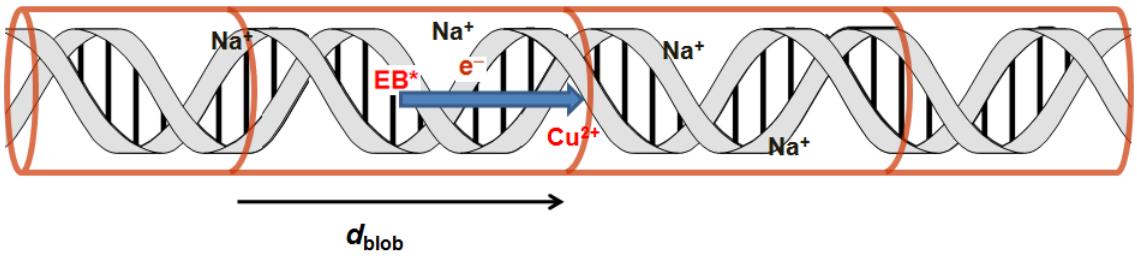

Figure 3.1: The DNA helix partitioned into a string of electrostatic blobs where EB is assumed to be near the center of a blob.

This report questions the nature of $N_{blob}(\infty)$ by investigating how $N_{blob}(\infty)$ varies as a function of solution ionic strength, metal cation, and chromophore lifetime. Considering the complexity of the photophysical processes considered, the conclusions drawn from the study are startlingly simple: $d_{blob} = N_{blob}(\infty) \times 3.4$ Å equals, within experimental error, the Debye length (κ^{-1}) which suggests that these fluorescence measurements report on the average distance of minimal approach for metal cations subject to electrostatic repulsion along the DNA backbone. The implications of so simple a conclusion are wide ranging, from polymer science to biochemistry, where interactions between polyelectrolytes and metal cations are commonly encountered and applied to numerous ends. How this conclusion was reached is developed hereafter.

3.3 Experimental

Materials. Calf Thymus DNA (CT DNA, product number D1501), anhydrous copper sulfate, anhydrous nickel sulfate, and ethidium bromide were purchased from Sigma-Aldrich (Milwaukee, WI). Sodium sulfate and deuterium oxide were purchased from Cambridge Isotope Laboratories, Inc. (Andover, MA) and EMD Chemicals (Gibbstown, NJ), respectively. All materials were used as received except for ethidium bromide, which was recrystallized three times from 50:50 water:methanol to ensure its fluorescence purity.[15] All solutions were prepared using doubly distilled water (deionized from Millipore Milli-RO 10 Plus and Milli-Q UF Plus (Bedford, MA)).

Solution Preparation. ET between DNA-EB and copper and nickel cations were studied for at least five sodium sulfate concentrations of 5×10^{-4}, 5×10^{-3}, 1.25×10^{-2}, 2×10^{-2}, and 3×10^{-2} M. The ratio of divalent metal cation to DNA phosphates was always smaller than 0.2 to minimize binding of the metal cations to the DNA bases.[16] At least five CT DNA concentrations ranging from 0.02 wt% to 0.09 wt% were studied for each ionic strength. DNA stock solutions (0.30 wt%) were prepared by dissolving CT DNA overnight in water or deuterium oxide (D_2O) containing the appropriate sodium sulfate concentration. The absolute concentration of the DNA stock solution was obtained spectrophotometrically. Molar extinction coefficients per mole of bp of ε_{260} = 11,300 $M^{-1}cm^{-1}$ and ε_{260} = 10,000 $M^{-1}cm^{-1}$ were determined experimentally for DNA in 5×10^{-3} M sodium sulfate aqueous or D_2O solution, respectively. Samples were freshly made on the day of use and all remaining CT DNA stock was discarded at the end of each day.

Steady-State Fluorescence Spectroscopy. Steady-state fluorescence measurements were carried out on a Photon Technology International (PTI) LS-100 steady-state fluorometer. The instrument was equipped with an Ushio UXL-75Xe Xenon arc flash lamp and a PTI 814 photomultiplier detection system using the right angle geometry. Samples were excited at 340 nm and the emission spectrum was collected from 450 to 650 nm. The fluorescence intensity was taken as the integral under the fluorescence spectrum from 583 nm to 603 nm which spans the fluorescence maximum of DNA-intercalated ethidium bromide located near 590 nm.

Time-Resolved Fluorescence Spectroscopy. Fluorescence decays were acquired with an IBH Ltd. time-resolved fluorometer equipped with an IBH 340 nm NanoLED. All solutions were excited at 340 nm and the emission was collected at 605 nm. Decays were acquired using the right angle geometry and a filter with a cutoff of 570 nm to block potential light scattering from reaching the detection system. Fluorescence decays of solutions in H_2O or D_2O were acquired over 1024 or 4096 channels, respectively, with a 1 MHz repetition rate and a time per channel of 0.24 ns/channel. A Ludox solution was used to obtain the instrument response function (IRF). To ensure a high signal-

to-noise ratio, the fluorescence decays and IRF were acquired until a peak maximum of 20,000 counts was reached. A least-squares analysis was used to fit the decays to the desired function and all decays were deconvoluted from the IRF profile.

Analysis of the Fluorescence Decays. The fluorescence decays of DNA-EB were first fit with Equation 3.1 using n = 2 or 3 in the absence and presence of quencher, respectively. Equation 3.1 is a sum of exponentials that provides only qualitative information on the time scale over which quenching occurs.

$$i(t) = \sum_{i=1}^{n} a_i e^{-t/\tau_i} \tag{3.1}$$

Quantitative information on how the excited ethidium bromide is being quenched via electron transfer to either copper or nickel is described by Equation 3.2 which is the FBM equation. In Equation 3.2, the function $f(t)$ represents the natural decay of DNA-EB in the absence of quencher found to be biexponential and whose pre-exponential factors and decay times are fixed in the analysis. The resulting fits were characterized as "good" when the residuals and autocorrelation function of the residuals were randomly distributed around zero and the χ^2 parameter was smaller than 1.3. A background and light scattering correction were applied to fit the fluorescence decays.

$$[EB^*] = [EB^*]_o \left| f_{slow} \times f(t) \times \exp\left[-A_2 t - A_3\left(1 - \exp(-A_4 t)\right)\right] + f_{fast} \exp(-t/\tau_{fast}) \right| \tag{3.2}$$

The expressions of the parameters A_2, A_3, and A_4 used in Equation 3.2 are given in Equation 3.3.

$$A_2 = \langle n \rangle \frac{k_{blob} k_e [blob]}{k_{blob} + k_e [blob]} \qquad A_3 = \langle n \rangle \frac{k_{blob}^2}{\left(k_{blob} + k_e [blob]\right)^2} \qquad A_4 = k_{blob} + k_e [blob] \tag{3.3}$$

A_2, A_3, and A_4 are functions of the three parameters k_{blob}, $k_e[blob]$, and $<n>$ that describe the kinetics of electron transfer from DNA-EB to divalent metal cations. These three parameters are obtained from the fits of the fluorescence decays with the FBM equation (Equation 3.2). k_{blob} is the rate constant of quenching of DNA-EB by one quencher inside the same blob, $k_e[blob]$ is the product of the rate constant describing the exchange of quenchers between blobs (k_e) and the local blob concentration ([*blob*]), and $<n>$ is the average number of divalent metal cations per blob. An excited EB can be quenched quasi-instantaneously by nearby divalent metal cations with a decay time of 1 – 2 ns and this decay time is represented by the fraction f_{fast}. The fraction f_{slow} represents EB that is quenched with a decay time greater than τ_{fast} and can be handled by the FBM equation.

Blob Size and Binding Constant. The size of a blob (N_{blob}) and the binding constant (K) of divalent metal cations to DNA are found through the FBM parameter $<n>$. The FBM parameter $<n>$ represents the average number of quenchers per blob and is expressed in Equation 3.4.

$$< n >= \frac{[M^{2+}]_{bound} - [M^{2+}]_o}{[blob]} \tag{3.4}$$

In Equation 3.4, $[M^{2+}]_o$ is the onset quencher concentration representing the concentration of divalent metal cation required to induce a minimum amount of quenching that can be detected through our analysis and whose origin has been investigated earlier.[14] $[M^{2+}]_{bound}$ represents the concentration of divalent metal cations bound to DNA. The equilibrium between free and DNA-bound divalent metal cations is given in Equation 3.5. The equilibrium constant K in Equation 3.5 can be used to derive the expression for $[M^{2+}]_{bound}$ shown in Equation 3.6.

$$M^{2+}_{free} + DNA \underset{}{\overset{K}{\rightleftharpoons}} M^{2+}_{bound} \tag{3.5}$$

$$[M^{2+}]_{bound} = \frac{[M^{2+}]_T}{\frac{1}{K[DNA]} + 1} \tag{3.6}$$

$[M^{2+}]_T$ in Equation 3.6 is the total divalent metal concentration and is equal to $[M^{2+}]_{free} + [M^{2+}]_{bound}$. The blob concentration, [*blob*], in Equation 3.4 is equal to $[DNA]/N_{blob}$ where N_{blob} represents the number of bp constituting a blob. The expression of $[M^{2+}]_{bound}$ in Equation 3.6 can be introduced into Equation 3.4 to yield Equation 3.7.

$$\langle n \rangle = \frac{[M^{2+}]_T}{\frac{1}{KN_{blob}} + \frac{[DNA]}{N_{blob}}} - \frac{[M^{2+}]_o N_{blob}}{[DNA]} \tag{3.7}$$

Equation 3.7 implies that a plot of <*n*> versus $[M^{2+}]_T$ yields a straight line with a slope that depends on N_{blob}, *K*, and DNA concentration. A plot of the inverse of the slope of Equation 3.7 is expected to be linear with respect to DNA concentration as depicted in Equation 3.8.

$$\frac{1}{slope} = \frac{1}{KN_{blob}} + \frac{[DNA]}{N_{blob}} \tag{3.8}$$

Therefore, according to Equation 3.8, a plot of $slope^{-1}$ versus [DNA] yields a straight line whose slope and intercept give *K* and N_{blob}, respectively. This procedure has been successfully validated in an earlier report.[14]

3.4 Results and Discussion

The fluorescence decays of DNA-EB without quencher were always slightly biexponential for all salt concentrations. The strongest contribution to the fluorescence decay of DNA-EB was the exponential with a 23 ns decay time which is characteristic of EB intercalated between the base pairs

of DNA. The other contribution to the decay was a shorter decay time around 9 – 14 ns which has been attributed to EB bound electrostatically to the DNA helix.[17,18] It has been reported that electrostatic associations that would stabilize a groove-bound form of ethidium are expected only at very low ionic strengths and intercalative binding is favoured at higher ionic strengths.[19] Since no change in the contributions of the lifetimes of DNA-EB (see Tables SI 3.1a-g, entries with $[Cu^{2+}] = 0$ M and Tables SI 3.2a-e, entries with $[Ni^{2+}] = 0$ M) was observed as a function of salt concentration, it can be concluded that no change in the binding mode of EB to DNA takes place for the ionic strengths used in this study.

The fluorescence decays of DNA-EB quenched by divalent metal cations were acquired and fit with Equation 3.1 using $n = 2$ or 3 depending on the quenching efficiency. The fluorescence decays of EB in a 0.09 wt% CT DNA solution quenched by 5×10^{-4} M copper cations are plotted in Figure 3.2 for different ionic strengths.

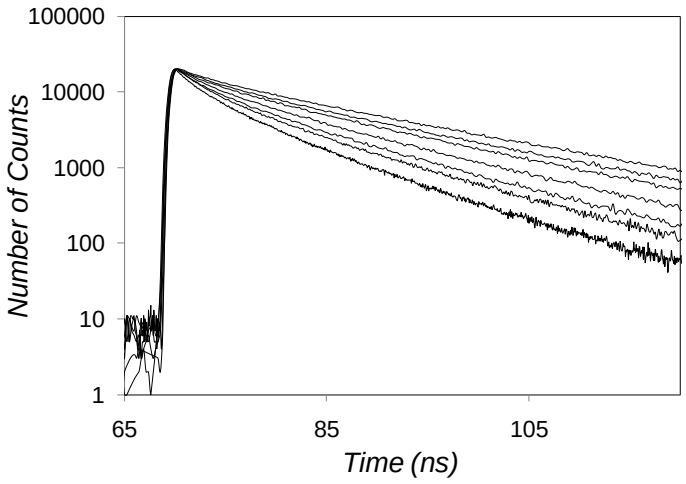

Figure 3.2: Time-resolved fluorescence decays of DNA-intercalated EB quenched by copper cations with increasing salt concentration. From top to bottom: $[Na_2SO_4] = 4\times10^{-2}$ M, 3×10^{-2} M, 2×10^{-2} M, 1.25×10^{-2} M, 7.5×10^{-3} M, 5×10^{-3} M, 5×10^{-4} M (0.09 wt% DNA equivalent to $[bp] = 1.4\times10^{-3}$ M, $[EB] = 1\times10^{-5}$ M, $[Cu^{2+}] \cong 5\times10^{-4}$ M).

The most striking feature of the fluorescence decays of DNA-EB quenched by copper cations is the increasing curvature observed in the decays with decreasing salt concentration which indicates a distribution of decay times. Curved fluorescence decays have been observed in many instances where a distribution of quenching rate constants are required and these types of decays have been successfully fit with an FBM equation.[14,20,21] The less pronounced curvature observed in the fluorescence decays at high ionic strength also indicates a decrease in quenching efficiency with increasing ionic strength.

The Stern-Volmer plots were obtained from the steady-state emission spectra by plotting the ratio I_o/I_M as a function of divalent metal concentration. I_o and I_M are the fluorescence intensity of DNA-EB in the absence and presence of quencher, respectively. The Stern-Volmer plots describing the quenching of DNA-EB by copper and nickel at the lowest ionic strength studied corresponding to a 5×10^{-4} M sodium sulfate solution are shown in Figure 3.3A for 0.09 wt% CT DNA. The ratio I_o/I_M increases exponentially with increasing quencher concentration indicating that quenching might be occurring in a restricted geometry similar to the ones encountered for micellar quenching.[22] Fluorescence quenching experiments between a chromophore covalently attached onto a polyanion and positively charged metal cations also show an upward curvature in the Stern-Volmer plots indicating that fluorescence quenching between reactants bound to polyelectrolytes occurs in a restricted geometry.[23] An interesting feature of Figure 3.3A is that copper seems to quench DNA-EB more efficiently than nickel. At high salt concentration, however, the Stern Volmer plots obtained for quenching of DNA-EB by copper and nickel overlap (Figure 3.3 B) suggesting that copper and nickel have the same quenching efficiency at high ionic strengths. The Stern-Volmer plots ($<\tau>_o/<\tau>_M$) resulting from the analysis of the fluorescence decays with Equation 3.1 were obtained and plotted together with the I_o/I_M ratios as a function of quencher concentration for salt concentrations of 5×10^{-4} M (Figure 3.3C) and 3×10^{-2} M (Figure 3.3D). $<\tau>_o$ and $<\tau>_M$ are the number average fluorescence lifetime in the absence and presence of quencher, respectively. Differences between Stern-Volmer

plots that use $<\tau>_o/<\tau>_M$ and I_o/I_M are indicative of static quenching, a quenching process that occurs instantaneously and cannot be probed by lifetime measurements.[24] As previously reported, Figure 3.3C shows that static quenching occurs for copper at low ionic strength.[14] No static quenching of DNA-EB by nickel is observed with a salt concentration of 5×10^{-4} M. At a salt concentration of 3×10^{-2} M, no static quenching is observed for both copper and nickel. Copper cations from $Cu(ClO_4)_2$ are known to bind to DNA bases at copper to phosphate ratios greater than 0.25 at a $NaClO_4$ salt concentration of 6×10^{-3}M.[16] Therefore, at low ionic strengths, electrostatic repulsion between the negatively charged DNA strands might allow some copper cations to bind to the bases, even for copper to phosphate ratios smaller than 0.2.

Quenching of DNA-EB by copper bound to the DNA bases would be expected to occur on very fast time scales, time scales that appear to be too fast to be probed by our time-resolved fluorometer, as both DNA-EB and copper might be within the π-stacked array of the DNA helix. Ultrafast ET between EB tethered to DNA and 7-deazaguanine (Z), a modified base, required femtosecond resolution for observation of this ET event.[25] Nickel does not have an affinity for the DNA bases[26] and therefore Ni^{2+} binds solely to the negatively charged DNA backbone so that no static quenching is observed. At a high ionic strength, copper is not likely bound to the DNA bases under the copper to phosphate ratios employed in this study, and no static quenching is observed. The ultra-fast quenching processes that occur between species located inside the DNA helix are beyond the resolution of our time-resolved fluorometer and the present study focuses only on the photophysical processes that occur more slowly over ~ 140 ns.

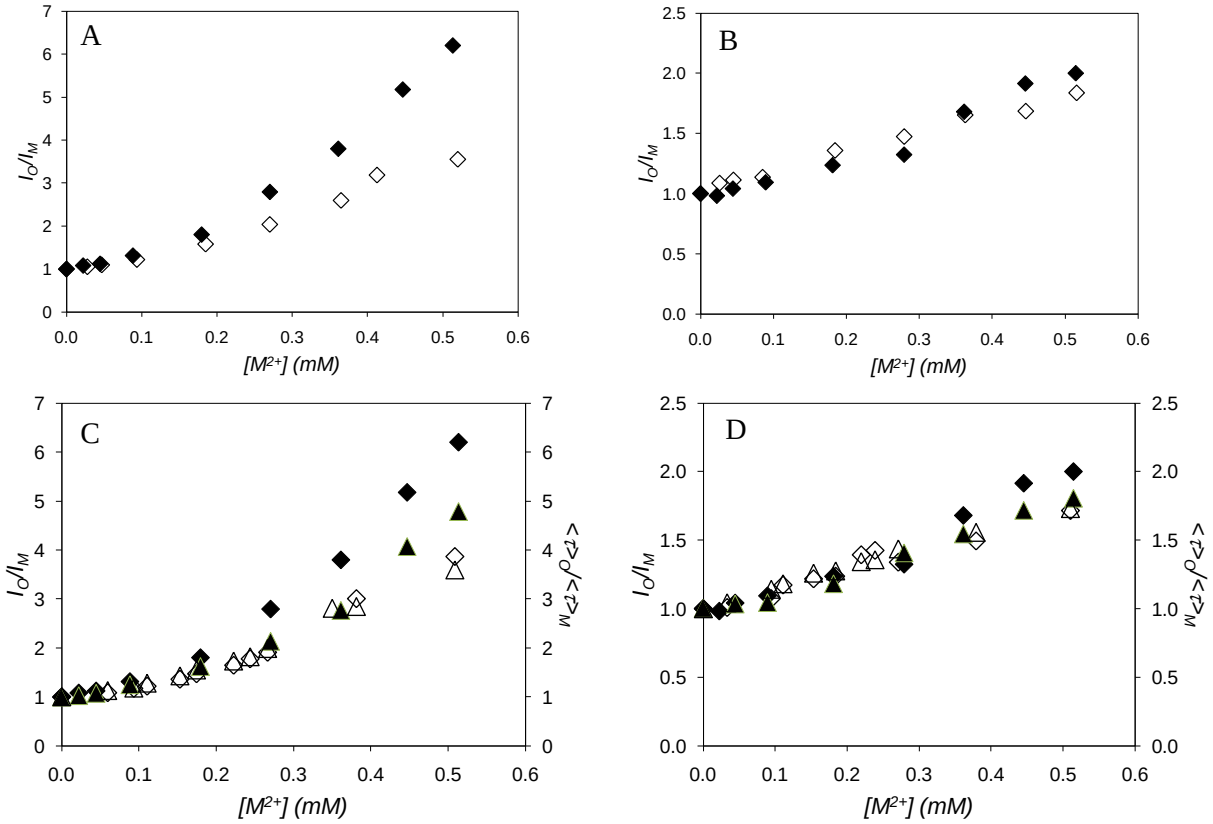

Figure 3.3: Stern-Volmer plots of DNA-EB quenched by copper and nickel cations. A) I_o/I_M as a function of divalent metal (copper (◆) and nickel (◇)) concentration with $[Na_2SO_4] = 5 \times 10^{-4}$ M and 0.09 wt% CT DNA or [bp] = 1.4×10^{-3} M. B) I_o/I_M as a function of divalent metal (copper (◆) and nickel (◇)) concentration with $[Na_2SO_4] = 3 \times 10^{-2}$ M 0.09 wt% CT DNA or [bp] = 1.4×10^{-3} M. C) I_o/I_M (copper (◆) and nickel (◇)) and $<\tau>_o/<\tau>_M$ (copper (▲) and nickel (△)) as a function of divalent metal concentration with $[Na_2SO_4] = 5 \times 10^{-4}$ M and 0.09 wt% CT DNA or [bp] = 1.4×10^{-3} M. D) I_o/I_M (copper (◆) and nickel (◇)) and $<\tau>_o/<\tau>_M$ (copper (▲) and nickel (△)) as a function of divalent metal concentration with $[Na_2SO_4] = 3 \times 10^{-2}$ M and 0.09 wt% CT DNA or [bp] = 1.4×10^{-3} M.

The fluorescence decays of DNA- EB quenched by copper cations were fit with Equation 3.2 to yield the parameters $<n>$, k_{blob}, and $k_e[blob]$ for each ionic strength studied. The FBM parameter $<n>$

increased linearly with increasing quencher concentration for all salt concentrations studied above an onset quencher concentration referred to as $[Cu^{2+}]_o$. The onset copper concentration arises from electrostatic repulsion between DNA-EB and Cu^{2+}.[14] Both ethidium and Cu^{2+} are positively charged so that, at low salt and low copper concentrations, copper cations are repelled by the positive charge of ethidium and bind to the DNA helix away from the intercalated chromophore. Thus, at low salt concentrations, a threshold copper concentration ($[Cu^{2+}]_o$) in Equation 3.4 needs to be reached before quenching can be detected. At a high salt concentration, repulsion between the positively charged ethidium and copper cations is reduced, the copper cations are no longer repelled by the positive charge exerted by ethidium, and no onset copper concentration is observed.[14] This phenomenon was observed as the concentration of salt was increased from 5×10^{-4} M to 4×10^{-2} M. Figure 3.4A shows how $<n>$ varies as a function of copper concentration for each salt concentration studied and for a DNA concentration of 0.09 wt%. As the concentration of salt increases, the onset copper concentration decreases until a high enough salt concentration is reached where no onset copper concentration is required. Analysis of all the FBM data obtained for each salt concentration and DNA concentrations reveals that if the [phosphate]/[salt] ratio is less than a value of approximately 0.13, then no onset copper concentration is observed, whereas a [phosphate]/[salt] ratio greater than 0.13 always results in an onset copper concentration. Figure 3.4A also shows that as the concentration of salt increases from 5×10^{-4} M to 4×10^{-2} M, $<n>$ decreases for a same quencher concentration which indicates that there are less quenchers per blob at higher salt concentrations. The inverse of the slope of the lines shown in Figure 3.4A for each DNA concentration and each salt concentration studied was plotted as a function of DNA concentration in Figure 3.4B to obtain N_{blob} and K according to Equation 3.8. The dashed line represents the trend obtained by conducting a set of experiments with

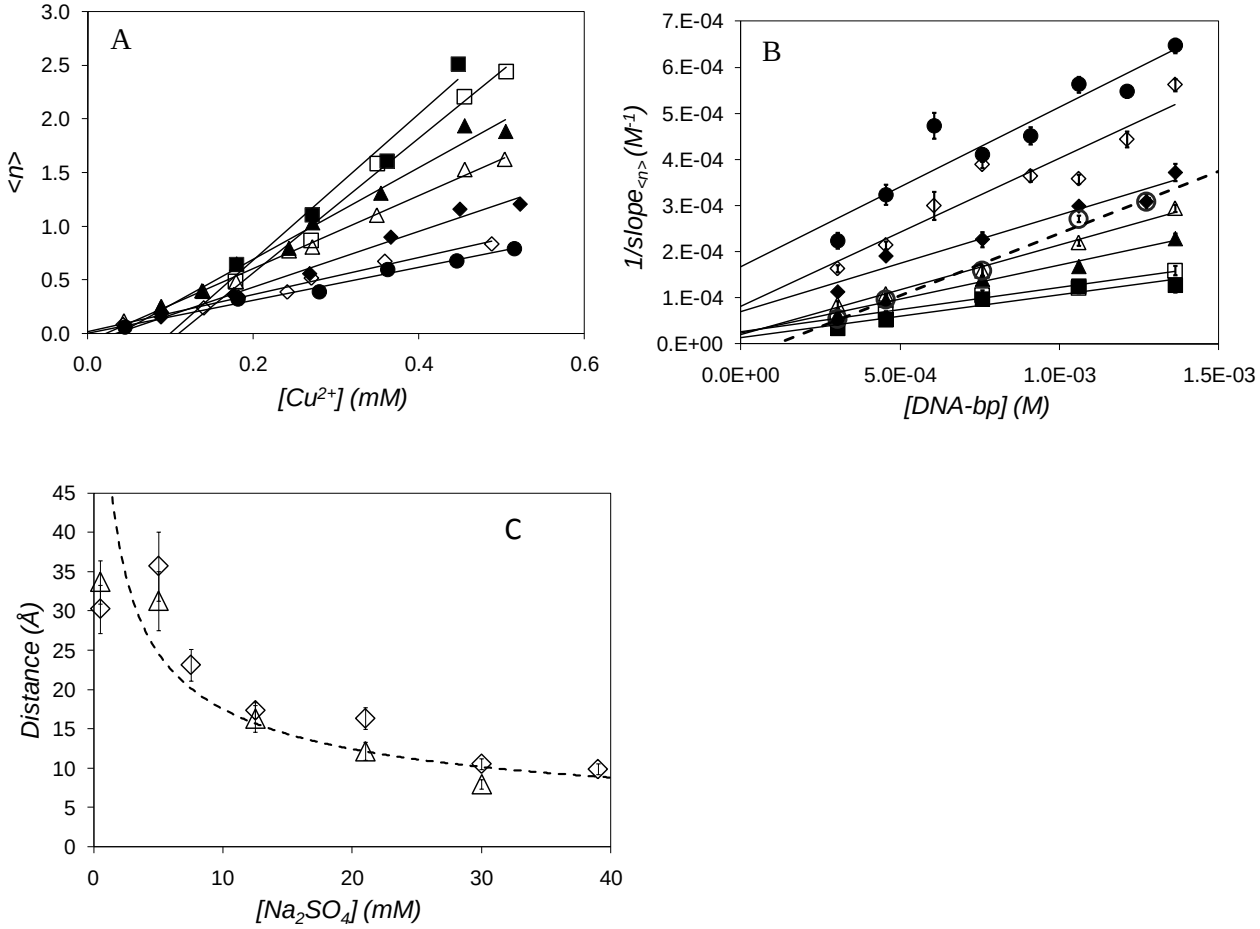

Figure 3.4: Effect of ionic strength on <*n*>, the inverse of the slope of <*n*> versus copper concentration, and d_{blob}. A) <*n*> as a function of copper concentration (0.09 wt% DNA or [bp] = 1.4×10^{-3} M, [EB] = 1×10^{-5} M). B) $slope^{-1}$ of <*n*> plotted as a function of DNA concentration expressed in moles of base pair per L. The hollow circles and dashed treadline represent a ratio of [salt]/[phosphate] of 8 ([EB] = 1×10^{-5} M); [Na_2SO_4] = (■) 5×10^{-4} M (R^2 = 0.98), (□) 5×10^{-3} M (R^2 = 0.99), (▲) 7.5×10^{-3} M (R^2 = 0.99), (△) 1.25×10^{-2} M (R^2 = 0.99), (◆) 2×10^{-2} M (R^2 = 0.95), (◇) 3×10^{-2} M (R^2 = 0.89), (●) 4×10^{-2} M (R^2 = 0.88). C) The distance of electron transfer, d_{blob}, for Cu^{2+} (diamonds) and Ni^{2+} (triangles) for varying ionic strengths. The dashed line represents the Debye length as a continuous function of ionic strength.

the [phosphate]/[salt] ratio set to equal 0.13. Data points obtained below and above this dashed line, respectively, did and did not require an onset copper concentration to fit $<n>$.

The N_{blob} and K values obtained as a result of this analysis are listed in the Supporting Information in Table SI 3.5. Note that the near zero intercept obtained at a salt concentration of 5×10^{-4} M in Figure 3.4B made it impossible to retrieve an accurate value of K. Taking advantage of the well-defined spacing existing between DNA bps, N_{blob} was converted to a distance expressed in Å, d_{blob} (= $N_{blob} \times 3.4$ Å), and is plotted as a function of ionic strength in Figure 3.4C. d_{blob} is small at high salt concentration but increases steadily with decreasing salt concentration until it reaches a value of 33 ± 4 Å. This trend suggests that the distance over which ET occurs becomes shorter at higher salt concentrations or that ET is less efficient as the concentration of salt is increased.

For ET to occur, copper cations must be in the vicinity of the DNA helix.[14] The negatively charged DNA backbone attracts positively charged copper cations to enable ET between DNA-EB and copper. As the ionic strength is increased, more sodium counterions will populate the binding sites along the DNA helix and the charges along the DNA helix become more screened from one another. The distance over which screening occurs is characterized by the Debye length and its effect on the distance over which ET takes place, namely d_{blob}, will now be considered.

It is well known that the efficiency of ET between electron donors and acceptors which are both cations or both anions is enhanced in the presence of an oppositely charged polyion.[24,27] The catalytic effect observed is due to the large increase in the concentrations of reactant ions in the vicinity of the polyelectrolyte due to counterion condensation. This catalytic effect is only observed if the charge density of the polyelectrolyte, ξ, is greater than the critical charge density parameter, ξ_c.[23] In Manning's counterion condensation theory, the critical charge density is defined as $\xi_c = N^{-1}$, where N

is the counterion valence.[28] When $\xi > \xi_c$, counterions condense until the charge density of the polyelectrolyte equals ξ_c. The charge density of a polyelectrolyte is given by

$$\xi = \frac{q^2}{\varepsilon k_B b T} \tag{3.9}$$

where q is the protonic charge, ε is the bulk dielectric constant of the solution, k_B is Boltzmann's constant, T is the absolute temperature in Kelvin, and b is the average axial spacing between charged groups on the polelectrolyte.[28] Studies have shown that when $\xi > \xi_c$, an upward curvature in the Stern-Volmer plots is observed.[23] The upward curvature is usually explained by evoking an active sphere where quenching occurs with unity or zero efficiency if a quencher is located inside or outside the sphere, respectively. Within the framework of the FBM, this sphere can be viewed as a blob which is defined in the FBM as a restricted volume over which quenching takes place with a rate constant k_{blob}.

DNA in aqueous solution is negatively charged with a charge density equivalent to two electronic charges per base pair or every 3.4 Å along the DNA helix. For water at 25 °C, $\xi = 7.1/b$ (if b is expressed in Å) where b = 1.7 Å and ξ = 4.2 for B-DNA.[25] According to Manning's theory, many copper counterions condense around the DNA helix due to its large charge density. The critical charge density is respectively 1 and 0.5 for monovalent and divalent counterions. The fraction of polyelectrolyte charges that are neutralized by condensed counterions is given in Equation 3.10,

$$N\theta_N = 1 - (N\xi)^{-1} \tag{3.10}$$

where θ_N is the number of condensed N-valent counterions per polyelectrolyte charge.[29] Therefore, the charge fractions of DNA in aqueous solutions of Na^+ and Cu^{2+} are 0.24 and 0.12 respectively. In

the case of DNA-EB quenched by Cu^{2+} in a sodium sulfate solution, the Na^{+} and Cu^{2+} counterions compete to condense onto DNA. In this case, selective binding is expected to take place where the species of higher valence (Cu^{2+}) predominates in the population of bound counterions even if the concentration of the species of lower valence (Na^{+}) is much higher.[29]

The screening of charges located near the DNA helix can be characterized by the Debye length (κ^{-1}).[25] κ^{-1} is given by Equation 3.11.

$$\kappa^{-1} = \frac{1}{\sqrt{8\pi b_B N_A I}} \tag{3.11}$$

where b_B is the Bjerrum length (7.1 Å in water at 25 °C), N_A is the Avogadro number and I is the ionic strength of the solution calculated from the concentrations of all free (uncondensed) small ions and is given by Equation 3.12.

$$I = \frac{1}{2}\left((\nu N^2 + \nu' N'^2)c_s + N(1 - N\theta_N)c_p\right) \tag{3.12}$$

In Equation 3.12, c_s is the molarity of the simple salt, c_p is the molarity of the charged polymer groups, N and N' are the assigned valances of the counterion and co-ion, respectively, ν and ν' are the number of counterions and co-ions, respectively, and θ_N is the number of condensed N-valent counterions per polyelectrolyte charge.[29] The ionic strength was calculated in mol/m^3 for each salt concentration studied and these values were used in Equation 3.12 to calculate κ^{-1}. κ^{-1} and d_{blob} were calculated in Å and are plotted as a function of salt concentration in Figure 3.4C.

Interestingly, the plot of κ^{-1} versus salt concentration yields a trend which is quite similar to that of d_{blob} obtained with Cu^{2+} at salt concentrations above 5×10^{-3} M. Equation 3.11 holds when salt is present in excess over the polyelectrolyte. This is no longer the case for salt concentrations lower

than 5×10^{-3} M. Therefore, if κ^{-1} and d_{blob} are supposed to yield similar trends, κ^{-1} is expected to diverge from the d_{blob} trend at lower salt concentrations as observed in Figure 3.4C since Equation 3.11 no longer holds. The highest and lowest concentrations of DNA used in this study correspond to a phosphate concentration of 2.7×10^{-3} M and 6.1×10^{-4} M, respectively, and these concentrations were used as c_p in Equation 3.12. κ^{-1} did not change with DNA concentrations ranging from 0.02 to 0.09 wt%, i.e. the range of DNA concentrations used in this study. Therefore Figure 3.4C shows the κ^{-1} values calculated for the highest DNA concentration (0.09 wt%). At low salt concentrations, d_{blob} reaches a constant value of 33 ± 4 Å indicating a maximum distance is reached over which an electron can be transferred from an excited DNA-EB to Cu^{2+}. The close agreement obtained between κ^{-1} and d_{blob} at salt concentrations above 5×10^{-3} M suggests that d_{blob} is the average distance of minimal approach between copper cations. Why this might be the case is rationalized as follows.

The phosphate anions lining the DNA backbone generate an electric field that extends in all directions, along the DNA and into the solution, over a distance equal to κ^{-1}. As a positively charged copper cation in solution experiences this electric field and binds to DNA, its binding is expected to induce a local dent in the electric field which is decreased at the locus where Cu^{2+} has bound (see second panel in Figure 3.5). Other Cu^{2+} cations tend to bind to DNA where the electric field is strongest, i.e. at distances d away from the first bound Cu^{2+} and where the electric field has recovered its original value corresponding to $d > \kappa^{-1}$. As the Cu^{2+} concentration is increased further, a crossover concentration is reached where, in order to have Cu^{2+} binding at a locus corresponding to an electric field maximum, the Cu^{2+} cations must arrange themselves in a more or less periodic manner along the DNA with an average periodicity given by κ^{-1} (see fourth panel in Figure 3.5).

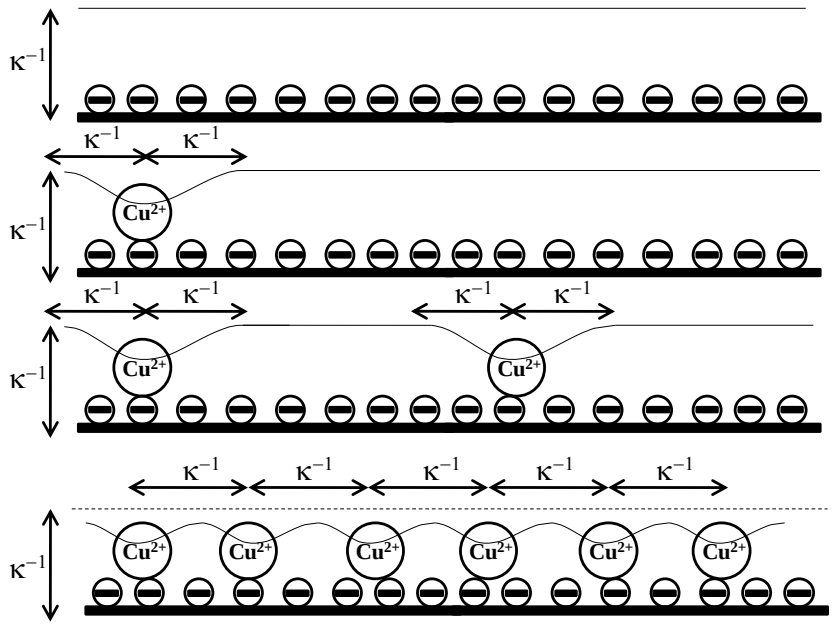

Figure 3.5: Description of the binding of copper cations along the DNA helix.

Some deviation from the ideal periodicity shown in Figure 3.5 is expected as such a representation is entropically disfavoured. Nonetheless, the fourth panel in Figure 3.5 suggests that electrostatic repulsion between Cu^{2+} cations leads them to bind to DNA at a distance greater than or equal to κ^{-1}. In effect, κ^{-1} represents a distance of minimal approach between DNA bound to Cu^{2+} cations at low concentrations of Cu^{2+}. The periodical arrangement of the Cu^{2+} cations along the DNA helix defines the boundaries over which ET from an excited DNA-EB and Cu^{2+} occurs. These boundaries result in an apparent compartmentalization of the Cu^{2+} cations which appears to be probed nicely by the FBM analysis. The relationship $d_{blob} = \kappa^{-1}$ obtained in our fluorescence experiments is expected to hold as long as the distance over which ET occurs is greater than κ^{-1}. For this statement to hold true, however, d_{blob} should not depend on the type of divalent metal quencher used or the lifetime of the chromophore since κ^{-1} depends only on the ionic strength of the solution according to Equation 3.11.

To check whether this was the case, the distance of electron transfer, d_{blob}, between DNA-EB and divalent nickel cations was obtained and plotted in Figure 3.4C to compare its values to d_{blob} obtained for copper cations and κ^{-1}. Figure 3.4C shows that d_{blob} is exactly the same whether divalent copper or nickel cations are employed as an electron acceptor and the quenching distance from both divalent metal cations follows κ^{-1} at high salt concentrations. At low salt concentrations, d_{blob} plateaus at 33 ± 3 Å which is the same value obtained for copper cations within experimental error. This "plateau" region represents the maximum distance over which divalent metal cations can quench DNA-EB. Equation 3.12 holds when the salt concentration is larger than the DNA concentration. The largest DNA concentration used in this study was 0.09 wt% which corresponds to a 2.7×10^{-3} M phosphate concentration. Therefore, when the concentration of sodium sulfate is decreased to 5×10^{-3} M, it becomes of the same order of magnitude as the concentration of DNA and Equation 3.11 does not hold. However, DNA being negatively charged enables metal cations to condense around the helix, regardless of the ionic strength of the solution. Therefore, the "plateau" region at low salt concentrations might represent the maximum distance where cations bound to DNA are screened from one another by the cloud of counterions surrounding the DNA double helix. At low salt concentrations, an onset divalent metal cation concentration was observed indicating that a minimum amount of Cu^{2+} or Ni^{2+} needed to be added to the solution before they could induce quenching. This effect was rationalized by noting that at low salt concentration, repulsion between the positively charged EB and the divalent metal cations induces them to bind to the DNA double helix away from the intercalated chromophore.[14]

The influence of the lifetime of the fluorescent electron donor on d_{blob} was also investigated. d_{blob} was obtained for ET between DNA-EB by copper cations taking place in D_2O. In D_2O, the lifetime of DNA-EB almost doubles from 23 ns in aqueous solution to 40 ns (see Tables SI 3.7a, entries with $[Cu^{2+}] = 0$ M). Intuitively, an increase in the lifetime of DNA-EB should allow more time for copper cations to diffuse along the DNA helix, resulting in a larger d_{blob}. However, d_{blob} for electron transfer

between DNA-EB and copper cations in D_2O at an ionic strength of 5×10^{-3} M was found to equal 35 ± 4 Å, a value identical to that of 36 ± 4 Å found for d_{blob} in water at the same ionic strength. This result demonstrates that the lifetime of DNA-EB does not affect d_{blob} and that d_{blob} depends solely on the electrostatic potential generated by the DNA phosphates and the solution ionic strength, as would be expected if d_{blob} and κ^{-1} were equivalent quantities.

The FBM parameters k_{blob} and $k_e[blob]$ were plotted as a function of the ratio of divalent metal cation to DNA phosphate for all ionic strengths in Figures 3.6 and 3.7. Whereas $k_e[blob]$ was found to yield similar trends for Cu^{2+} and Ni^{2+} within experimental error, k_{blob} did not change with ionic strength but took an average value of $4.1 \pm 0.3 \times 10^7$ s^{-1} and $2.9 \pm 0.6 \times 10^7$ s^{-1}, for Cu^{2+} and Ni^{2+}, respectively. The value of k_{blob} obtained for the quenching of DNA-EB by nickel cations is slightly lower than that obtained for quenching by copper cations. Nickel has been reported to be a less efficient quencher of DNA-EB than copper, an observation which is supported by the k_{blob} trend shown in Figure 3.6.[30] The Stern Volmer plots in Figure 3.3A would lead one to believe that nickel quenches DNA-EB much less efficiently than copper, but the results obtained from the time-resolved fluorescence decays indicate that the difference is certainly due to static quenching, most likely arising from copper binding to the DNA bases at low ionic strengths, a binding capability which seems to elude nickel cations.

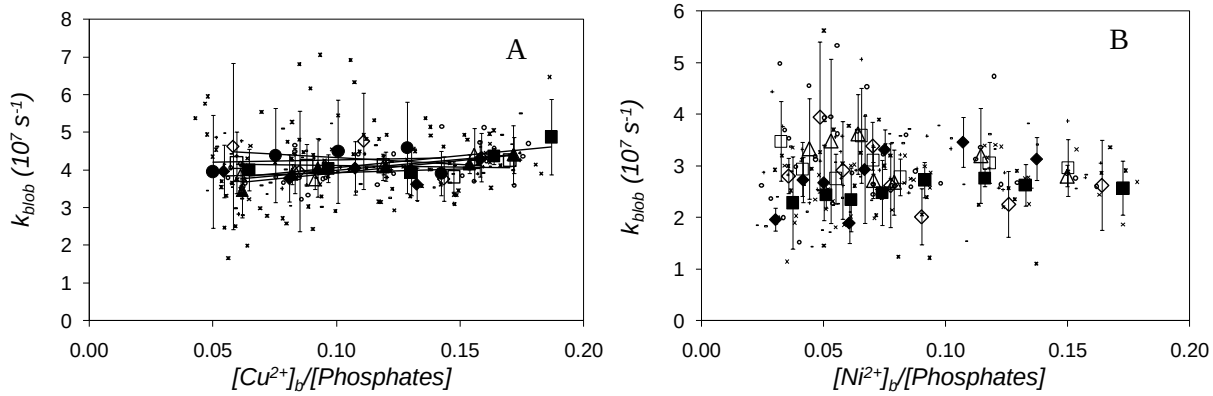

Figure 3.6: k_{blob} plotted as a function of the ratio of divalent metal cation to DNA phosphate for all ionic strengths. k_{blob} averaged over all DNA concenrations plotted as a function of copper bound (A) and nickel bound (B) to phosphate ratio for each salt concentration. Individual data points are the smaller data points represented by crosses, stars, and dashes. [Na_2SO_4] = (■) 5×10^{-4} M, (□) 5×10^{-3} M, (▲) 7.5×10^{-3} M, (△) 1.25×10^{-2} M, (◆) 2×10^{-2} M, (◇) 3×10^{-2} M, (●) 4×10^{-2} M ([EB] = 1×10^{-5}M).

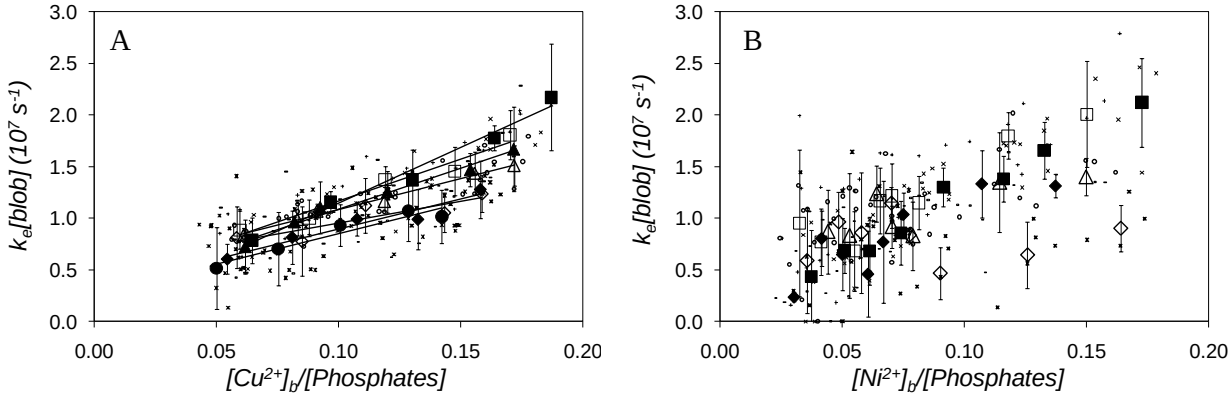

Figure 3.7: k_e[blob] plotted as a function of the ratio of divalent metal cation to DNA phosphate for all ionic strengths. k_e[blob] averaged over all DNA concentrations plotted as a function of copper bound (A) and nickel bound (B) to phosphate ratio for each salt concentration. Individual data points are the smaller data points represented by crosses, stars, and dashes. [Na_2SO_4] = (■) 5×10^{-4} M, (□) 5×10^{-3} M, (▲) 7.5×10^{-3} M, (△) 1.25×10^{-2} M, (◆) 2×10^{-2} M, (◇) 3×10^{-2} M, (●) 4×10^{-2} M ([EB] = 1×10^{-5}M).

3.5 Conclusions

This work illustrates how DNA was used as a molecular ruler to establish the equivalence that exists between d_{blob}, determined experimentally via the FBM analysis of the fluorescence decays of DNA-EB quenched by metal cations, and the Debye screening length, κ^{-1}. The quenching of DNA-EB by Cu^{2+} and Ni^{2+} was characterized by steady-state and time-resolved fluorescence. The Stern Volmer plots in Figure 3.2 demonstrated that static quenching occurred between DNA-EB and Cu^{2+}. This could be due to Cu^{2+} binding to the DNA bases at low ionic strength. At high ionic strength, quenching by Cu^{2+} and Ni^{2+} occurs solely from the binding of these cations to the negatively charged backbone phosphates at the less than 0.2 metal to phosphate ratios used in this study.

The fluorescence decays of DNA-EB quenched by Cu^{2+} and Ni^{2+} were acquired and fit with Equation 3.2 for varying ionic strengths. The number of quenchers per blob, $\langle n \rangle$, was linear with respect to quencher concentration (Figure 3.4A) and N_{blob} was obtained from the slopes of these lines using Equation 3.8. N_{blob} was multiplied by 3.4 Å to yield the distance over which ET takes place, d_{blob}. κ^{-1} was calculated for each ionic strength studied and d_{blob} was found to follow κ^{-1} when the salt was present in excess over the DNA phosphates and was independent of the type of divalent metal cation used (Figure 3.4C) and the lifetime of the chromophore, whether it be 23 ns in aqueous solution or 40 ns in D_2O. This result was rationalized by considering that the Debye length represents a distance of minimal approach between divalent metal cations bound along the DNA helix. At low ionic strengths, when the DNA concentration is in excess of the salt concentration, d_{blob} reached a plateau of 33 ± 4 Å and 33 ± 3 Å for Cu^{2+} and Ni^{2+}, respectively, providing the maximum screening distance experienced by the divalent metal cations condensed near the DNA helix. The rate constant for electron transfer, $k_{blob,}$ between DNA-EB and Cu^{2+} and Ni^{2+} were $4.1 \pm 0.3 \times 10^7$ s^{-1} and $2.9 \pm 0.6 \times 10^7$ s^{-1}, respectively, suggesting that copper and nickel bound to the outside of the DNA helix quench the fluorescence of DNA-EB in a similar manner.

These results provide a simple explanation to a very complex problem, namely by finding the limiting length scale that controls ET between electron donors and acceptors randomly distributed along a polyelectrolyte, the DNA helix in this report. In the case of DNA-EB quenched by Cu^{2+} and Ni^{2+} cations, the limiting length scale is found to be κ^{-1}, the average distance of minimal approach between two cations. The corollary to this conclusion is that the distance over which electrons are transferred to metal cations bound to DNA from DNA-EB is irrelevant as long as this distance is larger than κ^{-1}. In these experiments, the limiting length scale was that of minimal approach between divalent metal cations randomly distributed along the DNA helix, which represents a purely electrostatic process and implies that a limiting length scale would arise from any anions or cations randomly distributed along an oppositely charged polyelectrolyte. This inherent limit in length scale over which ET occurs is expected to provide novel insights to rationalize the process of ET taking place in complex synthetic and biological polyelectrolytes.

Chapter 4
Characterization of the Behavior of a Pyrene Substituted Gemini Surfactant in Water by Fluorescence

4.1 Overview

Time-resolved fluorescence was applied to characterize the behavior in solution of a gemini surfactant substituted with pyrene (Py-3-12). Upon association in water, excimer formation by Py-3-12 can be probed by acquiring pyrene monomer and excimer fluorescence decays which can be fitted globally according to the Model Free (MF) analysis to yield quantitative information about the internal dynamics of the Py-3-12 surfactant micelles as well as a complete description of the distribution of the different pyrene species in solution either incorporated inside the micelles or free in solution. A proof of procedure for the MF analysis was established by noting that the concentrations of free surfactant in solution, $[\text{Py-3-12}]_{\text{free}}$, was found to equal the critical micelle concentration (CMC) for surfactant concentrations larger than the CMC. $(I_E/I_M)^{SPC}$, the ratio of pyrene monomer to excimer fluorescence intensities, was calculated from parameters retrieved from the MF analysis of the fluorescence decays and was found to be independent of sample geometry. This work demonstrates how time-resolved fluorescence can be used to study the properties of pyrene-labeled macromolecules under conditions where large absorptions and inner filter effects usually distort the steady-state fluorescence signals. It was found that the pyrene excimer is formed mostly by diffusion within Py-3-12 micelles, which suggests that the pyrene microenvironment is fluid, an important feature for future studies on the interactions of Py-3-12 with DNA.

4.2 Introduction

Gemini surfactants have a unique structure consisting of two amphiphilic surfactant moieties connected chemically at or near the head group by a spacer. Since the early 1990's, these types of surfactants have attracted considerable research interest due to their improved properties over conventional surfactants.[1–7] Gemini surfactants have a critical micelle concentration (CMC) that is

generally at least one order of magnitude lower than that of the corresponding monomeric surfactants. Gemini surfactants are more efficient at reducing the surface tension of water and the interfacial tension of the oil–water interface than conventional surfactants.[3–9] A remarkable feature of gemini surfactants is their ability to form micelles of different shapes and dimensions, such as spherical, rod–like, or thread–like, even at low concentrations.[7,10–14]

Cationic gemini surfactants have shown potential as delivery vectors in gene therapy[15–20] making the study of the complexes formed between cationic gemini surfactants and DNA one of significant importance. The transfection efficiency of diammonium type gemini surfactants has been found to correlate closely with the morphologies of gemini aggregates in aqueous solution which were studied by atomic force microscopy (AFM).[21] However, a potential drawback of studying the morphologies of gemini surfactant – DNA complexes adsorbed onto the surfaces of mica slides used in AFM imaging is that these complexes may have structures and aggregation properties that are different from the solution state. Therefore, the interactions of cationic gemini surfactants with DNA are more realistically studied in solution. This can be done by labeling the gemini surfactant with a fluorophore and studying the complexes in solution by fluorescence spectroscopy.

This strategy was applied successfully by Wang et al.[22] who introduced a 1-pyrenehexyl unit as one of the hydrophobic tails of a 12-3-12 gemini surfactant to yield the pyrene–substituted surfactant Py-3-12 whose structure is given in Figure 4.1. Taking advantage of the ability of pyrene to form an excimer upon encounter between an excited and a ground-state pyrene, they were able to determine the critical micelle concentration (CMC) of Py-3-12 in water (CMC = 0.22 mM) which was confirmed by surface tension and conductivity measurements, as well as to monitor the interactions between Py-3-12 and DNA. However further information about the fluidity of the micellar interior or the distribution of the surfactants bound to DNA either as unimers or aggregates was not investigated.

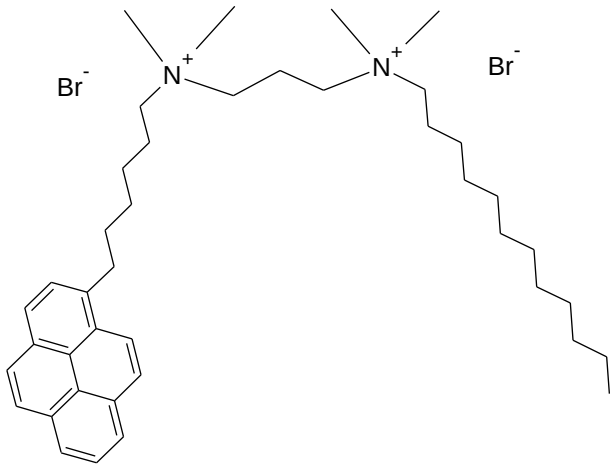

Figure 4.1: Structure of the gemini surfactant Py-3-12.

Knowledge about the internal dynamics of a surfactant aggregate bound to DNA is important as a rigid aggregate might hinder cell transfection by hampering the interactions that need to occur between surfactants and lipids as the surfactant coated DNA passes across the cell membrane. Furthermore the distribution of the surfactant molecules along the DNA needs to be characterized as it should also influence the interactions between the surfactants bound to DNA and the cell membrane. In the case of Py-3-12, such information can only be obtained from a detailed analysis of the fluorescence decays of the pyrene monomer and excimer of Py-3-12 in the presence of DNA. Before this can be done however, the behaviour of Py-3-12 in aqueous solution without DNA needs be fully characterized by time-resolved fluorescence, a task which was not done in the earlier study.[22] This work describes how a Model Free (MF) analysis of the pyrene monomer and excimer fluorescence decays was conducted that yields quantitative information about the internal dynamics of the Py-3-12 surfactant micelles as well as a complete description of the distribution of the different pyrene species in solution, either incorporated inside the micelles or present as unimers. Since the study of the micellization of Py-3-12 requires dealing with pyrene concentrations below and above the CMC = 0.22 mM, the fluorescence measurements were fraught with the inner filter effect, which

is a problem for any fluorescence study dealing with solution absorptions greater than 0.1,[23] as the absorption of the solution reached a value of 22 for a Py-3-12 concentration of 1 mM. Regardless of this complication which is inherent to any study carried out by steady-state fluorescence using the right angle geometry, our study based on the global analysis of the pyrene monomer and excimer fluorescence decays was found to be impervious to this artefact.[24-25] Most importantly, the full characterization of the Py-3-12 gemini surfactant in solution enables the future study of the interactions taking place between Py-3-12 and DNA by time-resolved fluorescence.

4.3 Theory

In water, the pyrene substituted gemini surfactants can be located in two environments, namely the aqueous phase and the surfactant micelles. The heterogeneity of environments experienced by pyrene results in a distribution of pyrene species in solution, similar to those encountered with pyrene-labeled polymers or lipids.[26–31] In such instances, several pyrene species are considered, as is being done hereafter with the Py-3-12 surfactant. At surfactant concentrations that are low enough, the gemini surfactants are isolated in the aqueous phase and the excited pyrene emits as a pyrene monomer. When excited, these pyrenes emit with the lifetime of the pyrene monomer τ_M as if they were free in solution and they are referred to as (Py^*_{free}). In the micelles, the presence of the alkyl chains of the gemini surfactants provides a fluid medium which enables diffusive excimer formation. The pyrenes that are involved in diffusive excimer formation are referred to as (Py^*_{diff}). The rate of excimer formation by diffusion is given by the function $f(t)$; however, the restricted geometry of the surfactant micelles does not enable all excited pyrenes to form well-stacked pyrene excimers. As such, two excimer species are assumed to be present in the surfactant micelles, one with a lifetime τ_{E0} of about 55 ns that is typical of the pyrene excimer (*E0**) formed in organic solvents,[32] and a second, shorter lifetime τ_D of about 35 ns that indicates that some excimer emission results from poorly

stacked pyrene dimers (*D**).[26] Based on these considerations, excimer formation was assumed to proceed according to Scheme 4.1.

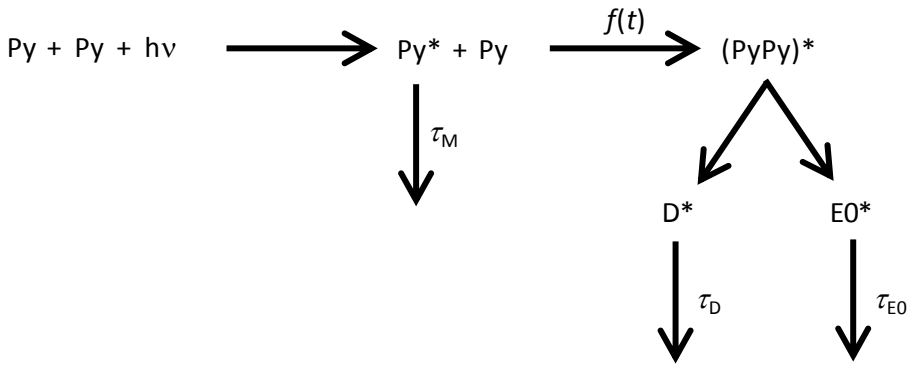

Scheme 4.1: Proposed reaction scheme for excimer formation inside the surfactant micelles.

In Scheme 4.1, excimer dissociation is neglected, a reasonable assumption when working at room temperature.[32] Based on Scheme 4.1, the following set of differential equations could be derived to describe the time-dependent profiles of the different pyrene species present in solution.

$$\frac{d[Py^*_{diff}]}{dt} = -f(t) - \frac{1}{\tau_M}[Py^*_{diff}] \tag{4.1}$$

$$\frac{d[Py^*_{free}]}{dt} = -\frac{1}{\tau_M}[Py^*_{free}] \tag{4.2}$$

$$\frac{d[E0^*]}{dt} = \alpha \times f(t) - \frac{1}{\tau_E}[E0^*] \tag{4.3}$$

$$\frac{d[D^*]}{dt} = (1-\alpha) \times f(t) - \frac{1}{\tau_E}[D^*] \tag{4.4}$$

The fractions α in Equation 4.3 and (1 – α) in Equation 4.4 represent the fractions of (Py^{*}_{diff}) that form *E0** and *D** by diffusion, respectively. As has been done in several instances,[26-27] $f(t)$ is estimated by assuming that $[Py^{*}_{diff}]_{(t)}$ decays as the sum of exponentials shown in Equation 4.5 where the sum of the a_i pre-exponential factors equals unity ($\sum_{i=1}^{n} a_i = 1$).

$$[Py^{*}_{diff}]_{(t)} = [Py^{*}_{diff}]_{(t=0)} \times \sum_{i=1}^{n} a_i \times \exp(-t/\tau_i) \tag{4.5}$$

Using Equation 4.5, Equation 4.1 can be re-arranged to yield the expression for $f(t)$ given in Equation 4.6.

$$f(t) = -\frac{d[Py^{*}_{diff}]}{dt} - \frac{1}{\tau_M}[Py^{*}_{diff}] = [Py^{*}_{diff}]_{(t=0)} \times \sum_{i=1}^{n} a_i \left(\frac{1}{\tau_i} - \frac{1}{\tau_M}\right) \times \exp(-t/\tau_i) \tag{4.6}$$

The function $f(t)$ being a sum of exponentials can be easily integrated when dealing with the first order differential equations shown in Equations 4.3 and 4.4. The result of this integration is given in Equations 4.7 and 4.8.

$$[E0^{*}]_{(t)} = -\alpha \times [Py^{*}_{diff}]_{(t=0)} \times \sum_{i=1}^{n} a_i \frac{\frac{1}{\tau_i} - \frac{1}{\tau_M}}{\frac{1}{\tau_i} - \frac{1}{\tau_{E0}}} \exp(-t/\tau_i)$$

$$+ \left([E0^{*}]_{(t=0)} + \alpha \times [Py^{*}_{diff}]_{(t=0)} \times \sum_{i=1}^{n} a_i \frac{\frac{1}{\tau_i} - \frac{1}{\tau_M}}{\frac{1}{\tau_i} - \frac{1}{\tau_{E0}}} \right) \times \exp(-t/\tau_{E0}) \tag{4.7}$$

$$[D^*]_{(t)} = -(1-\alpha)\times[Py^*_{diff}]_{(t=0)} \times \sum_{i=1}^{n} a_i \frac{\frac{1}{\tau_i} - \frac{1}{\tau_M}}{\frac{1}{\tau_i} - \frac{1}{\tau_D}} \exp(-t/\tau_i)$$

$$+ \left([D^*]_{(t=0)} + (1-\alpha)\times[Py^*_{diff}]_{(t=0)} \times \sum_{i=1}^{n} a_i \frac{\frac{1}{\tau_i} - \frac{1}{\tau_M}}{\frac{1}{\tau_i} - \frac{1}{\tau_D}} \right) \times \exp(-t/\tau_D) \qquad (4.8)$$

The integration of Equation 4.2 is trivial and yields Equation 4.9.

$$[Py^*_{free}]_{(t)} = [Py^*_{free}]_{(t=0)} \times \exp(-t/\tau_M) \qquad (4.9)$$

Summing Equations 4.5 and 4.9 and Equations 4.7 and 4.8 yields Equations 4.10 and 4.11 which were used to fit the monomer $[Py^*]_{(t)}$ and excimer $[E^*]_{(t)}$ decays, respectively. The monomer decays also needed a small contribution (less than 6 %) of an additional exponential which could be due to quenching of the excited pyrene by nearby bromide counterions or a residual impurity that would emit with a lifetime τ_{imp} and is referred to as $[Py^*_{imp}]_{(t=0)}$ in Equation 4.10.

$$[Py^*]_{(t)} = [Py^*_{diff}]_{(t=0)} \times \sum_{i=1}^{n} a_i \times \exp(-t/\tau_i) + [Py^*_{free}]_{(t=0)} \times \exp(-t/\tau_M) + [Py^*_{imp}]_{(t=0)} \times \exp(-t/\tau_{imp})$$

(4.10)

$$[E^*]_{(t)} = -\alpha \times [Py^*_{diff}]_{(t=0)} \times \sum_{i=1}^{n} a_i \frac{\frac{1}{\tau_i} - \frac{1}{\tau_M}}{\frac{1}{\tau_i} - \frac{1}{\tau_{E0}}} \exp(-t/\tau_i)$$

$$+ \left([E0^*]_{(t=0)} + \alpha \times [Py^*_{diff}]_{(t=0)} \times \sum_{i=1}^{n} a_i \frac{\frac{1}{\tau_i} - \frac{1}{\tau_M}}{\frac{1}{\tau_i} - \frac{1}{\tau_{E0}}} \right) \times \exp(-t/\tau_{E0})$$

$$-(1-\alpha) \times [Py^*_{diff}]_{(t=0)} \times \sum_{i=1}^{n} a_i \frac{\frac{1}{\tau_i} - \frac{1}{\tau_M}}{\frac{1}{\tau_i} - \frac{1}{\tau_D}} \exp(-t/\tau_i)$$

$$+ \left([D^*]_{(t=0)} + (1-\alpha) \times [Py^*_{diff}]_{(t=0)} \times \sum_{i=1}^{n} a_i \frac{\frac{1}{\tau_i} - \frac{1}{\tau_M}}{\frac{1}{\tau_i} - \frac{1}{\tau_D}} \right) \times \exp(-t/\tau_D) \qquad (4.11)$$

Experimentally, it was found that a single exponential was sufficient (n = 1 in all summations) to handle $[Py^*_{diff}]_{(t)}$ in Equation 4.5. The monomer and excimer fluorescence decays were fitted globally to ensure that the decay time τ_1 (only one decay time since n = 1) would be the same in Equations 4.10 and 4.11. Most importantly, the pre-exponential factors shown in Equation 4.11 for the excimer were optimized as a function of all the parameters used in their expression. For instance, the pre-exponential factor of the exponential $exp(-t/\tau_{E0})$ in Equation 4.11, referred to as b_{E0} in Equation 4.12, was optimized as a function of the parameters $[E0^*]_{(t=0)}$, $\alpha \times [Py^*_{diff}]_{(t=0)}$, τ_1, and τ_{E0}.

$$b_{E0} = [E0^*]_{(t=0)} + \alpha \times [Py^*_{diff}]_{(t=0)} \times \frac{\frac{1}{\tau_1} - \frac{1}{\tau_M}}{\frac{1}{\tau_1} - \frac{1}{\tau_{E0}}} \tag{4.12}$$

This procedure lengthens somewhat the coding of the optimization program, but it brings the benefit of ensuring that the set of parameters optimized through the fit of the fluorescence decays satisfies perfectly both Equations 4.10 and 4.11.

The set of parameters $[E0^*]_{(t=0)}$, $[D^*]_{(t=0)}$, $\alpha \times [Py^*_{diff}]_{(t=0)}$, $(1-\alpha) \times [Py^*_{diff}]_{(t=0)}$, and $[Py^*_{free}]_{(t=0)}$ retrieved from the analysis of the fluorescence decays with Equations 4.10 and 4.11 yields the fractions of pyrene species that contribute to the monomer (f_{Mdiff} and f_{Mfree}) and to the excimer (f^{E0}_{Ediff}, f^{D}_{Ediff}, f_{EE0}, and f_{ED}) decays. The expressions of the fractions f_{Mdiff}, f_{Mfree}, f^{E0}_{Ediff}, f^{D}_{Ediff}, f_{EE0}, and f_{ED} are listed in Equations 4.13 – 4.18. The contribution of $[Py^*_{imp}]_{(t=0)}$ in Equation 4.10 has been omitted as it remains small over the range of surfactant concentrations studied and was found to hardly change the results if it was taken into account.

$$f_{Mdiff} = \frac{[Py^*_{diff}]_{(t=0)}}{[Py^*_{diff}]_{(t=0)} + [Py^*_{free}]_{(t=0)}} \tag{4.13}$$

$$f_{Mfree} = \frac{[Py^*_{free}]_{(t=0)}}{[Py^*_{diff}]_{(t=0)} + [Py^*_{free}]_{(t=0)}} \tag{4.14}$$

$$f_{Ediff}^{E0} = \frac{\alpha \times [Py_{diff}^{*}]_{(t=0)}}{[Py_{diff}^{*}]_{(t=0)} + [E0^{*}]_{(t=0)} + [D^{*}]_{(t=0)}} \tag{4.15}$$

$$f_{Ediff}^{D} = \frac{(1-\alpha) \times [Py_{diff}^{*}]_{(t=0)}}{[Py_{diff}^{*}]_{(t=0)} + [E0^{*}]_{(t=0)} + [D^{*}]_{(t=0)}} \tag{4.16}$$

$$f_{EE0} = \frac{[E0^{*}]_{(t=0)}}{[Py_{diff}^{*}]_{(t=0)} + [E0^{*}]_{(t=0)} + [D^{*}]_{(t=0)}} \tag{4.17}$$

$$f_{ED} = \frac{[D^{*}]_{(t=0)}}{[Py_{diff}^{*}]_{(t=0)} + [E0^{*}]_{(t=0)} + [D^{*}]_{(t=0)}} \tag{4.18}$$

The subscripts *M* and *E* in Equations 4.13 – 4.18 are introduced as a reminder that the parameters used in these equations are obtained from the fit of the monomer and excimer decays with Equations 4.10 and 4.11, respectively.

In turn, the fractions f_{Mdiff}, f_{Mfree}, f_{Ediff}^{E0}, f_{Ediff}^{D}, f_{EE0}, and f_{ED} can be used to determine the fractions of pyrene units that constitute a ground-state dimer giving an excimer *E0** upon direct excitation (f_{E0}), a ground-state dimer giving a shorter-lived excimer *D** upon direct excitation (f_{D}), form an excimer *E0** by diffusion (f_{diff}^{E0}), form a short-lived excimer *D** by diffusion (f_{diff}^{D}), and are not involved in the formation of excimer (f_{free}). The expressions of f_{diff}^{E0}, f_{diff}^{D}, f_{free}, f_{E0}, and f_{D} are given in Equations 4.19 – 4.23, respectively.

$$f_{diff}^{E0} = \frac{f_{Ediff}^{E0}}{f_{Ediff}^{E0} + f_{Ediff}^{D}} \times \left(1 + \frac{f_{Mfree}}{f_{Mdiff}} + \frac{f_{EE0}}{f_{Ediff}^{E0} + f_{Ediff}^{D}} + \frac{f_{ED}}{f_{Ediff}^{E0} + f_{Ediff}^{D}} \right)^{-1} \quad (4.19)$$

$$f_{diff}^{D} = \frac{f_{Ediff}^{D}}{f_{Ediff}^{E0} + f_{Ediff}^{D}} \times \left(1 + \frac{f_{Mfree}}{f_{Mdiff}} + \frac{f_{EE0}}{f_{Ediff}^{E0} + f_{Ediff}^{D}} + \frac{f_{ED}}{f_{Ediff}^{E0} + f_{Ediff}^{D}} \right)^{-1} \quad (4.20)$$

$$f_{free} = (f_{diff}^{E0} + f_{diff}^{D}) \times \frac{f_{Mfree}}{f_{Mdiff}} \quad (4.21)$$

$$f_{E0} = (f_{diff}^{E0} + f_{diff}^{D}) \times \frac{f_{E0}}{f_{Ediff}^{E0} + f_{Ediff}^{D}} \quad (4.22)$$

$$f_{D} = (f_{diff}^{E0} + f_{diff}^{D}) \times \frac{f_{D}}{f_{Ediff}^{E0} + f_{Ediff}^{D}} \quad (4.23)$$

Multiplying the fractions f_{diff}^{E0}, f_{diff}^{D}, f_{free}, f_{E0}, and f_{D} by the total pyrene concentration ($[Py]_o$) yields the concentrations $[Py_{diff}^{*}]_{(t=0)}$, $[Py_{free}^{*}]_{(t=0)}$, $[E0^*]_{(t=0)}$, and $[D^*]_{(t=0)}$ which can be used in Equations 4.10 and 4.11 to obtain a quantitative expression of the pyrene monomer $[Py^*]_{(t)}$ and excimer $[E^*]_{(t)}$ decays. Integration from $t = 0$ to infinity of Equations 4.10 and 4.11 yields Equations 4.24 and 4.25.

$$\int_{t=0}^{\infty} [Py^*]_{(t)}\, dt = [Py]_o \times \left((f_{diff}^{E0} + f_{diff}^{D}) \times \sum_{i=1}^{n} a_i \times \tau_i + f_{free} \times \tau_M \right) \quad (4.24)$$

$$\int_{t=0}^{\infty}[E^*]_{(t)}\,dt = -[Py]_o \times \left[f_{diff}^{E0} \times \sum_{i=1}^{n} a_i \frac{\frac{1}{\tau_i} - \frac{1}{\tau_M}}{\frac{1}{\tau_i} - \frac{1}{\tau_{E0}}} \times \tau_i + \left(f_{E0} + f_{diff}^{E0} \times \sum_{i=1}^{n} a_i \frac{\frac{1}{\tau_i} - \frac{1}{\tau_M}}{\frac{1}{\tau_i} - \frac{1}{\tau_{E0}}} \right) \times \tau_{E0} \right.$$

$$\left. - f_{diff}^{D} \times \sum_{i=1}^{n} a_i \frac{\frac{1}{\tau_i} - \frac{1}{\tau_M}}{\frac{1}{\tau_i} - \frac{1}{\tau_D}} \times \tau_i + \left(f_D + f_{diff}^{D} \times \sum_{i=1}^{n} a_i \frac{\frac{1}{\tau_i} - \frac{1}{\tau_M}}{\frac{1}{\tau_i} - \frac{1}{\tau_D}} \right) \times \tau_D \right] \qquad (4.25)$$

Since all the parameters used in Equations 4.24 and 4.25 are obtained from the fitting of the fluorescence decays, the ratio $\int_{t=0}^{\infty}[E^*]_{(t)}\,dt \,/\, \int_{t=0}^{\infty}[Py^*]_{(t)}\,dt$, where $[Py]_o$ cancels out, is an absolute value representative of the I_E/I_M ratio, i.e. the ratio of the fluorescence intensity of the excimer over that of the monomer. This ratio obtained from the analysis of the fluorescence decays which were acquired by single photon counting (SPC) is referred to as the $(I_E/I_M)^{SPC}$ ratio so that it can be differentiated from the $(I_E/I_M)^{SS}$ ratio obtained from steady-state fluorescence experiments. Whereas $(I_E/I_M)^{SS}$ depends on the fluorometer, the sample geometry, and the procedure applied to determine the fluorescence intensities of the pyrene monomer and excimer, $(I_E/I_M)^{SPC}$ is an absolute quantity.

Information about the average rate constant $<k>$ describing excimer formation by diffusion can also be obtained using Equation 4.26.[26–27,33]

$$< k > = \left(\sum_{i=1}^{n} a_i \times \tau_i \right)^{-1} - \frac{1}{\tau_M} \qquad (4.26)$$

4.4 Experimental

Materials. The pyrene substituted surfactant, Py-3-12, was prepared by Dr. Shawn Wettig's research group from the School of Pharmacy at the University of Waterloo. The procedure is described in an earlier publication.[22] Its ^{1}H NMR and 2-D COSY NMR spectra are given in, respectively, Figures SI 4.1 and SI 4.2 in Supporting Information (SI). Doubly distilled water (deionized from Millipore Milli-RO 10 Plus and Milli-Q UF Plus (Bedford, MA)) was used in the preparation of all solutions.

Sample Preparation. An aqueous solution of Py-3-12 was lyophilized using a Labconco Freezone 6 freeze drier prior to careful weighing of the gemini surfactant. The lyophilized gemini surfactant was dissolved in water and the concentration of the stock solution was calculated by mass. Aerated aqueous solutions of Py-3-12 were used for all the fluorescence measurements. Solutions were prepared on the day of use and all the remaining stock was stored in the fridge at 5 °C.

UV-Vis Absorption Measurements. Absorption spectra were acquired on a CARY 100 Bio UV-Vis spectrophotometer. Cells with a 1 cm, 0.3 cm, and 0.1 cm path length were used for solutions with concentrations between 0.001 – 0.01 mM, 0.02 – 0.08 mM, and 0.16 – 0.60 mM, respectively. The use of different UV cells having different path lengths ensured that the absorbance of the Py-3-12 aqueous solution was never larger than 2.0. The OD of all absorbance spectra obtained with the 0.3 cm and 0.1 cm path length were scaled to the OD corresponding to a 1 cm path length.

Steady-State Fluorescence Spectroscopy. Steady-state fluorescence measurements were performed on a Photon Technology International (PTI) LS-100 steady-state fluorometer with an Ushio UXL-75Xe Xenon arc flash lamp and PTI 814 photomultiplier detection system. The fluorescence spectra of the Py-3-12 solutions were acquired with the front-face and right-angle geometry. Samples were excited at 344 nm and the emission spectrum was collected from 350 to 600 nm. The monomer and excimer intensities, I_M and I_E, were obtained by taking the integral of the fluorescence spectra from 374 – 378 nm and 500 – 530 nm for the monomer and excimer, respectively, to yield the $(I_E/I_M)^{SS}$ ratio.

Time-Resolved Fluorescence Spectroscopy. Fluorescence decays were acquired with an IBH Ltd. time-resolved fluorometer equipped with an IBH 340 nm NanoLED. All solutions were excited at 344 nm and the fluorescence from the pyrene monomer and excimer was monitored at 375 and 510 nm, respectively. To block potential light scattering leaking through the detection system, filters were used with a cutoff at 370 nm and 495 nm to acquire the fluorescence decays of the pyrene monomer and excimer, respectively. Decays of the Py-3-12 solutions were acquired with both the front-face and the right-angle geometry. Fluorescence decays were acquired over 1024 channels with a 1 MHz repetition rate using times per channel of 1.02 ns/ch and 0.24 ns/ch. The peak maximum was 20,000 counts for the instrument response function (IRF) and decay curves to ensure a high signal-to-noise ratio. A Ludox solution was used to obtain the IRF. The fit of the fluorescence decays was accomplished by convoluting the function of interest to the IRF and optimizing the parameters of the function by comparing the convolution product with the experimental decays.

Analysis of the Fluorescence Decays. The fluorescence decays of the pyrene monomer and excimer were fit independently with a sum of exponentials according to Equation 4.27. The fluorescence decays of the pyrene monomer were fit with a biexponential (n = 2 in Equation 4.27) for very low Py-3-12 concentrations. For concentrations of Py-3-12 near and above the CMC, the pyrene monomer and excimer were fit with a triexponential (n = 3 in Equation 4.27).

$$i(t) = \sum_{i=1}^{n} a_i e^{-t/\tau_i} \tag{4.27}$$

Analysis of the fits of the fluorescence decays with sums of exponentials revealed that one decay time was coupled between the pyrene monomer and excimer decays. Therefore, the fluorescence decays of the pyrene monomer and excimer of Py-3-12 were also fit globally with, respectively, Equations 4.10 and 4.11, using n = 1.

4.5 Results and Discussion

Absorbance spectra were obtained for Py-3-12 and are shown in Figure 4.2A. They are typical of what is expected from pyrene, with a strong 0–1 transition band from 300 – 360 nm and a weakly allowed 0–0 transition at 375 nm.[34–35] The broadening of the absorption band at 344 nm is usually indicative of pyrene association in solution. A relative measure of the broadening of the absorption band is provided by the peak to valley ratio, P_A.[36–37] P_A is the ratio of the absorption of the most intense band of the 0–1 transition to that of the adjacent minimum at a shorter wavelength and their positions in the absorbance spectrum are shown in Figure 4.2A. A P_A value greater than 3.0 indicates that pyrene is molecularly dissolved whereas a value less than 3.0 indicates the presence of associated pyrenes.[37] The P_A value was determined for the Py-3-12 solutions and plotted as a function of surfactant concentration in Figure 4.2B. The P_A value of Py-3-12 was always lower than 3.0, even below 0.22 mM which represents the CMC.

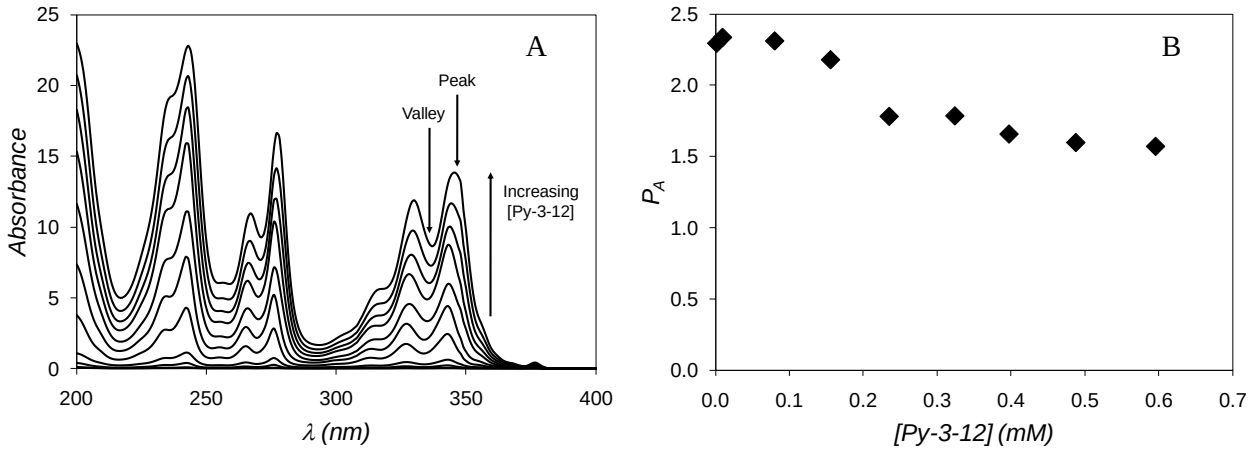

Figure 4.2: Absorbance spectra and the corresponding P_A values for a range of Py-3-12 concentrations. Absorbance spectra for Py-3-12 concentrations increasing from 0.001 to 0.60 mM (A). The peak-to-valley ratio, P_A, as a function of [Py-3-12] in mM (B).

To investigate the origin of the small P_A value found for Py-3-12, 0.06 mM Py-3-12 was mixed with 100 mM of SDS. At this SDS concentration, SDS forms micelles that should allow Py-3-12 to be

molecularly dissolved in the SDS micelles. Indeed, assuming an N_{agg} value of 60 and a CMC of 8 mM for SDS in water,[38] a very small occupancy equal to 0.06×60/(100 – 8) ~ 0.04 Py-3-12 molecule per micelle is expected which ensures that no ground-state pyrene dimers are being formed. The P_A value for this solution was found to be 2.3, which was the same value obtained for the Py-3-12 solutions without SDS. Therefore, one reason for the lower than 3.0 P_A value obtained for small Py-3-12 concentrations seems to be due to the 1–pyrenehexyl pendant of Py-3-12 having different photophysical properties than the 1–pyrenemethyl or 1–pyrenebutyl derivatives typically used to covalently label macromolecules.[39,40]

The absorbance maximum of the most intense band of the 0–1 transition was followed as a function of Py-3-12 concentration and is given in Table 4.1. The absorbance maximum shifts to higher wavelengths as the concentration of Py-3-12 is increased above the CMC. The shift in the absorbance maximum makes the peak appear broader due to competing absorbance maxima which results in an artificially low P_A value at concentrations larger than the CMC. The absorbance maximum of the most intense band of the 0–1 transition of Py-3-12 molecularly dissolved in SDS micelles also appears at longer wavelengths than for Py-3-12 free in water and suggests that the most intense band of the 0–1 transition of Py-3-12 shifts from 343 nm to 345 nm when the environment of 1–pyrenehexyl is switched from polar water to the apolar interior of SDS micelles.

The weak absorption peak at ~ 375 nm overlaps the 0–0 vibrational peak of the fluorescence spectrum of the pyrene monomer. The absorption at 375 nm becomes more significant at Py-3-12 concentrations greater than 1.0 mM (Figure SI 4.3). Therefore, solutions having a concentration up to 1.0 mM were studied to minimize artifacts due to re-absorption in the steady-state experiments.

Table 4.1: Position of the most intense band of the 0–1 transition for aqueous solutions of Py-3-12 and 0.06 mM Py-3-12 in 100 mM SDS micelles.

[Py-3-12] mM	Position of the absorbance maximum (nm)
0.01	343
0.02	343
0.08	343
0.16	343
0.24	343
0.32	343
0.40	344
0.49	344
0.60	344
Py-3-12 in SDS	345

The steady-state fluorescence spectra were obtained for solutions of Py-3-12. Figure 4.3A shows the fluorescence spectra of Py-3-12 acquired with the right-angle geometry. The spectra in Figure 4.3 are normalized to 1 at the 0–0 vibrational peak of the pyrene monomer (375 nm). The fluorescence of the pyrene excimer at 480 nm increases with increasing concentration of Py-3-12 due to the continued formation of micelles. The normalization of the fluorescence spectra in Figure 4.3A illustrates that as the concentration of Py-3-12 increases, the monomer spectra for the wavelength range of 370 – 420 nm do not overlap and the noise in the monomer signal increases. This observation could be a result of re-absorption of the monomer fluorescence by the 0–0 absorption band of pyrene at 375 nm (see Figure SI 4.2).

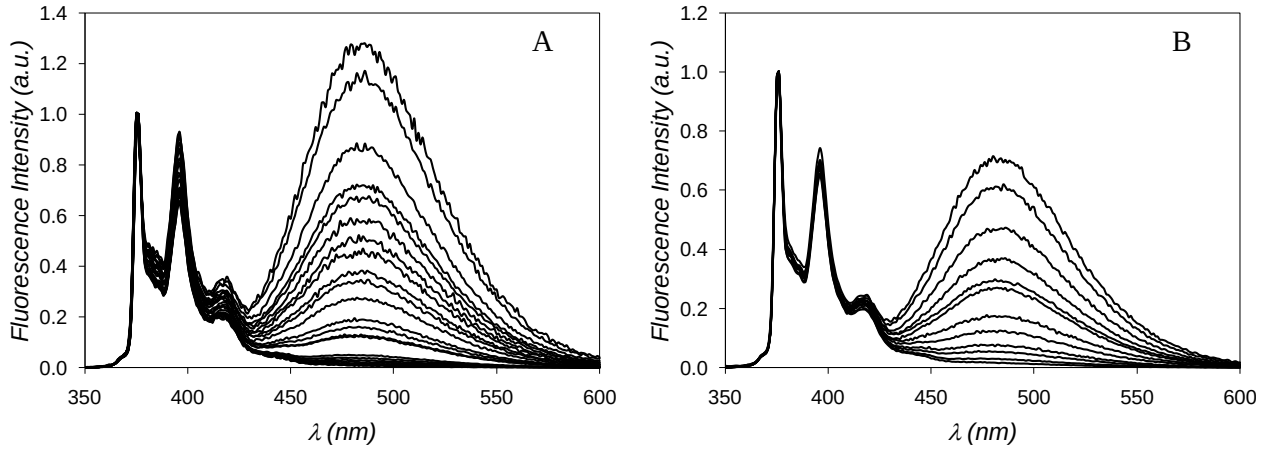

Figure 4.3: Effect of sample acquisition geometry on the steady-state fluorescence of Py-3-12. Steady state fluorescence spectra of Py-3-12 acquired with the right angle geometry (A) and the front-face geometry (B) ([Py-3-12] = 0.02 to 1.0 mM; λ_{ex} = 344 nm).

To check whether this was the case, the steady-state fluorescence spectra were then re-acquired with a triangular cell using the front-face geometry. Figure 4.3B shows the steady-state fluorescence spectra of Py-3-12 acquired with the front-face geometry and normalized to 1 at 375 nm. The monomer fluorescence spectra overlapped perfectly for all Py-3-12 concentrations when the spectra were acquired with the front-face geometry. To further illustrate that the inconsistencies observed in Figure 4.3A were due to re-absorption of the monomer fluorescence, the fluorescence spectrum of a 2 mM Py-3-12 solution was acquired with both the right-angle and front-face geometry and compared in Figure 4.4 to emphasize the effect of the fluorescence cell geometry on the monomer signal. At this Py-3-12 concentration, the solution has an absorbance of ~ 1.0 at the 0–0 vibrational transition and therefore re-absorption of the monomer emission cannot be ignored.

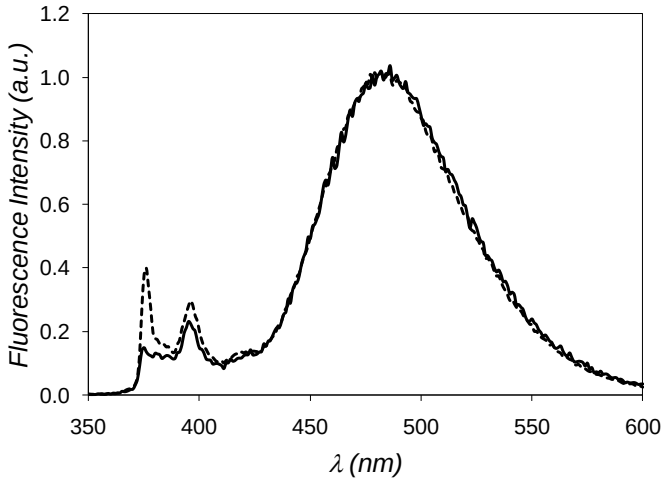

Figure 4.4: Effect of sample acquisition geometry on the monomer fluorescence of Py-3-12. Steady state fluorescence spectra of a 2.0 mM Py-3-12 aqueous solution acquired with the right angle geometry (solid line) and the front-face geometry (dashed line); λ_{ex} = 344nm.

Since re-absorption of the fluorescence does not take place at longer wavelengths, the fluorescence spectra were normalized to 1 at the excimer emission maximum. Figure 4.4 clearly demonstrates that the fluorescence emission of the pyrene monomer at 375 nm is substantially lower when the right-angle geometry is used. The differences in the fluorescence intensity of the excimer relative to that of the monomer can be visualized by determining the $(I_E/I_M)^{SS}$ ratio and plotting it as a function of Py-3-12 concentration in Figure 4.5 for both the right-angle and front-face geometries. Both trends show an increase in $(I_E/I_M)^{SS}$ after the CMC at 0.22 mM. However, the increase in $(I_E/I_M)^{SS}$ observed for the fluorescence spectra acquired with the right-angle geometry is much more pronounced due to the smaller monomer emission reduced by re-absorption (Figure 4.4). Overstated I_E/I_M ratios due to self-absorption effects have been reported in the literature.[41,42] These effects are expected to be reduced in time-resolved fluorescence experiments and therefore the sample geometry should matter less when acquiring fluorescence decays.

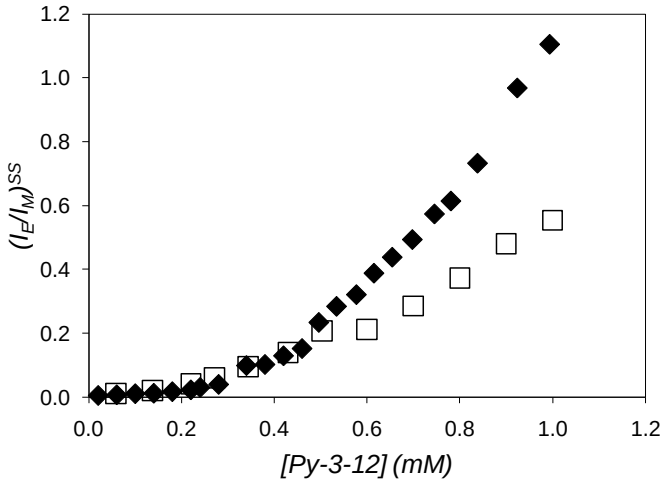

Figure 4.5: $(I_E/I_M)^{SS}$ as a function of [Py-3-12] in mM. Acquired with the right angle (◆) and front-face (□) geometries.

The monomer and excimer fluorescence decays of Py-3-12 were acquired for all samples with a large time per channel (TPC) equal to 1.02 ns/ch and a small TPC equal to 0.24 ns/ch for both the monomer and excimer decays to capture the long and short time-behavior of the decays, respectively. Sample fluorescence decays acquired at a TPC of 1.02 ns/ch and 0.24 ns/ch are shown in Figures SI 4.4 and SI 4.5, respectively, for 1.0 mM of Py-3-12. Since the small TPC captured all the information present in the decays, all decays were analyzed for the samples acquired at a TPC of 0.24 ns/ch. The monomer and excimer decays were fit with a sum of exponentials according to Equation 4.27. The decay times and pre-exponential factors are given in Table SI 4.1 and SI 4.2 acquired both with the right-angle and front-face geometries, respectively. At very low concentrations of Py-3-12, the pyrene monomer decays biexponentially with a small contribution (~0.03) for a decay time of about 10 ns. The major contribution (~0.97) of the pyrene monomer decay is for a decay time equal to 97 ns which is assigned to the natural lifetime of Py-3-12 (τ_M). The small contribution to the monomer decay is thought to be either residual quenching of pyrene by bromide ions or a fluorescence impurity present in too small an amount to be detected by NMR. We are not too concerned with this small impurity as

the MF analysis described in the theory section allows for the fraction of the impurity to be determined and isolated from the rest of the pyrene fractions. The fits of the pyrene monomer and excimer decays with a sum of exponentials show that one decay time around 1 ns appears as a decay (positive pre-exponential factor) in the monomer decay and as a rise time (negative pre-exponential factor) in the excimer decay. The magnitude of the pre-exponential factors associated with the decay– and rise–times increases with increasing surfactant concentration above the CMC. This observation suggests that the disappearance of the monomer is coupled with the appearance of the excimer. Furthermore, the short decay– and rise–times of 1 ns found in the analysis of the fluorescence decays indicates that pyrene excimer formation by diffusion occurs on a fast time scale, as would be expected of pyrenes located close from each other inside surfactant micelles.

The ratio of the negative pre-exponential factor divided by the sum of the positive pre-exponential factor(s), the A_-/A_+ ratio, obtained from the analysis of the excimer decays gives an indication of whether the excimer is formed via diffusion or excitation of pre-associated pyrenes.[26] A value of A_-/A_+ equal to −1 indicates that the pyrene excimer is formed via diffusion and values of A_-/A_+ approaching 0 indicate that the pyrene excimer is formed from the direct excitation of pyrene aggregates. Values between −1 and 0 indicate that pyrene excimer is formed by a mixture of both processes. Figure 4.6 shows how A_-/A_+ varies as the concentration of Py-3-12 increases above the CMC. This plot shows that as the concentration of Py-3-12 increases, more excimer is formed via diffusion. Once the CMC is reached, the A_-/A_+ ratio plateaus at a value of -0.70 ± 0.04, which is closer to −1.0 than to 0.0 suggesting that most of the pyrene excimer is formed via diffusion. Not only does the A_-/A_+ ratio remain constant above the CMC but so do the decay times (~30 ns and 58 ns) and rise time (~ 1 ns). The constancy with surfactant concentration of the pre-exponential factors and decay times obtained from the analysis of the excimer decays indicates that regardless of surfactant concentration, the excimer is generated in the same manner, as is expected of the surfactant micelles which are the loci of excimer formation. Increasing the surfactant concentration increases

the number of micelles and the number of loci for excimer formation, but it does not affect the process of excimer formation since the micelles are independent of one another.

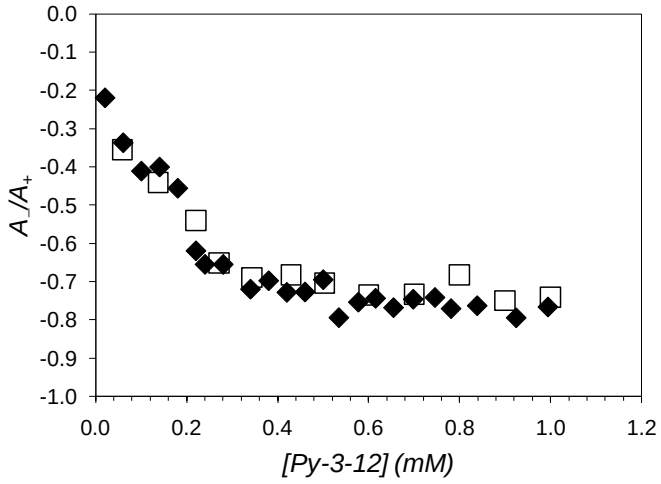

Figure 4.6: A_-/A_+ as a function of [Py-3-12] in mM. Acquired with the right angle (◆) and front-face (□) geometries.

The monomer and excimer decays were fit globally with Equations 4.10 and 4.11 and the fractions of pyrene in solution were calculated using Equations 4.13 – 4.23. The global analysis was performed on the monomer and excimer decays acquired with the small TPC of 0.24 ns/ch. The decay times and pre-exponential factors retrieved from the global analysis of the pyrene monomer and excimer decays have been listed in Tables SI 4.3 and SI 4.4 for the decays acquired with right-angle and front-faced geometries, respectively. The resulting fits were excellent with all χ^2 smaller than 1.20 and residuals and autocorrelation function of the residuals randomly distributed around zero. A sample fit of the fluorescence decays of the pyrene monomer and excimer analyzed globally with, respectively, Equation 4.10 and 4.11 is shown in Figure 4.7.

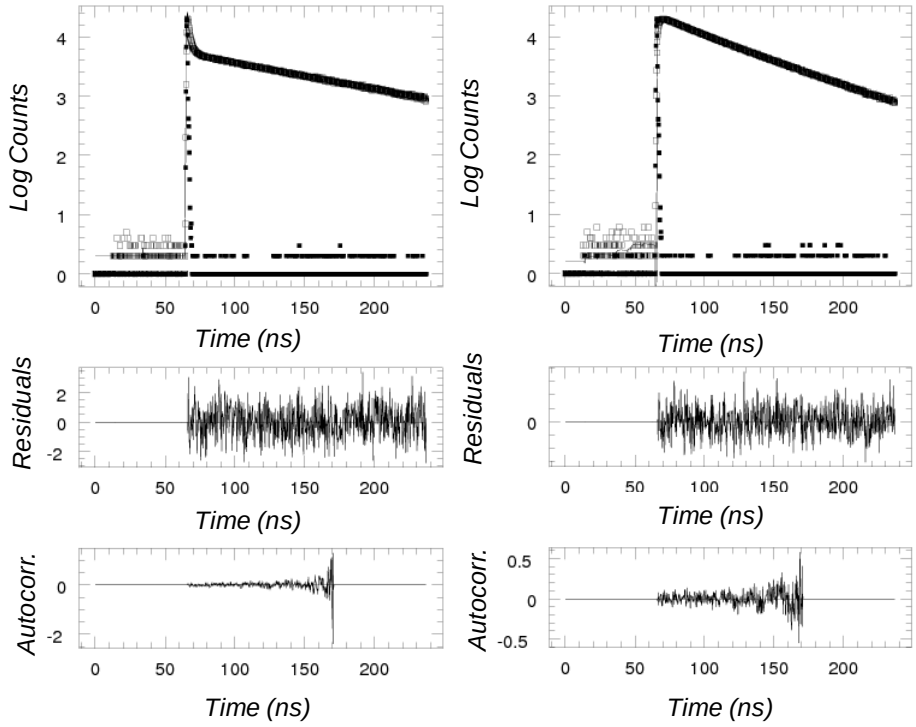

Figure 4.7: Fluorescence decays of Py-3-12. Decays of the pyrene monomer (left; λ_{ex} = 344 nm, λ_{em} = 375 nm) and excimer (right; λ_{ex} = 344 nm, λ_{em} = 510 nm) of a 1.0 mM Py-3-12 aqueous solution fit globally with Equations 4.10 and 4.11, respectively. (TCP = 0.24 ns/ch, acquired with the right angle geometry).

The benefit in analyzing the monomer and excimer decays globally is that the molar fraction of each pyrene species present in solution can be assigned. The fraction of the fluorescent impurity found in the monomer decay was isolated and found to be present in all solutions with a fraction of 0.03 ± 0.01 and 0.05 ± 0.02 for the right-angle and front-face geometries. This fraction is small, but shows up in the fluorescence decays (and not the NMR spectra), certainly due to the sensitivity of fluorescence. The advantage of the MF procedure is that the fraction of the impurity in the sample could be accounted for. The pyrene fractions, f_{free}, f_{diff}, and f_{agg} were plotted as a function of Py-3-12 concentration and are shown in Figure 4.8. The total fraction of pyrene that forms excimer via

diffusion, f_{diff}, is the sum of f_{diff}^{E0} + f_{diff}^{D} and the total fraction of aggregated pyrenes, f_{agg}, is the sum of $f_{E0} + f_{D}$. The first conclusion that can be drawn from this plot is that these fractions, determined from the global analysis of the pyrene monomer and excimer fluorescence decays, are independent of sample geometry as the trends obtained for the fractions of pyrene in solution are identical when using both the right-angle and front-faced geometries. The trends shown in Figure 4.8 are also consistent with the expected behavior of the pyrene fractions if the excimer is formed inside the surfactant micelles by diffusion. As the concentration of Py-3-12 increases above the CMC of 0.22 mM, f_{free} decreases due to the formation of Py-3-12 micelles in solution. f_{diff} is small below the CMC and increases above the CMC as more micelles are formed. f_{agg} is small compared to the other pyrene fractions with a value of 0.13 ± 0.03. Below the CMC, f_{agg} and f_{diff} are small and similar in value. Above the CMC, f_{diff} increases much more strongly than f_{agg}. This behavior is internally consistent with that of A_{-}/A_{+} in Figure 4.6 which suggests that with increasing Py-3-12 concentration, excimer formation by diffusion inside the micelle is favoured. These results suggest that the microenvironment of the micellar core is sufficiently fluid to allow the closely packed pyrenes to form excimers by diffusion on a fast time scale described by the decay time τ_1 of 1.4 ± 0.2 ns in Tables SI 4.3 and SI 4.4.

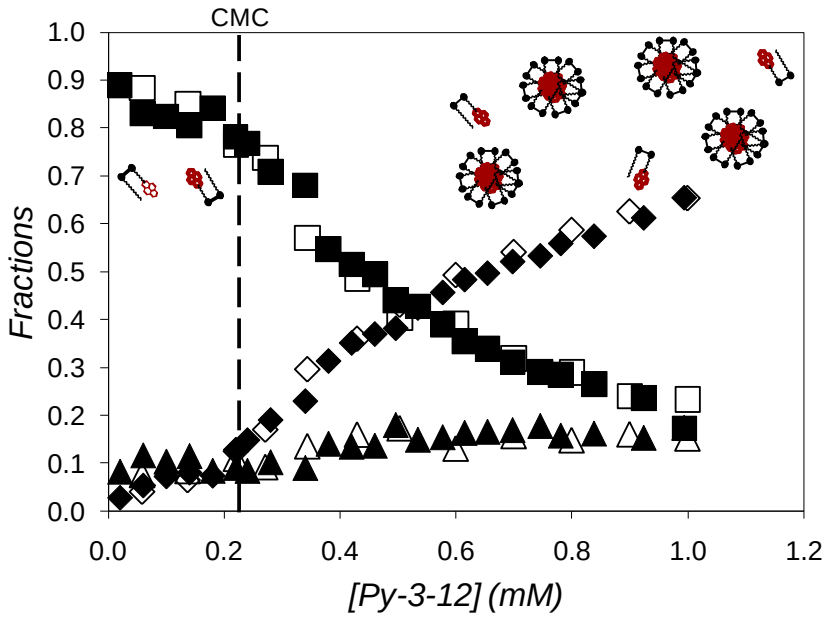

Figure 4.8: Molar fractions of pyrene species in solution as a function of [Py-3-12] in mM; f_{free} (squares), f_{diff} (diamonds), and f_{agg} (triangles). The filled and hollow data points were acquired with the right angle and front-face geometries, respectively. The dashed line represents the CMC of Py-3-12 equal to 0.22 mM.

Spectroscopic data are not always easy to interpret. Taken at their face value, the P_A ratios smaller than 3.0 in Figure 4.2B suggest that pyrene aggregation takes place as the concentration of Py-3-12 is increased, a conclusion made in an earlier study.[22] The lifetime measurements conflicted with this observation as the A_-/A_+ ratio in Figure 4.6 plateaued at a negative value of -0.70 ± 0.04 for Py-3-12 concentrations larger than the CMC indicating that the bulk of excimer formation occurs via diffusion. Furthermore, the pyrene molar fractions obtained from the MF analysis shown in Figure 4.8 revealed that only 13 ± 3 % of all pyrenes were aggregated in the Py-3-12 solutions. The discrepancy observed between the results obtained by UV-Vis absorption and fluorescence can be rationalized as follows. It was observed in Table 4.1 that the wavelength of the 0–1 transition shifts to higher wavelengths as the concentration of Py-3-12 was increased, suggesting that Py-3-12 absorbs

at higher wavelengths when present in micelles. This claim was supported by finding the position of the absorption maximum of Py-3-12 molecularly dissolved in SDS micelles which also resulted in a shifted 0–1 transition band. As the environment of the pyrenyl pendant of Py-3-12 is switched from water to the micellar interior, the absorption maximum shifts from 343 nm to 344 nm. In the transition region close to the CMC, equal to 0.22 mM, both species coexist resulting in an artificially broadened absorption band, as reflected by the P_A values shown in Figure 4.2. Despite the small P_A values, most pyrenes are not aggregated, present either as monomers in water with an absorption maximum at 343 nm or solvated inside the micellar interior with an absorption maximum at 344 nm. The thorough analysis of the absorption measurements combined with the results obtained from the fluorescence decays and their MF analysis reveals that Py-3-12 micelles have a fluid core where the pyrenyl pendants are not aggregated. This result was somewhat unexpected as the large local concentration of pyrenyl pendants found in the Py-3-12 micelles would be expected to enhance pyrene aggregation. That this is not the case indicates that the dodecyl chains brought by the Py-3-12 surfactants into the micelles are enough to solvate the pyrene moieties even at a ratio of dodecyl chain to pyrene as low as 1:1.

The analysis of fluorescence data can also be complicated by artifacts encountered when dealing with large chromophore concentrations as was shown in Figures 4.3 and 4.4. Inner filter effects resulted in an over estimated $(I_E/I_M)^{SS}$ ratio when the fluorescence spectra were acquired using the right-angle geometry suggesting increased levels of excimer formation than was truly the case, as was demonstrated by acquiring the steady-state fluorescence spectra with the front-face geometry. This artifact was not encountered with the $(I_E/I_M)^{SPC}$ ratio obtained from the MF analysis of the fluorescence decays. As shown in Figure 4.9A, $(I_E/I_M)^{SPC}$ is an absolute value that does not depend on whether right-angle or front-face geometries are being used. The trends in Figure 4.9A demonstrate that $(I_E/I_M)^{SPC}$ is independent of sample geometry whereas $(I_E/I_M)^{SS}$ in Figure 4.5 was not. A comparison between $(I_E/I_M)^{SS}$ and $(I_E/I_M)^{SPC}$ obtained with the right-angle geometry is shown in

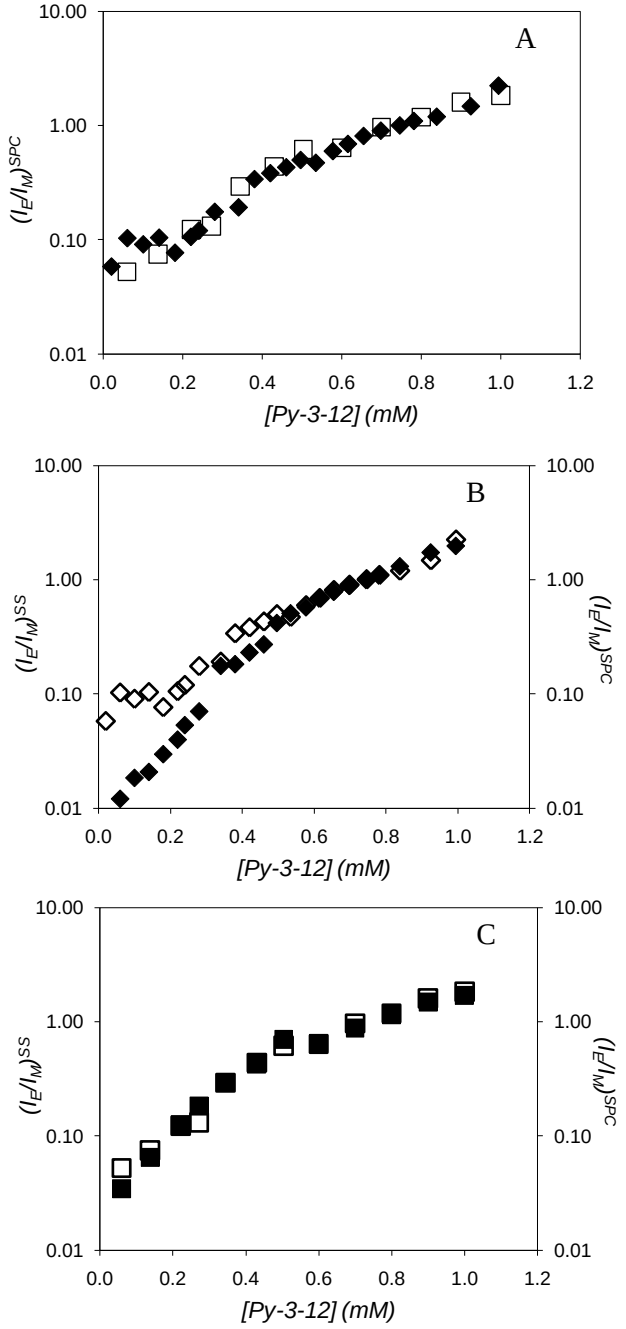

Figure 4.9: Effect of sample geometry on $(I_E/I_M)^{SS}$ and $(I_E/I_M)^{SPC}$. A) $(I_E/I_M)^{SPC}$ as a function of [Py-3-12] in mM acquired with the right angle (◆) and front-face (□) geometries. B) $(I_E/I_M)^{SS}$ (filled diamonds) and $(I_E/I_M)^{SPC}$ (hollow diamonds) as a function of [Py-3-12] in mM acquired with the right angle geometry. C) $(I_E/I_M)^{SS}$ (filled squares) and $(I_E/I_M)^{SPC}$ (hollow squares) as a function of [Py-3-12] in mM acquired with the front-faced geometry.

Figure 4.9B, where the data points for $(I_E/I_M)^{SS}$ are scaled by a constant multiplication factor equal to 1.8 which represents the average value of the $(I_E/I_M)^{SPC}/(I_E/I_M)^{SS}$ ratio obtained over the range on Py-3-12 concentrations where the $(I_E/I_M)^{SPC}/(I_E/I_M)^{SS}$ ratio did not change, namely from a Py-3-12 concentration of 0.5 to 1.0 mM. $(I_E/I_M)^{SS}$ and $(I_E/I_M)^{SPC}$ were plotted on a logarithmic scale to show that $(I_E/I_M)^{SS}$ and $(I_E/I_M)^{SPC}$ do not compare at low Py-3-12 concentrations where the ratios take small values. Figure 4.9C compares $(I_E/I_M)^{SS}$ and $(I_E/I_M)^{SPC}$ obtained with the front-face geometry, where the data points for $(I_E/I_M)^{SS}$ were scaled in the same way as those shown in Figure 4.9B, but with a constant multiplications factor equal to 3.1. After normalization, $(I_E/I_M)^{SPC}$ and $(I_E/I_M)^{SS}$ show identical trends. This result confirms the importance of using a front-face geometry when fluorescence spectra are being acquired with high optical density solutions.

The CMC of a surfactant represents the concentration of surfactant above which micelles are spontaneously formed. In other words, the CMC represents the concentration of free surfactant molecules in solution. Therefore, the concentration of free Py-3-12 surfactant in solution, $[\text{Py-3-12}]_{free}$, is expected to remain constant and equal to 0.22 mM at Py-3-12 concentrations greater than the CMC. $[\text{Py-3-12}]_{free}$ can be calculated from the MF analysis by multiplying the total Py-3-12 concentration, [Py-3-12], by f_{free}. Figure 4.10 is a plot of $[\text{Py-3-12}]_{free}$ as a function of [Py-3-12]. Figure 4.10 indicates that once [Py-3-12] reaches the CMC, $[\text{Py-3-12}]_{free}$ plateaus at a concentration near the CMC of 0.22 mM obtained by surface tension measurements.[22] Not only is it comforting that independent experimental procedures yields the same result (i.e. identical CMC obtained by surface tension and conductivity measurements in reference 22 and fluorescence decay measurements in Figure 4.10), but this result also demonstrates that the global analysis of the pyrene monomer and excimer fluorescence decays conducted by fitting the kinetic parameters directly in the decay times and pre-exponential factors, as done with the MF,[26,27] the Fluorescence Blob Model,[28,29] or the Birks Scheme,[30] analyses conducted in this laboratory, provides a robust procedure to obtain the molar fraction of all the pyrene species present in solution.

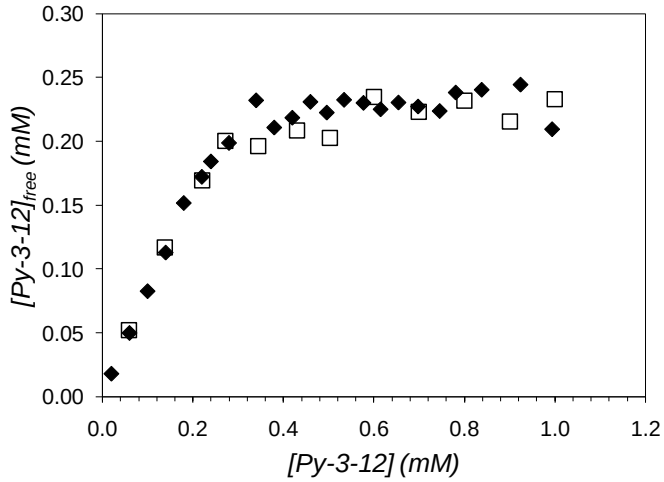

Figure 4.10: $[\text{Py-3-12}]_{free}$ calculated from the MF analysis as a function of the total Py-3-12 concentration. Data acquired with the right angle (◆) and front-face (□) geometries.

The average rate constant $\langle k \rangle$ at which excimers are formed in the Py-3-12 micelles was calculated using Equation 4.26 with n = 1. $\langle k \rangle$ was found to equal $79 \pm 2 \times 10^7$ s^{-1} and $78 \pm 8 \times 10^7$ s^{-1}, using the decays acquired with the right-angle and front-face geometries, respectively. $\langle k \rangle$ in Py-3-12 micelles is over 10 times greater than the rate constant of excimer formation for pyrene dissolved in SDS micelles which has been reported to be 2.1×10^7 s^{-1}.[41] The increase in the rate constant of excimer formation for Py-3-12 compared to pyrene molecularly dissolved in micelles is likely due to the higher local pyrene concentrations found in the Py-3-12 micelles. The constancy of $\langle k \rangle$ with Py-3-12 concentration suggests that, as the I_E/I_M ratio in Figure 4.5 for the front-face results increases 13 fold when the Py-3-12 concentration increases from the CMC to 1 mM, the structure of the Py3-12 micelles remains unchanged.

4.6 Conclusion

The interior of the Py-3-12 micelles was described using time-resolved fluorescence. Despite the large local pyrene concentration located inside the micelles and their inherent propensity to π-stack,

the 1:1 ratio of dodecyl chain to pyrene moiety present in the micelles ensured that the pyrenyl pendants are solvated inside the micelles providing a fluid micellar interior. This conclusion was drawn by observing that excimer formation between two pyrene groups occurs principally by diffusion. Indeed, most pyrene species are present in the solution as surfactant molecules either isolated in the water phase or solvated inside the micellar interior. As the Py-3-12 concentration increases, the molar fraction of surfactant free in solution (f_{free}) decreases at the expense of the molar fraction of surfactant forming excimer diffusionally inside the micelles (f_{diff}). Together, the fractions f_{free} and f_{diff} account for over 85% of all the pyrene species present in solution for the range of Py-3-12 concentrations studied. The rate of intramolecular excimer formation, $<k>$, was found to equal $79 \pm 2 \times 10^7$ s^{-1}. This value is similar to that obtained for a 4th generation dendrimer containing 16 pyrenyl moieties and having a diameter estimated to equal 2.5 nm,[27] similar to that of the Py-3-12 micelles determined by surface tension measurements.[22]

The useful information gathered on the Py-3-12 micelles was not straightforward to obtain. Starting with the UV-Vis absorption measurements shown in Figure 4.2A, direct analysis of the absorption spectra in terms of the P_A value leads to the erroneous conclusion that the pyrenyl pendants are aggregated as expected from a P_A value smaller than 3.0. Yet closer inspection of the absorption spectra suggested that the observed broadening of the 0–1 band was due to a shift in the absorption spectrum as the pyrene monomer switches its environment from polar water to the apolar micelle interior. In short, the absorption results were inconclusive in characterizing the Py-3-12 micelles. Analysis of the steady-state fluorescence spectra provided little information besides indicating the onset of excimer formation at surfactant concentration larger than the CMC; however the analysis was complicated by the inner filter effect. Indeed different trends for the $(I_E/I_M)^{SS}$ ratios were obtained whether the spectra were acquired with the right-angle or front-face geometry (Figure 4.5) due to the inner filter effect that cannot be neglected at the large pyrene concentrations used in these measurements. On the other hand, absolute $(I_E/I_M)^{SPC}$ ratios were obtained by analyzing

globally the monomer and excimer fluorescence decays. The MF analysis provided a robust procedure to determine the molar fractions of all pyrene species in solution (Figure 4.8). The robustness of the procedure was validated by determining the concentration of surfactant free in solution, $[\text{Py-3-12}]_{\text{free}}$, as a function of the overall surfactant concentration, [Py-3-12]. It was found in Figure 4.10 that $[\text{Py-3-12}]_{\text{free}}$ increased linearly with increasing [Py-3-12] up to 0.22 mM, i.e. the CMC of the surfactant, above which concentration, $[\text{Py-3-12}]_{\text{free}}$ remained constant and equal to 0.22 (±0.06) mM. The agreement found between $[\text{Py-3-12}]_{\text{free}}$ and the expected profile of the concentration of free surfactant suggests that the analysis conducted is reliable, as well as the conclusions drawn from it regarding the properties of the Py-3-12 micelles.

This study illustrates how time-resolved fluorescence can be applied to study the properties of pyrene-labeled macromolecules and their supramolecular assemblies under conditions where large absorptions and the associated inner filter effect usually cripple the analysis of fluorescence data. It also confirms that the global analysis of the pyrene monomer and excimer fluorescence decays, be it conducted with the "Model Free" procedure,[26,27] the Fluorescence Blob Model,[28,29] or the Birks Scheme,[30] provides a robust procedure to determine the molar fractions of all the pyrene species present in solution. This feature yields information about whether the process of excimer formation occurs via diffusive encounters or direct excitation of pyrene aggregates, as well as the fraction of pyrene moieties that participate in excimer formation via the fraction $1 - f_{\text{free}}$. In turn, knowing that excimer formation occurs by diffusion suggests that the pyrene microenvironment is fluid, important information necessary to describe the nature of the macromolecular assembly under study.

Chapter 5
Studying the Interactions of a Pyrene Substituted Gemini Surfactant with DNA by Fluorescence

5.1 Overview

The interactions of a pyrene substituted gemini surfactant (Py-3-12) and calf thymus (CT) DNA were studied using steady-state and time-resolved fluorescence. The fluorescence decays of the pyrene monomer and excimer were fit with the Model Free "MF" analysis program to provide quantitative information about the molar fractions of the different pyrene species, and therefore, gemini surfactants, present in solution. The binding of Py-3-12 to CT DNA was found to be time-dependent. All fluorescence data were acquired once equilibrium had been reached to ensure their reproducibility. The trends obtained with the $(I_E/I_M)^{SS}$ ratios and the molar fractions of the pyrene species in solution demonstrated that all gemini surfactants are bound to DNA at a charge ratio between DNA phosphates and surfactant ammonium cations equal to unity. The decay times of the pyrene excimer revealed that Py-3-12 is in a micellar form when bound to the DNA helix. The average rate constant of excimer formation, $\langle k \rangle$, was determined to be $50 \pm 3 \times 10^7$ s^{-1} which is smaller than $\langle k \rangle$ for Py-3-12 micelles with no DNA found to equal $79 \pm 2 \times 10^7$ s^{-1}. This difference in $\langle k \rangle$ values suggests that Py-3-12 surfactant molecules bound to the backbone phosphates experience a hindered mobility that results in a micellar interior that is stiffer for the micelles bound to DNA than for Py-3-12 micelles in water.

5.2 Introduction

A major challenge in gene therapy is the transport of therapeutic genes to the proper cell for gene expression.[1–3] An ideal gene delivery vehicle should protect the gene from degradation, transport it across the membrane into the nucleus of target cells, and not cause an immunogenic response. Gene delivery vectors can be categorized into two classes, depending on whether they are viral or non-viral.

Viral vectors used as gene delivery vehicles have two main advantages. First, they protect the gene against degradation and second, they provide high transfer efficiencies.[4-6] However, viral delivery vectors have the major disadvantage of generating severe immune responses.[7] In addition, viral gene delivery vectors are limited in the size of the gene they can encapsulate. In comparison, non-viral gene delivery vectors are non toxic and non immunogenic, they have no size limitation of the gene they can encapsulate, and they are relatively cheap.[4,8,9] Some non-viral vectors include surfactants,[10–12] gemini surfactants,[13–15] lipids/liposomes,[16–18] cationic polymers,[19,20] dendrimers,[21] and cell penetrating peptides.[22,23] The major disadvantage of non-viral delivery vectors is their low transfection efficiency. These combined factors have driven researchers to develop non-viral gene delivery vectors with enhanced transfection efficiencies.

In recent years, cationic gemini surfactants have attracted considerable research interest as gene delivery vehicles. The physical properties of gemini surfactants are diverse and can be modified through variations in the length of the hydrophobic tails, the nature of the head groups, and the nature and length of the spacer.[13-15,22-24] Gemini surfactants offer basic benefits for gene delivery compared to their monomeric counterparts such as achieving similar transfection efficiencies with less surfactant.[13,14] This reduces the risk of toxicity since lower *in vivo* concentrations are used. Gemini surfactants are of particular interest as gene delivery vehicles due to their ability to self-assemble into micelles of different shapes (spherical, rod-like) even at low concentrations.[22,24] Recently, it has been shown that certain cationic gemini surfactants combine a superior ability to introduce genes into cells with a low toxicity.[23,27,28] In particular, Wang *et al.* found that the DNA transfection efficiency correlated closely with the morphologies of aggregates of gemini surfactants with DNA in aqueous solution.[29] Their conclusions were drawn from the analysis of atomic force microscopy (AFM) images of the complexes formed between the gemini surfactants and DNA. A disadvantage of using AFM to study DNA – gemini surfactant complexes is that the complexes are not imaged in solution but rather adsorbed on mica surfaces which may alter their aggregation properties. To address this

issue, Wang *et al.* substituted one of the alkyl chains of a gemini surfactant with the hydrophobic chromophore pyrene (Py-3-12 shown in Figure 5.1) and studied its interactions with DNA by UV-Vis absorption and fluorescence spectroscopy.[30] These pyrene-substituted gemini surfactants belong to a family of dissymmetrical gemini surfactants, which have shown varying levels of complexation with DNA depending on the degree of dissymmetry exhibited by the surfactant tails.[30] Using fluorescence, Wang *et al.* found that as the concentration of DNA was increased, the amount of gemini surfactant bound to DNA increased, as was evident from the observed enhancement in excimer formation between the two pyrenyl tails of the Py-3-12 molecules brought in close proximity by the polyphosphate backbone.

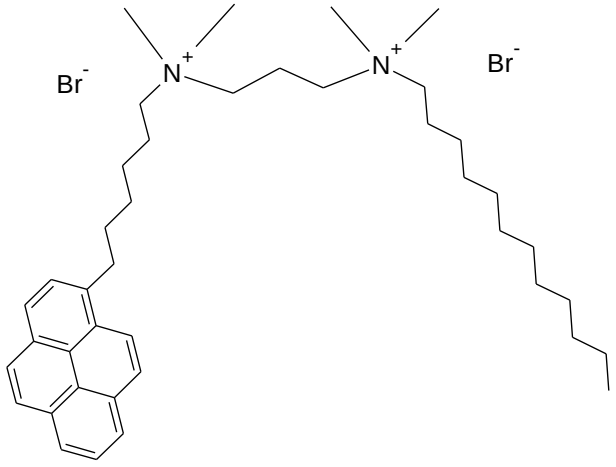

Figure 5.1: Structure of the gemini surfactant, Py-3-12.

To date, the micellization of gemini surfactants and their interactions with DNA have been studied essentially by steady-state fluorescence.[30–34] Most of these experiments use chromophores non-covalently attached to surfactant molecules as fluorescent probes. The interaction between gemini surfactants and DNA is highly co-operative which results in an increase of the local concentration of surfactant molecules along the DNA helix where the hydrophobic tails of the

surfactants interact with one another.[33,34] In water, these interactions provide a hydrophobic environment for a hydrophobic chromophore, such as pyrene. Information about the local polarity of the environment surrounding pyrene is obtained from monitoring the I_1/I_3 ratio of molecular pyrene.[35,36] The I_1/I_3 ratio of pyrene in aqueous solution with DNA and gemini surfactants is lower than when in water alone, revealing that hydrophobic domains are formed between surfactant molecules along the DNA helix.[33,34] These hydrophobic domains can also promote the formation of pyrene excimer. However, when pyrene is used as a free probe, pyrene only reports on the surfactant aggregates which form hydrophobic microdomains, not the isolated surfactant molecules. Therefore, the use of pyrene as a free probe yields a partial description of the surfactant population. In comparison, the interactions between pyrene-substituted gemini surfactants like Py-3-12 and DNA are more inclusive as the individual surfactant molecules can be followed by monitoring the relative amounts of pyrene monomer and excimer in solution by fluorescence.

The steady-state fluorescence spectrum of pyrene provides information about the extent of excimer formation in terms of the ratio of the fluorescence intensity of the excimer over that of the monomer, the $(I_E/I_M)^{SS}$ ratio,[37] where the SS superscript indicates that the I_E/I_M ratio was obtained from steady-state fluorescence measurements. A large $(I_E/I_M)^{SS}$ ratio usually indicates that the pyrenes are close to one another and this observation applies also to the Py-3-12 gemini surfactants. Indeed, Wang *et al.* found that at low ratios of DNA to Py-3-12, which in terms of charges translates into small (–/+) ratios, the $(I_E/I_M)^{SS}$ ratio was small and pyrene was present in the monomer form until a (–/+) ratio near 0.75. At this (–/+) ratio, $(I_E/I_M)^{SS}$ increased drastically indicating an increase in the local concentration of Py-3-12 as expected when the positively charged surfactants cluster along the DNA helix into a lipoplex form.[30] Though the analysis of the steady-state fluorescence of Py-3-12 provides valuable information about the binding of Py-3-12 to DNA, it does not provide quantitative information about the actual molar fractions of Py-3-12 free in solution or bound to DNA. This information can be obtained quantitatively through the analysis of the time-resolved fluorescence

decays of the pyrene monomer and excimer of Py-3-12 with the "Model Free" (MF) procedure.[38,39] The MF analysis can be performed when the kinetics of monomer consumption and excimer formation are coupled. This is usually the case when excimer formation occurs by diffusion. In the MF analysis, the monomer and excimer decays are fit globally by ensuring that the decay times used to describe excimer formation are held the same in both the monomer and excimer decays which results in parameters that are retrieved with greater accuracy. This report builds on the results obtained in Chapter 4 which demonstrated that the MF analysis of the monomer and excimer decays of Py-3-12 yielded a complete description of the population of gemini surfactants in solution. It is now extended to study the population of Py-3-12 gemini surfactants as they interact with DNA.

5.3 Theory

As for the case of excimer formation in Py-3-12 micelles in water described in Chapter 4, excimer formation for Py-3-12 complexed to DNA was assumed to proceed according to Scheme 5.1. All experiments investigating the interactions of Py-3-12 with DNA are performed below the CMC of 0.22 mM for Py-3-12 to ensure that excimer formation is solely a result of the binding of Py-3-12 to DNA. At low ratios of DNA to Py-3-12 ((–/+) ratios), most of the gemini surfactants are isolated in solution and an excited pyrene emits as a pyrene monomer with a lifetime τ_M. These pyrenes are referred to as Py^*_{free}. The rate of excimer formation by diffusion is given by the function $f(t)$ and these pyrenes are referred to as Py^*_{diff}. As with Py-3-12 micelles in water, two excimer species are assumed to be generated in the surfactant micelles complexed with DNA. One has a lifetime, τ_{E0}, of about 55 ns that is typical of pyrene excimer (*E0**) generated by properly stacked pyrenes[40] and a second has a shorter lifetime, τ_D of about 35 ns, which we suspect is originating from pyrene dimers (*D**) that cannot stack properly due to the restricted geometry of the Py-3-12 micelles. Excimer dissociation is small when working at room temperature[40] and it is omitted from Scheme 5.1.

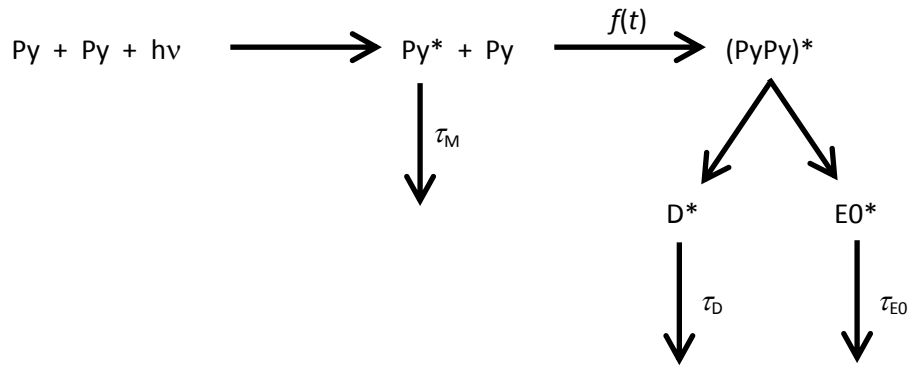

Scheme 5.1: Proposed reaction scheme for excimer formation inside the surfactant micelles.

The derivations of Equations 5.1 and 5.2 used to fit the fluorescence decays of the pyrene monomer and excimer have been described in Chapter 4. Contrary to Py-3-12 micelles in water which required a single exponential to handle $[Py^*_{diff}]_{(t)}$, the process of excimer formation in the Py-3-12 micelles complexed to DNA required two exponentials to describe $[Py^*_{diff}]_{(t)}$. Thus *n* in Equation 5.1 and 5.2 was set to equal 2.

$$[Py^*]_{(t)} = [Py^*_{diff}]_{(t=0)} \times \sum_{i=1}^{n} a_i \times \exp(-t/\tau_i) + [Py^*_{free}]_{(t=0)} \times \exp(-t/\tau_M) + [Py^*_{imp}]_{(t=0)} \times \exp(-t/\tau_{imp}) \quad (5.1)$$

$$[E^*]_{(t)} = -\alpha \times [Py^*_{diff}]_{(t=0)} \times \sum_{i=1}^{n} a_i \frac{\frac{1}{\tau_i} - \frac{1}{\tau_M}}{\frac{1}{\tau_i} - \frac{1}{\tau_{E0}}} \exp(-t/\tau_i)$$

$$+ \left([E0^*]_{(t=0)} + \alpha \times [Py^*_{diff}]_{(t=0)} \times \sum_{i=1}^{n} a_i \frac{\frac{1}{\tau_i} - \frac{1}{\tau_M}}{\frac{1}{\tau_i} - \frac{1}{\tau_{E0}}} \right) \times \exp(-t/\tau_{E0})$$

$$-(1-\alpha) \times [Py^*_{diff}]_{(t=0)} \times \sum_{i=1}^{n} a_i \frac{\frac{1}{\tau_i} - \frac{1}{\tau_M}}{\frac{1}{\tau_i} - \frac{1}{\tau_D}} \exp(-t/\tau_i)$$

$$+ \left([D^*]_{(t=0)} + (1-\alpha) \times [Py^*_{diff}]_{(t=0)} \times \sum_{i=1}^{n} a_i \frac{\frac{1}{\tau_i} - \frac{1}{\tau_M}}{\frac{1}{\tau_i} - \frac{1}{\tau_D}} \right) \times \exp(-t/\tau_D) \qquad (5.2)$$

A short ~ 10 ns decay time in the monomer decay (τ_{imp} in Equation 5.1) could not be accounted for in the global analysis of the monomer and excimer decays. The contribution of this short decay time was small and equaled 0.03 ± 0.01. This contribution might be due to residual quenching of the pyrene monomer by the bromide counterions or a fluorescence impurity generated during the synthesis of Py-3-12. Its contribution was isolated by the MF analysis, and since it was small, it was neglected when determining the molar fractions of the pyrene species, as taking it into account was found not to affect the reported trends (see Chapter 4). The lifetime of the monomer, τ_M, was held constant at 97 ns in the analysis of the fluorescence decays which is the natural lifetime of free Py-3-12 in water. The expressions of the fractions of the pyrene species that contribute to the monomer

(f_{Mdiff} and f_{Mfree}) and to the excimer (f_{Ediff}^{E0} , f_{Ediff}^{D} , f_{EE0}, and f_{ED}) decays are listed in Equations 5.3 – 5.8.

$$f_{Mdiff} = \frac{[Py^{*}_{diff}]_{(t=0)}}{[Py^{*}_{diff}]_{(t=0)} + [Py^{*}_{free}]_{(t=0)}} \tag{5.3}$$

$$f_{Mfree} = \frac{[Py^{*}_{free}]_{(t=0)}}{[Py^{*}_{diff}]_{(t=0)} + [Py^{*}_{free}]_{(t=0)}} \tag{5.4}$$

$$f_{Ediff}^{E0} = \frac{\alpha \times [Py^{*}_{diff}]_{(t=0)}}{[Py^{*}_{diff}]_{(t=0)} + [E0^{*}]_{(t=0)} + [D^{*}]_{(t=0)}} \tag{5.5}$$

$$f_{Ediff}^{D} = \frac{(1-\alpha) \times [Py^{*}_{diff}]_{(t=0)}}{[Py^{*}_{diff}]_{(t=0)} + [E0^{*}]_{(t=0)} + [D^{*}]_{(t=0)}} \tag{5.6}$$

$$f_{EE0} = \frac{[E0^{*}]_{(t=0)}}{[Py^{*}_{diff}]_{(t=0)} + [E0^{*}]_{(t=0)} + [D^{*}]_{(t=0)}} \tag{5.7}$$

$$f_{ED} = \frac{[D^{*}]_{(t=0)}}{[Py^{*}_{diff}]_{(t=0)} + [E0^{*}]_{(t=0)} + [D^{*}]_{(t=0)}} \tag{5.8}$$

Rearrangement of Equations 5.3 – 5.8 into Equations 5.9 – 5.13 yielded the molar fractions of pyrene units that constitute a ground-state dimer giving an excimer *E0** upon direct excitation (f_{E0}), a ground-state dimer giving a shorter-lived excimer *D** upon direct excitation (f_{D}), form an excimer

*E0** by diffusion (f_{diff}^{E0}), form a short-lived excimer *D** by diffusion (f_{diff}^{D}), and are not involved in the formation of excimer (f_{free}).

$$f_{diff}^{E0} = \frac{f_{Ediff}^{E0}}{f_{Ediff}^{E0} + f_{Ediff}^{D}} \times \left(1 + \frac{f_{Mfree}}{f_{Mdiff}} + \frac{f_{EE0}}{f_{Ediff}^{E0} + f_{Ediff}^{D}} + \frac{f_{ED}}{f_{Ediff}^{E0} + f_{Ediff}^{D}} \right)^{-1} \tag{5.9}$$

$$f_{diff}^{D} = \frac{f_{Ediff}^{D}}{f_{Ediff}^{E0} + f_{Ediff}^{D}} \times \left(1 + \frac{f_{Mfree}}{f_{Mdiff}} + \frac{f_{EE0}}{f_{Ediff}^{E0} + f_{Ediff}^{D}} + \frac{f_{ED}}{f_{Ediff}^{E0} + f_{Ediff}^{D}} \right)^{-1} \tag{5.10}$$

$$f_{free} = (f_{diff}^{E0} + f_{diff}^{D}) \times \frac{f_{Mfree}}{f_{Mdiff}} \tag{5.11}$$

$$f_{E0} = (f_{diff}^{E0} + f_{diff}^{D}) \times \frac{f_{E0}}{f_{Ediff}^{E0} + f_{Ediff}^{D}} \tag{5.12}$$

$$f_{D} = (f_{diff}^{E0} + f_{diff}^{D}) \times \frac{f_{D}}{f_{Ediff}^{E0} + f_{Ediff}^{D}} \tag{5.13}$$

The $(I_E/I_M)^{SPC}$ ratio, i.e. the ratio of the fluorescence intensity of the excimer over that of the monomer, can be obtained from the analysis of the fluorescence decays. The superscript SPC differentiates the $(I_E/I_M)^{SPC}$ ratio obtained by single photon counting (SPC) from the $(I_E/I_M)^{SS}$ ratio obtained from steady-state fluorescence experiments. The expression of $(I_E/I_M)^{SPC}$ is obtained by dividing $(I_E)^{SPC}$ calculated using Equation 5.14 by $(I_M)^{SPC}$ calculated using Equation 5.15.

$$\left(I_M\right)^{SPC} = \int_{t=0}^{\infty} [Py^*]_{(t)}\, dt = [Py]_o \times \left((f_{diff}^{E0} + f_{diff}^{D}) \times \sum_{i=1}^{n} a_i \times \tau_i + f_{free} \times \tau_M \right) \tag{5.14}$$

$$\left(I_E\right)^{SPC} = \int_{t=0}^{\infty} [E^*]_{(t)}\, dt = -[Py]_o \times \left[f_{diff}^{E0} \times \sum_{i=1}^{n} a_i \frac{\frac{1}{\tau_i} - \frac{1}{\tau_M}}{\frac{1}{\tau_i} - \frac{1}{\tau_{E0}}} \times \tau_i + \left(f_{E0} + f_{diff}^{E0} \times \sum_{i=1}^{n} a_i \frac{\frac{1}{\tau_i} - \frac{1}{\tau_M}}{\frac{1}{\tau_i} - \frac{1}{\tau_{E0}}} \right) \times \tau_{E0} \right.$$

$$\left. - f_{diff}^{D} \times \sum_{i=1}^{n} a_i \frac{\frac{1}{\tau_i} - \frac{1}{\tau_M}}{\frac{1}{\tau_i} - \frac{1}{\tau_D}} \times \tau_i + \left(f_D + f_{diff}^{D} \times \sum_{i=1}^{n} a_i \frac{\frac{1}{\tau_i} - \frac{1}{\tau_M}}{\frac{1}{\tau_i} - \frac{1}{\tau_D}} \right) \times \tau_D \right] \tag{5.15}$$

$(I_E/I_M)^{SPC}$ is an absolute value that depends solely on the parameters obtained from the MF analysis of the monomer and excimer decays.

The average rate constant $<k>$, which describes excimer formation by diffusion, can also be obtained using Equation 5.16.[38,39,41]

$$< k > = \left(\sum_{i=1}^{n} a_i \times \tau_i \right)^{-1} - \frac{1}{\tau_M} \tag{5.16}$$

5.4 Experimental

Materials. The pyrene substituted surfactant, Py-3-12, was prepared by Dr. Shawn Wettig's research group from the School of Pharmacy at the University of Waterloo. The procedure is described in an earlier publication.[30] Calf Thymus DNA (CT DNA) was purchased from Sigma-Aldrich (Milwaukee, WI). Doubly distilled water (deionized from Millipore Milli-RO 10 Plus and Milli-Q UF Plus (Bedford, MA)) was used in the preparation of all solutions.

Sonicated Calf Thymus DNA. A 0.30 wt% stock solution of CT DNA was left to dissolve in water overnight. The CT DNA stock solution was sonicated for about 30 min with 1 min sonication durations interspaced by 30 sec rest periods. A sonifier cell disrupter (Heat Systems-Ultrasonic Inc, model W-225) set at about 20 W output was used to sonicate CT DNA. The sonicated CT DNA (sCT DNA) was purified by ethanol precipitation and was lyophilized using a Labconco Freezone 6 freeze drier.

Preparation of DNA Stock Solution. Py-3-12 was dissolved in water and freeze dried. An amount of the dried gemini surfactant was weighed and dissolved in water and the concentration of the stock solution was calculated by mass. Stock solutions of 0.3 mM of CT DNA and sCT DNA were prepared in Milli-Q water and the absolute concentrations of the stock solutions were determined spectrophotometrically. A stock solution of 23.6 mM of sCT DNA in water was also prepared for samples having very high DNA concentrations. An extinction coefficient per mole of bp of ε_{260} = 12,000 $M^{-1}cm^{-1}$ was determined experimentally for CT DNA in Milli-Q water. Solutions of Py-3-12 and CT DNA were prepared on the day of use and all the remaining stock was stored in a fridge at 5 °C.

Py-3-12 and DNA Sample Preparation. The interaction of Py-3-12 with CT DNA was studied by fluorescence as a function of the ratio of [DNA] in mM of bp to [Py-3-12] in mM, or the (–/+) ratio. The concentration of Py-3-12 used in the DNA – surfactant solution was kept below the CMC of 0.22 mM[30] so that any excimer formation observed was due to the interaction of Py-3-12 with DNA and not from Py-3-12 micelles in solution. Considering that pyrene has a high absorption coefficient and quantum yield, one would intuitively believe that very low surfactant concentrations could be used.[37] Initially, a concentration of 0.005 mM Py-3-12 was tested, which is well below the CMC of Py-3-12. However, a decrease in the fluorescence signal of Py-3-12 was observed with time, even without DNA. The steady-state fluorescence spectra of the 0.005 mM Py-3-12 solution are shown in Figure 5.2A as a function of time. Gemini surfactants are known for their excellent adsorption properties at

both air/water[42] and solid/water interfaces,[33,43] such that their study requires careful sample preparation to obtain accurate and reproducible results.[32] Therefore, the decrease in fluorescence intensity of Py-3-12 with time shown in Figure 5.2A is likely due to surfactant molecules adsorbing onto the cell walls and migrating out of the path of the incident beam. The lowest concentration of Py-3-12 that resulted in a minimal decrease in fluorescence intensity with respect to time, while still being below the CMC, was 0.1 mM. The steady-state fluorescence spectra of 0.1 mM Py-3-12 with increasing time are shown in Figure 5.2B which demonstrates that any adsorption onto the sides of the cuvette does not affect the fluorescence signal. Therefore, the concentration of Py-3-12 was kept at 0.1 mM for DNA – surfactant solutions having a (–/+) ratio of 2.0 and less.

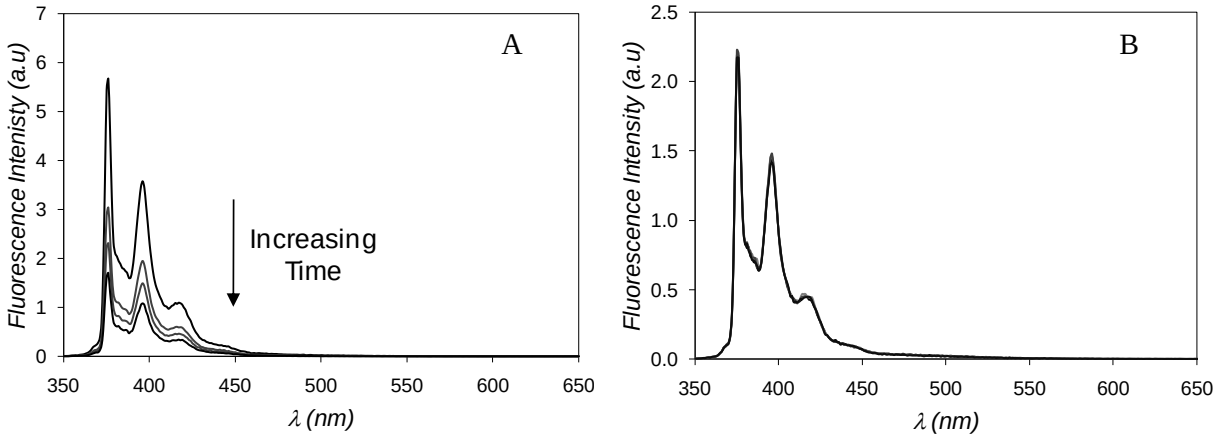

Figure 5.2: Steady-state fluorescence spectra of high and low concentrations of Py-3-12 with time. A) 0.005 mM Py-3-12 and B) 0.1 mM with increasing time intervals of 40 min up to 2 hrs.

The concentration of CT DNA was varied to change the (–/+) ratio. For (–/+) ratios greater than 2.0, sCT DNA was used exclusively. The shorter average length of sCT DNA minimized the increase in solution viscosity that was experienced at large CT DNA concentrations. Nevertheless, solutions were prepared with (–/+) ratios as large as 1,000. For so large (–/+) ratios, the amount of sCT DNA required while maintaining a 0.1 mM Py-3-12 concentration was so large that either a substantial increase in viscosity was observed, or the sCT DNA was no longer soluble. Therefore, a lower

concentration of Py-3-12 had to be used to maintain a same (–/+) ratio. To overcome the problem of Py-3-12 adsorbing onto the cuvette walls at very low Py-3-12 concentration, a stock solution with a (–/+) ratio of 2.0 was prepared. This stock solution was diluted to yield a final [Py-3-12] equal to 0.01 mM and sCT DNA was added to generate the desired (–/+) ratio. It was observed that once Py-3-12 was complexed with DNA, dilution of this solution did not result in changes in the intensity of the steady-state fluorescence spectrum. Figures SI 5.1A and B in the Supporting information (SI) show the steady-state fluorescence spectra of DNA – surfactant solutions having a (–/+) ratio of 2.0 and a 10-fold dilution of that solution, respectively. Very little change was observed in the fluorescence spectrum over time. This suggests that the driving force of Py-3-12 to adsorb onto the cuvette walls is reduced once Py-3-12 is complexed with DNA.

Steady-State Fluorescence Spectroscopy. Steady-state fluorescence measurements were acquired with a Photon Technology International (PTI) LS-100 steady-state fluorometer equipped with an Ushio UXL-75Xe Xenon arc flash lamp and a PTI 814 photomultiplier. Samples were excited at a wavelength of 344 nm. The resulting emission spectrum was collected from 350 to 600 nm. The monomer intensity, I_M, and the excimer intensity, I_E, were obtained by taking the integral of the fluorescence spectrum from 374 – 378 nm and 500 – 530 nm for the monomer and excimer, respectively. The spectra of all solutions were acquired with the right angle geometry.

Steady-State Fluorescence Time Studies. Although conditions were found to minimize the effect that Py-3-12 adsorbing onto the cell walls has on the fluorescence data, the binding of Py-3-12 to DNA was found to occur over approximately 1 hr so that the fluorescence intensity of the pyrene monomer and excimer for Py-3-12 binding to CT DNA varied within this time frame. This effect was more pronounced near the transition around a (–/+) ratio of 1.0. To ensure that the $(I_E/I_M)^{SS}$ ratio was taken when the binding of Py-3-12 to CT DNA reached equilibrium, the steady-state fluorescence spectrum of each sample was monitored over time and acquired until changes were no longer observed in the fluorescence spectrum of Py-3-12. Figure SI 5.2A shows the steady-state fluorescence spectra

acquired until equilibrium was reached for a (–/+) ratio of 1.0. The $(I_E/I_M)^{SS}$ ratio was calculated from the fluorescence spectra acquired over a 1 hour time period for the solution with a (–/+) ratio of 1.0 and its values are plotted in Figure SI 5.2B. The intensity of the scattered light (I_S) centered around 688 nm resulting from irradiating the solution with an excitation wavelength of 344 nm was also plotted as a function of time in Figure SI 5.2B. Figure SI 5.2B shows that I_S does not change with respect to time whereas $(I_E/I_M)^{SS}$ does, suggesting that the change in $(I_E/I_M)^{SS}$ results from rearrangements of Py-3-12 with DNA and is not due to precipitation of large complexes.

Time-Resolved Fluorescence Spectroscopy. Time-resolved fluorescence decays were acquired when each sample had reached equilibrium as determined by steady-state fluorescence. A steady-state fluorescence spectrum was also obtained after the monomer and excimer decays were acquired for each sample. It was compared to the fluorescence spectrum obtained before the fluorescence decays were acquired. Similar fluorescence spectra that were obtained before and after the decay acquisition confirmed that binding of Py-3-12 to DNA had reached equilibrium. Fluorescence decays were acquired with an IBH Ltd. time-resolved fluorometer. The light source was an IBH 340 nm NanoLED. All solutions were excited at 344 nm and the fluorescence emission from the pyrene monomer and excimer was monitored at 375 and 510 nm, respectively. Filters were used with a cutoff at 370 nm and 495 nm to acquire the fluorescence decays of the pyrene monomer and excimer, respectively. This was done to block potential light scattering leaking through the detection system. Fluorescence decays were acquired over 1024 channels with a 1 MHz repetition rate. Decays were acquired at a time per channel of 0.24 ns/ch using the right angle geometry. To ensure a high signal-to-noise ratio, the instrument response function (IRF) and fluorescence decays were acquired until a peak maximum of 20,000 counts was reached. A Ludox solution was used to obtain the IRF. All decays were deconvoluted from the IRF and fitted to the desired function using a least-squares analysis.

Analysis of the Fluorescence Decays. The fluorescence decays of the pyrene monomer and excimer were fit independently with a sum of exponentials according to Equation 5.17 with n = 2 – 4 depending on the level of binding of Py-3-12 to DNA. All excimer decays were fit with n = 4 in Equation 5.17.

$$i(t) = \sum_{i=1}^{n} a_i e^{-t/\tau_i} \tag{5.17}$$

Analysis of the fits of the fluorescence decays with Equation 5.17 revealed that two decay times were coupled between the pyrene monomer and excimer. Therefore, the fluorescence decays of the pyrene monomer and excimer of Py-3-12 were also fit globally with Equations 5.1 and 5.2, respectively, with n = 2.

5.5 Results and Discussion

The steady-state fluorescence spectra were first obtained for CT DNA to Py-3-12 ratios, or more concisely, (–/+) ratios, up to 2. The steady-state fluorescence spectra are shown in Figure 5.3 and have been normalized to 1 at the monomer peak which occurs between 375 – 377 nm depending on the DNA concentration used. Very low DNA concentrations resulted in no excimer formation. As the DNA concentration was increased, some excimer began to form. Further increase in the concentration of DNA resulted in a large increase in the fluorescence emission of the pyrene excimer until a point was reached where the fluorescence spectrum no longer changed with further addition of DNA. The fluorescence spectra in Figure 5.3 show that the addition of DNA to Py-3-12 induces excimer formation and the extent of excimer formation for each (–/+) ratio can be quantified with the $(I_E/I_M)^{SS}$ ratio.

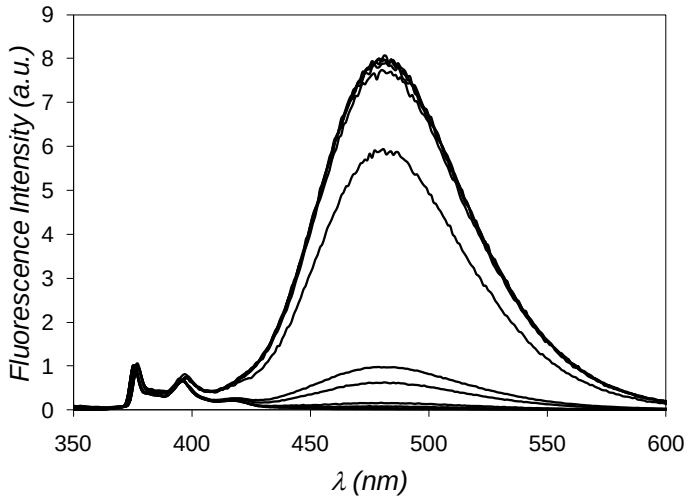

Figure 5.3: Steady-state fluorescence spectra of solutions of DNA and Py-3-12. The concentration of DNA was increased from 0 to 0.2 mM in terms of base pairs for a constant Py-3-12 concentration of 0.1 mM, λ_{ex} = 344 nm.

The $(I_E/I_M)^{SS}$ ratios were determined for mixtures of Py-3-12 with two DNA solutions, one prepared with CT DNA and the other with sCT DNA. The viscosity of CT DNA solutions increases with increasing CT DNA concentration, making sample preparation more difficult for large DNA concentrations. To minimize the increase in viscosity, CT DNA was sonicated to yield sCT DNA with a reduced average length. In so doing, sCT DNA solutions could be prepared with DNA concentrations as high as 6.6 g/L with no apparent increase in solution viscosity. However, to reach (–/+) ratios as large as 1,000 would have required a sCT DNA equal to 66 g/L which could not be prepared due to solubility issues. Consequently, for (–/+) ratios greater than 2.0, a Py-3-12 concentration of 0.01 mM was used with the required amount of sCT DNA to obtain the desired (–/+) ratio. As demonstrated in the Experimental section, small concentrations of Py-3-12 were found to be less likely to adsorb onto the cell walls if they were complexed with DNA beforehand (Figures A 5.1A and B).

The $(I_E/I_M)^{SS}$ ratios were obtained and are plotted in Figure 5.4A and B as a function of the (–/+) ratio for CT DNA and sCT DNA, respectively. Similar trends were obtained at low (–/+) ratios where very little excimer is formed and the $(I_E/I_M)^{SS}$ ratio is small. As the (–/+) ratio approaches unity, the $(I_E/I_M)^{SS}$ ratio begins to increase as more excimer is formed following the binding of Py-3-12 to the negative charges of the DNA backbone. At a (–/+) ratio of 1 for CT DNA and 1.2 for sCT DNA, the $(I_E/I_M)^{SS}$ ratio increases drastically before reaching a plateau.

For (–/+) ratios larger than 2.0, the $(I_E/I_M)^{SS}$ ratios were obtained for solutions of sCT DNA and Py-3-12 and are shown in Figure 5.4B. The $(I_E/I_M)^{SS}$ ratio reached a maximum value near 4.5 and a slight decrease in $(I_E/I_M)^{SS}$ was observed after a (–/+) ratio of 2.0. The maximum obtained for the complexation of Py-3-12 with sCT DNA was lower than the maximum around 6 obtained for CT DNA. Once the (–/+) ratio reaches 10, the $(I_E/I_M)^{SS}$ ratio keeps decreasing. After a (–/+) ratio of 100, no excimer is observed and the fluorescence emission is solely due to the pyrene monomer.

Traces similar to that shown in Figure 5.4A and B for (–/+) ratios smaller than 2.0 have been observed for the binding of Py-3-12 and other gemini surfactants onto DNA, with a dramatic change found at some critical $(–/+)_o$ ratio for variables like the $(I_E/I_M)^{SS}$ ratio, surface tension, enthalpy change, or the I_1/I_3 ratio.[30–34] The position of $(–/+)_o$ reported in these other studies departs somewhat from the value of 1.0 and 1.2 found in the present study, certainly due to the facile adsorption of gemini surfactants onto surfaces which complicates its accurate determination. In any case, pronounced S-shaped traces like the one shown in Figures 5.4A and B around $(–/+)_o$ are usually taken as indicative of cooperative binding. In fact, such traces are misleading. Intuitively, electrostatic forces are expected to induce binding of the cationic Py-3-12 surfactant onto the DNA polyanion at (–/+) ratios that are smaller than $(–/+)_o$. In this regime of (–/+) ratios, each DNA molecule is in the presence of a large excess of surfactant molecules which are driven to interact with DNA via electrostatic forces. Whether this binding occurs cooperatively can only be answered by determining the actual action mass laws that exist between the states in which the Py-3-12 molecules distribute

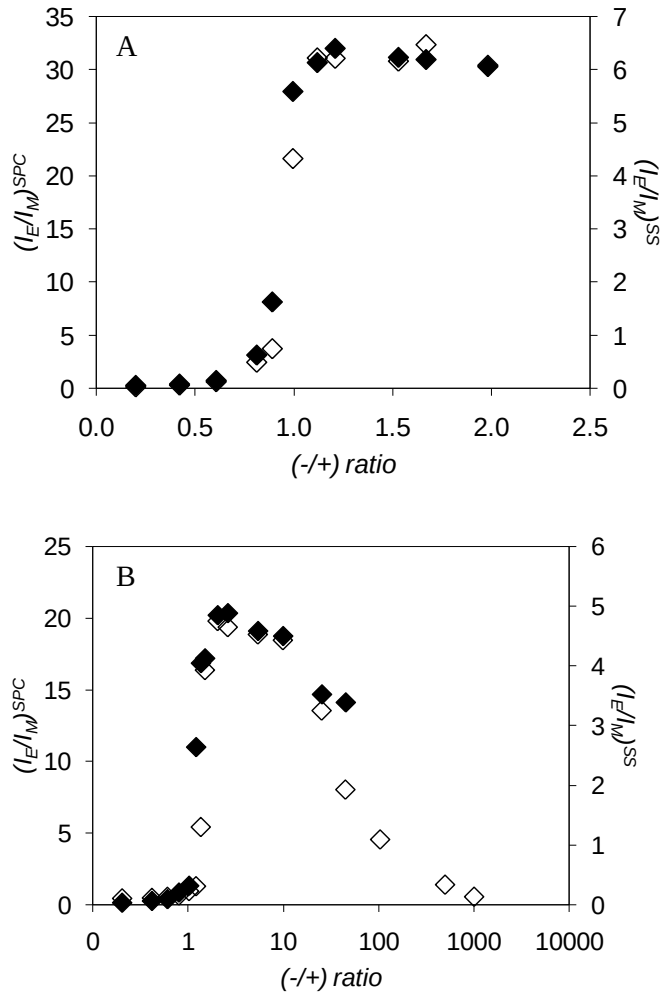

Figure 5.4: $(I_E/I_M)^{SS}$ and $(I_E/I_M)^{SPC}$ versus the (–/+) ratio. A) $(I_E/I_M)^{SPC}$ (filled diamonds) and $(I_E/I_M)^{SS}$ (hollow diamonds) and $(I_E/I_M)^{SPC}$ (hollow diamonds) as a function of (–/+) ratio for the complexation of Py-3-12 with CT DNA. B) $(I_E/I_M)^{SPC}$ (filled diamonds) and $(I_E/I_M)^{SS}$ (hollow diamonds) and $(I_E/I_M)^{SPC}$ (hollow diamonds) as a function of (–/+) ratio in logarithmic scale for the complexation of Py-3-12 with sheared CT DNA.

themselves when DNA is present. In turn, this requires the knowledge of the molar fractions of the different Py-3-12 species found in solution, an information that can be obtained by conducting the global analysis of the monomer and excimer fluorescence decays acquired with solutions of DNA and

Py-3-12 mixtures.[34,35] To this end, time-resolved fluorescence measurements were carried out on the Py-3-12 and DNA solutions.

The monomer and excimer fluorescence decays of solutions of CT DNA and Py-3-12 were acquired for all samples with a TPC equal to 0.24 ns/ch since the decay times which are coupled between the monomer and excimer describe processes that occur on a time scale of about 4 ns or less. MF analysis of the fluorescence decays acquired with this TPC was found to provide sufficiently accurate information about the longer decay times and their pre-exponential factors. However, before the MF analysis was applied, the monomer and excimer decays were fit with a sum of exponentials according to Equation 5.17 and the decay times and pre-exponential factors retrieved from this analysis are listed in Table SI 5.1 in the Supporting Information. At a (–/+) ratio of zero, the pyrene monomer decays biexponentially with a small contribution (~0.03) for a decay time of about 9 ns and a major contribution (~0.97) for a decay time equal to 97 ns. The 97 ns decay time was assigned to the natural lifetime of Py-3-12 (τ_M) as was done in Chapter 4. The small contribution to the monomer decay was assigned to a fluorescence impurity present in too small an amount to be detected by NMR. It was found to have the same contribution at all (–/+) ratios. At a (–/+) ratio of 1 and larger, when a large increase in excimer fluorescence is observed (Figure 5.4), the pre-exponential factor a_{M1} in Table SI 5.1 becomes negligible (< 0.01) and τ_{M1} becomes unreliable. Nevertheless, the small a_{M1} value suggests that little pyrene monomer remains free in solution. The excimer decay times, τ_{E1} and τ_{E2}, remain constant with increasing DNA concentration and equal to, respectively, 60 ± 2 ns and 30 ± 2 ns which correspond to the excimer decay times τ_{E0} and τ_D found for the Py-3-12 micelles obtained without DNA in Chapter 4. This observation indicates that the fluorescence emission observed around 480 nm in the steady-state fluorescence spectra in Figure 5.2 occurs as a result of Py-3-12 aggregates bound to DNA, i.e. the formation of the "beads on a string" complex, and is not due to the formation of a pyrene exciplex with the bases on DNA.

The fits of the pyrene monomer and excimer decays with a sum of exponentials show that two decay times, one around 3 ns (τ_{M3}) and one around 0.8 ns (τ_{M4}), appear as a decay time (positive pre-exponential factor) in the monomer decays and as a rise time (negative pre-exponential factor) in the excimer decays. The magnitude of the pre-exponential factors associated with the decay- and rise-times increases with DNA concentration, a "telltale" sign that the disappearance of the monomer is coupled with the appearance of the excimer. As with Py-3-12 micelles, the short decay- and rise-times of 3.0 ns and 0.8 ns found in the analysis of the fluorescence decays indicate that pyrene excimer formation by diffusion occurs on a fast time scale, as would be expected of pyrenes located close to each other. In Py-3-12 micelles alone (i.e. not complexed to DNA), only one fast decay time of about 1 ns was found for excimer formed by diffusion. In the case of Py-3-12 complexed to DNA, an additional slightly longer decay time of 3 ns is obtained suggesting that slower dynamics are involved in the process of excimer formation. The ratio of the negative pre-exponential factor divided by the sum of the positive pre-exponential factor(s), the A_-/A_+ ratio, retrieved from the analysis of the excimer decays with a sum of exponentials according to Equation 5.17, gives an indication of whether the excimer is formed via diffusion or excitation of pre-associated pyrenes. A value of A_-/A_+ of -1 indicates that the pyrene excimer is formed via diffusion and values of A_-/A_+ approaching 0 indicate that the pyrene excimer is formed from the direct excitation of pyrene aggregates. The A_-/A_+ ratios for the binding of Py-3-12 to CT DNA are listed in Table SI 5.1. The A_-/A_+ ratio was constant and took an average value of -0.78 ± 0.06 which indicates that most of the excimer is formed via diffusion. The A_-/A_+ ratio of -0.78 is similar to that of -0.70 ± 0.04 obtained for Py-3-12 micelles in solution with no DNA (see Chapter 4).

The monomer and excimer fluorescence decays of solutions of sCT DNA and Py-3-12 were also acquired with a TPC equal to 0.24 ns/ch for all (–/+) ratios. The monomer and excimer decays were fit with a sum of exponentials according to Equation 5.17 and the decay times and pre-exponential factors are listed in Table SI 5.2 in the Supporting Information. Up to a (–/+) ratio of 10, the results

obtained for the complexation of Py-3-12 with sCT DNA are the same as the results obtained with CT DNA up to a (–/+) ratio of 2. For (–/+) ratios larger than 10, the A_-/A_+ ratio becomes more positive, i.e. its absolute value decreases. Beyond a (–/+) ratio of 100, no rise time can be found and very fast decay times are observed which show up as a "spike" in the excimer decays. This trend is illustrated in Figure 5.5 which shows the early times of the excimer decays for (–/+) ratios of 10 and higher.

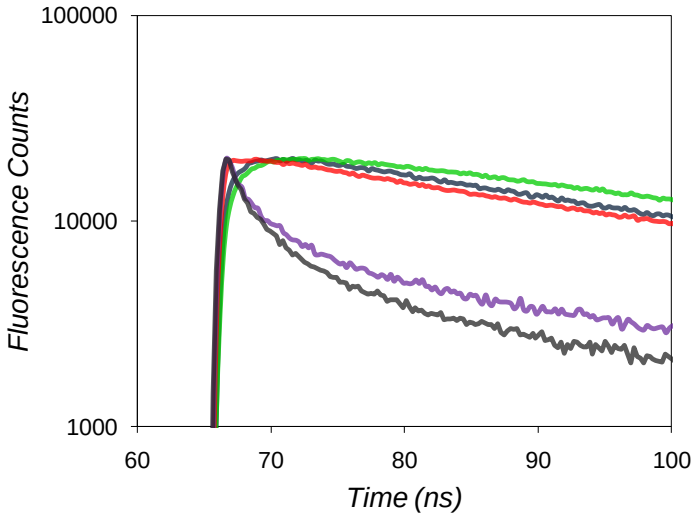

Figure 5.5: Early times of the fluorescence decays of the pyrene excimer of Py-3-12. Decays were acquired for solutions having (–/+) ratios of 10 (green), 50 (blue), 100 (red), 500 (purple), 1000 (grey); λ_{ex} = 344 nm, λ_{em} = 510 nm, TPC = 0.42 ns/ch.

The decay times of the pyrene monomer seemed to be less affected at high (–/+) ratios. The absence of a rise time in the excimer decays for large (–/+) ratios prevents the application of the global analysis of the decays with the MF equations because the pyrene monomer and excimer are no longer coupled.

At first glance, the decrease in the absolute value of the A_-/A_+ ratio at (–/+) ratios greater than 10 would suggest that excimer formation proceeds more readily via direct excitation of pyrene aggregates rather than diffusive encounter. However, as previously stated, trends obtained by steady-

state fluorescence indicate that less excimer is being formed at ratios greater than 10 (Figure 5.4B). These contradicting conclusions led us to question whether all fluorescent species had been considered in our analysis, especially when working at these high DNA concentrations. DNA is known to absorb at 260 nm. Solutions of Py-3-12 and DNA were excited at 344 nm where pyrene is the only species that should absorb at this wavelength. At very high (–/+) ratios, the concentration of DNA is obviously very high. At the largest (–/+) ratio studied, the 6.6 g/L DNA solution has an equivalent base pair (bp) concentration of 0.01 M. Using the molar extinction coefficient of CT DNA expressed in mole of bp in Milli-Q water of 12,000 $M^{-1}cm^{-1}$ at 260 nm, a DNA concentration of 0.01 M in bp, and a 0.3 cm path length cell, the optical density of this solution equals 36.0. A sCT DNA solution this concentrated results in an absorbance of about 0.1 at 344 nm even though it was free of Py-3-12. The absorption at 344 nm due to sCT DNA is no longer negligible when compared to that of the 0.01 mM solution of Py-3-12 which equals 0.12 (1×10^{-4}M × 40,000 cm/M^{-1} × 0.3 cm). Interestingly, the 6.6 g/L sCT DNA solution without Py-3-12 fluoresced when excited at 344 nm. The absorbance and steady-state fluorescence spectra of the sCT DNA solution free of Py-3-12 are shown in the Supporting Information in Figures SI 5.3A and B, respectively. The fluorescence decays of a 6.6 g/L sCT DNA solution without Py-3-12 were acquired with an excitation wavelength of 344 nm and emission wavelengths set at 375 nm and 510 nm, where the pyrene monomer and excimer decays were acquired, respectively. These decays were fit with a sum of exponentials according to Equation 5.17 with $n = 3$ and the decay times and pre-exponential factors are given in Table SI 5.3. The fluorescence decay profiles of the 6.6 g/L sCT DNA solution acquired at 375 nm and 510 nm are shown in Figure 5.6. The steady-state fluorescence and decay times of DNA have been reported in the literature. Although the absorption and emission of DNA depends on several factors such as DNA sequence and length,[44,45] as well as excitation wavelength,[46] the fluorescence spectra compare well with those found for DNA shown in Figure SI 5.3 and 5.6, respectively. The

decay profiles in Figure 5.6 resemble the excimer decays acquired for solutions of Py-3-12 and sCT DNA at (–/+) ratios of 500 and 1000 which are shown in Figure 5.5.

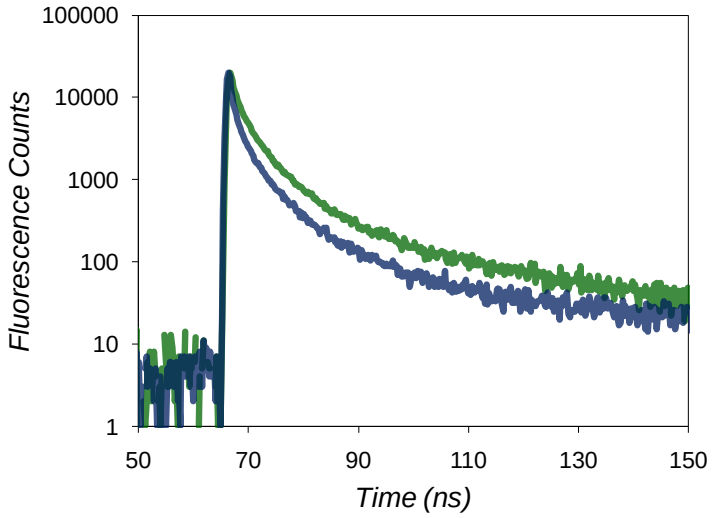

Figure 5.6: Fluorescence decay profiles of 0.01 M CT DNA. Decays were acquired at λ_{em} = 375 nm (blue) and λ_{em} = 510 nm (green); λ_{ex} = 344 nm, TPC = 0.42 ns/ch.

The decay times obtained from the analysis of the fluorescence decays of the 6.6 g/L sCT DNA solution acquired at 375 nm and 510 nm were compared to the decay times obtained from the analysis of the decays acquired with solutions of Py-3-12 and sCT DNA having a (–/+) ratio equal to 500 and 1000. They too were found to be similar equal to ~ 1 ns and 4 ns. The fast decay times of ~ 1 ns and ~4 ns found in the analysis of the excimer decays acquired with the Py-3-12 and sCT DNA solutions at (–/+) ratios of 500 and 1000 should not be confused with the rise times observed in the excimer decays at lower (–/+) ratios. A rise time has a negative pre-exponential factor and indicates that excimer is formed via the diffusive encounter of an excited and a ground-state pyrene monomer as is the case with Py-3-12 micelles bound to CT DNA. For solutions having a (–/+) ratio of 500 and 1000, the excimer decays show no rise time and only a decay time which appears as a "spike". In

fact, this "spike" seems to arise from the fluorescence emission of CT DNA itself and not from Py-3-12. This fast decay was also observed by Costa *et al.* who used molecular pyrene to probe the interactions between gels of cross-linked DNA and the cationic surfactant, cetyltrimethylammonium bromide (CTAB), at DNA concentrations of 10 g/L.[47] In these fluorescence experiments, DNA contaminates the fluorescence of the probe so that experiments performed at high DNA concentrations should be interpreted with caution, especially when quantitative results are required. In the present study, the results obtained from the MF analysis are discussed for (–/+) ratios smaller than 10.

The monomer and excimer decays of Py-3-12 and DNA were fit globally with Equations 5.7 and 5.8, respectively, with $n = 2$. For all samples, two rise times were found in the excimer decays. The molar fractions of all pyrene species in solution were calculated using Equations 5.9 – 5.13. The total fraction of pyrene that forms excimer via diffusion, f_{diff}, is the sum $f_{diff}^{E0} + f_{diff}^{D}$ and the total fraction of aggregated pyrenes, f_{agg}, is the sum $f_{E0} + f_{D}$. The decay times and pre-exponential factors retrieved from the global analysis of the pyrene monomer and excimer decays with CT DNA and sCT DNA have been listed in the Supporting Information in Table SI 5.4 and Table SI 5.5, respectively. The resulting fits were excellent with all χ^2 smaller than 1.20 and residuals and autocorrelation function of the residuals randomly distributed around zero. As with Py-3-12 without DNA, the fraction of the fluorescent impurity found in the monomer decays was isolated and found to be present in all solutions with a fraction of 0.03 ± 0.01 and 0.05 ± 0.01 when monitoring the interactions of Py-3-12 with CT DNA and sCT DNA, respectively.

The $(I_E/I_M)^{SPC}$ ratio for the complexation of Py-3-12 with CT DNA and sCT DNA was found by taking the ratio of $(I_E)^{SPC}$ to $(I_M)^{SPC}$ which were calculated using Equation 5.15 and 5.14, respectively. The $(I_E/I_M)^{SS}$ and $(I_E/I_M)^{SPC}$ are compared in Figure 5.4A and B for the interaction on Py-3-12 with CT DNA and sCT DNA, respectively. Figure 5.4A shows that the trends observed for $(I_E/I_M)^{SS}$ and $(I_E/I_M)^{SPC}$ are in excellent agreement for the complexation of Py-3-12 with CT DNA. Figure 5.4B

shows that $(I_E/I_M)^{SS}$ and $(I_E/I_M)^{SPC}$ only compare well for (–/+) ratios smaller than 10 but they differ for (–/+) ratios larger than 10. This result correlates well with the decrease in the ratio A_-/A_+ observed for (–/+) ratios greater than 10 and indicates that this decrease is not due to an increase in the aggregation of Py-3-12. If the decrease in the ratio A_-/A_+ was due to the fluorescence of pyrene aggregates, then the ratios $(I_E/I_M)^{SS}$ and $(I_E/I_M)^{SPC}$ would still match as they both take into account all pyrene species that fluoresce. The discrepancy observed for the ratios $(I_E/I_M)^{SS}$ and $(I_E/I_M)^{SPC}$ at (–/+) ratios of 10 and higher for solutions of sCT DNA and Py-3-12 is due to the fluorescence of sCT DNA which contaminates the excimer decays of Py-3-12 and prevents the global analysis of the decays.

The pyrene fractions, f_{free}, f_{diff}, and f_{agg} were calculated for (–/+) ratios smaller than 10 for the CT DNA and sCT DNA solutions and they are plotted in Figure 5.7 as a function of the (–/+) ratio. The fractions of Py-3-12 without DNA were the fractions obtained from the MF analysis carried out in Chapter 4 for a Py-3-12 concentration of 0.l mM. Without DNA, a small fraction of pre-associated surfactant is present in solution as evidenced by the non zero f_{diff} and f_{agg} fractions, probably due to the presence of pre-micellar aggregates.[30,48] At low (–/+) ratios, the surfactant is in excess. The fraction f_{free} is the largest which indicates that most of the surfactant is free in solution. Since the concentration of DNA is small in this regime, DNA molecules are expected to maximize their interactions with bound surfactants since the binding of gemini surfactants to DNA is highly co-operative.[33–34] Py-3-12 cluster near one another along the DNA helix to promote interactions between the hydrophobic tails. This binding induces bending and condensation of long DNA strands into a "beads on a string" structure.[30,49–52] The fraction f_{free} decreases until a point is reached where there is almost no free surfactant in solution and almost all Py-3-12 is bound to the DNA. At a (–/+) ratio of 1.0, the point of charge neutrality, the Py-3-12 molecules are all bound to the DNA. Excimer lifetimes of 30 ± 2 ns and 61 ± 2 ns were obtained for, respectively, τ_D and τ_{E0} in Scheme 5.1. These lifetimes are identical to those obtained in Chapter 4 for the excimer in Py-3-12 micelles without DNA. This observation suggests that the binding of Py-3-12 onto DNA results in the formation of

structures similar to those formed in water, possibly micelles. Once the Py-3-12 aggregates are formed along the DNA helix, an increase in CT DNA concentration does not affect the manner in which excimer is formed since the Py-3-12 aggregates are the loci of excimer formation.

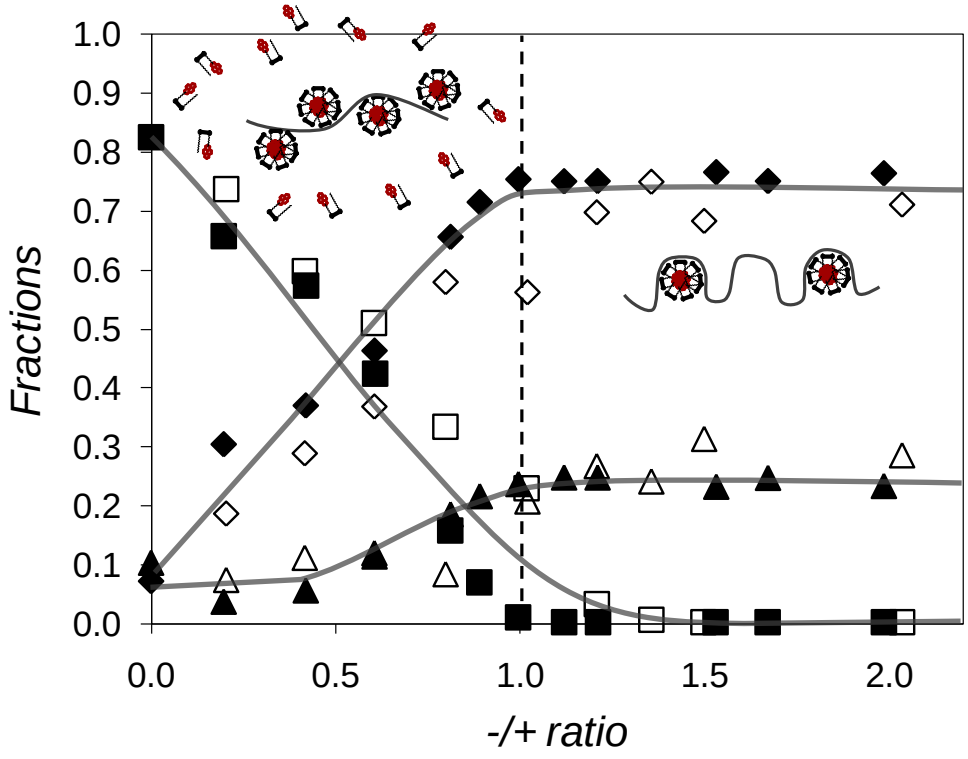

Figure 5.7: The fractions of the Py-3-12 species in solution a function of (–/+) ratio; f_{free} (squares), f_{diff} (diamonds), and f_{agg} (triangles), filled CT DNA, hollow sCT DNA. The dashed line represents the transition occurring at a (–/+) ratio of 1.0.

The average rate constant $\langle k \rangle$ at which excimer is formed in the Py-3-12 aggregates complexed to CT DNA was calculated using Equation 5.16 with $n = 2$. $\langle k \rangle$ was plotted as a function of the (–/+) ratio in Figure 5.8 for solutions of Py-3-12 and CT DNA or sCT DNA. At low (–/+) ratios, $\langle k \rangle$ is similar to $\langle k \rangle$ obtained for Py-3-12 micelles in water which was found to equal $79.2 \pm 2.3 \times 10^7$ s^{-1}. Although the Py-3-12 aggregates must be bound to DNA since the Py-3-12 concentration is smaller

than the CMC of 0.22 mM, their internal dynamics seem to be unaffected by the presence of DNA and are similar to those formed in the Py-3-12 micelles. The similar internal dynamics, and short (30 ns) and long (61 ns) lifetimes of the excimer found for the Py-3-12 micelles or aggregates bound to DNA, suggest that the Py-3-12 aggregates bound to DNA adopts a structure that is similar to that of the Py-3-12 micelles in solution as would be expected from a "beads on a string" model.[30,49–52] Furthermore, the internal dynamics of the Py-3-12 micelles free in solution or bound to DNA also suggests that when the concentration of Py-3-12 is in excess of the concentration of DNA, the micelles are bound to the DNA via a minimal number of contact points. As the (–/+) ratio increases, more Py-3-12 micelles are formed along the DNA helix and more DNA is available to bind to the Py-3-12 micelles, and <*k*> decreases. At a (–/+) ratio of 1.0, all surfactants in solution are bound to DNA (Figure 5.7) and <*k*> plateaus and equals $50 \pm 3 \times 10^7$ s^{-1} for CT DNA and 42 ± 5 for sCT DNA.

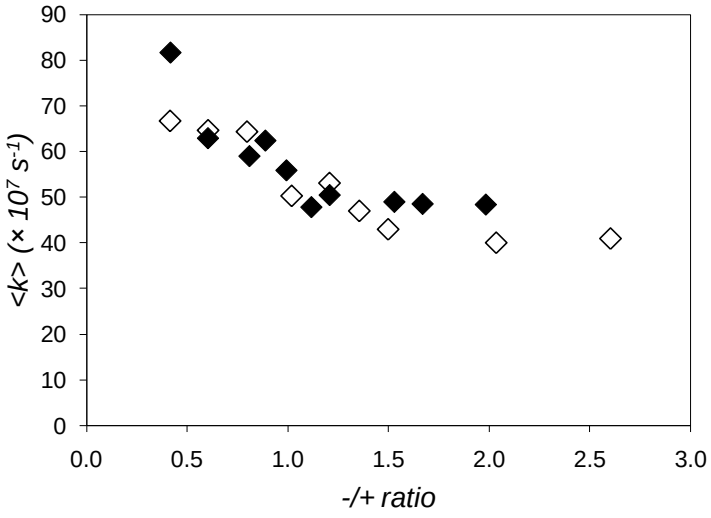

Figure 5.8: Plot of <*k*> as a function of the (–/+) ratio for solutions of Py-3-12 and DNA; CT DNA (filled diamonds) and sCT DNA (hollow diamonds).

The plateau reached by <*k*> for (–/+) ratios greater than 1 suggests that the Py-3-12 micelles bound to DNA retain the same structure as the (–/+) ratio varies from 1.0 to 10. The decrease in <*k*> with increasing (–/+) ratios observed for micelles bound to the DNA helix might be due to a slowed mobility of the surfactant molecules. Addition of more DNA to the solution increases the number of DNA – surfactant contacts which further reduce the internal dynamics of the Py-3-12 micelles bound to DNA. Even though <*k*> for excimer formation in micelles bound to DNA is smaller than that for micelles in water, their interior is still relatively fluid as most of the excimer is formed via diffusion, an important feature for effective gene delivery.

Taken at face value, the trends obtained for the I_E/I_M ratios in Figure 5.4 suggest that a major transition is occurring for the binding of Py-3-12 to DNA near the point of charge neutrality. However, this conclusion is contradicted by the trends of the molar fractions f_{free}, f_{diff}, and f_{agg} in Figure 5.7 which show no discontinuity but rather a gradual relationship with increasing DNA concentration up to a (–/+) ratio of 1. Intuitively, $(I_M)^{SPC}$ and $(I_E)^{SPC}$ should display a trend similar to that obtained for the molar fractions of pyrene in solution since f_{free} is the main contribution to the monomer fluorescence whereas f_{diff} and f_{agg} are associated with the generation of excimer fluorescence. The values of $(I_M)^{SPC}$ and $(I_E)^{SPC}$ were calculated using Equations 5.14 and 5.15, respectively, and they are plotted as a function of the (–/+) ratio in Figure 5.9. The trends of $(I_M)^{SPC}$ and $(I_E)^{SPC}$ also show a gradual relationship with increasing DNA concentration up to a (–/+) ratio of 1. As the (–/+) ratio is increased from 0 to 1, $(I_M)^{SPC}$ decreases and $(I_E)^{SPC}$ increases in a continuous manner that together combine to yield the $(I_E/I_M)^{SPC}$ trends shown in Figure 5.4 and in the inset of Figure 5.9 with the same discontinuity observed in the $(I_E/I_M)^{SS}$ trends.

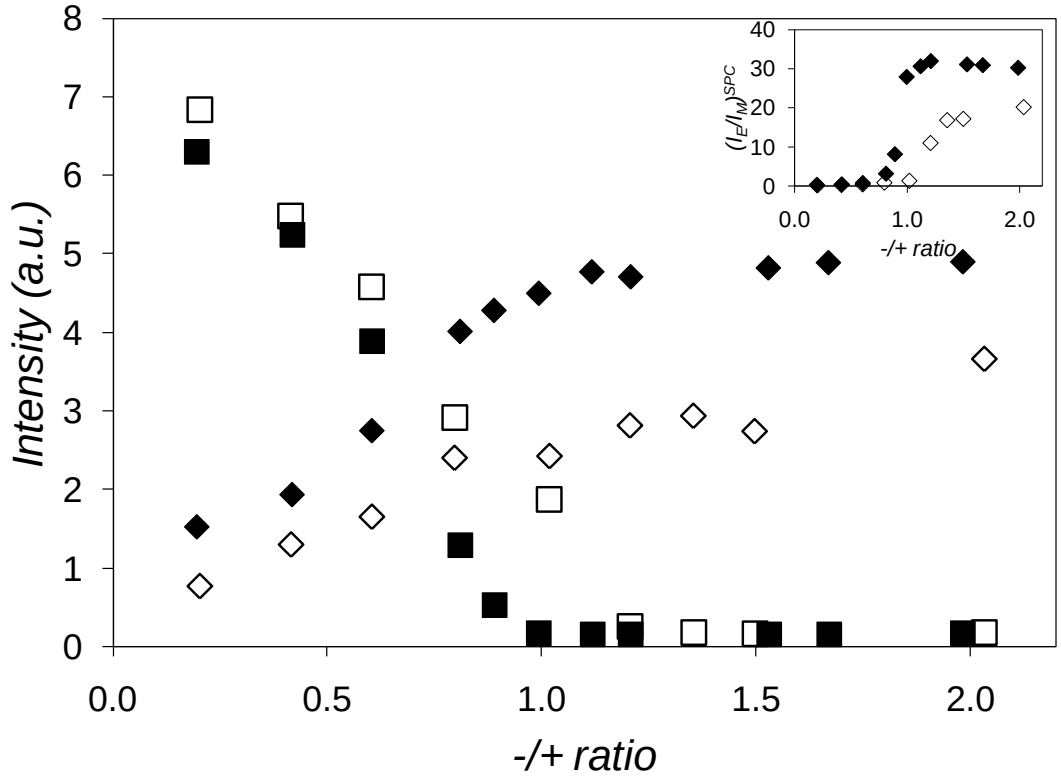

Figure 5.9: Plot of $(I_M)^{SPC}$, $(I_E)^{SPC}$ and $(I_E/I_M)^{SPC}$ as a function of (–/+) ratio. Plot of $(I_M)^{SPC}$ (squares) and $(I_E)^{SPC}$ (diamonds) and sCT DNA (hollow diamonds) as a function of the (–/+) ratio for solutions of Py-3-12 and CT DNA (filled) and sCT DNA (hollow). Inset: Plot of $(I_E/I_M)^{SPC}$ as a function of the (–/+) ratio for solutions of Py-3-12 and CT DNA (filled) and sCT DNA (hollow).

5.6 Conclusion

Numerous time-dependent studies were performed in this work to establish the conditions where stable $(I_E/I_M)^{SS}$ ratios and molar fractions of the various pyrene species in solution could be determined reliably. In particular, a range of surfactant concentrations was determined where the inherent adsorption of the surfactant to the cuvette walls would minimally affect the fluorescence results. Equilibrium conditions were also established for the time-dependent binding of Py-3-12 to

DNA. Establishing equilibrium conditions was found to be critical to obtain reliable and reproducible readings by fluorescence.

Having determined conditions where the fluorescence signal remained constant, the interaction between Py-3-12 and CT DNA could be studied using time-resolved fluorescence. The fluorescence decays of the pyrene monomer and excimer were fit with the "Model Free" (MF) analysis program to obtain the molar fractions of all the pyrene species present in solution namely, f_{free}, f_{diff}, and f_{agg}. The total concentration of Py-3-12 was held constant at a value lower than the CMC to ensure that any excimer formed was due to the binding of Py-3-12 to DNA. As the (–/+) ratio of DNA to Py-3-12 increased, f_{free} decreased at the expense of f_{diff}. Near a (–/+) ratio of 1.0, the point of charge neutrality, all surfactants were bound to DNA. Above this (–/+) ratio, the molar fractions of the pyrene species in solution remained unchanged with increasing DNA concentration, as well as the excimer lifetimes τ_{E0} and τ_D and the average rate constant of excimer formation $<k>$. Together, these observations indicate that pyrene excimer is generated in the same manner when bound to DNA, such as was the case with Py-3-12 micelles. The rate of intramolecular excimer formation, $<k>$, was found to equal $50 \pm 3 \times 10^7$ s^{-1} and $43 \pm 5 \times 10^7$ s^{-1} for, respectively, CT DNA and sCT DNA. These values are smaller than $<k>$ for Py-3-12 micelles without DNA found to equal $79 \pm 2 \times 10^7$ s^{-1} in Chapter 4. This suggests that the binding of Py-3-12 to the phosphates along the DNA backbone results in micelles that are more hindered than when no DNA is present in solution. Nonetheless, the large $<k>$ values obtained for Py-3-12 bound to DNA indicate that the pyrene microenvironment near the DNA helix is fluid, as was the case with the Py-3-12 micelles in water. The decay times of the pyrene excimer of ~30 ns and 55 ns are the same as those found for the Py-3-12 micelles in water which suggests that Py-3-12 clusters in a micellar form near the DNA helix where it adopts a "beads on a string" structure. The time-resolved fluorescence measurements conducted in this study provide a precise description of the state of the Py-3-12 molecules as they bind onto the DNA and information on the internal dynamics of the Py-3-12 micelles bound to DNA.

This work provides a solid start for the study of how the morphologies of aggregates of gemini surfactants with DNA is related to transfection efficiency. The next step of this work is to establish how $\langle k \rangle$ influences transfection efficiency. In other words, how the fluidity of the micellar interior enables DNA to be transferred to cells. This can be done by adding a helper lipid such as dioleoylphosphatidylethanolamine (DOPE) which has been shown to improve the transfection efficiency of DNA-gemini surfactant complexes.[29]

Chapter 6

Summary

The purpose of this thesis was to characterize the interactions between DNA and oppositely charged species in solution using fluorescence spectroscopy. The interactions between DNA and divalent metal cations were considered since these cations, namely Cu^{2+} and Ni^{2+}, can efficiently quench the fluorescence of ethidium bromide intercalated in DNA (DNA-EB) via an electron transfer (ET) mechanism. This thesis demonstrated that a quantitative description of the process of ET between DNA-EB and Cu^{2+} and Ni^{2+} cations randomly distributed around the DNA helix, can be achieved by applying the Fluorescence Blob Model (FBM) to the analysis of the fluorescence decays. This analysis yields the distance over which ET takes place (d_{blob}) and the rate constant of ET (k_{blob}) and it was applied to determine how d_{blob} varies with the size of the DNA construct and the solution ionic strength. Next, the interactions between DNA and a positively charged pyrene substituted gemini surfactant (Py-3-12), were studied as the complexes formed between these species have large implications for enabling gene delivery. Pyrene was used as a fluorescent probe since it is hydrophobic like the surfactant tails and its ability to form an excimer enables the straightforward detection of Py-3-12 associations. Excimer formation indicates that two pyrene molecules have come in contact with one another in a process that reflects the interactions between two surfactant molecules. The molar fractions of the pyrene species in water, with and without DNA, were obtained using the "Model Free" (MF) analysis program to analyze the pyrene monomer and excimer fluorescence decays globally. These molar fractions are f_{free}, the fraction of free pyrene that does not form excimer, f_{diff}, the fraction of pyrene that forms excimer by diffusion, and f_{agg}, the fraction of aggregated pyrene. A summary of the results obtained for the interactions between, on the one hand, DNA and divalent metal cations and on the other hand, DNA and gemini surfactants is presented below.

In Chapter 2, ET between DNA-EB and Cu^{2+} randomly distributed around the DNA helix was studied using the Fluorescence Blob Model (FBM). The FBM proved successful in analyzing the complicated fluorescence decays resulting from the random distribution of the electron donors and acceptors. In this work, it was observed that an onset copper concentration in the DNA-EB solution needed to be reached before quenching could occur. This onset copper concentration arose from the electrostatic repulsion taking place between the positively charged ethidium and copper cations. This onset copper concentration occurred at a salt concentration of 5×10^{-3} M. The onset copper concentration was found to vanish at high salt concentrations as the repulsion between the positively charged ethidium and copper cations was reduced by the screening of the charges. For a salt concentration of 5×10^{-3} M, the size of a blob, equivalent to the average distance over which electron transfer takes place was determined to be 11 bp with a quenching rate constant of 4×10^{7} s^{-1} for CT DNA.

An assumption in the FBM analysis of ET between DNA-EB and Cu^{2+} is that ET occurs locally inside a blob. This means that the parameters retrieved from the FBM analysis should not depend on the size of the DNA construct as long as the size of the DNA construct is larger than a blob. To ensure that this requirement was obeyed, the size of DNA was decreased from 15,000 bp (calf thymus) to 6 bp. The parameters retrieved from the FBM analysis of the fluorescence decays were found not to depend on the size of the DNA constructs as long as the size of the construct was substantially larger than a blob. The size of a blob was constant until the length of DNA was decreased below 11 bp. At this point the size of a blob "adapted" to the smaller size of the DNA construct yielding N_{blob} values that were smaller than the size of the DNA fragment. The quenching rate constant increased to a maximum value of 7×10^{7} s^{-1} for the smallest DNA hairpin where the electron donor and acceptor are forced to occupy a smaller volume and thus are located closer to each other. The binding constant of copper to DNA was found to decrease with decreasing DNA length as end effects are no longer negligible.

Chapter 3 focused on the effect of ionic strength on the distance over which ET occurred between DNA-EB and Cu^{2+} (d_{blob}) determined by the FBM analysis of the fluorescence decays and to establish the equivalence that exists between d_{blob} and the Debye screening length, κ^{-1}. κ^{-1} was calculated for each ionic strength studied and d_{blob} was found to follow κ^{-1} when the salt was present in excess over the DNA phosphates. d_{blob} was found to be independent of the type of divalent metal cation used, either Cu^{2+} or Ni^{2+}, and the lifetime of the chromophore, as would be expected if d_{blob} equals κ^{-1}. This result suggested that $\kappa^{-1} = d_{blob}$ represents a distance of minimal approach between divalent metal cations bound along the DNA helix. At low ionic strengths, when the DNA concentration is in excess of the salt concentration, d_{blob} reached a plateau of 33.0 ± 3.8 Å and 32.5 ± 3.3 Å for Cu^{2+} and Ni^{2+}, respectively, providing the maximum screening distance experienced by the divalent metal cations condensed near the DNA helix. The rate constant for electron transfer, $k_{blob,}$ between DNA-EB and Cu^{2+} and Ni^{2+} equaled $4.1 \pm 0.3 \times 10^7$ s^{-1} and $2.9 \pm 0.6 \times 10^7$ s^{-1}, respectively, suggesting that Ni^{2+} quenches the fluorescence of DNA-EB slightly less efficiently than Cu^{2+}. These results provided a simple explanation to a very complex problem, namely by finding the limiting length scale that controls ET between electron donors and acceptors randomly distributed along the DNA helix. In the case of DNA-EB quenched by Cu^{2+} and Ni^{2+} cations, this parameter is found to be κ^{-1}, a parameter suspected of representing the average distance of minimal approach between two cations.

Chapters 4 and 5 involved the characterization of the interactions between DNA and pyrene substituted gemini surfactant (Py-3-12) in solution. This work demonstrated how a Model Free (MF) analysis of the pyrene monomer and excimer fluorescence decays yielded quantitative information about the internal dynamics of the Py-3-12 surfactant micelles in water and bound to the DNA helix as well as a complete description of the distribution of the different pyrene species in solution. First, the MF procedure was used to characterize the micellization of Py-3-12 with increasing surfactant

concentration and this work was presented in Chapter 4. Chapter 5 then uses the MF procedure to characterize the complexes formed between DNA and Py-3-12.

Chapter 4 revealed that the interior the Py-3-12 micelles was fluid based on the fact that excimer formation between two pyrene groups occurs principally by diffusion. As the Py-3-12 concentration was increased, the molar fraction of surfactant free in solution (f_{free}) decreases at the expense of the molar fraction of surfactant forming excimer diffusionally inside the micelles (f_{diff}). Together, the fractions f_{free} and f_{diff} account for over 85% of all the pyrene species present in solution for the range of Py-3-12 concentrations studied and the rate of intramolecular excimer formation, $\langle k \rangle$, was found to equal $79 \pm 2 \times 10^7$ s^{-1}. The concentration study required to analyze the steady-state fluorescence signal of Py-3-12 above and below the CMC was complicated by inner filter effects. However, the global analysis of the monomer and excimer fluorescence decays enabled the calculation of the $(I_E/I_M)^{SPC}$ ratio, which is an absolute measure of how efficient excimer formation is. The robustness of the MF procedure was validated by determining the concentration of surfactant free in solution, $[\text{Py-3-12}]_{free}$, as a function of the overall surfactant concentration, [Py-3-12]. It was found that $[\text{Py-3-12}]_{free}$ increased linearly with increasing [Py-3-12] up to 0.22 mM, which is the CMC of the surfactant obtained by surface tension. Above this concentration, $[\text{Py-3-12}]_{free}$ remained constant and equal to 0.22 (±0.06) mM. The agreement between the $[\text{Py-3-12}]_{free}$ trend and what is expected of the behaviour of surfactants validated the MF procedure applied to study the Py-3-12 surfactant and provided a solid start to probe the interactions of Py-3-12 with DNA.

In Chapter 5, the MF procedure was used to yield the molar fractions of all the pyrene species present in solutions of Py-3-12 and DNA, namely, f_{free}, f_{diff}, and f_{agg}. The total concentration of Py-3-12 was held constant at a value lower than the CMC to ensure that any excimer formed was due to the binding of Py-3-12 to DNA. As the (–/+) ratio of DNA to Py-3-12 increased, f_{free} decreased as f_{diff} increased. Near a (–/+) ratio of 1.0 all surfactants were bound to DNA and above this (–/+) ratio, the molar fractions of the pyrene species in solution remained unchanged with increasing DNA

concentration. $\langle k \rangle$ for Py-3-12 bound to DNA was found to equal $50 \pm 3 \times 10^7$ s^{-1} for CT DNA which is smaller than the $\langle k \rangle$ value of $79 \pm 2 \times 10^7$ s^{-1} obtained for Py-3-12 micelles. This suggests that the binding of Py-3-12 to the phosphates along the DNA backbone results in micelles that are more hindered than when no DNA is present in solution. Nonetheless, the large $\langle k \rangle$ values obtained for Py-3-12 bound to DNA indicate that the pyrene microenvironment near the DNA helix is fluid which is an important feature for the use of Py-3-12 as a gene carrier in gene therapy. The decay times of the pyrene excimer of ~30 ns and 55 ns were the same as those found for the Py-3-12 micelles in water which suggests that Py-3-12 clusters in a micellar form near the DNA helix and possibly adopt a "beads on a string" structure.

The characterization of the interactions between Py-3-12 and DNA provides a solid start for the investigation of how the morphologies of these complexes influence transfection efficiency. The next step of this work would be to establish how $\langle k \rangle$ varies under physiological conditions and then to study how $\langle k \rangle$ is related to transfection efficiency. This work did not take into account how pyrene substitution affects the morphologies formed between the gemini surfactant and DNA. Thus, it is recommended that future work investigate the complexes formed between DNA and mixtures of Py-3-12 and its non-fluorescent analog, 12-3-12, which has a 12 carbon tail in place of the 1-pyrenehexyl unit. Other studies involve adding a helper lipid such as DOPE (dioleoyl phosphatidylethanolamine) to complexes of DNA and Py-3-12 to investigate how $\langle k \rangle$ in the presence of a helper lipid is related to transfection efficiency.

Overall, this thesis demonstrated that fluorescence spectroscopy, especially time-resolved fluorescence spectroscopy, combined with an appropriate protocol for analyzing the fluorescence decays, can provide quantitative and insightful information on the interactions between DNA and oppositely charged species in solution. The ideas presented in this thesis should be applicable to study the interactions between any polyelectrolyte and its counterions, an area of science of considerable interest.

Appendices

Chapter 2 Supporting Information

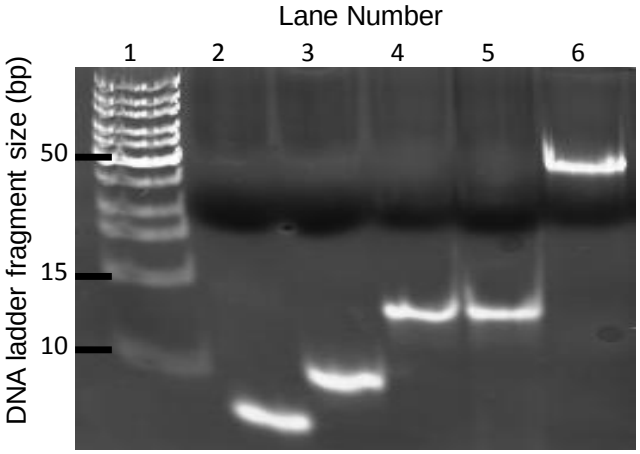

Figure SI 2.1: Polyacrylamide gel (20%) of DNA duplexes and hairpins (Lane 1: DNA Ladder, Lane 2: 6 bp hairpin, Lane 3: 8 bp hairpin, Lane 4: 12 bp hairpin, Lane 5: 12 bp duplex, Lane 6: 43 bp duplex).

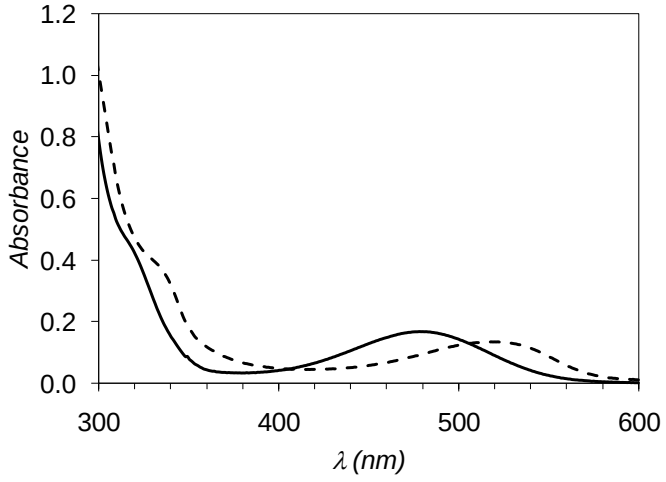

Figure SI 2.2: Absorbance of EB in sodium sulfate solution (solid line) and intercalated in calf thymus DNA (dashed line) acquired with a 0.3 cm path length cell ([DNA] = 0.09 wt%, [EB] = 1×10^{-4} M, [Na_2SO_4] = 5×10^{-3} M).

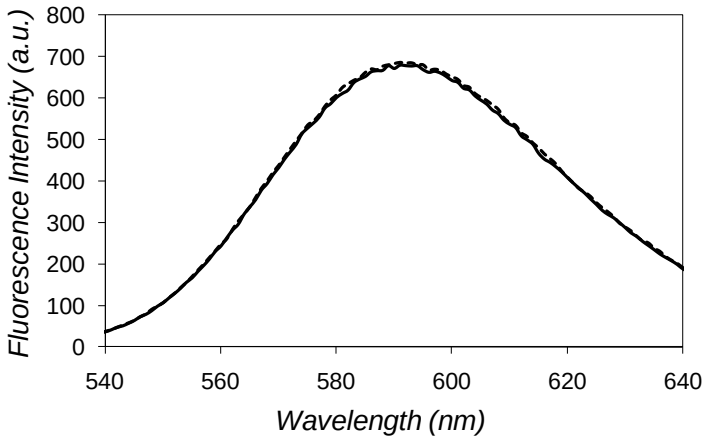

Figure SI 2.3: Fluorescence intensity of EB intercalated in calf thymus DNA (solid line) and calf thymus DNA dialyzed against sodium sulfate solution ([DNA] = 0.02 wt%, [EB] = 1×10^{-5} M, $[Na_2SO_4] = 5\times10^{-3}$ M).

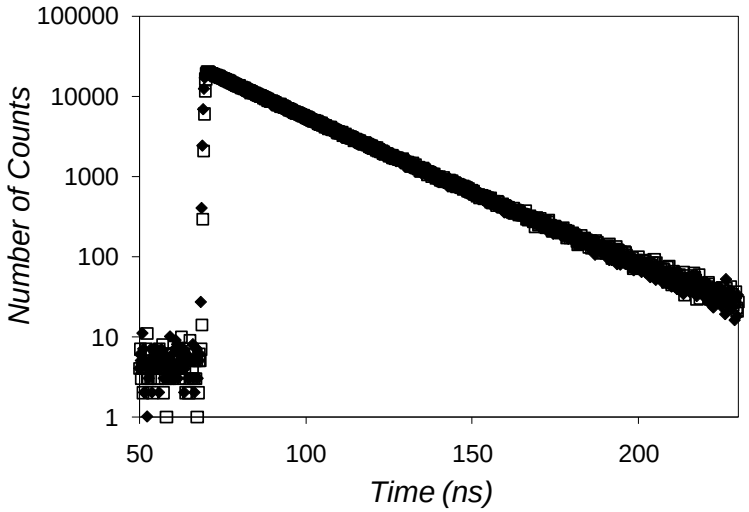

Figure SI 2.4: Fluorescence decay of EB intercalated in calf thymus DNA (solid diamonds, $\tau_1 = 22.9$, $a_1 = 0.96$, $\tau_2 = 9.54$, $a_2 = 0.04$, $\chi^2 = 1.06$) and calf thymus DNA dialyzed against sodium sulfate solution (hollow squares, $\tau_1 = 23.5$, $a_1 = 0.91$, $\tau_2 = 13.7$, $a_2 = 0.09$, $\chi^2 = 0.96$) ([DNA] = 0.02 wt%, [EB] = 1×10^{-5} M, $[Na_2SO_4] = 5\times10^{-3}$ M).

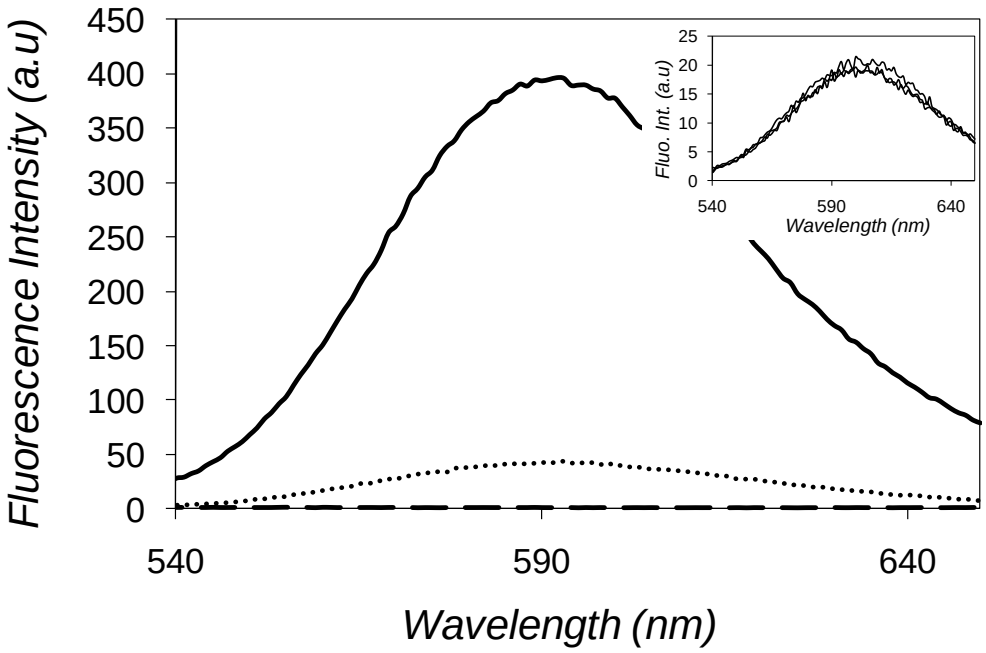

Figure SI 2.5: 0.09 wt% CT DNA, 1×10^{-5} M EB, 3.5×10^{-5} M Cu^{2+} (solid line); 0.09 wt% CT DNA, 1×10^{-5} M EB, 3.5×10^{-5} M Cu^{2+} filtered through a 200 nm membrane (dotted line); 0.09 wt% CT DNA, 1×10^{-5} M EB, 3.5×10^{-5} M Cu^{2+} filtered through a 20 nm membrane (dashed line). Inset: 1×10^{-5} M EB, 3.5×10^{-5} M Cu^{2+} solution; same solution filtered through a 200 nm membrane, same solution filtered through a 20 nm membrane.

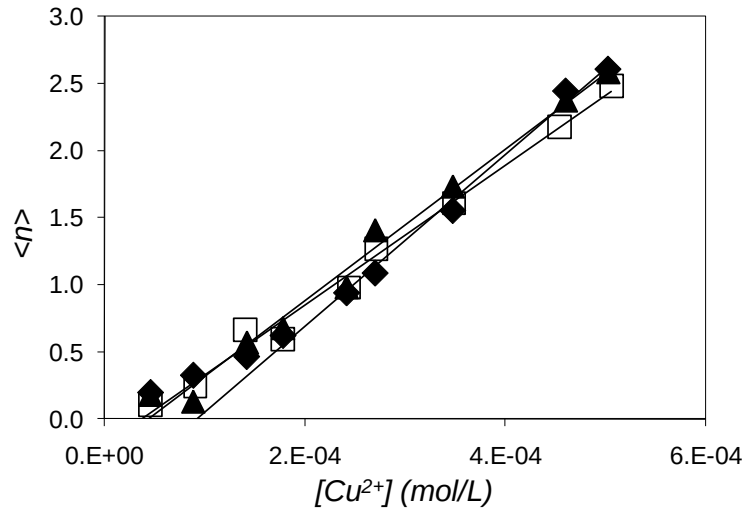

Figure SI 2.6: <*n*> as a function of copper concentration (◆) 136 bp between EBs (□) 75 bp between EBs (▲) 30 bp between EBs (0.09 wt% CT DNA, $[Na_2SO_4] = 5\times10^{-3}$M).

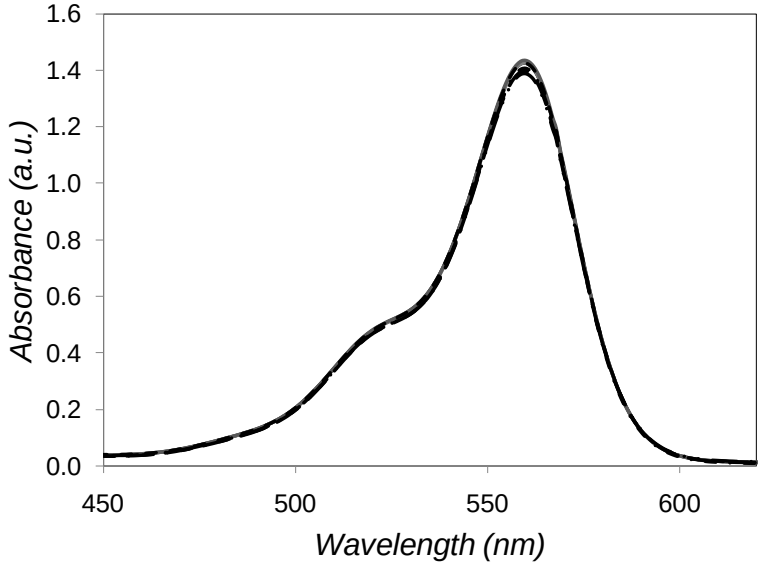

Figure SI 2.7: Absorbance spectra of 12 bp hairpin labeled with rhodamine, $[CuSO_4] = 0$ to 4.5×10^{-4} M (0.09 wt% DNA, $[Na_2SO_4] = 5\times10^{-3}$M).

Table SI 2.1a: Decay times and pre-exponential factors retrieved from fitting the fluorescence decays of EB intercalated in the 6 bp hairpin quenched by Cu^{2+} cations with Equation 2.2.

wt % DNA	$[Cu^{2+}]$ (mM)	$[Cu^{2+}]/[P]$	τ_1 ns	τ_2 ns	τ_3 ns	a_1	a_2	a_3	χ^2
0.02	0	0.00	20.7	7.51		0.78	0.22		1.19
	21	0.03	20.6	8.63	1.38	0.51	0.29	0.20	1.05
	32	0.05	20.3	7.86	1.31	0.47	0.29	0.24	1.10
	44	0.07	20.1	7.48	1.79	0.44	0.30	0.26	1.30
	55	0.09	20.0	7.79	1.59	0.36	0.34	0.30	1.19
	63	0.10	19.9	7.72	1.61	0.32	0.34	0.35	1.23
	76	0.13	19.6	7.67	1.63	0.29	0.34	0.38	1.02
	104	0.17	18.8	6.73	1.42	0.24	0.36	0.40	1.10
0.03	0	0.00	22.0	9.07		0.90	0.10		1.11
	31	0.03	22.9	14.9	2.70	0.63	0.27	0.11	1.14
	46	0.05	22.5	13.7	2.77	0.60	0.25	0.15	1.16
	59	0.06	21.7	8.67	1.49	0.62	0.23	0.15	1.15
	75	0.08	21.4	8.49	1.53	0.57	0.24	0.19	1.00
	90	0.10	21.3	8.29	1.66	0.46	0.30	0.24	1.04
	105	0.12	21.2	8.35	1.79	0.45	0.29	0.25	1.30
	122	0.13	20.4	6.87	0.99	0.33	0.34	0.34	1.09
	151	0.17	20.2	7.56	1.55	0.30	0.36	0.34	1.19
	173	0.19	19.8	7.27	1.60	0.28	0.37	0.35	1.07
0.05	0	0.00	22.1	10.3		0.85	0.15		1.07
	52	0.03	22.3	12.6	2.13	0.69	0.21	0.10	1.25
	76	0.05	12.3	22.3	2.79	0.24	0.63	0.13	1.19
	99	0.07	21.7	9.13	1.95	0.59	0.23	0.17	1.29
	124	0.08	21.4	8.30	1.79	0.56	0.25	0.19	1.04
	150	0.10	21.4	8.42	1.82	0.50	0.27	0.22	1.14
	175	0.12	21.0	7.80	1.45	0.40	0.30	0.30	1.05
	201	0.13	20.7	7.47	1.40	0.39	0.31	0.30	1.03
	251	0.17	19.9	6.80	1.38	0.30	0.34	0.35	1.17
	289	0.19	19.7	6.79	1.38	0.28	0.35	0.38	1.02

0.07	0	0.00	22.3	9.62		0.85	0.15		1.23
	72	0.03	22.6	14.5	3.64	0.65	0.22	0.12	1.16
	106	0.05	22.5	12.5	3.41	0.67	0.20	0.13	1.19
	140	0.07	21.7	9.07	1.73	0.57	0.24	0.19	1.06
	174	0.08	21.6	8.88	1.69	0.51	0.27	0.22	1.14
	209	0.10	21.4	8.08	1.37	0.47	0.28	0.25	1.27
	246	0.12	20.6	7.27	1.37	0.40	0.30	0.30	1.14
	281	0.13	20.9	7.96	1.69	0.39	0.31	0.30	1.12
	353	0.17	20.2	7.25	1.55	0.29	0.35	0.37	1.18
	406	0.19	20.2	7.60	1.61	0.26	0.34	0.40	1.11
0.09	0	0.00	22.5	10.1		0.82	0.18		1.17
	92	0.03	22.3	10.4	1.26	0.69	0.20	0.11	1.05
	138	0.05	22.3	9.59	1.51	0.66	0.22	0.12	1.16
	181	0.06	21.9	9.61	1.89	0.55	0.25	0.21	1.06
	223	0.07	21.5	8.18	1.59	0.50	0.27	0.23	1.15
	270	0.09	21.3	7.87	1.53	0.46	0.29	0.25	1.16
	315	0.10	21.1	8.17	1.73	0.37	0.31	0.32	1.00
	360	0.12	20.9	7.87	1.72	0.36	0.32	0.32	1.08
	453	0.15	20.2	7.34	1.48	0.26	0.34	0.41	1.18
	519	0.17	19.8	6.83	1.38	0.25	0.35	0.40	1.10

Table SI 2.1b: Decay times and pre-exponential factors retrieved from fitting the fluorescence decays of EB intercalated in the 8 bp hairpin quenched by Cu^{2+} cations with Equation 2.2.

wt % DNA	$[Cu^{2+}]$ (mM)	$[Cu^{2+}]/[P]$	τ_1 ns	τ_2 ns	τ_3 ns	a_1	a_2	a_3	χ^2
0.02	0	0.00	20.0	7.59		0.81	0.19		1.30
	11	0.02	19.9	8.35	0.97	0.66	0.23	0.11	1.16
	23	0.04	19.6	8.13	1.42	0.57	0.27	0.15	1.16
	32	0.05	19.5	7.86	1.25	0.53	0.28	0.19	1.09
	42	0.07	18.9	7.16	1.30	0.44	0.32	0.23	1.25
	53	0.09	19.0	7.57	1.53	0.37	0.34	0.28	1.14

	62	0.10	18.7	7.61	1.50	0.33	0.34	0.32	1.20
	81	0.13	17.9	6.84	1.44	0.28	0.36	0.36	1.18
	104	0.17	17.3	6.57	1.41	0.23	0.36	0.41	1.24
	117	0.19	17.2	6.67	1.40	0.20	0.37	0.43	1.21
0.03	0	0.00	20.9	9.31		0.82	0.18		1.07
	47	0.05	20.1	8.50	1.57	0.56	0.28	0.16	1.22
	61	0.07	20.1	9.02	1.98	0.47	0.30	0.23	1.10
	78	0.09	19.4	7.79	1.34	0.41	0.32	0.27	1.32
	90	0.10	19.2	8.02	1.79	0.37	0.33	0.30	1.17
	114	0.13	19.2	8.02	1.62	0.32	0.34	0.34	1.14
	151	0.17	17.9	7.01	1.49	0.22	0.36	0.41	1.25
0.05	0	0.00	21.6	10.9		0.80	0.20		1.01
	25	0.02	21.6	12.6	3.42	0.68	0.24	0.08	0.90
	44	0.03	21.1	10.4	2.08	0.67	0.23	0.10	1.02
	79	0.05	20.5	9.11	1.80	0.59	0.27	0.14	1.09
	98	0.06	20.3	8.74	1.52	0.52	0.30	0.17	1.14
	134	0.09	19.9	8.66	1.72	0.45	0.32	0.23	1.01
	151	0.10	19.8	8.43	1.83	0.42	0.33	0.25	1.04
	196	0.13	19.2	8.30	1.77	0.30	0.37	0.34	0.99
	251	0.17	17.7	6.75	1.39	0.24	0.38	0.38	1.30
	280	0.18	17.2	6.46	1.46	0.22	0.38	0.40	1.13
0.07	0	0.00	21.7	10.4		0.82	0.18		1.16
	110	0.05	20.8	8.94	1.29	0.59	0.27	0.14	1.01
	139	0.07	20.9	10.7	2.56	0.50	0.30	0.20	1.07
	187	0.09	19.8	7.95	1.50	0.46	0.33	0.21	1.14
	210	0.10	19.5	7.44	1.29	0.42	0.35	0.23	1.19
	269	0.13	18.8	7.56	1.43	0.31	0.37	0.33	1.09
	353	0.17	17.9	6.90	1.39	0.23	0.38	0.39	1.11
	389	0.18	17.0	6.39	1.40	0.23	0.38	0.39	1.20
0.09	0	0.00	21.8	10.1		0.82	0.18		1.01
	45	0.02	21.5	10.3	1.47	0.74	0.20	0.06	1.04
	91	0.03	21.6	9.61	1.50	0.68	0.23	0.09	1.04
	142	0.05	20.8	9.16	1.37	0.61	0.27	0.12	1.06
	181	0.07	20.7	9.47	1.95	0.53	0.31	0.16	1.18

	239	0.09	19.8	8.2	1.68	0.47	0.32	0.21	1.23
	301	0.11	18.2	6.86	1.36	0.32	0.37	0.31	1.18
	390	0.14	17.1	6.62	1.42	0.21	0.38	0.41	1.20
	461	0.17	15.7	5.51	1.25	0.17	0.40	0.42	1.11
	498	0.18	15.3	5.55	1.28	0.15	0.40	0.45	1.47

Table SI 2.1c: Decay times and pre-exponential factors retrieved from fitting the fluorescence decays of EB intercalated in the 12 bp hairpin quenched by Cu^{2+} cations with Equation 2.2.

wt % DNA	$[Cu^{2+}]$ (mM)	$[Cu^{2+}]/[P]$	τ_1 ns	τ_2 ns	τ_3 ns	a_1	a_2	a_3	χ^2
0.02	0	0.00	22.1	11.0		0.83	0.17		1.07
	31	0.05	21.5	11.4	2.10	0.53	0.34	0.12	1.05
	46	0.08	21.2	11.4	2.42	0.41	0.42	0.17	1.05
	60	0.10	19.9	10.1	2.25	0.41	0.38	0.21	1.02
	75	0.12	18.3	7.64	1.36	0.40	0.37	0.23	1.05
	91	0.15	17.8	7.68	1.37	0.32	0.39	0.29	1.13
	104	0.17	17.2	7.37	1.54	0.27	0.40	0.33	1.07
	120	0.20	16.2	6.61	1.31	0.25	0.39	0.37	1.08
0.04	0	0.00	22.2	10.8		0.83	0.17		1.02
	50	0.04	22.6	15.4	5.28	0.42	0.40	0.19	1.19
	74	0.06	20.8	10.6	2.38	0.47	0.37	0.16	1.04
	102	0.08	19.7	8.88	1.44	0.42	0.39	0.20	0.99
	124	0.10	19.0	8.8	1.80	0.34	0.40	0.26	1.02
	151	0.12	17.6	7.45	1.55	0.31	0.39	0.30	1.01
	176	0.15	16.6	6.67	1.23	0.25	0.40	0.35	1.22
	200	0.17	16.4	7.06	1.59	0.20	0.39	0.41	1.11
0.05	0	0.00	22.7	12.1		0.76	0.24		1.04
	72	0.05	22.1	11.9	2.39	0.50	0.36	0.14	0.96
	104	0.07	20.8	9.61	1.66	0.47	0.38	0.15	1.07
	138	0.09	20.0	9.53	1.91	0.39	0.40	0.21	0.95
	174	0.12	19.0	8.38	1.63	0.33	0.42	0.25	1.09

	208	0.14	17.9	7.74	1.45	0.29	0.40	0.31	1.10
	271	0.18	15.8	6.50	1.33	0.17	0.40	0.43	1.06
	295	0.19	14.2	5.59	1.14	0.14	0.38	0.48	1.21
0.07	0	0.00	22.7	11.9		0.77	0.23		1.27
	88	0.04	23.9	15.2	3.99	0.33	0.50	0.17	1.23
	133	0.06	20.6	9.67	1.85	0.48	0.36	0.16	1.08
	181	0.09	19.8	9.30	1.88	0.40	0.39	0.21	1.07
	224	0.11	19.0	8.57	1.68	0.31	0.42	0.28	1.10
	269	0.13	18.1	8.20	1.79	0.26	0.41	0.34	1.08
	320	0.15	16.1	6.96	1.65	0.16	0.39	0.45	1.16
	365	0.17	14.6	5.84	1.29	0.14	0.39	0.46	1.24
0.09	0	0.00	21.8	10.5		0.87	0.13		0.99
	88	0.03	20.9	9.73	1.78	0.63	0.28	0.09	1.05
	141	0.05	19.9	8.54	1.14	0.52	0.34	0.14	1.10
	179	0.07	19.5	8.96	1.59	0.43	0.37	0.19	1.13
	242	0.09	18.1	8.16	1.56	0.34	0.39	0.28	1.26
	268	0.10	15.8	6.46	1.32	0.21	0.39	0.39	1.20
	375	0.14	12.9	4.98	1.15	0.14	0.39	0.47	1.20
	482	0.18	11.7	4.46	1.06	0.11	0.38	0.51	1.33
	515	0.19	10.6	4.11	0.98	0.11	0.37	0.52	1.25

Table SI 2.1d: Decay times and pre-exponential factors retrieved from fitting the fluorescence decays of EB intercalated in the 12 bp duplex quenched by Cu^{2+} cations with Equation 2.2.

wt % DNA	$[Cu^{2+}]$ (mM)	$[Cu^{2+}]/[P]$	τ_1 ns	τ_2 ns	τ_3 ns	a_1	a_2	a_3	χ^2
0.02	0	0.00	21.7	12.3		0.74	0.26		1.10
	32	0.05	20.6	10.3	1.91	0.62	0.29	0.10	1.04
	46	0.08	20.8	11.5	2.36	0.50	0.35	0.15	1.07
	59	0.10	19.8	10.2	2.41	0.46	0.34	0.20	1.19
	75	0.12	19.3	9.05	1.86	0.42	0.35	0.23	1.08
	89	0.15	18.3	7.90	1.67	0.35	0.37	0.27	1.03

	103	0.17	18.3	8.14	1.84	0.30	0.39	0.32	1.13
	118	0.19	17.5	7.21	1.62	0.27	0.39	0.34	1.12
0.04	0	0.00	22.0	12.4		0.76	0.24		0.99
	33	0.03	20.8	10.1	1.47	0.60	0.28	0.12	1.02
	74	0.06	20.5	9.96	1.63	0.51	0.33	0.16	1.01
	100	0.08	19.6	8.91	1.73	0.45	0.35	0.20	1.03
	124	0.10	19.6	9.77	2.40	0.34	0.39	0.27	1.10
	148	0.12	18.9	8.28	1.75	0.31	0.40	0.29	1.15
	174	0.14	17.7	7.08	1.53	0.29	0.41	0.30	1.11
	199	0.16	17.1	6.83	1.53	0.24	0.40	0.36	1.12
0.06	0	0.00	22.0	11.5		0.80	0.20		0.89
	69	0.04	21.5	11.8	2.55	0.55	0.34	0.11	1.08
	107	0.06	20.7	9.96	1.94	0.50	0.35	0.15	1.06
	140	0.08	19.9	9.06	1.75	0.41	0.37	0.21	1.08
	173	0.10	19.1	8.44	1.75	0.35	0.39	0.27	1.04
	209	0.11	18.0	7.55	1.86	0.32	0.40	0.29	1.05
	235	0.13	17.2	6.83	1.65	0.20	0.42	0.38	1.21
	276	0.15	15.9	6.20	1.55	0.18	0.42	0.40	1.24
0.07	0	0.00	21.8	10.8		0.85	0.15		1.06
	90	0.04	23.3	15.7	4.41	0.34	0.51	0.16	1.09
	134	0.06	21.3	11.5	2.33	0.43	0.39	0.18	1.09
	177	0.08	20.3	9.8	1.99	0.40	0.38	0.22	1.10
	221	0.10	19.1	8.43	1.87	0.26	0.42	0.32	1.26
	275	0.13	17.9	7.45	1.79	0.22	0.42	0.36	1.18
	330	0.16	16.5	6.52	1.54	0.19	0.42	0.39	1.16
	372	0.18	16.1	6.5	1.64	0.14	0.42	0.44	1.16
0.09	0	0.00	21.4	9.22		0.80	0.20		1.00
	93	0.03	21.0	9.74	1.98	0.60	0.28	0.12	1.17
	139	0.05	21.2	11.5	2.98	0.47	0.35	0.18	0.94
	183	0.07	20.2	8.99	1.86	0.45	0.36	0.20	1.13
	240	0.09	20.0	9.00	1.99	0.35	0.40	0.25	1.18
	285	0.10	18.3	7.17	1.55	0.24	0.42	0.34	1.18
	375	0.14	17.3	6.54	1.51	0.18	0.43	0.39	1.18
	465	0.17	15.9	6.13	1.55	0.14	0.42	0.43	1.24

Table SI 2.1e: Decay times and pre-exponential factors retrieved from fitting the fluorescence decays of EB intercalated in the 43 bp duplex quenched by Cu^{2+} cations with Equation 2.2.

wt % DNA	$[Cu^{2+}]$ (mM)	$[Cu^{2+}]/[P]$	τ_1 ns	τ_2 ns	τ_3 ns	a_1	a_2	a_3	χ^2
0.02	0	0.00	20.8	10.0		0.88	0.12		1.13
	11	0.02	19.8	8.00	0.43	0.66	0.16	0.18	1.16
	22	0.04	19.4	9.11	1.64	0.65	0.25	0.11	1.03
	32	0.05	18.7	8.09	1.25	0.57	0.30	0.14	1.10
	40	0.07	17.8	7.67	1.24	0.49	0.31	0.20	1.23
	55	0.09	17.1	7.74	1.50	0.42	0.36	0.23	1.08
	60	0.10	16.6	7.21	1.50	0.40	0.37	0.23	1.28
	77	0.13	15.8	7.14	1.69	0.33	0.38	0.30	1.13
	102	0.17	15.5	7.38	1.66	0.27	0.39	0.33	1.16
	113	0.19	14.2	6.38	1.48	0.24	0.40	0.36	1.37
0.03	0	0.00	21.5	8.58		0.93	0.07		1.13
	17	0.02	20.8	9.24	0.82	0.70	0.19	0.11	1.09
	30	0.03	19.8	7.64	0.71	0.64	0.21	0.15	1.19
	49	0.05	19.4	8.64	1.35	0.53	0.31	0.16	1.07
	59	0.06	18.6	8.19	1.37	0.46	0.35	0.19	1.20
	80	0.09	17.8	8.46	1.89	0.37	0.37	0.26	1.16
	91	0.10	17.2	7.90	1.67	0.34	0.39	0.27	1.17
	120	0.13	15.4	6.66	1.40	0.29	0.39	0.31	1.27
	153	0.17	14.2	6.50	1.55	0.20	0.42	0.38	1.23
	170	0.19	13.2	5.72	1.33	0.20	0.42	0.38	1.18
0.05	0	0.00	22.1	9.99		0.90	0.10		1.21
	27	0.02	21.2	9.45	1.51	0.75	0.19	0.07	0.97
	51	0.03	20.6	9.44	1.41	0.62	0.27	0.11	1.14
	78	0.05	19.8	8.84	1.10	0.53	0.30	0.16	1.06
	101	0.07	18.9	8.17	1.45	0.47	0.33	0.20	1.11
	133	0.09	17.9	7.87	1.43	0.39	0.36	0.25	1.19
	151	0.10	17.0	6.97	1.09	0.33	0.39	0.27	1.27
	194	0.13	15.3	6.60	1.15	0.26	0.40	0.34	1.19

	253	0.17	13.1	5.49	1.13	0.22	0.42	0.36	1.26
	280	0.18	12.6	5.38	1.13	0.20	0.42	0.38	1.17
0.07	0	0.00	22.8	12.5		0.84	0.16		1.21
	36	0.02	22.7	14.7	3.77	0.61	0.30	0.09	1.09
	70	0.03	21.1	8.83	0.81	0.62	0.25	0.13	1.13
	112	0.05	20.1	8.41	0.92	0.51	0.30	0.20	1.12
	139	0.07	19.6	8.64	1.33	0.43	0.35	0.22	1.18
	188	0.09	18.2	8.24	1.49	0.33	0.38	0.29	1.22
	213	0.10	15.7	7.12	1.49	0.24	0.42	0.34	1.21
	304	0.14	13.0	5.66	1.22	0.20	0.42	0.38	1.25
	375	0.18	10.7	4.70	1.10	0.18	0.42	0.40	1.33
	408	0.19	10.3	4.76	1.25	0.17	0.43	0.40	1.26
0.09	0	0.00	22.8	12.7		0.83	0.17		1.06
	46	0.02	21.8	9.09		0.78	0.22		1.16
	89	0.03	21.3	9.72	1.57	0.63	0.28	0.09	1.05
	143	0.05	20.5	9.73	1.69	0.49	0.33	0.18	1.13
	184	0.07	19.4	8.64	1.69	0.45	0.35	0.19	1.04
	242	0.09	18.0	7.97	1.63	0.36	0.38	0.26	1.15
	268	0.10	15.9	7.02	1.52	0.27	0.42	0.31	1.18
	358	0.13	12.6	5.29	1.16	0.23	0.43	0.34	1.12
	430	0.16	11.1	4.71	1.05	0.20	0.43	0.37	1.21
	515	0.19	10.1	4.43	0.94	0.17	0.43	0.41	1.29

Table SI 2.1f: Decay times and pre-exponential factors retrieved from fitting the fluorescence decays of EB intercalated in CT DNA quenched by Cu^{2+} cations with Equation 2.2.

wt % DNA	$[Cu^{2+}]$ (mM)	$[Cu^{2+}]/[P]$	τ_1 ns	τ_2 ns	τ_3 ns	a_1	a_2	a_3	χ^2
0.02	0	0.00	22.9	9.54		0.96	0.04		1.06
	20	0.03	22.5	8.48		0.87	0.13		1.08
	40	0.07	20.7	8.00	0.75	0.58	0.24	0.17	1.09
	60	0.10	19.3	8.50	1.59	0.46	0.33	0.21	1.18

	79	0.13	17.5	7.24	1.20	0.38	0.36	0.25	1.15
	99	0.16	16.2	7.47	1.78	0.32	0.38	0.29	1.20
	115	0.19	14.9	6.66	1.51	0.29	0.40	0.31	1.19
0.03	0	0.00	23.8	17.2		0.84	0.16		0.99
	8	0.01	23.0	9.59		0.93	0.07		1.05
	15	0.02	22.8	8.09		0.91	0.09		1.03
	30	0.03	22.5	7.86		0.85	0.15		1.02
	59	0.06	20.7	9.16	1.82	0.59	0.26	0.15	1.08
	90	0.10	19.0	8.22	1.68	0.46	0.33	0.21	1.07
	120	0.13	16.8	7.60	1.74	0.36	0.36	0.28	1.10
	149	0.16	15.1	6.87	1.68	0.29	0.40	0.31	1.21
	172	0.19	14.0	6.40	1.64	0.26	0.40	0.34	1.15
0.05	0	0.00	24.0	17.9		0.81	0.19		1.17
	13	0.01	23.5	15.6		0.86	0.14		1.13
	25	0.02	23.1	10.2		0.91	0.09		1.06
	50	0.03	22.2	8.80	1.35	0.78	0.15	0.06	1.18
	100	0.07	21.0	9.30	1.80	0.61	0.25	0.14	1.07
	148	0.10	20.0	9.50	2.08	0.45	0.34	0.21	0.98
	200	0.13	17.3	7.57	1.53	0.36	0.37	0.28	1.10
	249	0.16	15.8	7.64	1.89	0.26	0.40	0.33	1.06
	287	0.19	14.4	6.60	1.70	0.27	0.39	0.33	1.15
0.07	0	0.00	24.1	17.8		0.81	0.19		1.11
	17	0.01	23.3	11.1		0.91	0.09		1.25
	35	0.02	22.9	8.95		0.88	0.12		1.23
	69	0.03	22.3	7.95		0.81	0.19		1.12
	138	0.07	21.3	10.1	2.55	0.59	0.27	0.14	1.15
	208	0.10	19.3	8.13	1.41	0.46	0.34	0.20	1.27
	280	0.13	16.9	7.77	1.78	0.32	0.39	0.29	1.12
	347	0.16	13.5	6.09	1.58	0.26	0.39	0.35	1.22
	399	0.19	11.7	5.21	1.36	0.24	0.41	0.35	1.32
0.09	0	0.00	23.7	17.4		0.84	0.16		1.17
	22	0.01	23.3	12.9		0.89	0.11		1.11
	45	0.02	22.7	8.42		0.89	0.11		1.13
	90	0.03	22.4	9.67	1.25	0.75	0.17	0.08	1.05

	179	0.07	21.1	8.61	1.52	0.61	0.26	0.13	1.05
	269	0.10	19.3	8.03	1.34	0.46	0.33	0.21	1.05
	349	0.13	16.6	7.68	1.79	0.32	0.37	0.31	1.05
	455	0.17	14.3	6.55	1.58	0.26	0.40	0.34	1.12
	505	0.19	12.9	6.28	1.77	0.23	0.40	0.37	1.11

Table SI 2.2a: FBM parameters obtained from fitting the fluorescence decays of EB intercalated in the 6 bp hairpin quenched by Cu^{2+} cations with Equation 2.3.

wt % DNA	$[Cu^{2+}]$ (mM)	$[Cu^{2+}]/[P]$	$k_e[blob]$ $\times 10^7\ s^{-1}$	k_{blob} $\times 10^7\ s^{-1}$	<n>	τ_{fast}	a_{fast}	a_2	χ^2
0.02	21	0.03	0	3.56	0.26	1.24	0.20	0.80	1.06
	32	0.05	0.006	4.53	0.31	1.29	0.24	0.76	1.08
	44	0.07	0.047	4.19	0.40	1.78	0.25	0.75	1.25
	55	0.09	0.13	5.08	0.54	1.49	0.28	0.72	1.24
	63	0.10	0.16	5.21	0.63	1.48	0.33	0.67	1.29
	76	0.13	0.29	5.18	0.71	1.50	0.35	0.65	0.99
	104	0.17	0.43	6.30	0.93	1.30	0.37	0.63	1.03
0.03	46	0.05	0	4.21	0.17	1.53	0.12	0.88	1.08
	59	0.06	0.28	6.53	0.24	1.36	0.15	0.85	1.12
	75	0.08	0.14	4.88	0.32	1.61	0.19	0.81	0.98
	90	0.10	0.36	6.62	0.49	1.42	0.22	0.78	1.04
	105	0.12	0.28	5.56	0.49	1.73	0.24	0.76	1.25
	122	0.13	0.48	7.84	0.75	0.82	0.33	0.67	1.73
	151	0.17	0.40	6.30	0.90	1.33	0.31	0.69	1.16
0.05	52	0.03	0.77	9.09	0.07	0.66	0.14	0.86	1.19
	76	0.05	0.25	6.10	0.14	1.31	0.11	0.89	1.17
	99	0.07	0.38	6.17	0.21	1.82	0.16	0.84	1.27
	124	0.08	0.49	7.58	0.28	1.60	0.17	0.83	1.06
	150	0.10	0.44	7.24	0.35	1.61	0.20	0.80	1.08
	175	0.12	0.43	7.41	0.52	1.27	0.29	0.71	1.05
	201	0.13	0.59	8.91	0.56	1.02	0.27	0.73	1.02

	251	0.17	0.61	8.39	0.82	1.12	0.31	0.69	1.19
	289	0.19	0.60	7.93	0.89	1.18	0.34	0.66	1.09
0.07	106	0.05	0	3.48	0.11	2.35	0.10	0.90	1.19
	140	0.07	0.23	4.23	0.27	1.79	0.19	0.81	1.06
	174	0.08	0.46	5.76	0.32	1.56	0.21	0.79	1.09
	209	0.10	0.52	7.50	0.40	1.11	0.24	0.76	1.19
	246	0.12	0.64	7.49	0.54	1.25	0.29	0.71	1.05
	281	0.13	0.59	7.07	0.55	1.44	0.28	0.72	1.06
	353	0.17	0.47	6.54	0.85	1.44	0.34	0.66	1.19
	406	0.19	0.51	6.33	0.92	1.40	0.36	0.64	1.03
0.10	138	0.05	0.59	7.75	0.11	1.24	0.12	0.88	1.16
	181	0.06	0.58	5.49	0.23	1.73	0.20	0.80	1.07
	223	0.07	0.63	8.00	0.32	1.35	0.22	0.78	1.14
	270	0.09	0.64	9.66	0.41	1.00	0.23	0.77	1.15
	315	0.10	0.54	6.51	0.56	1.56	0.29	0.71	1.04
	360	0.12	0.56	7.01	0.59	1.55	0.30	0.70	1.07
	453	0.15	0.59	6.97	0.88	1.29	0.37	0.63	1.14

Table SI 2.2b: FBM parameters obtained from fitting the fluorescence decays of EB intercalated in the 8 bp hairpin quenched by Cu^{2+} cations with Equation 2.3.

wt % DNA	$[Cu^{2+}]$ (mM)	$[Cu^{2+}]/[P]$	$k_e[blob]$ $\times 10^7\ s^{-1}$	k_{blob} $\times 10^7\ s^{-1}$	<n>	τ_{fast}	a_{fast}	a_2	χ^2
0.02	11	0.02	0	1.84	0.14	1.12	0.11	0.89	1.14
	23	0.04	0	3.94	0.24	1.42	0.15	0.85	1.08
	32	0.05	0.36	4.74	0.27	1.38	0.17	0.83	1.06
	42	0.07	0.49	5.44	0.43	1.52	0.22	0.78	1.17
	53	0.09	0.33	5.12	0.58	1.58	0.26	0.74	1.06
	62	0.10	0.49	5.49	0.66	1.34	0.30	0.70	1.21
	81	0.13	0.73	6.61	0.85	1.27	0.32	0.68	1.15
	104	0.17	0.69	6.36	1.08	1.25	0.37	0.63	1.17
	117	0.19	0.63	5.97	1.20	1.22	0.39	0.61	1.22

0.03	47	0.05	0.45	4.91	0.30	1.56	0.16	0.84	1.21
	61	0.07	0.39	4.25	0.42	1.90	0.22	0.78	1.08
	78	0.09	0.66	5.81	0.54	1.25	0.26	0.74	1.29
	90	0.10	0.74	5.66	0.63	1.16	0.28	0.72	1.17
	114	0.13	0.60	0.52	0.74	1.43	0.31	0.69	1.07
	151	0.17	0.73	6.05	1.14	1.31	0.38	0.62	1.22
0.05	44	0.03	0.31	2.65	0.15	2.16	0.10	0.90	1.00
	79	0.05	0.64	4.26	0.29	1.90	0.14	0.86	1.06
	98	0.06	0.75	5.73	0.36	1.39	0.16	0.84	1.11
	134	0.09	0.82	5.49	0.49	1.56	0.22	0.78	1.00
	151	0.10	0.89	6.13	0.54	1.59	0.22	0.78	1.00
	196	0.13	0.65	5.04	0.88	1.59	0.31	0.69	0.99
	251	0.17	0.86	6.45	1.16	1.16	0.34	0.66	1.23
	280	0.18	0.90	6.83	1.26	1.26	0.35	0.65	1.12
0.07	139	0.07	0.34	2.83	0.24	2.44	0.19	0.81	1.05
	187	0.09	0.97	7.29	0.51	1.10	0.19	0.81	1.11
	210	0.10	0.96	7.51	0.60	0.99	0.21	0.79	1.15
	269	0.13	0.83	5.99	0.89	1.22	0.30	0.70	1.10
	353	0.17	0.94	7.00	1.18	1.03	0.35	0.65	1.03
0.09	142	0.05	0.80	4.70	0.27	1.25	0.12	0.88	1.04
	181	0.07	0.64	4.34	0.40	1.71	0.15	0.85	1.18
	239	0.09	1.01	6.19	0.50	1.38	0.19	0.81	1.18
	301	0.11	0.98	6.61	0.92	1.18	0.28	0.72	1.15
	390	0.14	0.98	6.35	1.37	1.17	0.37	0.63	1.15
	461	0.17	1.21	8.23	1.62	0.93	0.35	0.65	1.01
	498	0.18	1.08	7.04	1.87	1.08	0.38	0.62	1.35

Table SI 2.2c: FBM parameters obtained from fitting the fluorescence decays of EB intercalated in the 12 bp hairpin quenched by Cu^{2+} cations with Equation 2.3.

wt % DNA	$[Cu^{2+}]$ (mM)	$[Cu^{2+}]/[P]$	$k_e[blob]$ $\times 10^7\ s^{-1}$	k_{blob} $\times 10^7\ s^{-1}$	<n>	τ_{fast}	a_{fast}	a_2	χ^2
0.02	31	0.05	0.23	2.61	0.44	1.87	0.11	0.89	1.09
	46	0.08	0.14	2.38	0.74	2.13	0.16	0.84	1.08
	60	0.10	0.67	2.98	0.82	2.07	0.19	0.81	1.06
	75	0.12	1.28	5.58	0.84	1.12	0.21	0.79	1.07
	91	0.15	1.17	4.90	1.09	1.16	0.27	0.73	1.15
	104	0.17	1.07	4.81	1.33	1.33	0.30	0.70	1.08
	120	0.20	1.30	5.58	1.42	1.14	0.34	0.66	1.10
0.04	50	0.04	0.72	4.20	0.34	1.24	0.10	0.90	1.12
	74	0.06	0.53	3.04	0.60	2.08	0.01	0.85	1.06
	102	0.08	0.80	4.12	0.78	1.27	0.19	0.81	1.02
	124	0.10	0.82	3.78	1.02	1.61	0.24	0.76	1.04
	151	0.12	1.16	5.01	1.15	1.36	0.27	0.73	1.03
	176	0.15	1.24	5.67	1.38	1.02	0.32	0.68	1.24
	200	0.17	1.16	5.02	1.61	1.33	0.36	0.64	1.09
0.05	72	0.05	0.26	2.32	0.41	2.23	0.13	0.87	0.99
	104	0.07	0.83	4.51	0.53	1.38	0.14	0.86	1.10
	138	0.09	0.92	3.98	0.77	1.58	0.19	0.81	0.97
	174	0.12	0.97	4.77	0.98	1.29	0.22	0.78	1.10
	208	0.14	1.16	4.77	1.18	1.27	0.29	0.71	1.11
	271	0.18	1.11	5.20	1.85	1.12	0.39	0.61	1.06
	295	0.19	1.34	6.12	2.09	0.94	0.43	0.57	1.20
0.07	88	0.04	0.39	2.91	0.38	0.01	0.11	0.89	1.21
	133	0.06	1.01	4.35	0.53	0.02	0.14	0.86	1.10
	181	0.09	0.89	3.82	0.78	0.03	0.20	0.80	1.20
	224	0.11	0.86	4.20	1.06	0.04	0.25	0.75	1.12
	269	0.13	0.96	4.20	1.29	0.05	0.30	0.70	1.08
	320	0.15	1.01	4.64	1.90	0.09	0.40	0.60	1.13
	365	0.17	1.22	5.86	2.09	0.12	0.41	0.59	1.22

0.09	141	0.05	0.72	4.54	0.58	1.09	0.13	0.87	1.07
	179	0.07	0.54	3.81	0.82	1.12	0.22	0.78	1.41
	242	0.09	0.86	4.11	1.11	1.38	0.26	0.74	1.18
	268	0.10	1.36	6.06	1.57	1.02	0.35	0.65	1.12
	375	0.14	1.91	8.05	2.13	0.83	0.39	0.61	1.08
	482	0.18	1.92	8.21	2.50	0.78	0.42	0.58	1.23
	515	0.19	2.28	9.09	2.59	0.70	0.43	0.57	1.13

Table SI 2.2d: FBM parameters obtained from fitting the fluorescence decays of EB intercalated in the 12 bp duplex quenched by Cu^{2+} cations with Equation 2.3.

wt % DNA	$[Cu^{2+}]$ (mM)	$[Cu^{2+}]/[P]$	$k_e[blob]$ $\times 10^7\ s^{-1}$	k_{blob} $\times 10^7\ s^{-1}$	<n>	τ_{fast}	a_{fast}	a_2	χ^2
0.02	32	0.05	1.43	6.44	0.21	1.27	0.08	0.92	1.07
	46	0.08	0.46	2.42	0.41	2.25	0.15	0.85	1.10
	59	0.10	0.89	3.27	0.56	2.30	0.19	0.81	1.25
	75	0.12	1.12	5.55	0.58	1.47	0.20	0.80	1.12
	89	0.15	1.05	5.77	0.82	1.42	0.24	0.76	1.07
	103	0.17	0.95	5.20	0.97	1.58	0.28	0.72	1.13
	118	0.19	1.01	6.09	1.11	1.37	0.30	0.70	1.11
0.04	33	0.03	0.15	4.92	0.23	1.39	0.12	0.88	1.05
	74	0.06	0.91	4.49	0.40	1.45	0.15	0.85	1.03
	100	0.08	1.06	5.23	0.56	1.52	0.18	0.82	1.06
	124	0.10	0.70	3.69	0.84	2.16	0.24	0.76	1.13
	148	0.12	0.80	4.95	0.94	1.56	0.26	0.74	1.18
	174	0.14	1.05	6.65	1.08	1.16	0.26	0.74	1.12
	199	0.16	1.04	6.41	1.29	1.23	0.31	0.69	1.27
0.06	107	0.06	0.58	4.01	0.47	1.77	0.14	0.86	1.09
	140	0.08	0.75	4.61	0.66	1.51	0.20	0.80	1.11
	173	0.10	0.82	4.75	0.86	1.56	0.24	0.76	1.07
	209	0.11	1.05	5.80	1.02	1.55	0.24	0.76	1.07
	235	0.13	0.89	6.29	1.49	1.22	0.31	0.69	1.21

	276	0.15	1.04	6.48	1.70	1.21	0.33	0.67	1.22
	347	0.19	0.95	6.26	2.09	1.17	0.64	0.36	1.24
0.07	90	0.04	0	2.40	0.40	1.90	0.11	0.89	1.06
	134	0.06	0	2.38	0.66	2.12	0.17	0.83	1.13
	177	0.08	0.41	3.39	0.76	1.86	0.20	0.80	1.12
	221	0.10	0.49	4.20	1.22	1.65	0.29	0.71	1.28
	275	0.13	0.69	4.95	1.42	1.56	0.31	0.69	1.19
	330	0.16	0.93	5.94	1.63	1.24	0.33	0.67	1.17
	372	0.18	0.77	5.27	2.01	1.38	0.37	0.63	1.18
0.09	93	0.03	0.16	3.05	0.25	1.86	0.11	0.89	1.15
	139	0.05	0	2.09	0.47	2.58	0.15	0.85	0.96
	183	0.07	0.55	4.45	0.52	1.53	0.18	0.82	1.14
	240	0.09	0.30	3.67	0.79	1.82	0.23	0.77	1.17
	285	0.10	0.69	5.87	1.18	1.24	0.30	0.70	1.13
	375	0.14	0.84	6.65	1.64	1.07	0.32	0.68	1.08

Table SI 2.2e: FBM parameters obtained from fitting the fluorescence decays of EB intercalated in the 43 bp duplex quenched by Cu^{2+} cations with Equation 2.3.

wt % DNA	$[Cu^{2+}]$ (mM)	$[Cu^{2+}]/[P]$	$k_e[blob]$ $\times 10^7\ s^{-1}$	k_{blob} $\times 10^7\ s^{-1}$	<n>	τ_{fast}	a_{fast}	a_2	χ^2
0.02	11	0.02	0.99	4.72	0.20	0.92	0.11	0.89	1.15
	22	0.04	1.03	4.11	0.37	1.21	0.12	0.88	1.01
	32	0.05	1.23	5.27	0.51	0.89	0.15	0.85	1.05
	40	0.07	1.20	4.45	0.73	1.22	0.20	0.80	1.19
	55	0.09	1.25	4.24	0.98	1.39	0.21	0.79	1.14
	60	0.10	1.39	4.92	1.02	1.36	0.21	0.79	1.22
	77	0.13	1.17	4.03	1.42	1.42	0.29	0.71	1.36
	102	0.17	1.25	3.92	1.59	1.48	0.30	0.70	1.17
	113	0.19	1.84	5.67	1.67	1.15	0.31	0.69	1.32
0.03	17	0.02	0.36	3.62	0.27	0.65	0.14	0.86	1.04
	30	0.03	1.05	4.64	0.39	0.86	0.14	0.86	1.12

	49	0.05	0.92	4.22	0.63	1.21	0.16	0.84	1.04
	59	0.06	0.78	3.85	0.88	1.33	0.19	0.81	1.14
	80	0.09	0.81	3.38	1.22	1.69	0.24	0.76	1.12
	91	0.10	1.15	4.56	1.22	1.14	0.26	0.74	1.21
	120	0.13	1.43	4.79	1.55	1.19	0.30	0.70	1.16
	153	0.17	1.55	5.07	2.04	1.07	0.33	0.67	1.26
	170	0.19	1.53	4.94	2.28	1.16	0.34	0.66	1.09
0.05	27	0.02	0.87	3.53	0.23	1.56	0.07	0.93	1.00
	51	0.03	0.76	3.61	0.43	1.40	0.11	0.89	1.12
	78	0.05	0.78	3.61	0.64	1.19	0.16	0.84	1.22
	101	0.07	1.11	4.29	0.78	1.39	0.19	0.81	1.15
	133	0.09	1.17	4.20	1.05	1.32	0.24	0.76	1.14
	151	0.10	1.28	5.27	1.21	0.86	0.27	0.73	1.16
	194	0.13	1.39	4.66	1.70	0.99	0.32	0.68	1.10
	253	0.17	2.30	6.86	1.90	0.74	0.32	0.68	1.15
	280	0.18	1.99	5.76	2.20	0.89	0.33	0.67	1.13
0.07	70	0.03	1.37	7.15	0.30	0.47	0.17	0.83	1.10
	112	0.05	1.19	5.76	0.52	0.68	0.21	0.79	1.18
	139	0.07	1.07	4.84	0.76	1.05	0.21	0.79	1.13
	188	0.09	1.23	4.54	1.10	1.25	0.26	0.74	1.17
	213	0.10	1.32	4.30	1.78	1.25	0.31	0.69	1.12
	304	0.14	2.05	5.83	2.11	0.89	0.33	0.67	1.17
	375	0.18	2.53	6.35	2.58	0.82	0.34	0.66	1.22
	408	0.19	2.01	4.82	3.22	1.07	0.35	0.65	1.24
0.09	89	0.03	0.94	5.04	0.33	1.32	0.09	0.91	1.01
	143	0.05	0.71	3.77	0.64	1.69	0.18	0.82	1.12
	184	0.07	1.01	4.29	0.78	1.59	0.19	0.81	0.98
	242	0.09	1.25	4.70	1.08	1.40	0.24	0.76	1.10
	268	0.10	1.42	4.63	1.60	1.29	0.28	0.72	1.08
	358	0.13	1.83	5.35	2.20	1.02	0.31	0.69	1.06
	430	0.16	2.39	6.34	2.44	0.80	0.33	0.67	1.11
	515	0.19	2.66	6.24	2.81	0.75	0.36	0.64	1.12

Table SI 2.2f: FBM parameters obtained from fitting the fluorescence decays of EB intercalated in CT DNA quenched by Cu^{2+} cations with Equation 2.3.

wt % DNA	$[Cu^{2+}]$ (mM)	$[Cu^{2+}]/[P]$	$k_e[blob]$ $\times 10^7\ s^{-1}$	k_{blob} $\times 10^7\ s^{-1}$	<n>	τ_{fast}	a_{fast}	a_2	χ^2
0.02	20	0.03	0	2.39	0.16	1.30	0.07	0.93	1.13
	40	0.07	0.85	4.87	0.51	0.80	0.17	0.83	1.13
	60	0.10	0.80	3.51	0.96	1.64	0.21	0.79	1.17
	79	0.13	1.31	4.07	1.20	1.07	0.24	0.76	1.18
	99	0.16	1.48	4.04	1.60	1.60	0.27	0.73	1.17
	115	0.19	1.49	4.12	1.91	1.41	0.29	0.71	1.22
0.03	30	0.03	0.63	4.70	0.16	1.90	0.05	0.95	1.01
	59	0.06	1.04	4.16	0.57	1.81	0.15	0.85	1.20
	90	0.10	1.22	4.40	0.92	1.60	0.20	0.80	1.08
	120	0.13	1.60	4.43	1.35	1.57	0.25	0.75	1.12
	149	0.16	1.54	4.01	1.90	1.58	0.28	0.72	1.19
	172	0.19	1.66	4.09	2.18	1.54	0.31	0.69	1.09
0.05	13	0.01	0.40	3.48	0.04	2.00	0.01	0.99	1.04
	25	0.02	0.09	3.98	0.08	0.09	0.58	0.42	1.08
	50	0.03	1.02	5.98	0.21	1.35	0.06	0.94	1.20
	100	0.07	1.08	4.37	0.50	1.73	0.13	0.87	1.10
	148	0.10	0.84	3.61	0.91	1.93	0.20	0.80	1.11
	200	0.13	1.30	4.36	1.34	1.38	0.26	0.74	1.15
	249	0.16	1.09	3.11	2.13	1.84	0.30	0.70	1.03
	287	0.19	1.84	4.38	2.03	1.54	0.29	0.71	1.15
0.07	35	0.02	0.82	5.03	0.12	0.18	0.26	0.74	1.26
	69	0.03	0.15	2.25	0.33	2.37	0.08	0.92	1.09
	138	0.07	0.63	2.83	0.63	2.66	0.14	0.86	1.19
	208	0.10	1.06	4.32	0.93	1.35	0.19	0.81	1.26
	280	0.13	1.39	4.00	1.52	1.59	0.26	0.74	1.14
	347	0.16	1.73	4.05	2.27	1.51	0.33	0.67	1.18
	399	0.19	2.04	4.45	2.70	1.30	0.33	0.67	1.25
0.09	45	0.02	0.35	5.99	0.10	0.26	0.03	0.97	1.19
	90	0.03	0.80	6.77	0.21	0.84	0.06	0.94	1.13

	179	0.07	0.83	4.78	0.49	1.59	0.13	0.87	1.10
	269	0.10	1.08	4.81	0.86	1.24	0.20	0.80	1.14
	349	0.13	1.29	3.81	1.58	1.68	0.28	0.72	1.11
	455	0.17	1.43	3.90	2.20	1.47	0.31	0.69	1.12
	505	0.19	2.01	4.26	2.44	1.57	0.32	0.68	1.15

Table SI 2.3: Slope and intercept for <n> vs [Cu^{2+}].

DNA Construct	wt % DNA	[DNA] (in base pairs)	slope	intercept
6 bp hairpin	0.02	3.03E-04	9401 ± 206	0
	0.03	4.55E-04	7166 ± 553	-0.19 ± 0.05
	0.05	7.58E-04	3633 ± 149	-0.14 ± 0.03
	0.07	1.06E-03	2687 ± 152	-0.15 ± 0.04
	0.10	1.50E-03	2362 ± 107	-0.21 ± 0.03
8 bp hairpin	0.02	3.03E-04	10 354 ± 184	0
	0.03	4.55E-04	7722 ± 601	-0.07 ± 0.06
	0.05	7.58E-04	4912 ± 236	-0.12 ± 0.04
	0.07	1.06E-03	4335 ± 248	-0.32 ± 0.06
	0.09	1.36E-03	4579 ± 234	-0.46 ± 0.08
12 bp hairpin	0.02	3.52E-04	12 393 ± 429	0
	0.04	5.87E-04	8155 ± 283	-0.04 ± 0.04
	0.05	8.22E-04	7603 ± 515	-0.26 ± 0.10
	0.07	1.06E-03	6494 ± 483	-0.32 ± 0.12
	0.09	1.36E-03	5486 ± 447	-0.11 ± 0.02
12 bp duplex	0.02	3.76E-04	10 132 ± 663	-0.09 ± 0.05
	0.04	6.27E-04	6507 ± 364	-0.03 ± 0.05
	0.06	8.78E-04	7092 ± 498	-0.32 ± 0.11
	0.07	1.13E-03	5562 ± 337	-0.11 ± 0.08
	0.09	1.36E-03	4969 ± 434	-0.28 ± 0.10
43 bp duplex	0.02	3.03E-04	16 225 ± 895	0
	0.03	4.55E-04	13513 ± 234	0

	0.05	7.58E-04	7936 ± 158	0
	0.07	1.06E-03	8314 ± 574	-0.33 ± 0.15
	0.09	1.36E-03	6203 ± 411	-0.24 ± 0.13
CT DNA	0.02	3.03E-04	18 272 ± 486	-0.20 ± 0.04
	0.03	4.55E-04	14 357 ± 500	-0.30 ± 0.06
	0.05	7.58E-04	8614 ± 885	-0.30 ± 0.17
	0.07	1.06E-03	7327 ± 672	-0.36 ± 0.18
	0.09	1.36E-03	5699 ± 402	-0.46 ± 0.14

Chapter 3 Supporting Information

Table SI 3.1a: Decay times and pre-exponential factors retrieved from fitting the fluorescence decays of DNA-EB quenched by Cu^{2+} cations at an ionic strength of 5×10^{-4} M with Equation 3.1.

wt % DNA	$[Cu^{2+}]$ (μM)	$[Cu^{2+}]/[P]$	τ_1 ns	τ_2 ns	τ_3 ns	a_1	a_2	a_3	χ^2
0.02	0	0.00	23.2	10.9		0.95	0.05		1.08
	20	0.03	22.6	9.56		0.85	0.15		1.04
	40	0.07	21.6	7.73		0.76	0.24		1.09
	59	0.10	17.7	7.96	1.73	0.39	0.36	0.25	1.20
	79	0.13	16.2	7.85	1.87	0.27	0.40	0.33	1.18
	100	0.17	13.2	6.09	1.54	0.22	0.41	0.36	1.06
	115	0.19	12.4	5.80	1.51	0.20	0.42	0.37	1.02
0.03	0	0.00	23.7	18.2		0.81	0.19		1.09
	7	0.01	23.4	13.7		0.87	0.13		0.98
	15	0.02	22.8	9.68		0.89	0.11		1.04
	30	0.03	22.5	9.73		0.83	0.17		1.33
	60	0.07	20.8	9.12	1.80	0.54	0.28	0.17	1.06
	90	0.10	17.9	7.64	1.28	0.39	0.36	0.25	1.11
	119	0.13	14.8	6.49	1.46	0.30	0.39	0.30	1.04
	151	0.17	12.9	5.79	1.42	0.41	0.34	0.24	1.10
	172	0.19	11.3	5.30	1.58	0.24	0.42	0.34	1.07
0.05	0	0.00	23.7	16.6		0.85	0.15		1.09
	12	0.01	22.9	9.29		0.93	0.07		1.10
	25	0.02	22.8	9.93		0.90	0.10		1.11
	50	0.03	22.4	8.42		0.85	0.15		1.15
	99	0.07	20.5	8.77	1.38	0.55	0.29	0.16	0.96
	147	0.10	18.0	7.44	1.53	0.44	0.35	0.22	1.12
	201	0.13	15.2	6.60	1.38	0.31	0.38	0.30	1.11

	251	0.17	13.7	6.23	1.45	0.25	0.41	0.34	1.18
	287	0.19	11.4	4.97	1.24	0.25	0.41	0.34	1.07
0.07	0	0.00	23.4	14.9		0.90	0.10		1.05
	17	0.01	23.3	16.2		0.86	0.14		1.25
	35	0.02	22.8	9.61		0.90	0.10		1.00
	69	0.03	22.1	8.24		0.80	0.20		1.05
	139	0.07	20.6	9.09	1.89	0.57	0.28	0.15	1.13
	208	0.10	18.4	8.11	1.64	0.43	0.34	0.23	1.00
	280	0.13	15.8	7.16	1.64	0.32	0.39	0.30	1.08
	352	0.17	13.0	5.94	1.47	0.25	0.34	0.41	1.10
	402	0.19	11.8	5.29	1.31	0.22	0.37	0.41	1.16
0.09	0	0.00	23.9	10.9		0.95	0.05		1.08
	22	0.01	22.9	8.73		0.94	0.06		1.10
	45	0.02	22.7	9.08		0.88	0.12		1.11
	89	0.03	22.3	9.80	0.90	0.73	0.18	0.09	1.21
	180	0.07	20.5	8.87	1.56	0.54	0.30	0.16	1.07
	271	0.10	17.9	7.43	1.46	0.43	0.35	0.22	1.16
	361	0.13	15.7	6.97	1.58	0.32	0.39	0.29	1.10
	447	0.16	12.2	5.36	1.29	0.24	0.41	0.35	1.07
	514	0.19	10.2	1.09	4.37	0.25	0.33	0.42	1.16

Table SI 3.1b: Decay times and pre-exponential factors retrieved from fitting the fluorescence decays of DNA-EB quenched by Cu^{2+} cations at an ionic strength of 5×10^{-3} M with Equation 3.1.

wt % DNA	$[Cu^{2+}]$ (μM)	$[Cu^{2+}]/[P]$	τ_1 ns	τ_2 ns	τ_3 ns	a_1	a_2	a_3	χ^2
0.02	0	0.00	22.9	9.54		0.96	0.04		1.06
	20	0.03	22.5	8.48		0.87	0.13		1.08
	40	0.07	20.7	8.00	0.75	0.58	0.24	0.17	1.09
	60	0.10	19.3	8.50	1.59	0.46	0.33	0.21	1.18
	79	0.13	17.5	7.24	1.20	0.38	0.36	0.25	1.15

	99	0.16	16.2	7.47	1.78	0.32	0.38	0.29	1.20
	115	0.19	14.9	6.66	1.51	0.29	0.40	0.31	1.19
0.03	0	0.00	23.8	17.2		0.84	0.16		0.99
	8	0.01	23.0	9.59		0.93	0.07		1.05
	15	0.02	22.8	8.09		0.91	0.09		1.03
	30	0.03	22.5	7.86		0.85	0.15		1.02
	59	0.06	20.7	9.16	1.82	0.59	0.26	0.15	1.08
	90	0.10	19.0	8.22	1.68	0.46	0.33	0.21	1.07
	120	0.13	16.8	7.60	1.74	0.36	0.36	0.28	1.10
	149	0.16	15.1	6.87	1.68	0.29	0.40	0.31	1.21
	172	0.19	14.0	6.40	1.64	0.26	0.40	0.34	1.15
0.05	0	0.00	24.0	17.9		0.81	0.19		1.17
	13	0.01	23.5	15.6		0.86	0.14		1.13
	25	0.02	23.1	10.2		0.91	0.09		1.06
	50	0.03	22.2	8.80	1.35	0.78	0.15	0.06	1.18
	100	0.07	21.0	9.30	1.80	0.61	0.25	0.14	1.07
	148	0.10	20.0	9.50	2.08	0.45	0.34	0.21	0.98
	200	0.13	17.3	7.57	1.53	0.36	0.37	0.28	1.10
	249	0.16	15.8	7.64	1.89	0.26	0.40	0.33	1.06
	287	0.19	14.4	6.60	1.70	0.27	0.39	0.33	1.15
0.07	0	0.00	24.1	17.8		0.81	0.19		1.11
	17	0.01	23.3	11.1		0.91	0.09		1.25
	35	0.02	22.9	8.95		0.88	0.12		1.23
	69	0.03	22.3	7.95		0.81	0.19		1.12
	138	0.07	21.3	10.1	2.55	0.59	0.27	0.14	1.15
	208	0.10	19.3	8.13	1.41	0.46	0.34	0.2	1.27
	280	0.13	16.9	7.77	1.78	0.32	0.39	0.29	1.12
	347	0.16	13.5	6.09	1.58	0.26	0.39	0.35	1.22
	399	0.19	11.7	5.21	1.36	0.24	0.41	0.35	1.32
0.09	0	0.00	23.7	9.47		0.95	0.05		1.17
	22	0.01	23.3	12.9		0.89	0.11		1.11
	45	0.02	22.7	8.42		0.89	0.11		1.13
	90	0.03	22.4	9.67	1.25	0.75	0.17	0.08	1.05

	179	0.07	21.1	8.61	1.52	0.61	0.26	0.13	1.05
	269	0.10	19.3	8.03	1.34	0.46	0.33	0.21	1.05
	349	0.13	16.6	7.68	1.79	0.32	0.37	0.31	1.05
	455	0.17	14.3	6.55	1.58	0.26	0.40	0.34	1.12
	505	0.19	12.9	6.28	1.77	0.23	0.40	0.37	1.11

Table SI 3.1c: Decay times and pre-exponential factors retrieved from fitting the fluorescence decays of DNA-EB quenched by Cu^{2+} cations at an ionic strength of 7.5×10^{-3} M with Equation 3.1.

wt % DNA	$[Cu^{2+}]$ (μM)	$[Cu^{2+}]/[P]$	τ_1 ns	τ_2 ns	τ_3 ns	a_1	a_2	a_3	χ^2
0.02	0	0.00	22.6	13.0		0.93	0.07		1.00
	10	0.02	22.6	16.8	4.95	0.67	0.24	0.08	1.03
	22	0.04	21.5	12.8	2.83	0.64	0.24	0.12	1.21
	31	0.05	20.4	9.58	1.72	0.61	0.25	0.14	1.15
	40	0.07	19.6	8.08	1.35	0.57	0.28	0.15	1.07
	54	0.09	18.6	8.63	1.76	0.43	0.34	0.23	0.98
	60	0.10	18.6	8.47	1.46	0.42	0.34	0.24	1.26
	77	0.13	18.2	8.67	1.94	0.39	0.36	0.25	0.98
	101	0.17	16.2	7.13	1.36	0.30	0.40	0.30	1.45
	112	0.19	15.8	7.48	2.03	0.30	0.40	0.30	1.11
0.03	0	0.00	22.8	11.0		0.95	0.04		0.99
	16	0.01	22.9	20.9	7.84	0.49	0.40	0.11	1.17
	30	0.03	22.4	14.1	3.70	0.65	0.24	0.11	1.00
	48	0.02	21.2	11.0	2.81	0.61	0.25	0.14	1.12
	62	0.07	20.3	8.78	1.71	0.59	0.27	0.14	1.11
	79	0.03	19.7	8.66	1.75	0.52	0.30	0.18	0.93
	89	0.10	19.2	8.30	1.44	0.47	0.31	0.22	1.10
	118	0.05	18.1	8.32	1.73	0.38	0.36	0.26	1.17
	155	0.17	16.1	7.15	1.81	0.33	0.39	0.28	1.21
	171	0.19	15.5	7.03	1.59	0.29	0.38	0.33	1.17

0.05	0	0.00	23.1	11.6		0.93	0.07		1.14
	27	0.02	22.6	9.86		0.87	0.13		1.27
	50	0.03	23.0	16.6	5.30	0.58	0.29	0.13	1.21
	78	0.05	21.2	8.33	0.75	0.62	0.23	0.15	1.20
	99	0.07	20.7	9.79	1.97	0.56	0.27	0.17	1.09
	134	0.09	19.6	8.46	1.39	0.47	0.33	0.20	1.08
	154	0.10	19.3	8.96	1.83	0.43	0.35	0.22	1.06
	195	0.13	17.1	7.24	1.51	0.40	0.36	0.25	1.08
	257	0.17	15.4	7.20	1.92	0.27	0.40	0.33	0.99
	280	0.19	14.4	6.20	1.33	0.27	0.41	0.31	1.23
0.07	0	0.00	23.1	11.3		0.95	0.05		1.22
	36	0.02	23.9	16.9	3.89	0.64	0.29	0.07	1.16
	72	0.03	20.3	23.1	6.74	0.30	0.56	0.14	1.13
	110	0.05	21.7	10.2	2.02	0.64	0.25	0.12	1.13
	141	0.07	21.4	10.1	1.63	0.57	0.28	0.14	1.11
	187	0.09	20.0	8.66	1.53	0.50	0.32	0.18	1.15
	211	0.10	19.1	8.61	2.00	0.45	0.34	0.21	1.12
	274	0.13	17.6	7.92	1.65	0.35	0.38	0.27	1.07
	352	0.17	15.2	7.08	1.77	0.27	0.41	0.32	1.17
	392	0.18	14.1	6.50	1.75	0.27	0.41	0.32	1.33
0.09	0	0.00	23.2	11.0		0.94	0.06		1.04
	44	0.02	23.6	21.2	7.63	0.11	0.39	0.50	1.20
	89	0.03	22.3	9.88	1.23	0.74	0.17	0.09	1.23
	138	0.05	21.8	9.84	1.73	0.66	0.23	0.11	1.12
	180	0.07	21.4	10.6	2.38	0.55	0.30	0.15	1.08
	243	0.09	19.8	8.41	1.55	0.50	0.31	0.19	1.28
	272	0.10	19.6	9.32	1.97	0.44	0.34	0.22	1.19
	354	0.13	17.2	7.30	1.68	0.39	0.37	0.24	1.28
	455	0.17	14.7	6.78	1.66	0.28	0.39	0.33	1.10
	505	0.19	13.3	5.62	1.20	0.28	0.38	0.34	1.22

Table SI 3.1d: Decay times and pre-exponential factors retrieved from fitting the fluorescence decays of DNA-EB quenched by Cu^{2+} cations at an ionic strength of 1.25×10^{-2} M with Equation 3.1.

wt % DNA	$[Cu^{2+}]$ (μM)	$[Cu^{2+}]/[P]$	τ_1 ns	τ_2 ns	τ_3 ns	a_1	a_2	a_3	χ^2
0.02	0	0.00	22.5	12.0		0.95	0.05		0.97
	10	0.02	21.7	7.21		0.87	0.13		1.02
	22	0.04	21.1	8.96	1.60	0.74	0.19	0.08	1.24
	31	0.05	20.5	8.95	1.36	0.64	0.23	0.13	1.04
	40	0.07	20.3	8.87	1.23	0.59	0.26	0.15	1.10
	54	0.09	19.4	8.50	1.63	0.54	0.29	0.18	1.20
	60	0.10	19.1	8.67	1.97	0.51	0.30	0.19	1.27
	77	0.13	18.6	8.40	1.66	0.45	0.34	0.21	1.25
	101	0.17	17.3	7.18	1.35	0.42	0.34	0.24	1.18
	112	0.19	17.2	7.43	1.38	0.38	0.37	0.25	1.30
0.03	0	0.00	22.8	9.51		0.95	0.05		1.12
	15	0.02	23.3	19.5	7.67	0.55	0.36	0.09	1.10
	32	0.04	22.2	12.9	2.66	0.67	0.23	0.10	1.17
	46	0.05	20.8	7.78	0.79	0.65	0.23	0.13	1.28
	58	0.06	20.6	8.76	1.37	0.60	0.27	0.14	1.26
	80	0.09	19.7	8.83	1.93	0.52	0.31	0.17	1.08
	90	0.10	19.7	9.71	1.96	0.47	0.32	0.21	1.16
	118	0.13	18.5	8.36	1.82	0.43	0.34	0.22	1.11
	153	0.17	17.5	8.06	1.77	0.36	0.38	0.27	1.21
	166	0.18	16.7	7.21	1.56	0.36	0.36	0.28	1.14
0.05	0	0.00	23.2	12.0		0.94	0.06		1.03
	29	0.02	22.8	22.4	8.84	0.47	0.39	0.14	1.04
	51	0.03	22.7	16.2	5.04	0.65	0.22	0.13	1.15

	77	0.05	21.9	10.3	1.74	0.66	0.22	0.11	1.00
	99	0.07	21.3	9.46	1.79	0.61	0.27	0.12	1.14
	135	0.09	20.3	9.02	1.64	0.52	0.30	0.18	1.06
	148	0.10	19.9	8.82	1.72	0.50	0.31	0.19	1.03
	192	0.13	18.8	8.20	1.64	0.43	0.35	0.22	1.10
	252	0.17	17.5	8.16	1.81	0.34	0.37	0.29	1.19
	278	0.18	16.4	7.62	1.86	0.33	0.38	0.29	1.27
0.07	0	0.00	23.3	12.2		0.94	0.07		1.09
	36	0.02	24.1	19.3	4.97	0.52	0.40	0.08	1.15
	70	0.03	22.4	10.6	1.64	0.73	0.18	0.09	1.13
	110	0.05	21.6	9.77	1.26	0.61	0.26	0.13	1.11
	138	0.07	21.2	9.96	2.11	0.59	0.27	0.14	1.11
	185	0.09	20.0	8.58	1.36	0.49	0.33	0.18	1.15
	210	0.10	19.4	8.95	2.06	0.46	0.33	0.21	1.12
	274	0.13	18.0	8.17	1.69	0.38	0.37	0.25	1.25
	356	0.17	16.0	6.90	1.39	0.31	0.39	0.30	1.24
	391	0.18	15.6	7.08	1.53	0.28	0.41	0.31	1.26
0.09	0	0.00	23.2	9.81		0.94	0.06		1.14
	43	0.02	23.1	22.6	9.02	0.48	0.40	0.12	1.06
	89	0.03	23.2	14.5	4.12	0.67	0.25	0.09	1.02
	139	0.05	21.9	10.0	1.73	0.66	0.23	0.11	1.16
	179	0.07	21.6	9.97	1.88	0.61	0.26	0.13	1.17
	243	0.09	20.4	9.40	1.86	0.51	0.30	0.19	1.01
	271	0.10	19.9	8.91	1.73	0.49	0.32	0.20	1.04
	349	0.13	18.4	7.95	1.29	0.39	0.36	0.25	1.21
	455	0.17	16.2	6.91	1.31	0.33	0.37	0.29	1.20
	503	0.18	15.3	6.66	1.51	0.32	0.38	0.30	1.19

Table SI 3.1e: Decay times and pre-exponential factors retrieved from fitting the fluorescence decays of DNA-EB quenched by Cu^{2+} cations at an ionic strength of 2.1×10^{-2} M with Equation 3.1.

wt % DNA	$[Cu^{2+}]$ (μM)	$[Cu^{2+}]/[P]$	τ_1 ns	τ_2 ns	τ_3 ns	a_1	a_2	a_3	χ^2
0.02	0	0.00	22.4	8.11		0.97	0.03		1.01
	11	0.02	21.8	7.22		0.89	0.10		1.06
	20	0.03	21.8	11.3	2.04	0.74	0.18	0.08	0.98
	32	0.05	21.0	8.92	1.39	0.73	0.19	0.08	1.11
	39	0.06	21.9	15.1	3.24	0.51	0.33	0.16	1.19
	54	0.09	20.6	9.65	1.73	0.61	0.25	0.14	1.04
	61	0.10	20.1	8.81	1.65	0.62	0.23	0.15	1.05
	77	0.13	19.7	8.58	1.63	0.57	0.27	0.16	1.27
	102	0.17	19.3	8.83	1.91	0.52	0.30	0.19	1.06
	111	0.18	18.9	7.91	1.11	0.48	0.31	0.20	1.08
0.03	0	0.00	23.3	13.3		0.92	0.08		0.98
	15	0.02	23.0	10.5		0.90	0.10		1.07
	30	0.03	22.5	8.29		0.84	0.16		1.05
	59	0.06	22.1	10.6	1.28	0.66	0.22	0.12	1.05
	89	0.10	21.3	9.27	1.71	0.63	0.25	0.12	1.08
	121	0.13	20.6	8.43	1.22	0.56	0.28	0.16	1.10
	151	0.17	20.3	9.36	1.71	0.50	0.32	0.18	1.10
	173	0.19	19.6	9.03	1.89	0.48	0.33	0.19	1.07
0.05	0	0.00	23.1	10.3		0.96	0.04		1.10
	12	0.01	23.2	10.5		0.92	0.08		1.11
	25	0.02	22.9	9.99		0.91	0.09		1.08
	50	0.03	22.9	5.27		0.95	0.05		1.10
	101	0.07	21.9	8.84	1.38	0.72	0.19	0.09	1.12
	150	0.10	21.4	9.87	2.11	0.61	0.26	0.13	1.14
	199	0.13	20.0	8.84	1.95	0.54	0.30	0.16	1.24
	245	0.16	19.4	8.90	1.81	0.45	0.33	0.22	1.14
	292	0.19	18.1	7.62	1.38	0.42	0.34	0.24	1.29
0.07	0	0.00	23.4	13.4		0.91	0.09		1.08
	18	0.01	23.0	9.29		0.92	0.08		1.12
	35	0.02	22.6	7.94		0.91	0.09		1.16
	69	0.03	22.4	8.19		0.83	0.17		1.17

	140	0.07	21.7	9.43	1.18	0.64	0.23	0.13	1.03
	211	0.10	20.2	8.44	1.51	0.56	0.28	0.16	1.10
	282	0.13	19.0	8.39	1.61	0.46	0.32	0.22	0.95
	345	0.16	17.9	7.71	1.62	0.43	0.35	0.23	1.03
	397	0.19	17.0	7.19	1.51	0.40	0.36	0.24	1.08
0.09	0	0.00	23.3	13.2		0.93	0.07		1.00
	22	0.01	23.1	10.8		0.93	0.07		1.09
	45	0.02	22.7	7.01		0.92	0.08		0.96
	88	0.03	22.7	8.53		0.85	0.15		1.10
	176	0.06	22.0	9.64	1.66	0.68	0.22	0.10	1.10
	268	0.10	20.8	8.84	1.48	0.58	0.27	0.15	1.19
	366	0.13	19.6	8.92	1.67	0.46	0.33	0.21	0.99
	449	0.16	18.3	8.37	1.84	0.40	0.36	0.24	1.18
	522	0.19	16.7	7.21	1.48	0.40	0.34	0.26	1.17

Table SI 3.1f: Decay times and pre-exponential factors retrieved from fitting the fluorescence decays of DNA-EB quenched by Cu^{2+} cations at an ionic strength of 3×10^{-2} M with Equation 3.1.

wt % DNA	$[Cu^{2+}]$ (μM)	$[Cu^{2+}]/[P]$	τ_1 ns	τ_2 ns	τ_3 ns	a_1	a_2	a_3	χ^2
0.02	0	0.00	23.7	15.3		0.88	0.12		1.13
	21	0.03	23.3	16.0	5.15	0.69	0.22	0.08	1.17
	32	0.05	22.5	9.80	0.83	0.72	0.17	0.11	1.14
	41	0.07	22.2	9.98	1.64	0.72	0.20	0.08	1.08
	54	0.09	22.4	12.1	2.45	0.64	0.24	0.12	1.09
	59	0.10	22.0	11.2	1.95	0.66	0.23	0.11	1.01
	81	0.13	22.0	11.0	2.11	0.60	0.26	0.14	1.03
	101	0.17	21.5	11.1	2.47	0.55	0.29	0.16	1.10
	113	0.19	20.9	9.19	1.63	0.59	0.25	0.16	1.11
0.03	0	0.00	23.9	16.2		0.84	0.16		1.21

	25	0.02	23.2	12.5	1.54	0.80	0.13	0.07	1.12
	50	0.03	23.0	11.3	1.01	0.74	0.19	0.08	1.10
	80	0.05	22.7	11.9	2.11	0.70	0.22	0.10	1.06
	103	0.07	22.1	9.13	0.81	0.68	0.21	0.11	1.11
	138	0.09	22.0	10.9	1.98	0.62	0.25	0.13	1.17
	150	0.10	21.9	11.1	1.96	0.60	0.26	0.15	1.00
	196	0.13	21.2	9.19	1.23	0.58	0.27	0.15	1.01
	254	0.17	20.9	10.3	1.97	0.52	0.30	0.18	1.09
	281	0.19	20.5	9.90	2.04	0.51	0.30	0.19	1.12
0.04	0	0.00	24.2	16.4		0.80	0.20		1.11
	19	0.02	23.3	12.1	0.40	0.77	0.14	0.09	1.17
	41	0.03	22.8	10.9	1.10	0.75	0.17	0.08	1.18
	63	0.05	23.2	13.5	2.41	0.65	0.26	0.10	1.17
	81	0.07	22.2	11.2	2.22	0.65	0.24	0.12	1.13
	107	0.09	21.9	10.3	1.56	0.61	0.26	0.13	1.05
	120	0.10	21.8	9.86	1.16	0.58	0.26	0.15	1.15
	155	0.13	20.7	8.06	1.30	0.59	0.26	0.15	1.19
	202	0.17	20.4	9.59	2.07	0.52	0.29	0.18	1.13
	224	0.19	20.1	8.98	1.57	0.49	0.30	0.20	1.08
0.05	0	0.00	24.2	17.3		0.78	0.22		1.12
	25	0.02	24.0	16.5	4.57	0.72	0.24	0.04	1.02
	50	0.03	22.9	11.2	0.73	0.74	0.17	0.10	1.09
	80	0.05	22.5	9.70	1.36	0.75	0.18	0.07	1.04
	103	0.07	22.3	10.7	1.64	0.67	0.21	0.12	1.06
	138	0.09	21.9	9.65	1.33	0.65	0.24	0.11	1.18
	150	0.10	21.4	8.40	1.03	0.63	0.24	0.13	1.15
	196	0.13	21.1	9.14	1.42	0.58	0.26	0.16	1.15
	254	0.17	20.4	9.19	1.57	0.51	0.30	0.19	1.12

	281	0.19	19.8	8.51	1.57	0.51	0.29	0.20	1.29
0.06	0	0.00	23.83	16.62		0.86	0.14		1.11
	30	0.02	23.34	12.77	2.25	0.81	0.15	0.04	1.27
	60	0.03	23.08	12.16	2.09	0.74	0.20	0.06	1.06
	92	0.05	22.33	9.29	0.50	0.64	0.19	0.18	1.19
	120	0.07	22.25	11.02	2.20	0.63	0.24	0.12	1.14
	161	0.09	21.75	10.26	2.03	0.60	0.26	0.14	1.11
	232	0.13	20.09	8.86	1.54	0.49	0.30	0.20	1.10
	302	0.17	19.93	9.15	1.70	0.47	0.32	0.21	1.24
	336	0.18	19.41	8.57	1.61	0.46	0.33	0.20	1.06
0.07	0	0.00	23.6	12.3		0.92	0.08		1.09
	37	0.02	23.9	15.1	2.53	0.74	0.22	0.04	1.10
	71	0.03	23.7	14.2	2.12	0.67	0.26	0.07	1.09
	108	0.05	22.9	12.0	1.89	0.69	0.21	0.10	1.10
	140	0.07	22.6	12.3	2.86	0.65	0.23	0.12	1.08
	188	0.09	22.0	11.1	2.46	0.60	0.26	0.13	1.15
	189	0.09	21.6	10.6	2.13	0.56	0.28	0.16	1.08
	278	0.13	20.8	10.58	2.41	0.48	0.32	0.20	1.14
	386	0.18	19.0	8.70	1.75	0.43	0.33	0.23	1.17
0.08	0	0.00	24.0	16.8		0.84	0.16		1.19
	41	0.02	23.6	14.7	3.47	0.79	0.17	0.04	1.13
	81	0.03	23.1	11.4	1.23	0.74	0.19	0.07	1.15
	128	0.05	22.5	9.63	0.65	0.69	0.19	0.12	1.17
	160	0.07	22.6	10.9	1.88	0.64	0.26	0.10	1.12
	215	0.09	21.7	9.66	1.49	0.60	0.24	0.16	1.23
	237	0.10	22.1	11.4	2.02	0.54	0.29	0.17	1.21
	309	0.13	20.6	8.87	1.53	0.52	0.31	0.17	1.02
	398	0.16	19.5	9.10	1.79	0.45	0.33	0.22	1.09

	446	0.18	19.0	8.51	1.68	0.44	0.34	0.22	1.12
0.09	0	0.00	23.43	12.49		0.92	0.08		1.06
	43	0.02	23.92	18.59	4.87	0.66	0.28	0.06	1.17
	89	0.03	22.82	10.81	1.73	0.79	0.15	0.06	1.07
	140	0.05	22.51	9.85	0.83	0.69	0.18	0.13	1.04
	182	0.07	22.39	10.77	1.90	0.67	0.24	0.10	1.09
	241	0.09	21.54	8.52	0.97	0.64	0.23	0.13	1.17
	270	0.10	21.18	9.47	1.45	0.56	0.27	0.17	1.10
	359	0.13	20.08	8.30	1.06	0.50	0.29	0.21	1.02
	488	0.18	19.00	8.25	1.73	0.47	0.33	0.20	1.17

Table SI 3.1g: Decay times and pre-exponential factors retrieved from fitting the fluorescence decays of DNA-EB quenched by Cu^{2+} cations at an ionic strength of 4×10^{-2} M with Equation 3.1.

wt % DNA	$[Cu^{2+}]$ (μM)	$[Cu^{2+}]/[P]$	τ_1 ns	τ_2 ns	τ_3 ns	a_1	a_2	a_3	χ^2
0.02	0	0.00	23.7	16.7		0.84	0.16		1.16
	9	0.01	23.6	14.5		0.88	0.12		1.04
	20	0.03	23.7	16.9		0.82	0.18		1.00
	40	0.07	23.0	10.0		0.92	0.08		1.09
	59	0.10	23.0	15.1	4.21	0.61	0.27	0.12	1.10
	80	0.13	22.0	10.8	1.94	0.67	0.22	0.11	1.11
	100	0.17	21.8	11.0	2.35	0.64	0.23	0.12	1.00
	116	0.19	21.5	9.98	2.08	0.64	0.25	0.11	1.01
0.03	0	0.00	23.8	16.3		0.84	0.16		1.08
	15	0.02	23.9	17.2		0.80	0.20		1.08
	30	0.03	22.8	9.24		0.87	0.13		1.07
	60	0.07	22.4	10.0	1.25	0.75	0.16	0.09	1.08
	90	0.10	22.9	13.5	2.62	0.61	0.28	0.12	1.08
	120	0.13	21.9	9.72	1.43	0.64	0.23	0.12	1.13

	151	0.17	21.3	8.94	1.50	0.63	0.24	0.13	1.18
	173	0.19	21.2	9.59	1.58	0.58	0.26	0.15	1.05
0.04	0	0.00	23.8	16.2		0.85	0.15		0.97
	10	0.01	23.8	17.1		0.84	0.16		1.10
	20	0.02	23.9	17.3		0.82	0.18		1.11
	39	0.03	23.0	8.86		0.89	0.11		1.11
	80	0.07	22.5	8.49		0.84	0.16		1.19
	119	0.10	22.3	8.09		0.79	0.21		1.12
	160	0.13	21.8	7.35		0.77	0.23		1.15
	201	0.17	21.7	9.39	1.85	0.65	0.23	0.11	1.09
	230	0.19	21.3	10.4	2.03	0.55	0.28	0.16	1.14
0.05	0	0.00	23.9	18.1		0.81	0.19		1.15
	13	0.01	23.9	16.2		0.84	0.16		1.24
	24	0.02	23.3	10.6		0.89	0.11		1.12
	50	0.03	22.7	8.48		0.87	0.13		1.20
	101	0.07	22.8	8.79		0.85	0.15		1.15
	152	0.10	22.4	11.9	2.72	0.63	0.25	0.12	1.02
	203	0.13	21.2	8.83	1.36	0.58	0.26	0.16	1.03
	259	0.17	20.6	9.07	1.91	0.56	0.28	0.16	1.11
	287	0.19	20.4	9.85	2.12	0.51	0.31	0.19	1.08
0.06	0	0.00	23.8	14.6		0.88	0.12		1.02
	15	0.01	24.1	17.5		0.80	0.20		1.13
	30	0.02	23.5	12.8		0.86	0.14		1.19
	60	0.03	23.0	9.01		0.86	0.14		1.14
	119	0.07	22.3	7.63		0.81	0.19		1.08
	180	0.10	21.9	9.20	1.65	0.69	0.21	0.10	1.15
	231	0.13	21.3	10.5	2.44	0.58	0.25	0.17	1.14
	301	0.17	20.9	9.94	2.07	0.52	0.29	0.18	1.11
	343	0.19	20.3	9.42	2.12	0.52	0.30	0.18	1.13
0.07	0	0.00	23.9	17.2		0.82	0.19		1.06
	18	0.01	23.7	16.9		0.85	0.15		1.22
	35	0.02	23.3	11.8		0.88	0.12		1.17
	71	0.03	22.7	7.95		0.88	0.12		1.11

	140	0.07	22.6	11.4	1.45	0.73	0.19	0.08	1.15
	210	0.10	22.2	10.1	1.39	0.65	0.23	0.12	1.08
	280	0.13	20.8	9.41	1.66	0.56	0.27	0.17	1.10
	357	0.17	20.1	8.30	1.55	0.55	0.28	0.16	1.05
	398	0.19	19.7	8.30	1.45	0.51	0.30	0.18	1.13
0.08	0	0.00	24.4	18.3		0.85	0.15		1.06
	20	0.01	24.1	17.5		0.20	0.80		1.22
	40	0.02	23.5	12.0		0.14	0.86		1.17
	79	0.03	24.5	18.8	5.38	0.53	0.38	0.09	1.07
	160	0.07	23.0	12.3	2.31	0.66	0.24	0.10	1.07
	239	0.10	22.1	10.1	1.80	0.64	0.25	0.12	1.01
	320	0.13	20.6	8.94	1.70	0.55	0.28	0.17	1.16
	404	0.17	20.0	9.10	1.97	0.50	0.32	0.19	1.01
	468	0.19	19.3	8.86	1.92	0.48	0.31	0.21	1.12
0.09	0	0.00	24.1	12.2		0.93	0.07		1.07
	45	0.02	23.3	11.4		0.90	0.10		1.08
	90	0.03	23.1	9.57		0.90	0.10		1.09
	181	0.07	23.0	13.9	3.03	0.69	0.22	0.09	1.01
	279	0.10	21.7	9.63	1.41	0.64	0.23	0.14	1.24
	362	0.13	21.1	10.2	2.07	0.54	0.29	0.16	1.02
	446	0.16	20.1	8.95	1.65	0.51	0.29	0.19	1.04
	515	0.19	19.6	8.73	1.65	0.49	0.31	0.20	1.10

Table SI 3.2a: Decay times and pre-exponential factors retrieved from fitting the fluorescence decays of DNA-EB quenched by Ni^{2+} cations at an ionic strength of 5×10^{-4} M with Equation 3.1.

wt % DNA	$[Ni^{2+}]$ (μM)	$[Ni^{2+}]/[P]$	τ_1 ns	τ_2 ns	τ_3 ns	a_1	a_2	a_3	χ^2
0.02	0	0.00	23.2	12.1		0.93	0.07		1.04
	12	0.02	22.7	11.5	1.20	0.79	0.13	0.09	1.09
	20	0.03	22.1	10.9	2.07	0.75	0.15	0.10	1.09

	25	0.04	22.3	13.6	2.70	0.64	0.23	0.14	1.22
	34	0.06	21.4	11.1	1.89	0.57	0.24	0.19	1.10
	40	0.07	21.1	11.7	2.13	0.50	0.29	0.21	1.18
	54	0.09	19.4	10.2	1.83	0.44	0.28	0.28	1.10
	60	0.10	17.9	8.66	1.70	0.44	0.27	0.30	1.15
	85	0.14	15.5	7.55	1.59	0.33	0.32	0.35	1.00
	112	0.18	13.1	6.41	1.55	0.32	0.31	0.38	1.07
0.03	0	0.00	23.2	11.7		0.89	0.11		1.14
	19	0.02	23.0	13.7	1.62	0.76	0.17	0.07	1.05
	30	0.03	22.9	14.9	2.43	0.64	0.24	0.12	1.10
	36	0.04	22.7	14.2	2.77	0.62	0.25	0.13	1.07
	50	0.05	21.2	9.89	1.62	0.63	0.20	0.17	1.07
	60	0.07	20.7	10.7	1.80	0.54	0.24	0.22	1.24
	73	0.08	19.6	9.56	1.77	0.50	0.25	0.25	1.14
	80	0.09	19.4	9.66	1.82	0.47	0.26	0.26	1.08
	90	0.10	18.2	8.65	1.60	0.45	0.25	0.29	1.12
	128	0.14	16.0	8.39	1.73	0.33	0.31	0.36	1.20
	168	0.18	13.0	6.46	1.63	0.33	0.28	0.39	1.18
0.05	0	0.00	23.2	10.9		0.94	0.06		0.99
	30	0.02	24.0	18.5	4.63	0.58	0.35	0.08	1.07
	50	0.03	23.0	14.8	2.44	0.66	0.23	0.11	1.07
	61	0.04	22.4	13.8	2.37	0.68	0.20	0.13	1.29
	83	0.05	21.5	10.7	1.95	0.64	0.20	0.17	0.98
	100	0.07	21.3	11.2	1.91	0.55	0.26	0.19	1.16
	121	0.08	20.1	9.69	1.80	0.52	0.25	0.23	1.17
	150	0.10	18.3	8.17	1.69	0.49	0.23	0.28	1.10
	190	0.13	15.5	7.40	1.60	0.33	0.32	0.35	1.07
	217	0.14	14.6	7.03	1.61	0.35	0.27	0.38	1.04

	283	0.19	12.6	6.92	1.70	0.27	0.29	0.43	1.15
0.07	0	0.00	23.7	15.6		0.88	0.12		1.16
	43	0.02	23.7	17.8	3.53	0.60	0.33	0.07	1.09
	70	0.03	22.6	13.9	2.21	0.65	0.22	0.13	1.09
	85	0.04	22.3	12.4	2.08	0.58	0.26	0.16	1.05
	116	0.05	22.3	12.5	2.09	0.57	0.26	0.16	1.05
	141	0.07	21.2	10.8	1.71	0.55	0.24	0.21	1.14
	169	0.08	20.1	9.40	1.66	0.53	0.24	0.24	1.23
	187	0.09	19.7	9.62	1.80	0.49	0.24	0.27	1.08
	211	0.10	19.1	9.59	1.81	0.43	0.28	0.29	1.16
	270	0.13	15.5	7.50	1.58	0.34	0.32	0.34	1.07
	301	0.14	15.4	8.27	1.79	0.31	0.30	0.38	1.02
	385	0.18	12.5	6.46	1.65	0.33	0.26	0.42	1.16
0.09	0	0.00	23.5	12.2		0.92	0.08		1.04
	59	0.02	23.9	16.4	2.45	0.64	0.29	0.07	1.12
	93	0.03	23.5	15.5	2.81	0.62	0.28	0.10	1.10
	110	0.04	23.0	13.2	1.67	0.61	0.26	0.13	0.98
	153	0.06	21.6	10.7	1.71	0.61	0.22	0.18	1.04
	174	0.06	20.9	9.38	1.55	0.59	0.21	0.20	1.10
	222	0.08	20.4	10.7	1.90	0.48	0.26	0.26	1.10
	244	0.09	19.6	9.69	1.96	0.48	0.26	0.26	1.07
	266	0.10	18.8	8.95	1.72	0.46	0.25	0.29	1.16
	350	0.13	15.5	7.50	1.59	0.33	0.32	0.34	1.08
	381	0.14	15.1	7.55	1.65	0.35	0.27	0.38	1.18
	509	0.19	12.4	6.21	1.59	0.32	0.27	0.41	1.01

Table SI 3.2b: Decay times and pre-exponential factors retrieved from fitting the fluorescence decays of DNA-EB quenched by Ni^{2+} cations at an ionic strength of 5×10^{-3} M with Equation 3.1.

wt % DNA	$[Ni^{2+}]$ (μM)	$[Ni^{2+}]/[P]$	τ_1 ns	τ_2 ns	τ_3 ns	a_1	a_2	a_3	χ^2
0.02	0	0.00	23.4	13.2		0.90	0.10		1.10
	6	0.01	23.2	13.2	2.04	0.82	0.14	0.04	1.05
	12	0.02	23.1	13.9	1.66	0.74	0.19	0.07	1.06
	19	0.03	22.2	11.3	2.07	0.72	0.17	0.11	1.11
	24	0.04	22.0	10.6	1.69	0.70	0.18	0.12	1.10
	30	0.05	21.6	10.8	1.82	0.64	0.20	0.16	1.09
	42	0.07	21.3	11.1	1.96	0.56	0.25	0.19	1.16
	48	0.08	20.4	9.57	1.79	0.56	0.24	0.20	1.13
	55	0.09	19.5	8.92	1.57	0.52	0.24	0.24	1.18
	60	0.10	19.9	10.3	1.90	0.47	0.27	0.26	1.16
	89	0.15	17.5	8.08	1.66	0.42	0.28	0.30	1.12
	118	0.20	15.5	7.58	1.63	0.42	0.38	0.20	0.96
0.03	0	0.00	23.4	13.9		0.90	0.10		1.07
	9	0.01	22.5	10.2	1.19	0.81	0.12	0.07	1.00
	16	0.02	22.8	11.7	1.59	0.80	0.14	0.07	1.15
	30	0.03	22.4	11.7	2.00	0.72	0.18	0.10	1.21
	37	0.04	22.2	11.1	1.37	0.67	0.19	0.14	1.17
	52	0.06	22.1	11.1	1.55	0.62	0.22	0.16	1.08
	60	0.07	21.0	10.6	1.73	0.58	0.23	0.19	1.21
	73	0.08	20.1	9.46	1.74	0.55	0.23	0.22	1.17

	80	0.09	20.0	10.8	1.93	0.46	0.28	0.26	1.02
	92	0.10	19.2	9.79	1.77	0.44	0.27	0.29	1.07
	129	0.14	16.9	7.76	1.74	0.43	0.26	0.31	1.17
	171	0.19	16.0	8.33	1.90	0.34	0.28	0.38	1.20
0.05	0	0.00	25.4	19.2		0.56	0.44		1.13
	16	0.01	23.5	13.4	0.12	0.37	0.55	0.07	1.04
	30	0.02	23.1	12.7	1.42	0.77	0.16	0.07	1.09
	51	0.03	22.9	12.8	2.15	0.69	0.21	0.10	1.01
	61	0.04	22.1	10.6	1.83	0.71	0.17	0.12	1.02
	77	0.05	21.8	11.2	1.87	0.64	0.21	0.16	1.06
	103	0.07	21.1	10.2	1.66	0.57	0.23	0.19	1.12
	122	0.08	20.3	8.93	1.51	0.54	0.24	0.22	1.14
	131	0.09	20.1	10.0	1.96	0.51	0.24	0.25	1.09
	152	0.10	19.8	10.6	1.93	0.43	0.28	0.29	1.03
	220	0.15	16.7	8.26	1.73	0.38	0.26	0.36	1.27
	280	0.19	15.9	6.86	1.10	0.24	0.26	0.50	1.20
0.07	0	0.00	23.5	12.9		0.92	0.08		1.03
	23	0.01	23.0	11.0	1.43	0.88	0.09	0.03	1.12
	44	0.02	22.4	10.4	1.68	0.75	0.15	0.10	1.14
	71	0.03	22.7	11.7	1.80	0.73	0.16	0.11	1.09
	82	0.04	22.3	10.7	1.88	0.74	0.16	0.10	1.12
	102	0.05	22.0	10.8	1.83	0.65	0.20	0.15	1.13
	141	0.07	21.9	11.2	1.87	0.58	0.24	0.18	1.22
	174	0.08	20.4	9.67	1.71	0.52	0.25	0.23	1.11
	191	0.09	19.9	9.33	1.69	0.50	0.24	0.26	1.11
	210	0.10	19.8	10.3	1.90	0.45	0.27	0.28	1.04
	301	0.14	16.9	8.60	1.72	0.36	0.28	0.36	1.16
	389	0.18	14.9	7.44	1.65	0.34	0.28	0.39	1.03

0.09	0	0.00	23.3	11.1		0.94	0.06		1.13
	54	0.02	23.5	16.7	4.02	0.73	0.19	0.07	1.33
	91	0.03	22.9	11.8	1.67	0.72	0.18	0.10	1.05
	109	0.04	22.3	10.2	1.70	0.72	0.15	0.12	1.03
	150	0.05	21.9	10.8	1.98	0.64	0.21	0.14	1.02
	178	0.07	21.7	11.3	1.76	0.55	0.24	0.21	0.94
	221	0.08	20.4	9.34	1.73	0.52	0.24	0.24	1.17
	238	0.09	20.1	9.53	1.75	0.50	0.25	0.24	1.30
	272	0.10	19.1	8.30	1.60	0.49	0.24	0.27	1.17
	383	0.14	16.6	7.92	1.69	0.40	0.25	0.35	0.99
	504	0.18	14.1	6.42	1.53	0.38	0.26	0.37	1.17

Table SI 3.2c: Decay times and pre-exponential factors retrieved from fitting the fluorescence decays of DNA-EB quenched by Ni^{2+} cations at an ionic strength of 1.25×10^{-2} M with Equation 3.1.

wt % DNA	$[Ni^{2+}]$ (μM)	$[Ni^{2+}]/[P]$	τ_1 ns	τ_2 ns	τ_3 ns	a_1	a_2	a_3	χ^2
0.02	0	0.00	23.5	13.5		0.90	0.10		0.98
	13	0.02	23.3	16.4	4.58	0.76	0.19	0.05	1.11
	21	0.03	23.7	16.9	3.27	0.61	0.30	0.09	1.29
	24	0.04	23.2	15.3	2.57	0.66	0.25	0.09	1.13
	33	0.05	23.1	14.3	2.26	0.63	0.27	0.12	1.23
	40	0.07	23.2	15.9	2.65	0.53	0.33	0.14	1.18
	53	0.09	21.8	11.2	1.74	0.62	0.21	0.16	1.09
	61	0.10	21.8	11.8	2.02	0.59	0.23	0.18	1.15
	85	0.14	20.8	10.9	2.00	0.51	0.26	0.22	1.04
	111	0.18	19.8	9.15	1.77	0.55	0.24	0.22	1.13

0.03	0	0.00	23.6	14.6		0.89	0.11		1.13
	18	0.02	23.3	14.3	2.55	0.80	0.15	0.05	0.98
	30	0.03	22.9	12.5	0.25	0.78	0.15	0.07	1.19
	37	0.04	23.4	16.2	3.11	0.63	0.27	0.10	1.28
	50	0.05	22.9	15.1	2.63	0.61	0.25	0.13	1.08
	60	0.07	22.6	12.9	2.29	0.64	0.23	0.14	1.11
	72	0.08	21.7	10.2	1.64	0.65	0.20	0.15	1.30
	80	0.09	21.2	9.64	1.88	0.66	0.18	0.16	1.25
	91	0.10	21.6	11.2	1.77	0.57	0.25	0.18	1.28
	127	0.14	20.6	10.4	1.97	0.53	0.25	0.22	1.03
	167	0.18	19.6	9.70	1.82	0.49	0.26	0.25	1.11
0.05	0	0.00	23.9	15.9		0.85	0.15		1.05
	30	0.02	23.6	18.4	4.42	0.70	0.23	0.07	1.16
	49	0.03	23.7	15.8	1.98	0.63	0.27	0.09	1.20
	61	0.04	23.7	17.1	3.34	0.57	0.32	0.11	1.18
	84	0.06	22.2	9.83	1.64	0.71	0.17	0.11	1.06
	100	0.07	22.1	10.9	1.80	0.66	0.20	0.14	1.13
	121	0.08	21.9	11.5	1.95	0.59	0.23	0.18	1.04
	134	0.09	21.5	11.1	1.86	0.58	0.21	0.20	1.06
	150	0.10	21.7	11.6	1.80	0.52	0.27	0.21	1.04
	217	0.14	19.1	9.20	1.81	0.48	0.24	0.28	1.04
	284	0.19	18.0	8.93	1.70	0.42	0.27	0.31	1.04
0.07	0	0.00	24.5	17.9		0.75	0.25		1.15
	42	0.02	23.8	17.3	3.84	0.71	0.23	0.06	1.07
	70	0.03	22.7	10.9	1.77	0.80	0.12	0.08	1.22
	85	0.04	23.6	16.9	3.72	0.61	0.29	0.11	1.16
	117	0.05	23.9	17.1	3.00	0.46	0.40	0.14	1.15
	139	0.07	21.9	9.03	1.50	0.68	0.18	0.14	1.21

	170	0.08	21.5	10.1	1.85	0.63	0.20	0.17	1.07
	186	0.09	21.7	11.0	1.64	0.56	0.24	0.20	1.19
	210	0.10	21.0	9.73	1.82	0.58	0.23	0.20	1.18
	300	0.14	18.4	7.80	1.46	0.48	0.24	0.27	1.08
	384	0.18	17.7	8.77	1.77	0.41	0.27	0.32	1.17
0.09	0	0.00	23.7	15.1		0.87	0.13		1.00
	57	0.02	23.4	14.9	1.98	0.74	0.20	0.06	1.15
	94	0.03	23.2	15.4	2.46	0.64	0.24	0.12	1.10
	111	0.04	22.8	14.5	2.27	0.64	0.23	0.14	1.13
	156	0.06	21.8	10.1	1.47	0.65	0.19	0.16	1.09
	219	0.08	20.9	10.3	1.96	0.58	0.22	0.20	0.96
	242	0.09	20.9	10.7	1.92	0.52	0.26	0.22	1.11
	272	0.10	20.3	10.1	1.72	0.50	0.26	0.24	1.00
	382	0.14	19.0	9.66	1.73	0.42	0.28	0.30	1.11
	504	0.18	17.2	8.61	1.75	0.39	0.27	0.33	1.26

Table SI 3.2d: Decay times and pre-exponential factors retrieved from fitting the fluorescence decays of DNA-EB quenched by Ni^{2+} cations at an ionic strength of 2.1×10^{-2} M with Equation 3.1.

wt % DNA	$[Ni^{2+}]$ (μM)	$[Ni^{2+}]/[P]$	τ_1 ns	τ_2 ns	τ_3 ns	a_1	a_2	a_3	χ^2
0.02	0	0.00	23.4	13.2		0.90	0.10		1.07
	12	0.02	23.5	20.2	7.09	0.66	0.27	0.08	1.17
	20	0.03	23.5	16.8	3.25	0.68	0.25	0.07	1.09
	40	0.07	23.2	15.4	2.62	0.62	0.27	0.11	1.13
	60	0.10	21.8	9.81	1.52	0.71	0.16	0.13	1.26
	85	0.14	21.5	9.93	1.88	0.67	0.19	0.14	1.11

	112	0.18	21.1	9.54	1.51	0.62	0.22	0.16	1.07
0.03	0	0.00	23.5	13.7		0.91	0.09		1.11
	36	0.04	23.8	17.9	4.02	0.58	0.34	0.09	1.12
	50	0.06	23.8	18.8	4.21	0.47	0.41	0.13	1.21
	60	0.07	22.7	12.8	1.80	0.68	0.21	0.11	1.04
	80	0.09	22.4	12.8	2.14	0.64	0.22	0.14	1.09
	90	0.10	22.1	11.4	1.84	0.64	0.22	0.14	1.15
	135	0.15	20.9	8.77	1.36	0.61	0.20	0.18	1.26
	167	0.18	20.7	9.96	1.78	0.57	0.23	0.20	1.10
0.05	0	0.00	24.1	16.3		0.83	0.17		1.07
	30	0.02	23.9	17.6	4.18	0.69	0.25	0.06	1.03
	50	0.03	23.0	11.6	1.61	0.78	0.14	0.08	1.05
	61	0.04	23.0	12.7	1.56	0.72	0.17	0.11	1.05
	83	0.05	23.1	14.3	2.19	0.65	0.23	0.12	1.13
	100	0.07	22.5	11.3	1.68	0.68	0.19	0.13	1.10
	121	0.08	22.0	11.7	2.07	0.66	0.18	0.16	1.20
	134	0.09	22.2	11.5	2.02	0.62	0.22	0.16	1.06
	150	0.10	21.7	10.2	1.92	0.63	0.20	0.16	1.21
	215	0.14	21.0	11.0	1.88	0.50	0.27	0.23	1.06
	275	0.18	19.7	8.89	1.70	0.52	0.23	0.24	1.21
0.07	0	0.00	23.9	13.7		0.88	0.12		1.04
	35	0.02	23.6	14.1	2.26	0.81	0.16	0.03	1.08
	70	0.03	24.1	16.3	1.78	0.61	0.30	0.09	1.07
	140	0.07	22.8	14.1	2.48	0.62	0.24	0.14	1.30
	211	0.10	21.2	9.27	1.68	0.61	0.22	0.17	1.08
	348	0.16	19.8	9.33	1.54	0.49	0.26	0.25	1.08
	399	0.19	19.2	9.26	1.68	0.48	0.24	0.28	1.24
0.09	0	0.00	23.5	11.9		0.93	0.07		1.21

	57	0.02	23.7	14.5	1.72	0.73	0.21	0.07	1.04
	99	0.04	23.0	13.0	1.64	0.71	0.19	0.10	1.14
	113	0.04	23.4	16.0	3.16	0.61	0.29	0.10	1.25
	152	0.06	22.3	10.9	1.72	0.68	0.19	0.14	1.19
	246	0.09	21.1	9.12	1.60	0.62	0.20	0.18	1.13
	272	0.10	20.9	8.85	1.48	0.60	0.20	0.20	1.19
	378	0.14	19.7	8.72	1.75	0.55	0.23	0.23	1.13
	506	0.19	18.8	8.73	1.74	0.48	0.25	0.28	1.24

Table SI 3.2e: Decay times and pre-exponential factors retrieved from fitting the fluorescence decays of DNA-EB quenched by Ni^{2+} cations at an ionic strength of 3×10^{-2} M with Equation 3.1.

wt % DNA	$[Ni^{2+}]$ (μM)	$[Ni^{2+}]/[P]$	τ_1 ns	τ_2 ns	τ_3 ns	a_1	a_2	a_3	χ^2
0.02	0	0.00	23.00	9.35		0.95	0.05		1.07
	13	0.02	22.90	10.90		0.90	0.10		1.19
	20	0.03	23.10	22.70	11.5	0.47	0.38	0.15	1.13
	24	0.04	23.80	19.60	6.40	0.53	0.39	0.08	1.18
	41	0.07	23.90	16.90	2.74	0.56	0.35	0.09	1.08
	60	0.10	22.10	10.80	1.48	0.74	0.17	0.09	1.03
	76	0.13	22.50	15.30	3.62	0.60	0.25	0.14	1.11
	112	0.18	21.50	10.50	1.68	0.66	0.19	0.15	1.07
0.03	0	0.00	23.9	14.9		0.87	0.13		1.12
	18	0.02	23.9	17.2	2.04	0.69	0.27	0.04	1.11
	30	0.03	23.2	13.6	2.29	0.79	0.15	0.06	0.99
	37	0.04	23.0	13.4	2.57	0.78	0.15	0.07	1.11
	50	0.06	22.7	11.5	2.27	0.78	0.15	0.07	0.96
	60	0.07	23.3	15.6	3.08	0.63	0.27	0.10	1.03

	73	0.08	22.1	9.80	1.41	0.74	0.15	0.10	1.08
	80	0.09	22.8	15.0	2.88	0.63	0.25	0.18	1.04
	90	0.10	22.4	13.4	2.58	0.67	0.21	0.12	1.08
	127	0.14	21.7	10.2	1.82	0.68	0.19	0.13	1.26
	168	0.18	21.3	10.0	1.86	0.64	0.21	0.16	1.10
0.05	0	0.00	23.6	13.9		0.90	0.10		1.17
	31	0.02	23.0	9.43		0.89	0.11		1.11
	50	0.03	24.5	19.9	4.57	0.43	0.48	0.09	1.08
	61	0.04	22.7	10.6	1.89	0.81	0.13	0.06	1.10
	83	0.06	23.4	15.3	2.82	0.63	0.27	0.10	1.11
	100	0.07	23.3	14.9	2.49	0.61	0.27	0.12	1.05
	133	0.09	22.2	12.0	2.57	0.68	0.20	0.12	1.05
	217	0.14	21.4	10.3	1.80	0.61	0.20	0.18	0.92
	283	0.19	21.0	10.2	1.73	0.56	0.24	0.20	1.08
0.07	0	0.00	23.9	16.2		0.82	0.18		1.07
	43	0.02	22.9	8.05		0.89	0.11		1.11
	70	0.03	23.3	13.5	1.54	0.73	0.19	0.08	1.06
	85	0.04	22.6	9.57	1.01	0.78	0.13	0.09	1.10
	117	0.05	23.4	16.0	2.78	0.59	0.30	0.12	1.11
	141	0.07	24.2	17.7	3.02	0.40	0.45	0.14	1.15
	169	0.08	22.1	11.0	1.69	0.65	0.21	0.14	1.13
	210	0.10	23.0	15.2	2.35	0.53	0.31	0.16	1.13
	299	0.14	21.6	11.6	2.03	0.54	0.26	0.20	1.17
	390	0.18	21.4	13.3	2.69	0.45	0.30	0.24	1.24
0.09	0	0.00	23.6	12.9		0.91	0.09		1.04
	33	0.01	23.2	9.45		0.89	0.11		1.00
	94	0.03	25.5	19.0	3.37	0.37	0.53	0.10	1.05
	111	0.04	23.4	14.9	2.13	0.65	0.25	0.10	1.16

	184	0.07	22.8	13.9	2.56	0.61	0.25	0.14	1.09
	219	0.08	21.9	10.7	1.74	0.66	0.20	0.15	1.24
	271	0.10	21.6	10.8	1.77	0.61	0.21	0.18	1.05
	379	0.14	21.4	12.1	2.09	0.51	0.26	0.23	1.13
	510	0.19	20.2	9.76	1.76	0.51	0.24	0.25	1.12

Table SI 3.3a: FBM parameters obtained from fitting the fluorescence decays of DNA-EB quenched by Cu^{2+} cations at an ionic strength of 5×10^{-4} M with Equation 3.2.

wt % DNA	$[Cu^{2+}]$ (μM)	$[Cu^{2+}]/[P]$	$k_e[blob]$ $\times 10^7\ s^{-1}$	k_{blob} $\times 10^7\ s^{-1}$	<n>	τ_{fast}	a_{fast}	a_2	χ^2
0.02	20	0.03	0.00	3.10	0.16	1.27	0.04	0.96	1.08
	40	0.07	0.51	3.75	0.35	1.28	0.09	0.91	1.04
	59	0.10	1.08	3.62	1.30	1.69	0.24	0.76	1.20
	79	0.13	0.87	2.93	2.05	1.78	0.31	0.69	1.18
	100	0.17	1.68	4.18	2.45	1.40	0.32	0.68	1.07
	115	0.19	1.71	4.14	2.75	1.34	0.33	0.67	1.08
0.03	30	0.03	0.37	4.38	0.19	0.00	0.39	0.61	1.33
	60	0.07	0.81	4.32	0.60	1.67	0.17	0.83	1.08
	90	0.10	1.05	3.95	1.24	1.26	0.24	0.76	1.13
	119	0.13	1.44	4.09	1.91	1.40	0.29	0.71	1.15
	151	0.17	1.77	4.45	2.40	1.27	0.31	0.69	1.19
0.05	50	0.03	0.12	2.74	0.21	1.29	0.07	0.93	1.13
	99	0.07	0.96	4.12	0.65	1.40	0.16	0.84	1.06
	147	0.10	1.23	4.25	1.09	1.57	0.21	0.79	1.22
	201	0.13	1.45	4.12	1.79	1.32	0.29	0.71	1.15
	251	0.17	1.67	4.21	2.25	1.29	0.31	0.69	1.14
	287	0.19	2.18	4.90	2.59	1.17	0.31	0.69	1.23

0.07	139	0.07	0.62	3.22	0.68	2.08	0.15	0.85	1.15
	208	0.10	1.12	3.84	1.09	1.60	0.22	0.78	1.08
	280	0.13	1.44	3.95	1.72	1.51	0.28	0.72	1.13
	352	0.17	1.82	4.33	2.35	1.33	0.31	0.69	1.09
0.09	180	0.07	1.03	4.64	0.64	1.41	0.16	0.84	1.11
	271	0.10	1.30	4.54	1.11	1.42	0.21	0.79	1.17
	361	0.13	1.65	4.57	1.61	1.41	0.26	0.74	1.13
	447	0.16	1.96	4.69	2.51	1.19	0.32	0.68	1.12

Table SI 3.3b: FBM parameters obtained from fitting the fluorescence decays of DNA-EB quenched by Cu^{2+} cations at an ionic strength of 5×10^{-3} M with Equation 3.2.

wt % DNA	$[Cu^{2+}]$ (μM)	$[Cu^{2+}]/[P]$	$k_e[blob]$ $\times 10^7\ s^{-1}$	k_{blob} $\times 10^7\ s^{-1}$	<n>	τ_{fast}	a_{fast}	a_2	χ^2
0.02	20	0.03	0.00	2.39	0.16	1.30	0.07	0.93	1.13
	40	0.07	0.85	4.87	0.51	0.80	0.17	0.83	1.13
	60	0.10	0.80	3.51	0.96	1.64	0.21	0.79	1.17
	79	0.13	1.31	4.07	1.20	1.07	0.24	0.76	1.18
	99	0.16	1.48	4.04	1.60	1.60	0.27	0.73	1.17
	115	0.19	1.49	4.12	1.91	1.41	0.29	0.71	1.22
0.03	30	0.03	0.63	4.70	0.16	1.90	0.05	0.95	1.01
	59	0.06	1.04	4.16	0.57	1.81	0.15	0.85	1.20
	90	0.10	1.22	4.40	0.92	1.60	0.20	0.80	1.08
	120	0.13	1.60	4.43	1.35	1.57	0.25	0.75	1.12
	149	0.16	1.54	4.01	1.90	1.58	0.28	0.72	1.19
	172	0.19	1.66	4.09	2.18	1.54	0.31	0.69	1.09
0.05	50	0.03	1.02	5.98	0.21	1.35	0.06	0.94	1.20
	100	0.07	1.08	4.37	0.50	1.73	0.13	0.87	1.10
	148	0.10	0.84	3.61	0.91	1.93	0.20	0.80	1.11

	200	0.13	1.30	4.36	1.34	1.38	0.26	0.74	1.15
	249	0.16	1.09	3.11	2.13	1.84	0.30	0.70	1.03
	287	0.19	1.84	4.38	2.03	1.54	0.29	0.71	1.15
0.07	138	0.07	0.63	2.83	0.63	2.66	0.14	0.86	1.19
	208	0.10	1.06	4.32	0.93	1.35	0.19	0.81	1.26
	280	0.13	1.39	4.00	1.52	1.59	0.26	0.74	1.14
	347	0.16	1.73	4.05	2.27	1.51	0.33	0.67	1.18
	399	0.19	2.04	4.45	2.70	1.30	0.33	0.67	1.25
0.09	179	0.07	0.83	4.78	0.49	1.59	0.13	0.87	1.10
	269	0.10	1.08	4.81	0.86	1.24	0.20	0.80	1.14
	349	0.13	1.29	3.81	1.58	1.68	0.28	0.72	1.11
	455	0.17	1.43	3.90	2.20	1.47	0.31	0.69	1.12
	505	0.19	2.01	4.26	2.44	1.57	0.32	0.68	1.15

Table SI 3.3c: FBM parameters obtained from fitting the fluorescence decays of DNA-EB quenched by Cu^{2+} cations at an ionic strength of 7.5×10^{-3} M with Equation 3.2.

wt % DNA	$[Cu^{2+}]$ (μM)	$[Cu^{2+}]/[P]$	$k_e[blob]$ $\times 10^7\ s^{-1}$	k_{blob} $\times 10^7\ s^{-1}$	<n>	τ_{fast}	a_{fast}	a_2	χ^2
0.02	10	0.02	0.96	5.37	0.15	0.58	0.09	0.91	1.00
	22	0.04	1.07	4.32	0.33	1.34	0.10	0.90	1.17
	31	0.05	0.95	3.50	0.53	1.76	0.14	0.86	1.12
	40	0.07	1.10	4.63	0.63	1.40	0.15	0.85	1.03
	54	0.09	1.01	3.60	1.03	1.71	0.22	0.78	0.96
	60	0.10	1.45	5.11	0.90	1.09	0.23	0.77	1.22
	77	0.13	1.18	3.94	1.12	1.72	0.23	0.77	0.97
	101	0.17	1.32	4.55	1.55	1.18	0.28	0.72	1.41
	112	0.19	1.27	3.66	1.79	1.90	0.27	0.73	1.13

0.03	16	0.01	0.58	3.08	0.16	1.35	0.05	0.95	1.11
	30	0.03	0.33	2.63	0.33	2.64	0.08	0.92	0.97
	48	0.02	0.26	1.95	0.63	0.31	0.15	0.85	1.10
	62	0.07	0.79	3.65	0.62	1.85	0.15	0.85	1.12
	79	0.03	0.88	3.67	0.78	1.83	0.18	0.82	0.93
	89	0.10	1.17	4.45	0.83	1.35	0.21	0.79	1.06
	118	0.05	1.03	3.63	1.24	1.65	0.24	0.76	1.10
	155	0.17	1.28	3.91	1.63	1.76	0.26	0.74	1.09
	171	0.19	1.36	3.92	1.80	1.50	0.31	0.69	1.16
0.05	27	0.02	0.15	2.43	0.15	1.09	0.05	0.95	1.23
	50	0.03	0.56	3.56	0.28	1.64	0.07	0.93	1.14
	78	0.05	1.13	6.05	0.38	0.46	0.22	0.78	1.15
	99	0.07	0.77	2.98	0.65	2.05	0.17	0.83	1.05
	134	0.09	0.99	4.02	0.84	1.52	0.18	0.82	1.04
	154	0.10	1.04	3.79	0.97	1.67	0.21	0.79	1.08
	195	0.13	1.56	4.67	1.20	1.40	0.23	0.77	1.09
	257	0.17	1.56	4.16	1.84	1.68	0.28	0.72	1.04
	280	0.19	1.83	4.94	1.87	1.24	0.27	0.73	1.18
0.07	36	0.02	0.00	3.26	0.15	0.33	0.06	0.94	1.14
	72	0.03	0.59	4.21	0.16	2.62	0.06	0.94	1.09
	110	0.05	0.52	3.12	0.46	2.33	0.11	0.89	1.09
	141	0.07	0.47	3.24	0.57	1.78	0.14	0.86	1.06
	187	0.09	0.97	4.26	0.76	1.45	0.17	0.83	1.14
	211	0.10	1.11	3.94	0.95	1.91	0.20	0.80	1.15
	274	0.13	1.19	4.01	1.37	1.49	0.25	0.75	1.12
	352	0.17	1.52	4.02	1.93	1.58	0.28	0.72	1.18
	392	0.18	1.60	4.00	2.17	1.62	0.29	0.71	1.26

0.09	44	0.02	0.44	4.72	0.11	0.77	0.06	0.94	1.16
	89	0.03	0.58	3.78	0.24	1.31	0.09	0.91	1.21
	138	0.05	0.73	3.76	0.39	1.75	0.11	0.89	1.07
	180	0.07	0.47	2.80	0.65	2.45	0.15	0.85	1.06
	243	0.09	0.96	3.91	0.79	1.60	0.19	0.81	1.19
	272	0.10	0.76	3.03	1.03	1.96	0.22	0.78	1.23
	354	0.13	1.32	4.21	1.31	1.66	0.23	0.77	1.18
	455	0.17	1.66	4.17	1.94	1.48	0.30	0.70	1.12

Table SI 3.3d: FBM parameters obtained from fitting the fluorescence decays of DNA-EB quenched by Cu^{2+} cations at an ionic strength of 1.25×10^{-2} M with Equation 3.2.

wt % DNA	$[Cu^{2+}]$ (μM)	$[Cu^{2+}]/[P]$	$k_e[blob]$ $\times 10^7\ s^{-1}$	k_{blob} $\times 10^7\ s^{-1}$	<n>	τ_{fast}	a_{fast}	a_2	χ^2
0.02	10	0.02	0.79	5.94	0.15	0.37	0.16	0.84	0.93
	22	0.04	0.92	4.25	0.31	1.64	0.09	0.91	1.29
	31	0.05	0.91	3.86	0.48	1.50	0.13	0.87	1.05
	40	0.07	0.79	3.80	0.58	1.40	0.15	0.85	1.07
	54	0.09	1.00	3.81	0.74	1.68	0.18	0.82	1.15
	60	0.10	1.17	3.80	0.81	1.96	0.18	0.82	1.23
	77	0.13	1.24	4.42	0.92	1.47	0.20	0.80	1.26
	101	0.17	1.56	5.15	1.05	1.23	0.22	0.78	1.16
	112	0.19	1.37	4.74	1.21	1.21	0.24	0.76	1.29
0.03	15	0.02	0.25	2.49	0.18	0.39	0.13	0.87	1.04
	32	0.04	0.57	3.09	0.32	1.63	0.09	0.91	1.15
	46	0.05	1.08	5.19	0.41	0.93	0.12	0.88	1.18
	58	0.06	0.93	4.06	0.55	1.41	0.14	0.86	1.14
	80	0.09	1.02	3.67	0.78	1.90	0.17	0.83	1.10

	90	0.10	1.03	3.34	0.87	1.75	0.19	0.81	1.14
	118	0.13	1.07	3.62	1.08	1.76	0.21	0.79	1.11
	153	0.17	1.23	3.85	1.34	1.59	0.24	0.76	1.20
	166	0.18	1.55	4.58	1.32	1.41	0.26	0.74	1.12
0.05	51	0.03	0.57	3.21	0.27	2.37	0.07	0.93	1.06
	77	0.05	0.72	3.63	0.37	1.75	0.11	0.89	0.99
	99	0.07	0.82	4.17	0.50	1.74	0.12	0.88	1.17
	135	0.09	1.14	4.50	0.68	1.45	0.17	0.83	1.03
	148	0.10	1.02	3.98	0.77	1.68	0.19	0.81	0.99
	192	0.13	1.06	4.04	1.30	1.59	0.21	0.79	1.10
	252	0.17	1.24	3.70	1.42	1.69	0.27	0.73	1.19
	278	0.18	1.28	3.59	1.65	1.78	0.27	0.73	1.22
0.07	36	0.02	0.51	3.07	0.13	1.52	0.06	0.94	1.11
	70	0.03	0.60	3.43	0.26	1.70	0.10	0.91	1.11
	110	0.05	0.65	3.70	0.47	1.29	0.13	0.87	1.08
	138	0.07	0.87	3.56	0.54	2.08	0.13	0.87	1.09
	185	0.09	1.07	4.66	0.75	1.18	0.17	0.83	1.18
	210	0.10	1.11	3.77	0.93	1.93	0.20	0.80	1.20
	274	0.13	1.20	3.90	1.25	1.56	0.23	0.77	1.20
	356	0.17	1.71	5.13	1.49	1.10	0.27	0.73	1.26
	391	0.18	1.55	4.37	1.76	1.29	0.28	0.72	1.24
0.09	43	0.02	0.01	3.24	0.11	0.74	0.05	0.95	1.02
	89	0.03	0.26	3.64	0.25	0.87	0.08	0.92	0.99
	139	0.05	0.58	3.37	0.39	1.77	0.11	0.89	1.14
	179	0.07	0.77	3.66	0.48	1.79	0.12	0.88	1.14
	243	0.09	0.73	3.23	0.77	1.86	0.18	0.82	1.03
	271	0.10	1.02	3.80	0.80	1.65	0.19	0.81	1.03
	349	0.13	1.25	4.43	1.10	1.13	0.24	0.76	1.19

	455	0.17	1.44	4.23	1.53	1.25	0.28	0.72	1.19
	503	0.18	1.80	4.71	1.62	1.35	0.27	0.73	1.15

Table SI 3.3e: FBM parameters obtained from fitting the fluorescence decays of DNA-EB quenched by Cu^{2+} cations at an ionic strength of 2.1×10^{-2} M with Equation 3.2.

wt % DNA	$[Cu^{2+}]$ (μM)	$[Cu^{2+}]/[P]$	$k_e[blob]$ $\times 10^7\ s^{-1}$	k_{blob} $\times 10^7\ s^{-1}$	<n>	τ_{fast}	a_{fast}	a_2	χ^2
0.02	11	0.02	0.64	4.56	0.13	0.49	0.06	0.94	1.01
	32	0.05	0.81	3.76	0.35	1.55	0.08	0.92	1.08
	39	0.06	0.71	3.43	0.42	1.54	0.12	0.88	1.10
	54	0.09	0.75	3.45	0.54	1.70	0.14	0.86	1.03
	61	0.10	0.97	3.63	0.56	1.69	0.15	0.85	1.03
	77	0.13	0.94	3.72	0.67	1.68	0.16	0.84	1.21
	111	0.18	1.12	4.57	0.82	1.04	0.20	0.80	1.06
0.03	30	0.03	0.75	6.29	0.16	0.36	0.11	0.89	1.12
	59	0.06	0.53	3.46	0.34	1.31	0.12	0.88	1.12
	89	0.10	0.61	3.37	0.51	2.09	0.13	0.87	1.08
	121	0.13	1.06	5.24	0.55	1.09	0.15	0.85	1.08
	151	0.17	0.62	3.26	0.83	1.74	0.18	0.82	1.15
	173	0.19	0.92	3.53	0.90	1.85	0.19	0.81	1.12
0.05	25	0.02	0.00	3.52	0.08	1.55	0.02	0.98	1.13
	50	0.03	0.00	2.31	0.02	0.11	0.27	0.73	1.15
	101	0.07	0.57	4.98	0.31	0.87	0.11	0.89	1.19
	150	0.10	0.46	3.05	0.55	2.29	0.14	0.86	1.17
	199	0.13	0.77	3.43	0.79	2.06	0.16	0.84	1.20
	245	0.16	0.76	3.17	1.04	1.83	0.22	0.78	1.15
0.07	35	0.02	0.85	3.77	0.09	0.59	0.09	0.91	1.03
	69	0.03	0.70	5.78	0.18	0.19	0.39	0.61	1.04

	140	0.07	0.79	4.42	0.38	1.18	0.13	0.87	0.96
	211	0.10	1.05	4.34	0.63	1.56	0.16	0.84	1.00
	282	0.13	1.20	4.08	0.91	1.55	0.21	0.79	0.98
	345	0.16	1.32	4.19	1.12	1.55	0.22	0.78	1.02
	397	0.19	1.40	4.10	1.27	1.49	0.23	0.77	1.15
0.09	22	0.01	0.00	3.51	0.03	0.09	0.64	0.36	1.02
	45	0.02	0.64	8.00	0.07	1.74	0.00	1.00	0.94
	88	0.03	0.37	5.00	0.15	0.55	0.11	0.89	1.01
	176	0.06	0.43	3.55	0.36	1.94	0.11	0.89	1.04
	268	0.10	0.98	4.51	0.56	1.45	0.14	0.86	1.14
	366	0.13	0.98	3.80	0.90	1.59	0.20	0.80	0.95
	449	0.16	1.21	3.90	1.16	1.71	0.23	0.77	0.96

Table SI 3.3f: FBM parameters obtained from fitting the fluorescence decays of DNA-EB quenched by Cu^{2+} cations at an ionic strength of 3×10^{-2} M with Equation 3.2.

wt % DNA	$[Cu^{2+}]$ (μM)	$[Cu^{2+}]/[P]$	$k_e[blob]$ $\times 10^7\ s^{-1}$	k_{blob} $\times 10^7\ s^{-1}$	<n>	τ_{fast}	a_{fast}	a_2	χ^2
0.02	21	0.03	0.80	6.20	0.16	0.17	0.36	0.64	1.12
	32	0.05	0.85	5.40	0.22	0.79	0.11	0.89	1.08
	41	0.07	0.92	4.95	0.26	1.58	0.08	0.92	1.08
	54	0.09	0.25	2.17	0.41	2.69	0.13	0.87	1.15
	59	0.10	0.66	2.98	0.39	2.03	0.11	0.89	1.03
	81	0.13	0.63	3.30	0.45	2.10	0.13	0.87	1.04
	101	0.17	0.81	3.15	0.58	2.37	0.16	0.84	0.96
0.03	16	0.02	0.80	3.59	0.09	1.65	0.04	0.96	1.15
	32	0.03	0.71	5.20	0.17	0.81	0.07	0.93	1.26
	46	0.05	0.26	2.51	0.30	2.36	0.09	0.91	1.06

	56	0.06	0.93	5.96	0.28	0.68	0.12	0.88	1.22
	80	0.09	0.93	3.99	0.38	1.85	0.12	0.88	1.12
	91	0.10	0.42	2.72	0.51	1.82	0.16	0.84	1.12
	151	0.17	0.93	3.31	0.67	1.92	0.18	0.82	1.08
	172	0.19	0.93	3.34	0.74	1.99	0.18	0.82	1.15
0.04	19	0.02	0.18	1.95	0.12	2.00	0.03	0.97	1.13
	41	0.03	0.92	3.91	0.18	1.19	0.08	0.92	1.15
	63	0.05	0.39	2.14	0.32	2.44	0.10	0.90	1.19
	81	0.07	0.90	3.32	0.36	2.23	0.11	0.89	1.02
	107	0.09	0.95	4.08	0.41	1.47	0.13	0.87	0.94
	120	0.10	1.09	5.28	0.41	0.80	0.17	0.83	1.01
	155	0.13	1.49	6.92	0.47	0.95	0.15	0.85	1.04
	202	0.17	1.30	4.02	0.66	1.94	0.17	0.83	1.14
	224	0.19	1.37	4.80	0.69	1.36	0.19	0.81	1.23
0.05	25	0.02	0.00	1.55	0.11	4.39	0.04	0.96	1.03
	50	0.03	0.41	3.72	0.18	0.81	0.09	0.91	1.04
	80	0.05	1.08	6.86	0.20	0.87	0.08	0.92	0.96
	103	0.07	1.41	9.44	0.25	0.07	0.91	0.09	1.00
	138	0.09	1.07	5.30	0.35	1.15	0.11	0.89	1.02
	150	0.10	1.26	6.82	0.38	0.74	0.14	0.86	0.94
	196	0.13	1.15	4.93	0.50	1.28	0.15	0.85	1.01
	254	0.17	1.22	4.62	0.65	1.39	0.18	0.82	1.04
	281	0.19	1.24	4.38	0.72	1.54	0.19	0.81	1.21
0.06	30	0.02	0.16	3.03	0.12	2.47	0.05	0.95	1.01
	60	0.03	0.31	3.21	0.21	2.22	0.06	0.94	0.96
	92	0.05	0.94	6.13	0.27	0.41	0.20	0.80	1.08
	120	0.07	0.70	3.66	0.39	2.12	0.12	0.88	1.10

	161	0.09	0.91	4.45	0.46	1.73	0.13	0.87	1.03
	232	0.13	1.25	4.82	0.71	1.31	0.19	0.81	1.04
	302	0.17	1.14	4.18	0.82	1.49	0.20	0.80	1.14
	336	0.18	1.35	4.96	0.84	1.25	0.19	0.81	0.95
0.07	37	0.02	0.00	3.36	0.10	0.80	0.06	0.94	1.12
	71	0.03	0.11	2.95	0.23	0.51	0.14	0.86	1.05
	108	0.05	0.00	2.05	0.33	2.20	0.10	0.90	1.11
	140	0.07	0.62	2.50	0.36	2.77	0.12	0.88	1.09
	188	0.09	0.60	2.79	0.50	2.48	0.13	0.87	1.01
	189	0.09	0.50	2.58	0.63	2.24	0.16	0.84	1.21
	278	0.13	0.96	3.16	0.76	2.20	0.19	0.81	1.04
	386	0.18	1.16	3.53	1.05	1.70	0.23	0.77	1.20
0.08	41	0.02	0.00	2.01	0.12	3.34	0.04	0.96	1.01
	81	0.03	0.49	4.02	0.20	1.22	0.07	0.93	1.06
	128	0.05	1.05	6.48	0.24	0.38	0.17	0.83	1.15
	160	0.07	0.51	3.75	0.37	1.87	0.10	0.90	1.03
	215	0.09	1.08	5.24	0.40	1.24	0.16	0.84	1.17
	237	0.10	0.51	3.03	0.55	1.97	0.16	0.84	1.21
	309	0.13	1.20	5.32	0.64	1.20	0.16	0.84	1.19
	398	0.16	0.94	3.34	0.99	1.78	0.22	0.78	1.15
0.09	43	0.02	0.24	4.38	0.08	0.19	0.33	0.67	1.01
	89	0.03	0.00	2.27	0.19	2.29	0.07	0.93	0.96
	140	0.05	0.59	4.36	0.24	0.88	0.13	0.87	1.08
	182	0.07	0.52	3.49	0.34	1.91	0.10	0.90	1.06
	241	0.09	0.88	5.04	0.39	1.04	0.13	0.87	1.15
	270	0.10	1.01	4.40	0.52	1.30	0.16	0.84	1.19
	359	0.13	1.19	4.94	0.67	0.97	0.20	0.80	1.15
	488	0.18	1.52	5.06	0.84	1.41	0.18	0.82	1.18

Table SI 3.3g: FBM parameters obtained from fitting the fluorescence decays of DNA-EB quenched by Cu^{2+} cations at an ionic strength of 4×10^{-2} M with Equation 3.2.

wt % DNA	$[Cu^{2+}]$ (μM)	$[Cu^{2+}]/[P]$	$k_e[blob]$ $\times 10^7\ s^{-1}$	k_{blob} $\times 10^7\ s^{-1}$	<n>	τ_{fast}	a_{fast}	a_2	χ^2
0.02	20	0.03	0.00	3.49	0.01	0.15	0.31	0.69	1.03
	59	0.10	0.60	3.70	0.27	2.28	0.08	0.92	1.12
	80	0.13	0.49	2.78	0.39	2.17	0.11	0.89	1.14
	100	0.17	0.50	2.43	0.47	2.57	0.13	0.87	1.04
	116	0.19	0.93	3.99	0.43	2.01	0.11	0.89	1.10
0.03	30	0.03	0.67	5.12	0.10	1.25	0.05	0.95	1.09
	60	0.07	0.94	5.37	0.18	1.17	0.09	0.91	1.13
	90	0.10	0.00	1.99	0.40	2.72	0.12	0.88	1.09
	120	0.13	0.82	4.80	0.36	1.37	0.12	0.88	1.13
	151	0.17	1.15	6.33	0.40	1.00	0.13	0.87	1.19
	173	0.19	0.65	3.50	0.54	1.74	0.16	0.84	1.09
0.04	39	0.03	0.23	3.48	0.07	2.59	0.04	0.96	1.09
	80	0.07	0.73	5.76	0.17	0.40	0.13	0.87	1.19
	119	0.10	0.69	5.55	0.24	0.83	0.09	0.91	1.06
	160	0.13	1.07	7.06	0.29	0.22	0.37	0.63	1.02
	201	0.17	0.96	4.83	0.38	1.79	0.11	0.89	1.13
	230	0.19	0.82	3.57	0.57	1.92	0.16	0.84	1.18
0.05	24	0.02	0.00	4.94	0.08	1.33	0.01	0.99	1.14
	101	0.07	0.32	4.36	0.16	0.87	0.08	0.92	1.10
	152	0.10	0.66	4.20	0.36	2.05	0.09	0.91	1.16
	203	0.13	0.99	5.45	0.49	1.14	0.16	0.84	1.07

	259	0.17	1.00	4.27	0.61	1.88	0.15	0.85	1.11
	287	0.19	0.93	3.62	0.75	1.94	0.18	0.82	1.06
0.06	30	0.02	0.00	3.36	0.06	0.25	0.18	0.82	1.21
	60	0.03	0.33	3.10	0.13	1.27	0.07	0.93	1.10
	119	0.07	1.03	4.54	0.21	1.89	0.08	0.92	0.97
	180	0.10	1.28	6.17	0.30	1.25	0.09	0.91	1.19
	231	0.13	0.88	2.91	0.56	2.47	0.17	0.83	1.17
	301	0.17	0.93	3.45	0.67	2.03	0.18	0.82	1.12
	343	0.19	0.88	3.10	0.80	2.23	0.19	0.81	1.11
0.07	35	0.02	0.00	3.70	0.06	0.10	0.37	0.63	1.17
	71	0.03	0.64	7.58	0.10	0.17	0.39	0.61	1.08
	140	0.07	0.47	3.54	0.23	1.48	0.08	0.92	1.15
	210	0.10	0.67	4.75	0.34	1.28	0.12	0.88	1.06
	280	0.13	1.06	4.42	0.56	1.52	0.16	0.84	1.09
	357	0.17	1.35	5.38	0.60	1.41	0.15	0.85	1.06
	398	0.19	1.26	4.94	0.72	1.33	0.18	0.82	1.09
0.08	79	0.03	0.52	5.40	0.14	0.87	0.07	0.93	1.10
	160	0.07	0.13	2.47	0.34	2.56	0.10	0.90	1.12
	239	0.10	0.79	4.31	0.40	1.75	0.11	0.89	0.99
	320	0.13	1.10	4.50	0.61	1.65	0.17	0.83	1.15
	404	0.17	1.32	5.15	0.73	1.37	0.16	0.84	1.00
	468	0.19	1.41	4.31	0.84	1.73	0.20	0.80	1.15
0.09	45	0.02	0.00	3.81	0.06	0.52	0.06	0.94	1.00
	181	0.07	0.00	1.67	0.32	3.15	0.09	0.91	1.01
	279	0.10	0.92	4.47	0.39	1.39	0.13	0.87	1.22
	362	0.13	1.02	4.06	0.60	1.77	0.15	0.85	1.01
	446	0.16	1.38	4.92	0.67	1.37	0.18	0.82	1.06
	515	0.19	1.25	4.31	0.79	1.53	0.20	0.80	1.06

Table SI 3.4a: FBM parameters obtained from fitting the fluorescence decays of DNA-EB quenched by Ni^{2+} cations at an ionic strength of 5×10^{-4} M with Equation 3.2.

wt % DNA	$[Ni^{2+}]$ (μM)	$[Ni^{2+}]/[P]$	$k_e[blob]$ $\times 10^7\ s^{-1}$	k_{blob} $\times 10^7\ s^{-1}$	<n>	τ_{fast}	a_{fast}	a_2	χ^2
0.02	12	0.02	0.11	1.97	0.19	1.38	0.08	0.92	1.08
	20	0.03	0.47	2.00	0.31	2.27	0.10	0.90	1.02
	25	0.04	0.84	3.00	0.32	2.00	0.12	0.88	1.14
	34	0.06	0.60	2.35	0.59	1.92	0.19	0.81	1.08
	40	0.07	0.32	1.81	0.86	2.16	0.21	0.79	1.13
	54	0.09	1.03	2.40	1.06	1.79	0.27	0.73	1.09
	60	0.10	1.29	2.67	1.24	1.72	0.30	0.70	1.10
	85	0.14	1.70	3.16	1.76	1.55	0.34	0.66	1.04
	112	0.18	2.35	3.32	2.25	1.51	0.37	0.63	1.07
0.03	19	0.02	0.00	0.93	0.20	1.34	0.07	0.93	1.04
	30	0.03	0.00	1.07	0.36	2.10	0.11	0.83	1.08
	36	0.04	0.00	1.15	0.45	2.55	0.12	0.88	1.03
	50	0.05	1.07	2.83	0.41	1.69	0.18	0.82	1.05
	60	0.07	0.70	1.86	0.74	1.85	0.22	0.78	1.13
	73	0.08	0.63	1.99	0.98	1.86	0.25	0.75	0.98
	80	0.09	1.27	2.56	0.91	1.82	0.26	0.74	1.02
	90	0.10	1.48	2.73	1.06	1.63	0.29	0.71	1.06
	128	0.14	1.30	2.20	2.03	1.70	0.36	0.64	1.11
	168	0.18	1.96	2.44	2.65	1.67	0.39	0.61	1.10
0.05	61	0.04	0.96	3.35	0.27	1.49	0.13	0.87	1.18
	83	0.05	0.56	2.17	0.51	2.05	0.17	0.83	0.95
	100	0.07	0.39	2.02	0.70	1.97	0.19	0.81	1.08
	121	0.08	0.73	2.39	0.84	1.87	0.24	0.76	1.00
	150	0.10	1.53	2.99	0.98	1.76	0.28	0.72	1.03
	190	0.13	1.72	3.39	1.62	1.54	0.34	0.66	1.06
	217	0.14	1.85	2.76	2.03	1.63	0.38	0.62	1.02

	283	0.19	1.44	1.86	3.14	1.70	0.33	0.57	1.16
0.07	70	0.03	0.76	3.48	0.22	1.36	0.10	0.90	0.96
	85	0.04	0.39	1.90	0.37	2.08	0.13	0.87	1.03
	116	0.05	0.62	2.55	0.46	2.03	0.16	0.84	1.02
	141	0.07	1.03	3.03	0.56	1.69	0.20	0.80	1.10
	169	0.08	1.31	3.40	0.68	1.67	0.24	0.76	1.15
	187	0.09	1.43	3.20	0.79	1.77	0.26	0.74	1.14
	211	0.10	1.24	2.87	1.02	1.79	0.29	0.71	1.15
	270	0.13	1.73	3.41	1.61	1.54	0.34	0.66	1.12
	301	0.14	1.46	2.26	2.22	1.76	0.38	0.62	0.97
	385	0.18	2.46	2.54	2.76	1.65	0.41	0.59	1.13
0.09	174	0.06	0.98	3.00	0.55	1.64	0.20	0.80	1.00
	222	0.08	0.76	2.15	0.91	1.92	0.26	0.74	1.06
	244	0.09	1.25	2.75	0.89	1.95	0.26	0.74	1.08
	266	0.10	1.18	2.57	1.08	1.77	0.29	0.71	1.18
	350	0.13	1.72	3.37	1.63	1.54	0.34	0.66	1.06
	381	0.14	1.97	2.77	1.88	1.64	0.37	0.63	1.12
	509	0.19	2.41	2.69	2.73	1.60	0.41	0.59	1.02

Table SI 3.4b: FBM parameters obtained from fitting the fluorescence decays of DNA-EB quenched by Ni^{2+} cations at an ionic strength of 5×10^{-3} M with Equation 3.2.

wt % DNA	$[Ni^{2+}]$ (μM)	$[Ni^{2+}]/[P]$	$k_e[blob]$ $\times 10^7\ s^{-1}$	k_{blob} $\times 10^7\ s^{-1}$	<n>	τ_{fast}	a_{fast}	a_2	χ^2
0.02	6	0.01	0.00	0.00	0.13	2.00	0.04	0.96	1.03
	12	0.02	0.00	1.47	0.24	1.65	0.07	0.93	1.02
	19	0.03	0.68	2.29	0.30	2.15	0.12	0.88	1.02
	24	0.04	0.81	2.87	0.32	1.79	0.12	0.88	0.94
	30	0.05	0.48	2.01	0.51	1.99	0.16	0.84	1.13

	42	0.07	0.65	2.28	0.62	2.00	0.19	0.81	1.02
	48	0.08	1.28	3.39	0.61	1.79	0.20	0.80	1.14
	55	0.09	1.38	3.28	0.76	1.60	0.24	0.76	1.08
	60	0.10	0.97	2.37	0.94	1.91	0.26	0.74	1.13
	89	0.15	1.71	3.58	1.13	1.63	0.29	0.71	1.09
0.03	30	0.03	0.00	4.02	0.19	1.56	0.09	0.91	1.02
	37	0.04	0.16	4.44	0.21	1.33	0.13	0.87	1.02
	52	0.06	0.59	3.10	0.37	1.57	0.16	0.84	0.94
	60	0.07	0.18	2.55	0.53	1.84	0.20	0.80	1.13
	73	0.08	0.91	3.58	0.58	1.75	0.22	0.78	1.23
	80	0.09	0.97	2.91	0.77	1.84	0.25	0.75	1.13
	92	0.10	1.01	2.92	0.90	1.74	0.29	0.71	1.10
	129	0.14	1.74	3.34	1.22	1.76	0.31	0.69	1.16
	171	0.19	1.71	2.57	1.77	1.87	0.37	0.63	1.27
0.05	61	0.04	1.99	7.56	0.19	1.46	0.10	0.90	1.06
	77	0.05	1.30	3.32	0.36	1.86	0.16	0.84	1.12
	103	0.07	1.27	3.56	0.50	1.65	0.19	0.81	1.04
	122	0.08	1.63	5.07	0.53	1.42	0.21	0.79	1.18
	131	0.09	1.62	3.39	0.67	1.92	0.25	0.75	0.95
	152	0.10	1.60	3.22	0.83	1.81	0.27	0.73	1.08
	220	0.15	1.91	2.95	1.41	1.72	0.35	0.65	1.00
	280	0.19	1.97	3.87	2.02	1.06	0.49	0.51	1.03
0.07	82	0.04	1.29	3.77	0.22	1.85	0.10	0.90	0.99
	102	0.05	0.84	3.14	0.35	1.84	0.15	0.85	1.00
	141	0.07	0.61	2.76	0.48	1.87	0.18	0.82	1.06
	174	0.08	1.19	3.37	0.66	1.69	0.23	0.77	1.08
	191	0.09	1.28	3.21	0.74	1.70	0.26	0.74	1.18
	210	0.10	1.03	2.48	0.96	1.88	0.28	0.72	1.14
	301	0.14	1.52	2.57	1.58	1.70	0.35	0.65	1.15

	389	0.18	2.14	2.77	2.25	1.62	0.38	0.62	1.12
0.09	109	0.04	0.52	2.83	0.27	1.81	0.12	0.88	1.02
	150	0.05	0.64	3.10	0.40	1.72	0.16	0.84	1.02
	178	0.07	0.70	2.62	0.54	1.72	0.21	0.79	0.94
	221	0.08	0.83	2.54	0.75	1.77	0.24	0.76	1.13
	238	0.09	0.84	2.76	0.81	1.79	0.24	0.76	1.23
	272	0.10	1.13	2.94	0.91	1.74	0.28	0.72	1.13
	383	0.14	2.11	2.87	1.64	1.69	0.35	0.65	1.00
	504	0.18	2.79	3.06	2.35	1.55	0.37	0.63	1.26

Table SI 3.4c: FBM parameters obtained from fitting the fluorescence decays of DNA-EB quenched by Ni^{2+} cations at an ionic strength of 1.25×10^{-2} M with Equation 3.2.

wt % DNA	$[Ni^{2+}]$ (μM)	$[Ni^{2+}]/[P]$	$k_e[blob]$ $\times 10^7\ s^{-1}$	k_{blob} $\times 10^7\ s^{-1}$	<n>	τ_{fast}	a_{fast}	a_2	χ^2
0.02	13	0.02	2.07	8.75	0.07	0.19	0.19	0.81	1.10
	21	0.03	0.56	2.83	0.18	1.73	0.07	0.93	1.22
	24	0.04	0.81	26.26	0.21	1.83	0.08	0.92	1.08
	33	0.05	0.21	2.00	0.33	1.96	0.10	0.90	1.21
	40	0.07	0.00	1.52	0.46	2.08	0.13	0.87	1.12
	53	0.09	0.59	2.27	0.47	1.83	0.16	0.84	1.05
	61	0.10	0.47	1.88	0.57	2.09	0.18	0.82	1.16
	85	0.14	0.84	2.60	0.69	2.00	0.22	0.78	1.04
0.03	30	0.03	0.00	1.80	0.22	2.58	0.08	0.92	1.16
	37	0.04	0.55	2.36	0.23	2.29	0.08	0.92	1.23
	50	0.05	0.77	2.99	0.28	1.77	0.12	0.88	1.03
	60	0.07	0.76	3.13	0.31	1.97	0.13	0.87	1.07

	72	0.08	1.09	3.62	0.38	1.65	0.15	0.85	1.25
	80	0.09	1.13	2.86	0.44	2.05	0.16	0.84	1.18
	91	0.10	0.57	2.45	0.58	1.81	0.18	0.82	1.23
	127	0.14	1.01	2.66	0.70	1.98	0.22	0.78	1.04
	167	0.18	1.12	2.68	0.90	1.84	0.25	0.75	1.13
0.05	61	0.04	1.32	4.99	0.17	1.51	0.09	0.91	1.12
	84	0.06	1.16	4.55	0.25	1.68	0.11	0.89	1.00
	100	0.07	1.29	3.95	0.31	1.74	0.13	0.87	1.08
	121	0.08	1.21	3.67	0.39	1.79	0.17	0.83	1.00
	134	0.09	0.97	2.63	0.50	1.89	0.20	0.80	1.02
	150	0.10	0.75	2.61	0.59	1.78	0.21	0.79	1.02
	217	0.14	1.67	3.36	0.83	1.77	0.27	0.73	1.10
	284	0.19	1.56	2.85	1.19	1.69	0.30	0.70	1.00
0.07	70	0.03	1.55	4.13	0.14	1.86	0.08	0.92	1.16
	85	0.04	1.08	3.70	0.18	2.20	0.08	0.92	1.12
	117	0.05	1.00	3.19	0.29	1.95	0.12	0.88	1.07
	139	0.07	1.26	5.33	0.29	1.51	0.14	0.86	1.13
	170	0.08	1.63	4.54	0.35	1.77	0.17	0.83	1.03
	186	0.09	1.00	3.23	0.50	1.61	0.20	0.80	1.13
	210	0.10	1.24	3.60	0.52	1.84	0.20	0.80	1.08
	300	0.14	2.02	4.74	0.78	1.42	0.27	0.73	1.04
	384	0.18	1.55	2.76	1.27	1.76	0.32	0.68	1.10
0.09	94	0.03	0.37	2.31	0.23	1.96	0.11	0.89	1.05
	111	0.04	1.09	3.54	0.23	1.71	0.13	0.87	1.04
	156	0.06	1.21	3.93	0.33	1.47	0.16	0.84	1.03
	219	0.08	1.02	2.65	0.59	2.03	0.20	0.80	0.96
	242	0.09	0.89	2.62	0.69	1.94	0.22	0.78	1.06
	272	0.10	1.11	2.90	0.74	1.72	0.24	0.76	0.99
	382	0.14	1.20	2.64	1.10	1.71	0.30	0.70	1.14
	504	0.18	1.45	2.60	1.45	1.75	0.33	0.67	1.20

Table SI 3.4d: FBM parameters obtained from fitting the fluorescence decays of DNA-EB quenched by Ni^{2+} cations at an ionic strength of 2.1×10^{-2} M with Equation 3.2.

wt % DNA	$[Ni^{2+}]$ (μM)	$[Ni^{2+}]/[P]$	$k_e[blob]$ $\times 10^7\ s^{-1}$	k_{blob} $\times 10^7\ s^{-1}$	<n>	τ_{fast}	a_{fast}	a_2	χ^2
0.02	12	0.02	0.49	1.97	0.08	2.53	0.03	0.97	1.10
	20	0.03	0.50	2.51	0.13	1.70	0.06	0.94	1.03
	40	0.07	0.73	2.90	0.22	1.78	0.10	0.90	1.05
	60	0.10	0.97	3.07	0.30	1.64	0.13	0.87	1.20
	85	0.14	1.20	3.45	0.36	1.95	0.14	0.86	1.05
	112	0.18	1.12	3.53	0.45	1.56	0.16	0.84	1.02
0.03	36	0.04	0.18	1.83	0.21	2.63	0.07	0.93	1.07
	50	0.06	1.06	3.37	0.20	2.19	0.09	0.91	1.09
	60	0.07	0.27	2.11	0.32	1.82	0.11	0.89	1.05
	73	0.08	0.24	1.71	0.38	2.71	0.13	0.87	1.13
	80	0.09	0.62	2.38	0.39	1.97	0.13	0.87	1.01
	90	0.10	0.70	2.79	0.47	1.86	0.13	0.87	1.10
	115	0.13	1.34	3.44	0.56	1.88	0.19	0.81	0.92
0.05	30	0.02	0.27	2.11	0.08	1.61	0.04	0.96	0.99
	50	0.03	0.99	3.44	0.14	1.69	0.08	0.92	1.04
	61	0.04	0.25	1.87	0.25	1.67	0.11	0.89	1.04
	83	0.05	0.99	2.63	0.26	1.95	0.12	0.88	1.10
	100	0.07	1.11	3.87	0.26	1.63	0.12	0.88	1.07
	121	0.08	0.92	2.11	0.40	2.16	0.16	0.84	1.18
	134	0.09	1.21	3.98	0.34	1.83	0.15	0.85	1.04
	150	0.10	1.12	3.41	0.39	1.98	0.17	0.83	1.17
	215	0.14	0.98	2.64	0.71	1.85	0.23	0.77	1.05
0.07	35	0.02	0.29	2.29	0.16	2.16	0.03	0.97	1.08
	70	0.03	0.08	2.13	0.20	0.91	0.11	0.89	1.07
	140	0.07	0.82	2.24	0.34	2.10	0.13	0.87	1.24
	211	0.10	1.22	3.58	0.47	1.80	0.18	0.82	1.04

	348	0.16	1.72	3.82	0.70	1.46	0.24	0.76	0.99
	399	0.19	1.26	3.62	0.97	1.72	0.28	0.72	1.11
0.09	57	0.02	0.00	2.04	0.16	1.57	0.06	0.94	1.04
	99	0.04	0.30	2.46	0.24	1.49	0.10	0.90	1.09
	113	0.04	0.29	2.29	0.29	1.99	0.09	0.91	1.14
	152	0.06	0.49	2.52	0.35	1.81	0.14	0.86	1.15
	246	0.09	1.26	3.62	0.45	1.68	0.19	0.81	1.06
	272	0.10	1.18	3.72	0.49	1.56	0.20	0.80	1.10
	378	0.14	0.99	2.63	0.68	1.77	0.23	0.77	1.11
	506	0.19	1.11	3.87	1.00	1.79	0.28	0.72	1.14

Table SI 3.4e: FBM parameters obtained from fitting the fluorescence decays of DNA-EB quenched by Ni^{2+} cations at an ionic strength of 3×10^{-2} M with Equation 3.2.

wt % DNA	$[Ni^{2+}]$ (μM)	$[Ni^{2+}]/[P]$	$k_e[blob]$ $\times 10^7\ s^{-1}$	k_{blob} $\times 10^7\ s^{-1}$	<n>	τ_{fast}	a_{fast}	a_2	χ^2
0.02	13	0.02	0.08	2.13	0.09	0.61	0.04	0.96	1.15
	20	0.03	0.00	2.14	0.14	0.93	0.05	0.95	1.09
	24	0.04	0.30	2.92	0.14	0.45	0.12	0.88	1.13
	41	0.07	0.00	1.45	0.23	2.36	0.08	0.92	1.08
	60	0.10	0.27	2.38	0.31	1.52	0.09	0.91	0.98
	76	0.13	0.71	1.22	0.36	1.82	0.10	0.90	1.03
	112	0.18	0.73	1.11	0.53	1.55	0.15	0.85	1.09
0.03	30	0.03	1.79	2.75	0.12	2.17	0.05	0.95	0.98
	37	0.04	1.45	3.20	0.14	1.49	0.06	0.94	1.10
	50	0.06	0.95	2.94	0.21	2.53	0.08	0.92	1.00
	60	0.07	1.64	3.70	0.25	1.85	0.10	0.90	1.00
	73	0.08	1.31	3.25	0.29	1.93	0.11	0.89	1.05
	80	0.09	0.79	2.05	0.28	2.47	0.09	0.91	1.01

	90	0.10	0.34	1.24	0.32	3.07	0.09	0.91	0.96
	127	0.14	0.14	2.25	0.45	1.97	0.14	0.86	1.15
0.05	31	0.02	1.14	4.44	0.07	1.81	0.03	0.97	1.00
	50	0.03	1.33	5.44	0.11	0.96	0.08	0.92	1.02
	61	0.04	0.63	3.00	0.16	2.14	0.06	0.94	1.07
	83	0.06	0.68	3.27	0.22	1.78	0.09	0.91	1.09
	100	0.07	0.79	3.04	0.25	1.87	0.11	0.89	1.03
	133	0.09	0.88	3.20	0.31	2.16	0.11	0.89	0.99
	217	0.14	0.56	2.57	0.49	1.83	0.18	0.82	0.89
	283	0.19	0.74	2.86	0.59	1.71	0.20	0.80	1.07
0.07	43	0.02	1.26	12.26	0.06	0.65	0.05	0.95	1.07
	70	0.03	1.30	6.86	0.13	0.95	0.09	0.91	1.07
	85	0.04	0.16	2.52	0.15	1.59	0.08	0.92	1.06
	117	0.05	1.26	5.63	0.18	1.17	0.11	0.89	1.05
	141	0.07	0.94	3.78	0.24	1.53	0.13	0.87	1.05
	169	0.08	1.12	3.90	0.31	1.63	0.14	0.86	1.03
	210	0.10	0.43	2.06	0.40	1.94	0.15	0.85	1.06
	299	0.14	1.00	2.35	0.54	2.04	0.20	0.80	1.14
	390	0.18	1.26	3.36	0.72	1.94	0.21	0.79	1.22
0.09	33	0.01	0.11	2.95	0.07	0.83	0.07	0.93	0.94
	94	0.03	0.38	2.64	0.19	1.49	0.09	0.91	1.01
	111	0.04	0.41	2.38	0.23	1.69	0.09	0.91	1.17
	184	0.07	0.92	2.61	0.33	2.16	0.13	0.87	1.09
	219	0.08	1.01	3.01	0.37	1.76	0.15	0.85	1.23
	271	0.10	0.83	2.40	0.50	1.84	0.18	0.82	1.03
	379	0.14	0.82	2.91	0.56	1.77	0.21	0.79	1.10
	510	0.19	0.99	2.91	0.71	1.74	0.24	0.76	1.10

Table SI 3.5: Slope and intercept for <n> vs [Cu^{2+}].

[Na_2SO_4] (M)	wt % DNA	[DNA] (in base pairs)	slope	intercept
5×10^{-4}	0.02	3.03E-04	29729 ± 2690	-0.68 ± 0.29
	0.03	4.55E-04	19001 ± 892	-0.41 ± 0.11
	0.05	7.58E-04	10316 ± 286	-0.35 ± 0.05
	0.07	1.06E-03	7936 ± 364	-0.51 ± 0.10
	0.09	1.36E-03	6189 ± 884	-0.53 ± 0.21
5×10^{-3}	0.02	3.03E-04	18272 ± 486	-0.20 ± 0.04
	0.03	4.55E-04	14356 ± 500	-0.30 ± 0.06
	0.05	7.58E-04	9416 ± 885	-0.30 ± 0.17
	0.07	1.06E-03	8224 ± 695	-0.65 ± 0.20
	0.09	1.36E-03	6268 ± 383	-0.69 ± 0.14
7.5×10^{-3}	0.02	3.03E-04	15656 ± 2636	0
	0.03	4.55E-04	10428 ± 209	0
	0.05	7.58E-04	7084 ± 270	-0.10 ± 0.04
	0.07	1.06E-03	5932 ± 272	-0.22 ± 0.06
	0.09	1.36E-03	4368 ± 222	-0.16 ± 0.06
1.25×10^{-2}	0.02	3.03E-04	11632 ± 1019	0
	0.03	4.55E-04	9197 ± 170	0
	0.05	7.58E-04	6297 ± 440	-0.10 ± 0.08
	0.07	1.06E-03	4541 ± 126	-0.05 ± 0.03
	0.09	1.36E-03	3396 ± 86	-0.07 ± 0.03
2.1×10^{-2}	0.02	3.03E-04	8893 ± 396	0
	0.03	4.55E-04	5251 ± 166	0
	0.05	7.58E-04	4405 ± 320	-0.08 ± 0.05
	0.07	1.06E-03	3343 ± 72	-0.05 ± 0.02
	0.08	1.27E-03	3239 ± 184	-0.07 ± 0.05
	0.09	1.36E-03	2685 ± 132	-0.09 ± 0.04
3×10^{-2}	0.02	3.03E-04	6119 ± 286	0
	0.03	4.55E-04	4662 ± 190	0

	0.04	6.06E-04	3334 ± 344	0
	0.05	7.58E-04	2569 ± 49	0
	0.06	9.09E-04	2746 ± 95	0
	0.07	1.06E-03	2729 ± 81	0
	0.08	1.21E-03	2253 ± 89	0
	0.09	1.36E-03	1778 ± 42	0
4×10^{-2}	0.02	3.03E-04	4461 ± 341	0
	0.03	4.55E-04	3085 ± 126	0
	0.04	6.06E-04	2110 ± 126	0
	0.05	7.58E-04	2432 ± 89	0
	0.06	9.09E-04	2212 ± 94	0
	0.07	1.06E-03	1776 ± 55	0
	0.08	1.21E-03	1825 ± 44	0
	0.09	1.36E-03	1544 ± 37	0

Table SI 3.6: Slope and intercept for <n> vs [Ni^{2+}].

$[Na_2SO_4]$ (M)	wt % DNA	[DNA] (in base pairs)	slope	intercept
5×10^{-4}	0.02	3.03E-04	21548 ± 705	-0.11 ± 0.04
	0.03	4.55E-04	16796 ±1029	-0.25 ± 0.09
	0.05	7.58E-04	12534 ± 874	-0.63± 0.15
	0.07	1.06E-03	8308 ± 627	-0.54 ± 0.14
	0.09	1.36E-03	6552 ± 207	-0.63 ± 0.07
5×10^{-3}	0.02	3.03E-04	14316 ± 3101	0
	0.03	4.55E-04	11284 ± 361	-0.18 ± 0.03
	0.05	7.58E-04	8189 ± 403	-0.36 ± 0.06
	0.07	1.06E-03	6652 ± 324	-0.42 ± 0.07
	0.09	1.36E-03	5349 ± 217	-0.41 ± 0.06
1.25×10^{-2}	0.02	3.03E-04	8934 ± 394	0
	0.03	4.55E-04	5526 ± 124	0

	0.05	7.58E-04	4598 ± 157	-0.13 ± 0.03
	0.07	1.06E-03	3428 ± 268	-0.15 ± 0.06
	0.09	1.36E-03	3039 ± 104	-0.10 ± 0.03
2.1×10^{-2}	0.02	3.03E-04	4367 ± 245	0
	0.03	4.55E-04	3802 ± 273	0
	0.05	7.58E-04	3018 ± 139	0
	0.07	1.06E-03	2274 ± 107	0
	0.09	1.36E-03	1925 ± 67	0
3×10^{-2}	0.02	3.03E-04	4944 ± 182	0
	0.03	4.55E-04	3675 ± 95	0
	0.05	7.58E-04	2223 ± 63	0
	0.07	1.06E-03	1821 ± 26	0
	0.09	1.36E-03	1545 ± 74	0

Table SI 3.7a: Decay times and pre-exponential factors retrieved from fitting the fluorescence decays of DNA-EB quenched by Cu^{2+} cations at an ionic strength of 5×10^{-3} M in D_2O with Equation 3.1.

wt % DNA	$[Cu^{2+}]$ (μM)	$[Cu^{2+}]/[P]$	τ_1 ns	τ_2 ns	τ_3 ns	a_1	a_2	a_3	χ^2
0.02	0	0.00	40.2	3.12		0.97	0.03		1.25
	11	0.02	39.5	13.9	1.03	0.85	0.08	0.07	1.16
	21	0.04	38.7	15.7	1.78	0.77	0.16	0.06	0.96
	32	0.05	43.7	35.1	9.01	0.12	0.69	0.19	1.23
	39	0.06	36.4	15.0	2.72	0.62	0.24	0.14	1.22
	54	0.09	35.1	14.3	2.64	0.54	0.29	0.17	1.20
	61	0.10	33.2	14.0	2.73	0.43	0.34	0.23	1.20
	76	0.13	32.1	13.6	2.53	0.39	0.35	0.26	1.22
	100	0.16	28.7	11.7	2.31	0.34	0.37	0.29	1.30
	111	0.18	27.9	11.4	2.38	0.29	0.40	0.31	1.23

0.03	0	0.00	40.3	14.5		0.98	0.02		1.11
	15	0.02	39.7	14.9	0.90	0.88	0.07	0.05	1.16
	29	0.03	38.9	15.4	2.17	0.82	0.12	0.07	1.12
	60	0.07	38.1	16.8	2.83	0.70	0.20	0.11	1.30
	80	0.09	14.8	36.2	2.46	0.25	0.61	0.15	1.15
	91	0.10	15.3	36.1	2.66	0.28	0.56	0.16	1.30
	116	0.13	34.2	14.5	2.66	0.48	0.31	0.21	1.55
	152	0.17	29.1	13.0	2.71	0.30	0.39	0.31	1.41
	169	0.19	26.0	10.1	1.90	0.30	0.38	0.32	1.28
0.05	0	0.00	40.3	14.0		0.98	0.02		1.17
	50	0.03	37.7	14.0	1.79	0.72	0.18	0.10	1.18
	77	0.05	36.5	15.6	2.33	0.59	0.26	0.15	1.17
	104	0.07	35.0	14.9	2.42	0.52	0.30	0.18	1.14
	139	0.09	32.7	14.2	2.54	0.42	0.34	0.24	1.20
	155	0.10	31.5	14.0	2.79	0.38	0.35	0.27	1.20
	196	0.13	28.3	11.9	2.31	0.31	0.38	0.31	1.20
	255	0.17	22.3	9.58	2.02	0.20	0.40	0.39	1.19
	287	0.19	19.2	8.54	2.07	0.18	0.40	0.42	1.30
0.07	0	0.00	40.3	14.8		0.98	0.02		1.20
	62	0.03	38.0	15.2	2.29	0.75	0.16	0.09	1.26
	111	0.05	35.8	13.7	1.91	0.59	0.25	0.16	1.14
	143	0.07	34.5	14.4	2.44	0.52	0.28	0.20	1.22
	185	0.09	31.7	12.7	2.06	0.42	0.34	0.23	1.25
	217	0.10	29.8	12.8	2.43	0.35	0.36	0.29	1.17
	278	0.13	24.5	10.2	2.18	0.28	0.39	0.33	1.31
	354	0.17	19.6	8.07	1.67	0.21	0.42	0.37	1.27
	392	0.18	16.7	7.03	1.69	0.19	0.41	0.39	1.49
0.09	0	0.00	40.6	9.64		0.98	0.02		1.14

	46	0.02	39.6	15.4	1.91	0.87	0.08	0.05	1.24
	89	0.03	39.0	18.5	2.28	0.71	0.18	0.11	1.31
	141	0.05	40.0	27.2	5.80	0.42	0.38	0.20	1.28
	178	0.07	37.8	17.5	2.86	0.62	0.24	0.14	1.18
	241	0.09	32.8	14.9	2.77	0.39	0.35	0.27	1.21
	272	0.10	30.8	12.6	2.44	0.39	0.35	0.25	1.26
	351	0.13	27.4	11.1	2.09	0.31	0.38	0.31	1.16
	455	0.17	20.6	8.29	1.71	0.23	0.41	0.36	1.28
	505	0.19	18.1	7.32	1.63	0.21	0.42	0.38	1.24

Table SI 3.7b: FBM parameters obtained from fitting the fluorescence decays of DNA-EB quenched by Cu^{2+} cations at an ionic strength of 5×10^{-3} M in D_2O with Equation 3.2.

wt % DNA	$[Cu^{2+}]$ (μM)	$[Cu^{2+}]/[P]$	$k_e[blob]$ $\times 10^7\ s^{-1}$	k_{blob} $\times 10^7\ s^{-1}$	<n>	τ_{fast}	a_{fast}	a_2	χ^2
0.02	11	0.02	0.28	2.99	0.12	0.67	0.05	0.95	1.15
	21	0.04	0.36	2.77	0.26	1.31	0.06	0.94	0.95
	32	0.05	0.55	2.93	0.35	2.21	0.09	0.91	1.08
	39	0.06	0.60	2.88	0.51	2.51	0.11	0.89	1.18
	54	0.09	0.64	2.96	0.67	2.37	0.14	0.86	1.16
	61	0.10	0.63	2.67	0.98	2.37	0.22	0.78	1.10
	76	0.13	0.69	2.67	1.10	2.61	0.19	0.81	1.13
	100	0.16	0.76	2.74	1.47	2.22	0.25	0.75	1.26
0.03	60	0.07	0.31	2.05	0.37	3.01	0.11	0.89	1.27
	80	0.09	0.65	2.82	0.52	2.33	0.14	0.86	1.08
	91	0.10	0.56	2.68	0.60	2.43	0.16	0.84	1.27
	116	0.13	0.56	2.40	0.85	2.63	0.20	0.80	1.50

	152	0.17	0.67	2.25	1.65	2.53	0.29	0.71	1.30
0.05	77	0.05	0.55	2.58	0.54	2.18	0.15	0.85	1.13
	104	0.07	0.54	2.44	0.75	2.32	0.18	0.82	1.10
	139	0.09	0.68	2.46	1.03	2.35	0.23	0.77	1.13
	155	0.10	0.72	2.41	1.20	2.55	0.25	0.75	1.14
	196	0.13	0.92	2.98	1.48	2.01	0.28	0.72	1.12
	255	0.17	1.06	2.93	2.41	1.77	0.36	0.64	1.10
0.07	111	0.05	0.67	3.12	0.53	1.85	0.16	0.84	1.10
	143	0.07	0.64	2.49	0.73	2.42	0.19	0.81	1.10
	185	0.09	0.82	3.12	1.00	1.80	0.22	0.78	1.16
	217	0.10	0.83	2.60	1.33	2.44	0.27	0.73	1.08
	278	0.13	1.06	2.94	1.88	2.01	0.31	0.69	1.20
	354	0.17	1.46	3.76	2.41	1.38	0.33	0.67	1.10
	392	0.18	1.79	4.08	2.74	1.40	0.33	0.67	1.32
0.09	178	0.07	0.40	2.09	0.49	2.63	0.13	0.87	1.18
	241	0.09	0.58	2.12	1.17	2.66	0.25	0.75	1.11
	272	0.10	0.85	2.88	1.16	2.16	0.23	0.77	1.21
	351	0.13	0.99	3.14	1.54	1.80	0.28	0.72	1.08
	455	0.17	1.48	3.83	2.20	1.42	0.32	0.68	1.16
	505	0.19	1.60	3.92	2.56	1.39	0.33	0.67	1.13

Table SI 3.8: Slope and intercept for <n> vs [Cu^{2+}] in D_2O.

wt % DNA	[DNA] (in base pairs)	slope	intercept
0.02	3.03E-04	15649 ± 874	-0.09 ± 0.05
0.03	4.55E-04	13727 ± 2180	-0.57 ± 0.23
0.05	7.58E-04	10174 ± 912	-0.34 ± 0.15
0.07	1.06E-03	7995 ± 186	-0.40 ± 0.05

0.09	1.36E-03	5878 ± 394	-0.44 ± 0.14

Table SI 3.9: Slope and intercept for <n> vs $[Cu^{2+}]$ in for $[Na_2SO_4]/[P] = 8.25$.

wt % DNA	[DNA] (in base pairs)	slope	intercept
0.02	3.03E-04	18272 ± 486	-0.20 ± 0.04
0.03	4.55E-04	10428 ± 209	0
0.05	7.58E-04	6297 ± 440	-0.10 ± 0.08
0.07	1.06E-03	3678 ± 93	-0.05 ± 0.02
0.08	1.27E-03	3239 ± 184	-0.07 ± 0.05

Chapter 4 Supporting Information

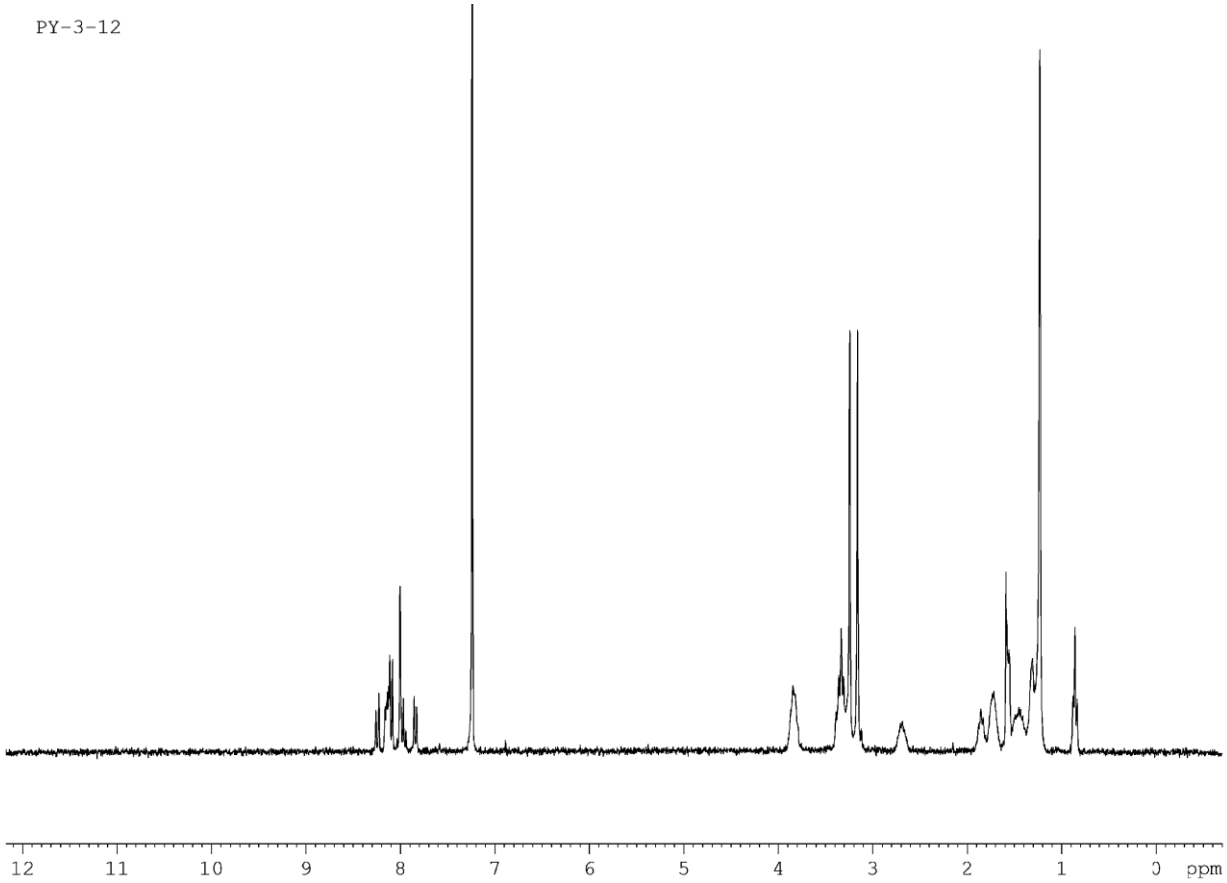

Figure SI 4.1: ^{1}H NMR spectrum of Py-3-12 in $CDCl_3$, 500 MHz, □ (ppm): 8.2 – 7.8 (m, 9H, py-H), 3.8 (broad, 4H, ^{+}N-CH_2), 3.4 – 3.3 (m, 6H, py-CH_2 and CH_2N^{+}), 3.2 (s, 6H, $^{+}N(CH_3)_2$ with py tail), 3.1 (s, 6H, $^{+}N(CH_3)_2$ with alkyl tail), 2.7 (broad, 2H, CH_2 between amines), 1.8 – 1.2 (m, 28H, CH_2 of alkyl chains), 0.9 (d, 3H, CH_3).

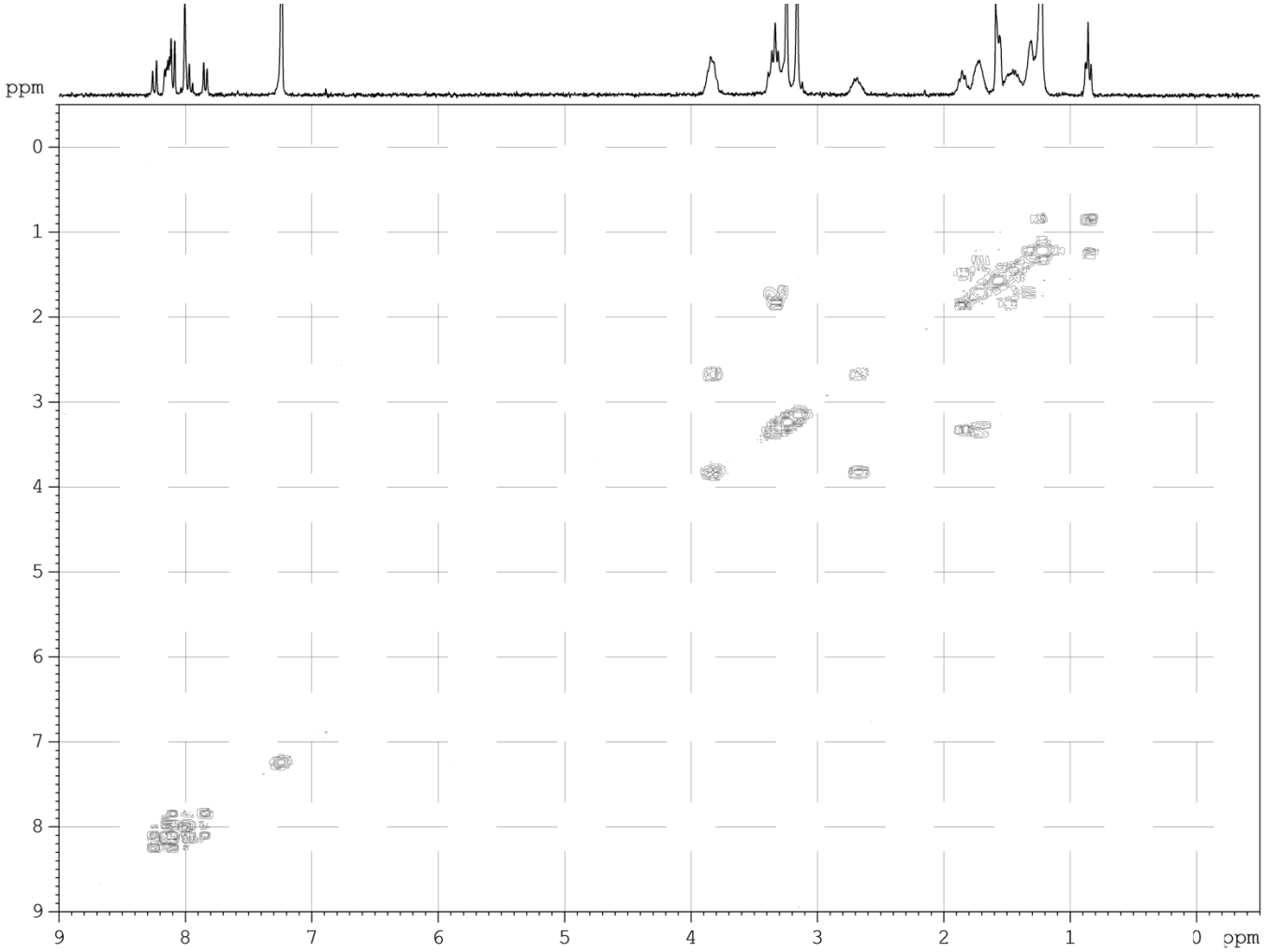

Figure SI 4.2: 2-D COSY NMR spectrum of Py-3-12 in $CDCl_3$.

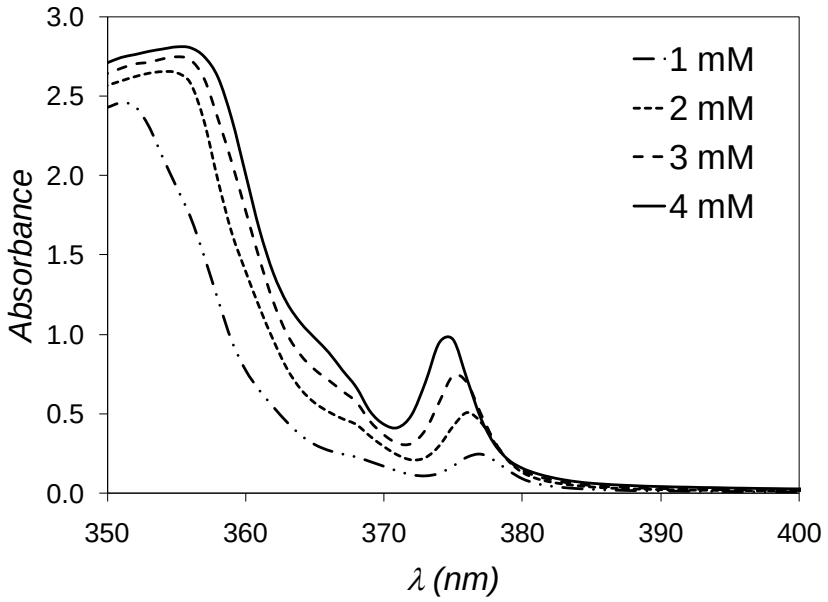

Figure SI 4.3: The absorbance spectra of Py-3-12 at concentrations greater than 1 mM show the 0–0 absorbance peak between 370 – 380 nm.

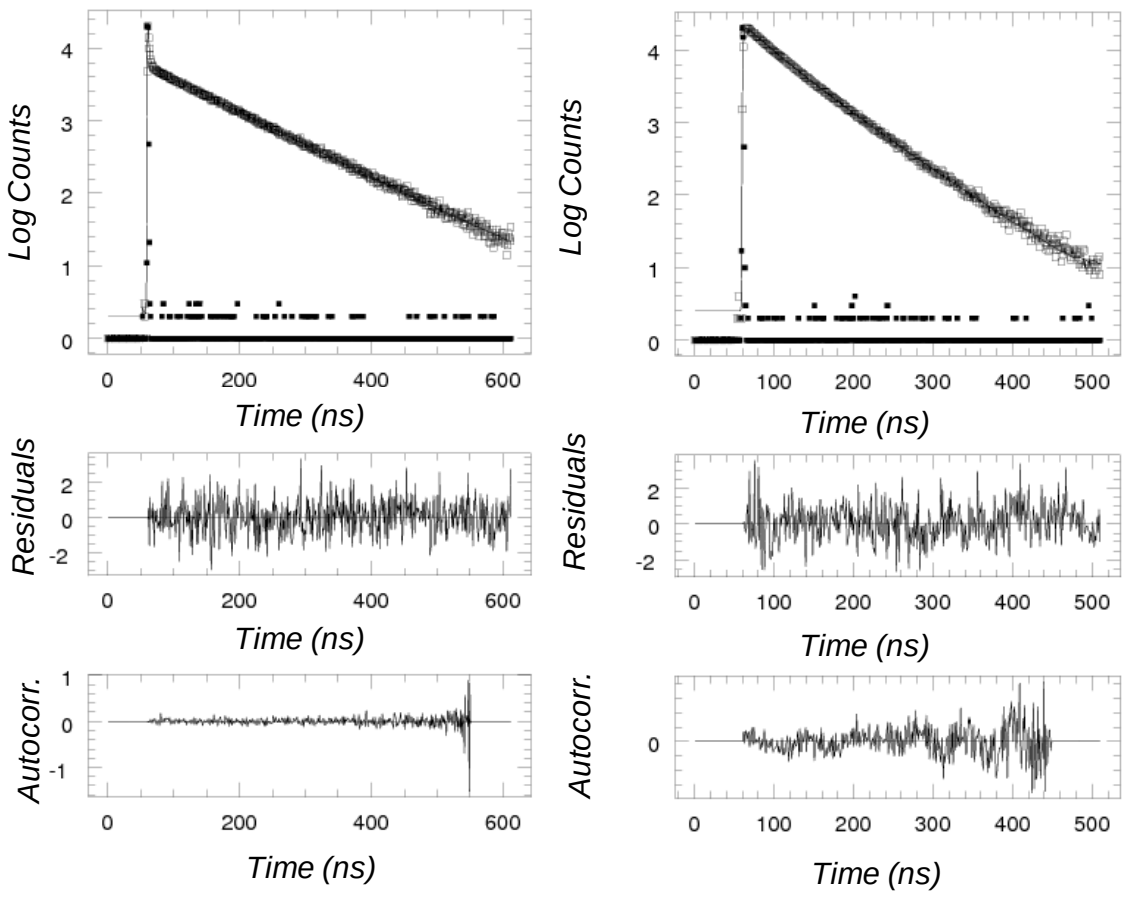

Figure SI 4.4: Fluorescence decays of the pyrene monomer (left; λ_{ex} = 344 nm, λ_{em} = 375 nm) and excimer (right; λ_{ex} = 344 nm, λ_{em} = 510 nm) of a 1.0 mM Py-3-12 aqueous solution at a TPC of 1.02ns/ch acquired with the right angle geometry and fit globally with Equations 4.10 and 4.11, respectively.

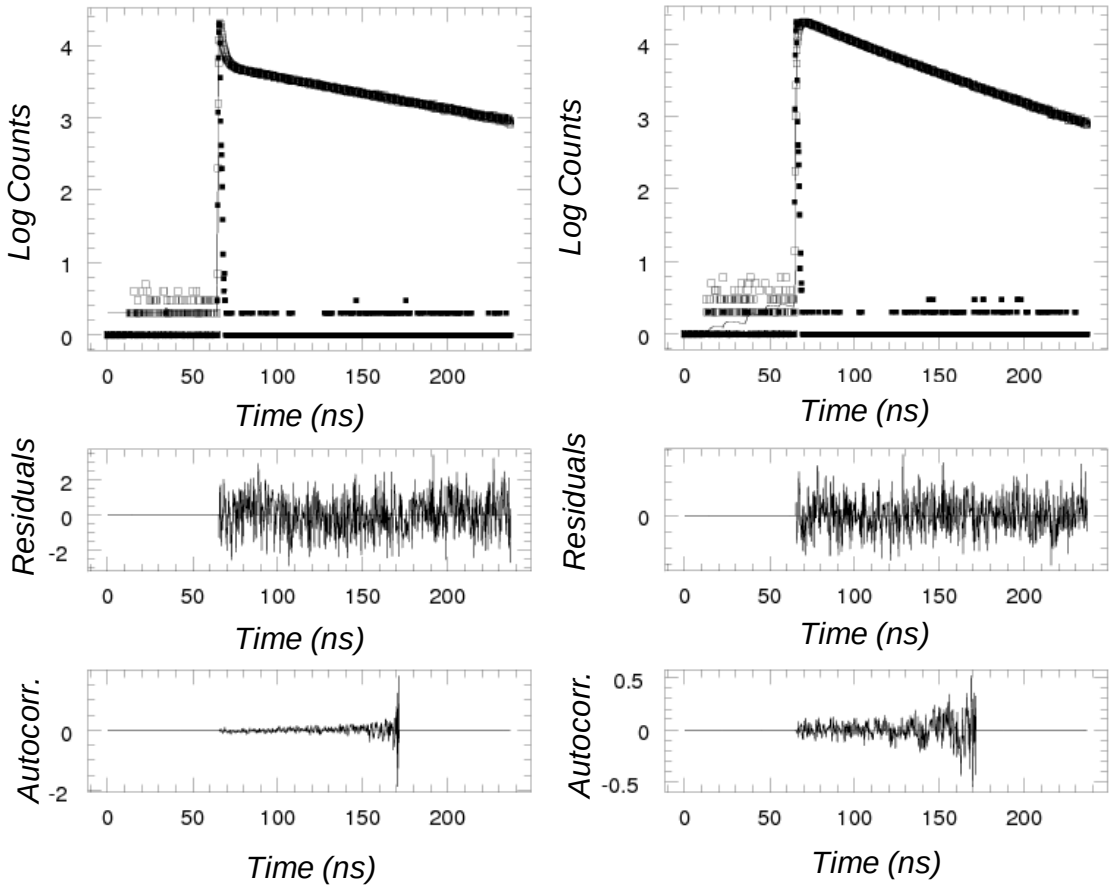

Figure SI 4.5: Fluorescence decays of the pyrene monomer (left; λ_{ex} = 344 nm, λ_{em} = 375 nm) and excimer (right; λ_{ex} = 344 nm, λ_{em} = 510 nm) of a 1.0 mM Py-3-12 aqueous solution acquired with a TPC of 0.24 ns/ch and the right angle geometry and globally fit with Equations 4.10 and 4.11, respectively.

Table SI 4.1: Decay times and pre-exponential factors of the pyrene monomer and excimer decays of Py-3-12, fit with Equation 4.27 and acquired with the right angle geometry and a TPC of 0.24 ns/ch.

	Monomer							Excimer						
[Py-3-12] (mM)	τ_1 (ns)	τ_2 (ns)	τ_3(ns)	a_1	a_2	a_3	χ^2	τ_1 (ns)	τ_2 (ns)	τ_3(ns)	a_1	a_2	a_3	χ^2
0.02	98.5	9.13		0.97	0.03		1.14	90.6	39.0	2.70	0.22	1.05	-0.28	1.18
0.06	98.1	8.86		0.97	0.03		1.14	73.2	34.5	0.60	0.65	0.86	-0.51	1.13
0.10	98.0	30.2	0.81	0.87	0.03	0.10	1.31	85.3	39.7	1.18	0.40	1.30	-0.70	1.20
0.14	97.2	14.4	1.04	0.89	0.02	0.09	0.99	87.4	41.0	1.13	0.43	1.24	-0.67	1.12
0.18	99.4	46.6	2.41	0.89	0.05	0.06	1.14	80.1	40.4	1.12	0.58	1.26	-0.84	1.15
0.22	99.0	37.9	1.34	0.84	0.04	0.12	1.14	75.7	39.4	0.99	0.94	1.69	-1.63	1.13
0.24	100.0	47.2	1.58	0.80	0.07	0.12	1.18	72.3	37.9	0.94	1.06	1.84	-1.90	1.17
0.28	96.0	18.1	1.25	0.78	0.02	0.20	0.99	64.8	34.2	0.99	1.43	1.50	-1.92	1.05
0.34	97.5	54.2	1.40	0.67	0.07	0.26	1.13	60.1	32.2	1.10	1.98	1.59	-2.57	1.11
0.38	96.9	8.86	1.18	0.61	0.03	0.36	1.11	59.4	31.5	1.11	1.88	1.43	-2.31	1.05
0.42	96.4	6.96	1.11	0.57	0.03	0.40	1.21	58.6	31.1	1.15	2.19	1.49	-2.68	1.11
0.46	96.4	3.97	0.98	0.53	0.07	0.40	1.09	57.1	29.2	1.18	2.33	1.30	-2.64	1.06
0.50	95.6	2.34	0.54	0.42	0.18	0.40	1.19	56.3	28.7	1.29	2.20	1.08	-2.28	1.12
0.53	95.9	3.42	0.82	0.43	0.10	0.47	0.98	57.9	31.0	1.24	2.59	1.20	-3.01	1.10
0.58	95.6	2.74	0.83	0.41	0.14	0.45	1.16	55.8	29.1	1.24	2.67	1.35	-3.03	1.16
0.62	95.5	2.84	0.83	0.37	0.14	0.49	1.18	57.0	30.4	1.26	2.41	1.50	-2.91	1.00
0.65	95.4	2.83	0.80	0.34	0.16	0.50	1.12	56.0	29.2	1.22	2.79	1.48	-3.28	1.13
0.70	95.5	3.54	0.97	0.33	0.10	0.57	1.11	55.9	28.9	1.26	2.53	1.37	-2.91	1.03
0.75	95.4	2.74	0.87	0.30	0.16	0.53	1.12	54.8	27.5	1.30	2.67	1.20	-2.87	1.13
0.78	95.2	2.46	0.72	0.27	0.24	0.80	1.00	55.0	27.6	1.25	2.95	1.41	-3.36	1.06
0.84	95.5	2.79	0.85	0.26	0.17	0.57	1.13	55.0	28.0	1.27	2.84	1.38	-3.22	0.97
0.92	94.9	2.22	0.72	0.22	0.28	0.51	1.14	55.0	28.5	1.23	3.23	1.59	-3.83	1.17
0.99	97.3	2.77	0.89	0.17	0.24	0.60	1.14	57.4	30.8	1.40	2.74	1.54	-3.28	1.13

2.00	94.7	2.69	0.95	0.06	0.27	0.67	1.16	54.2	26.4	1.48	2.58	0.98	-2.57	1.07

Table SI 4.2: Decay times and pre-exponential factors of the pyrene monomer and excimer decays of Py-3-12, fit with Equation 4.27 and acquired with the front-face geometry and a TPC of 0.24 ns/ch.

	Monomer							Excimer						
[Py-3-12] (mM)	τ_1 (ns)	τ_2 (ns)	τ_3(ns)	a_1	a_2	a_3	χ^2	τ_1 (ns)	τ_2 (ns)	τ_3(ns)	a_1	a_2	a_3	χ^2
0.06	97.5	9.42		0.97	0.03		1.12	84.5	40.6	1.74	0.36	1.19	-0.55	1.03
0.14	96.3	10.7	0.47	0.81	0.03	0.17	1.01	102	44.6	1.46	0.28	1.52	-0.79	1.15
0.22	98.5	42.2	1.27	0.80	0.06	0.14	1.04	105	45.9	1.25	0.27	1.93	-1.19	1.01
0.27	95.9	12.9	1.30	0.79	0.02	0.18	1.15	69.5	38.4	1.16	1.03	1.84	-1.87	0.98
0.34	95.6	14.9	1.18	0.64	0.02	0.34	1.07	61.2	34.6	1.19	1.60	1.62	-2.22	1.10
0.43	95.5	5.86	1.00	0.52	0.05	0.43	1.11	57.9	31.2	1.28	1.88	1.27	-2.15	1.11
0.50	96.0	6.14	1.07	0.44	0.05	0.51	1.02	56.7	30.2	1.29	2.12	1.26	-2.38	1.09
0.60	96.0	2.61	0.74	0.34	0.17	0.47	1.08	54.2	26.5	1.19	2.63	1.15	-2.78	0.99
0.70	96.1	3.29	0.90	0.31	0.12	0.57	1.09	54.1	26.3	1.23	2.57	1.14	-2.72	1.10
0.80	95.6	2.59	0.85	0.26	0.19	0.55	1.09	54.1	26.8	1.25	2.57	1.18	-2.56	1.01
0.90	95.3	3.54	1.04	0.22	0.11	0.67	1.14	54.3	27.0	1.24	2.72	1.28	-3.00	1.03
1.00	95.5	2.73	0.87	0.18	0.22	0.60	1.09	56.3	29.9	1.31	2.43	1.39	-2.83	1.03
2.00	94.6	2.63	0.89	0.06	0.29	0.66	1.07	55.8	29.8	1.37	2.67	1.50	-3.17	1.16

Table SI 4.3: Decay times and pre-exponential factors obtained from the global analysis of the monomer and excimer decays of Py-3-12 obtained with the right angle geometry and fit with Equations 4.10 and 4.11.

Monomer Decays:

[Py-3-12] (mM)	τ_1	$a_1 = f_{Mdiff}$	τ_M	$a_M = f_{Mfree}$	τ_{imp}	$a_{imp} = f_{imp}$	χ^2
0.02	2.68	0.03	100.0	0.93	40.9	0.04	1.15
0.06	0.64	0.06	98.4	0.91	15.9	0.02	1.13
0.10	1.17	0.08	98.5	0.88	37.7	0.04	1.26
0.14	1.06	0.09	97.2	0.89	14.9	0.02	1.04
0.18	1.06	0.08	97.5	0.89	16.3	0.03	1.13
0.22	1.02	0.14	98.0	0.83	24.9	0.03	1.10
0.24	0.96	0.16	98.4	0.79	30.3	0.04	1.12
0.28	1.00	0.21	95.7	0.76	9.94	0.03	1.02
0.34	1.09	0.25	93.7	0.72	5.48	0.03	1.12
0.38	1.11	0.36	96.6	0.61	7.38	0.04	1.08
0.42	1.15	0.40	96.4	0.57	8.06	0.03	1.16
0.46	1.16	0.42	96.5	0.54	6.15	0.04	1.07
0.50	1.29	0.46	95.9	0.52	6.99	0.03	1.19
0.53	1.27	0.49	96.2	0.48	8.10	0.03	1.08
0.58	1.24	0.53	95.9	0.44	8.37	0.03	1.18
0.62	1.23	0.57	96.1	0.41	9.38	0.03	1.10
0.65	1.24	0.58	95.8	0.38	7.04	0.04	1.15
0.70	1.22	0.61	95.7	0.35	6.83	0.04	1.09
0.75	1.26	0.63	95.6	0.33	6.25	0.03	1.12
0.78	1.21	0.64	95.5	0.31	4.93	0.05	1.06
0.84	1.22	0.66	95.8	0.29	5.55	0.05	1.08
0.92	1.20	0.69	95.2	0.25	4.53	0.06	1.17
0.99	1.32	0.74	97.8	0.18	4.85	0.07	1.19

Excimer Decays:

[Py-3-12] (mM)	f^{D}_{Ediff}	f^{E0}_{Ediff}	τ_D	τ_{E0}	$a_D = f_D$	$a_{E0} = f_{E0}$
0.02	0.10	0.16	39.2	92.2	0.73	0.05
0.06	0.07	0.24	34.4	72.9	0.49	0.19
0.10	0.23	0.18	39.7	85.7	0.54	0.05
0.14	0.28	0.13	44.4	116.2	0.59	0.00
0.18	0.32	0.14	44.6	107.9	0.53	0.00
0.22	0.38	0.20	43.1	91.8	0.41	0.00
0.24	0.33	0.30	37.6	71.8	0.29	0.07

0.28	0.29	0.36	34.1	64.6	0.21	0.14
0.34	0.33	0.38	32.3	60.3	0.11	0.17
0.38	0.31	0.38	31.6	59.7	0.13	0.18
0.42	0.32	0.41	31.2	58.8	0.09	0.19
0.46	0.30	0.43	29.5	57.2	0.06	0.21
0.50	0.37	0.31	30.6	57.5	0.00	0.32
0.53	0.45	0.29	32.6	59.5	0.00	0.26
0.58	0.38	0.36	30.7	57.0	0.00	0.25
0.62	0.39	0.35	31.1	57.5	0.00	0.25
0.65	0.34	0.41	29.3	56.0	0.00	0.25
0.70	0.36	0.40	29.8	56.4	0.01	0.24
0.75	0.33	0.42	28.8	55.4	0.00	0.25
0.78	0.33	0.45	28.4	55.4	0.00	0.22
0.84	0.34	0.44	29.9	55.5	0.00	0.22
0.92	0.34	0.46	29.3	55.4	0.00	0.20
0.99	0.38	0.41	32.8	58.7	0.03	0.18

Fractions of the pyrene species calculated with Equations 4.19 – 4.23:

[Py-3-12] (mM)	f_{diff}^{D}	f_{diff}^{E0}	f_{diff}	f_{free}	f_D	f_E	f_{agg}
0.02	0.01	0.02	0.03	0.01	0.08	0.01	0.08
0.06	0.01	0.04	0.05	0.08	0.08	0.03	0.12
0.10	0.04	0.03	0.07	0.06	0.09	0.01	0.10
0.14	0.05	0.03	0.08	0.08	0.11	0.00	0.11
0.18	0.05	0.02	0.07	0.07	0.08	0.00	0.08
0.22	0.08	0.04	0.13	0.13	0.09	0.00	0.09
0.24	0.08	0.07	0.15	0.15	0.07	0.02	0.08
0.28	0.08	0.11	0.19	0.20	0.06	0.04	0.10
0.34	0.11	0.12	0.23	0.22	0.04	0.05	0.09
0.38	0.14	0.17	0.31	0.29	0.06	0.08	0.14
0.42	0.15	0.20	0.35	0.31	0.04	0.09	0.13
0.46	0.15	0.22	0.37	0.33	0.03	0.11	0.14
0.50	0.21	0.17	0.38	0.30	0.00	0.18	0.18
0.53	0.26	0.17	0.42	0.34	0.00	0.15	0.15
0.58	0.23	0.22	0.46	0.38	0.00	0.15	0.15
0.62	0.25	0.23	0.48	0.40	0.00	0.16	0.16
0.65	0.22	0.27	0.50	0.41	0.00	0.17	0.17
0.70	0.25	0.27	0.52	0.44	0.00	0.16	0.17
0.75	0.23	0.30	0.53	0.44	0.00	0.18	0.18
0.78	0.24	0.32	0.56	0.48	0.00	0.16	0.16
0.84	0.25	0.32	0.57	0.48	0.00	0.16	0.16

0.92	0.26	0.35	0.61	0.53	0.00	0.15	0.15
0.99	0.31	0.34	0.65	0.50	0.02	0.15	0.17

Table SI 4.4: Decay times and pre-exponential factors obtained from the global analysis of the monomer and excimer decays of Py-3-12 obtained with the front-face geometry and fit with Equations 4.10 and 4.11.

Monomer Decays:

[Py-3-12] (mM)	τ_1	$a_1 = f_{Mdiff}$	τ_M	$a_M = f_{Mfree}$	τ_{imp}	$a_{imp} = f_{imp}$	χ^2
0.06	1.72	0.04	100.4	0.89	46.5	0.06	1.05
0.14	1.50	0.07	96.6	0.91	19.6	0.02	1.13
0.22	1.30	0.14	98.2	0.81	40.7	0.05	1.04
0.27	1.17	0.19	95.8	0.78	9.92	0.03	1.07
0.34	1.19	0.34	95.6	0.64	15.2	0.02	1.08
0.43	1.24	0.42	95.8	0.55	10.3	0.03	1.12
0.50	1.25	0.51	96.3	0.46	10.7	0.03	1.07
0.60	1.15	0.55	96.3	0.40	5.17	0.05	1.05
0.70	1.21	0.62	96.4	0.33	6.27	0.04	1.10
0.80	1.20	0.66	95.8	0.28	4.60	0.06	1.07
0.90	1.22	0.72	95.6	0.23	5.54	0.05	1.09
1.00	1.24	0.73	95.9	0.20	4.68	0.07	1.10

Excimer Decays:

[Py-3-12] (mM)	f_{Ediff}^{D}	f_{Ediff}^{E0}	τ_D	τ_{E0}	$a_D = f_D$	$a_{E0} = f_{E0}$
0.06	0.30	0.05	41.9	92.9	0.52	0.13
0.14	0.29	0.14	40.8	79.0	0.39	0.17
0.22	0.32	0.21	40.2	75.0	0.36	0.10
0.27	0.39	0.26	38.4	69.4	0.25	0.10
0.34	0.35	0.34	34.6	61.2	0.16	0.16
0.43	0.31	0.38	32.0	58.5	0.11	0.20
0.50	0.31	0.41	30.9	57.1	0.08	0.21
0.60	0.40	0.39	29.8	56.2	0.00	0.21
0.70	0.32	0.45	26.8	54.3	0.00	0.22
0.80	0.35	0.45	27.9	54.6	0.00	0.20
0.90	0.34	0.45	27.6	54.6	0.00	0.20
1.00	0.40	0.41	31.7	57.4	0.02	0.17

Fractions of the pyrene species calculated with Equations 19 – 23:

[Py-3-12] (mM)	f_{diff}^{D}	f_{diff}^{E0}	f_{diff}	f_{free}	f_D	f_E	f_{agg}
0.06	0.03	0.01	0.04	0.88	0.06	0.01	0.08
0.14	0.04	0.02	0.07	0.85	0.06	0.03	0.08
0.22	0.08	0.05	0.13	0.76	0.09	0.02	0.11
0.27	0.10	0.07	0.17	0.74	0.07	0.03	0.09
0.34	0.15	0.15	0.30	0.57	0.07	0.07	0.14
0.43	0.16	0.20	0.36	0.48	0.06	0.10	0.16
0.50	0.19	0.25	0.43	0.40	0.05	0.12	0.17
0.60	0.25	0.24	0.49	0.38	0.00	0.13	0.13
0.70	0.22	0.32	0.54	0.30	0.00	0.15	0.16
0.80	0.26	0.33	0.59	0.26	0.00	0.15	0.15
0.90	0.27	0.36	0.63	0.21	0.00	0.16	0.16
1.00	0.33	0.33	0.65	0.19	0.02	0.14	0.15

Chapter 5 Supporting Information

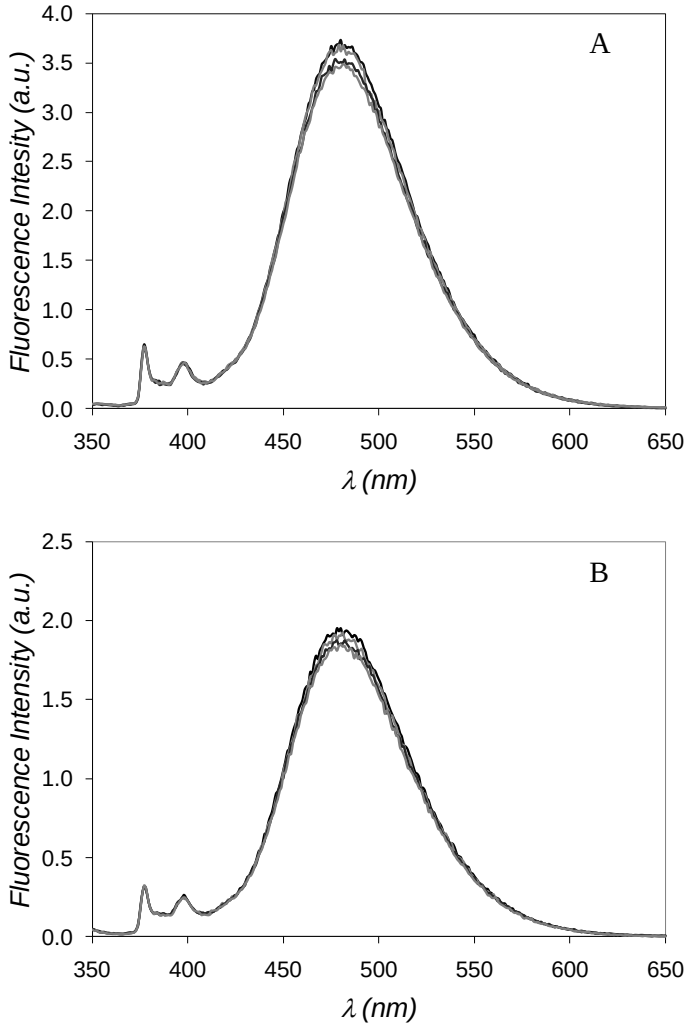

Figure SI 5.1. Steady-state fluorescence spectra of A) 0.2 mM CT DNA and 0.1 mM Py-3-12 and B) 0.02 mM CT DNA and 0.01 Py-3-12 diluted from the 2.0 mM CT DNA stock solution with increasing time up to 50 min.

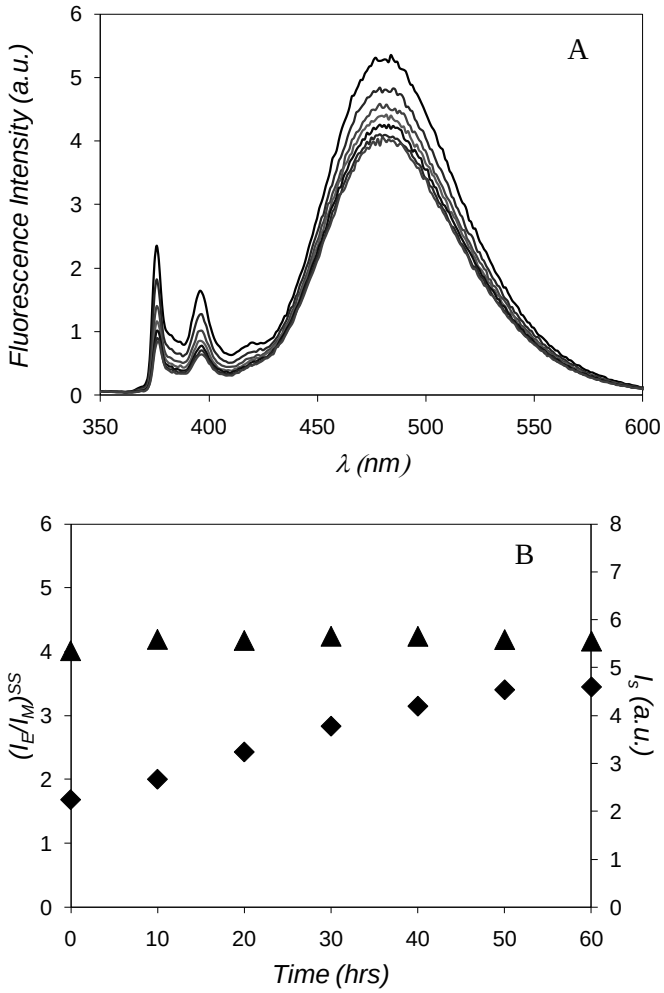

Figure SI 5.2. A) Steady-state fluorescence spectra of a Py-3-12 and DNA solution at a -/+ ratio of 1.0 with increasing time. B) $(I_E/I_M)^{SS}$ (filled diamonds) and the intensity of scattered light (I_S) (filled triangles) plotted as a function of time in hours [Py-3-12] = 1.0 mM, [CT DNA] = 1.0 mM.

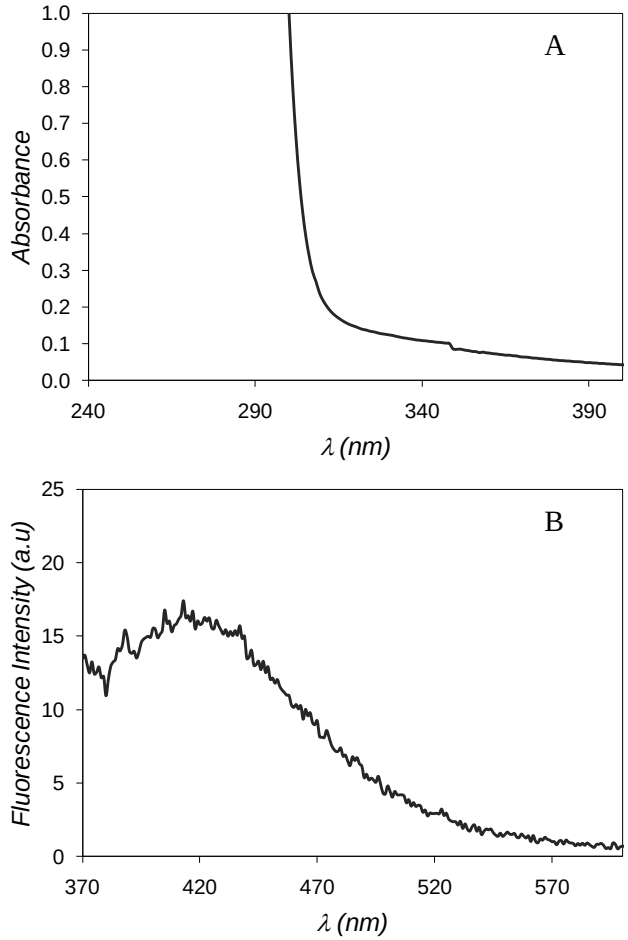

Figure SI 5.3. A) Absorbance spectrum and B) steady-state fluorescence spectrum (λ_{ex} = 344 nm) of 6.6 g/L sCT DNA solution.

Table SI 5.1: Decay times, pre-exponential factors, and A_-/A_+ ratios of the pyrene monomer and excimer fluorescence decays of Py-3-12 complexed with CT DNA acquired with a TPC of 0.24 ns/ch and analyzed with Equation 5.17.

	Monomer									Excimer									
-/+ ratio	τ_{M1} (ns)	τ_{M2} (ns)	τ_{M3} (ns)	τ_{M4} (ns)	a_{M1}	a_{M2}	a_{M3}	a_{M4}	χ^2	τ_{E1} (ns)	τ_{E2} (ns)	τ_{E3} (ns)	τ_{E4} (ns)	a_{E1}	a_{E2}	a_{E3}	a_{E4}	χ^2	A_-/A_+
0.00	98.5	8.89			0.97	0.03			1.05										
0.20	98.9	20.1	1.52		0.78	0.03	0.19		1.09	59.0	27.5	1.18		1.56	1.28	-1.84		1.13	-0.65
0.42	98.9	17.6	1.98	0.28	0.48	0.03	0.18	0.31	1.12	59.0	28.1	1.93	0.37	7.15	4.90	-5.72	-5.33	0.97	-0.92
0.61	99.4	30.8	3.36	0.71	0.42	0.02	0.20	0.36	1.01	60.9	30.1	2.31	0.64	2.83	1.95	-2.10	-1.67	1.00	-0.79
0.81	97.7	9.46	2.41	0.65	0.17	0.07	0.37	0.39	1.08	60.4	29.6	3.05	0.83	2.73	1.77	-1.46	-2.05	1.02	-0.78
0.89	97.2	8.94	2.55	0.66	0.08	0.07	0.38	0.48	1.01	57.8	27.2	2.50	0.62	2.74	1.83	-1.80	-1.77	1.23	-0.78
0.99	90.2	10.4	2.99	0.79	0.01	0.06	0.37	0.56	1.05	60.1	29.9	2.70	0.73	2.43	2.05	-1.62	-1.86	1.00	-0.78
1.12	59.3	9.90	3.23	0.90	0.00	0.07	0.33	0.59	1.08	62.3	31.5	3.11	0.90	2.47	1.73	-1.44	-1.75	1.08	-0.76
1.21	57.9	10.1	3.25	0.88	0.00	0.06	0.33	0.61	1.18	62.6	31.6	3.05	0.87	2.32	1.86	-1.36	-1.83	0.98	-0.76
1.53	56.1	9.29	2.83	0.71	0.01	0.08	0.38	0.53	1.10	63.9	33.3	2.97	0.76	2.92	2.26	-1.95	-2.23	1.09	-0.81
1.67	61.6	10.0	3.17	0.85	0.01	0.07	0.36	0.57	0.98	64.8	33.7	3.33	1.00	2.12	1.94	-1.13	-1.92	1.06	-0.75
1.98	67.8	10.4	3.28	0.87	0.01	0.06	0.34	0.59	1.08	61.4	30.1	3.92	1.11	2.52	1.52	-1.00	-2.03	1.07	-0.75

Table SI 5.2: Decay times, pre-exponential factors, and A_-/A_+ ratios of the pyrene monomer and excimer fluorescence decays of Py-3-12 complexed with sCT DNA acquired with a TPC of 0.24 ns/ch and analyzed with Equation 5.17.

	Monomer									Excimer									
-/+ ratio	τ_{M1} (ns)	τ_{M2} (ns)	τ_{M3} (ns)	τ_{M4} (ns)	a_{M1}	a_{M2}	a_{M3}	a_{M4}	χ^2	τ_{E1} (ns)	τ_{E2} (ns)	τ_{E3} (ns)	τ_{E4} (ns)	a_{E1}	a_{E2}	a_{E3}	a_{E4}	χ^2	A_-/A_+
0.00	98.5	8.89			0.97	0.03			1.05										
0.20	97.4	24.7	1.67		0.23	0.04	0.14		1.09	61.5	27.4	1.65	0.45	1.75	1.94	-1.29	-1.40	1.06	-0.73
0.41	97.4	19.7	3.13	0.64	0.62	0.03	0.12	0.23	1.00	59.4	27.7	2.60	0.80	1.82	1.63	-1.49	-0.96	1.10	-0.71

0.60	99.3	31.7	4.06	0.87	0.52	0.03	0.15	0.30	1.16	60.5	29.4	2.68	0.82	2.04	1.92	-1.19	-1.78	0.94	-0.75
0.80	96.8	10.8	2.62	0.56	0.33	0.06	0.27	0.34	1.05	63.0	32.1	2.61	0.56	3.89	4.02	-3.29	-3.61	0.94	-0.87
1.02	97.8	12.9	3.61	0.91	0.25	0.07	0.27	0.42	1.08	59.4	27.7	4.31	1.10	2.18	1.45	-1.80	-0.82	1.00	-0.72
1.21	94.2	10.5	3.14	0.83	0.04	0.09	0.37	0.50	1.02	61.7	31.3	2.72	0.61	2.15	2.36	-1.75	-1.77	1.03	-0.78
1.35	80.7	10.0	3.25	0.83	0.01	0.10	0.35	0.54	1.05	64.9	34.6	2.79	0.60	2.70	3.72	-2.66	-2.76	1.03	-0.84
1.50	49.1	11.1	3.50	0.87	0.01	0.12	0.38	0.50	1.11	76.8	43.0	3.59	0.88	1.50	2.82	-1.58	-1.74	1.05	-0.77
2.03	48.3	10.4	3.39	0.91	0.01	0.12	0.37	0.51	1.07	71.0	39.1	3.65	0.82	1.86	2.54	-1.57	-1.84	1.04	-0.78
2.60	44.7	10.1	3.22	0.77	0.01	0.12	0.38	0.49	1.05	81.3	43.8	3.33	0.86	1.11	3.02	-1.54	-1.58	1.04	-0.76
5.40	67.0	12.0	3.69	0.95	0.01	0.09	0.36	0.54	1.08	70.6	39.5	3.34	0.79	2.19	2.48	-1.74	-1.93	1.00	-0.79
9.89	67.1	11.7	3.30	0.78	0.02	0.12	0.39	0.48	1.06	69.0	37.0	4.64	1.21	1.81	1.59	-0.89	-1.50	1.02	-0.70
25.3	91.0	13.7	3.68	0.87	0.02	0.07	0.35	0.56	1.08	60.1	27.1	3.04	1.15	1.40	1.13	-0.52	-1.01	1.10	-0.60
45.0	103	16.2	3.83	0.81	0.03	0.07	0.31	0.60	1.04	60.4	28.9	2.21	0.98	1.03	0.96	-0.63	-0.36	1.00	-0.50
104	110	21.0	4.09	0.71	0.07	0.10	0.25	0.58	1.00	57.0	20.3	0.27	0.00	0.41	0.22	0.40	-0.02	1.06	-0.02
503	115	23.7	4.57	0.70	0.15	0.15	0.23	0.47	1.09	60.4	16.6	3.18	0.43	0.10	0.08	0.29	0.54	1.02	
1020	112	21.9	4.37	0.70	0.14	0.16	0.25	0.44	1.05	57.7	19.0	4.04	0.86	0.07	0.07	0.52	0.33	1.10	

Table SI 5.3: Decay times and pre-exponential factors of the pyrene monomer and excimer fluorescence decays of Py-3-12 complexed with sCT DNA and 0.01 M sCT DNA alone in solution. All decays were excited at 344 nm and acquired at a TPC of 0.24 ns/ch and analyzed with Equation 5.17.

	Monomer (λ_{em} = 375 nm)									Excimer (λ_{em} = 510 nm)								
-/+ ratio	τ_{M1} (ns)	τ_{M2} (ns)	τ_{M3} (ns)	τ_{M4} (ns)	a_{M1}	a_{M2}	a_{M3}	a_{M4}	χ^2	τ_{E1} (ns)	τ_{E2} (ns)	τ_{E3} (ns)	τ_{E4} (ns)	a_{E1}	a_{E2}	a_{E3}	a_{E4}	χ^2
503	115	23.7	4.57	0.70	0.15	0.15	0.23	0.47	1.09	60.4	16.6	3.18	0.43	0.10	0.08	0.29	0.54	1.02
1020	112	21.9	4.37	0.70	0.14	0.16	0.25	0.44	1.05	57.7	19.0	4.04	0.86	0.07	0.07	0.52	0.33	1.10
0.01 M DNA		29.8	4.94	1.03		0.01	0.25	0.77	1.14		24.3	4.49	0.86		0.02	0.27	0.71	1.14

Table SI 5.4: Decay times and pre-exponential factors obtained from the global analysis of the monomer and excimer fluorescence decays of Py-3-12 complexed with CT DNA and analyzed with Equations 5.1 and 5.2.

Monomer Decays:

-/+ ratio	τ_1	a_1	τ_2	a_2	τ_M	$a_M = f_{Mfree}$	τ_{imp}	$a_{imp} = f_{imp}$	χ^2
0.20	0.37	0.16	1.49	0.15	97.0	0.67	10.3	0.02	1.14
0.42	0.43	0.19	1.93	0.20	97.0	0.58	8.34	0.03	1.10
0.61	0.71	0.28	2.56	0.24	97.0	0.45	8.81	0.04	1.04
0.81	0.80	0.44	2.81	0.33	97.0	0.18	10.0	0.06	1.06
0.89	0.71	0.48	2.68	0.38	97.0	0.08	9.35	0.06	1.07
0.99	0.86	0.59	3.25	0.35	97.0	0.01	12.2	0.05	1.04
1.12	1.09	0.67	4.19	0.30	97.0	0.00	14.3	0.03	1.16
1.21	1.03	0.66	3.94	0.30	97.0	0.00	13.8	0.03	1.14
1.53	1.00	0.63	3.90	0.33	97.0	0.00	14.2	0.04	1.17
1.67	1.02	0.64	3.99	0.32	97.0	0.00	14.4	0.04	1.09
1.98	1.04	0.65	4.07	0.31	97.0	0.00	14.6	0.04	1.11

Excimer Decays:

-/+ ratio	f^{D}_{Ediff}	f^{E0}_{Ediff}	τ_D	τ_{E0}	$a_D = f_D$	$a_{E0} = f_{E0}$
0.20	0.51	0.38	29.4	61.4	0.00	0.11
0.42	0.44	0.43	29.4	60.2	0.00	0.13
0.61	0.36	0.45	29.4	60.5	0.03	0.16
0.81	0.39	0.39	31.2	61.4	0.03	0.19
0.89	0.39	0.38	27.2	57.8	0.00	0.23
0.99	0.18	0.58	28.0	58.7	0.24	0.00
1.12	0.20	0.55	28.9	60.8	0.16	0.09
1.21	0.22	0.53	29.0	60.9	0.17	0.08
1.53	0.16	0.61	29.8	61.6	0.20	0.03
1.67	0.15	0.60	29.5	61.6	0.23	0.02
1.98	0.24	0.53	29.0	60.8	0.11	0.12

Fractions:

-/+ ratio	f^{D}_{diff}	f^{E0}_{diff}	f_{diff}	f_{free}	f_D	f_{E0}	f_{agg}
0.20	0.17	0.13	0.30	0.66	0.00	0.04	0.04
0.42	0.19	0.18	0.37	0.57	0.00	0.06	0.06
0.61	0.21	0.26	0.46	0.42	0.02	0.09	0.11
0.81	0.33	0.33	0.66	0.16	0.03	0.16	0.19
0.89	0.37	0.35	0.71	0.07	0.00	0.22	0.22

0.99	0.18	0.58	0.75	0.01	0.24	0.00	0.24
1.12	0.20	0.55	0.75	0.00	0.16	0.09	0.25
1.21	0.22	0.53	0.75	0.00	0.17	0.08	0.25
1.53	0.16	0.61	0.77	0.00	0.20	0.03	0.23
1.67	0.15	0.60	0.75	0.00	0.23	0.02	0.25
1.98	0.24	0.53	0.76	0.00	0.11	0.12	0.23

Table SI 5.5: Decay times and pre-exponential factors obtained from the global analysis of the monomer and excimer fluorescence decays of Py-3-12 complexed with sCT DNA and analyzed with Equations 5.1 and 5.2.

Monomer Decays:

-/+ ratio	τ_1	a_1	τ_2	a_2	τ_M	$a_M = f_{Mfree}$	τ_{imp}	$a_{imp} = f_{imp}$	χ^2
0.20	0.49	0.11	1.75	0.09	97.0	0.77	18.4	0.03	1.08
0.41	0.76	0.20	2.61	0.13	97.0	0.64	13.4	0.03	1.05
0.60	0.79	0.25	2.68	0.16	97.0	0.54	10.1	0.05	1.06
0.80	0.58	0.33	2.67	0.28	97.0	0.33	11.5	0.06	0.99
1.02	0.98	0.43	3.64	0.25	97.0	0.25	11.1	0.07	1.05
1.21	0.82	0.50	3.23	0.38	97.0	0.04	11.5	0.08	1.03
1.35	0.98	0.60	4.09	0.33	97.0	0.01	13.6	0.06	1.10
1.50	0.99	0.56	4.28	0.36	97.0	0.00	14.2	0.08	1.18
2.03	1.17	0.60	4.72	0.34	97.0	0.00	14.7	0.06	1.13
2.60	1.10	0.58	4.53	0.35	97.0	0.00	14.8	0.07	1.13
5.40	1.10	0.60	4.54	0.34	97.0	0.00	15.7	0.06	1.14
9.89	1.10	0.56	4.57	0.35	97.0	0.01	16.7	0.08	1.16
25.3	0.98	0.59	4.06	0.33	97.0	0.02	15.5	0.06	1.13
45.0	0.79	0.51	3.48	0.32	97.0	0.03	13.9	0.08	1.05

Excimer Decays:

-/+ ratio	f_{Ediff}^{D}	f_{Ediff}^{E0}	τ_D	τ_{E0}	$a_D = f_D$	$a_{E0} = f_{E0}$
0.20	0.31	0.41	27.2	61.2	0.21	0.07
0.41	0.36	0.36	27.5	59.3	0.11	0.17
0.60	0.38	0.37	29.3	60.5	0.09	0.15
0.80	0.49	0.38	31.9	62.8	0.00	0.12
1.02	0.24	0.49	28.8	60.0	0.17	0.10
1.21	0.20	0.52	29.5	60.0	0.28	0.00
1.35	0.21	0.55	29.5	59.7	0.23	0.01
1.50	0.16	0.53	25.0	57.1	0.23	0.08
2.03	0.21	0.50	34.8	66.1	0.24	0.05

2.60	0.22	0.51	35.5	66.8	0.23	0.04
5.40	0.17	0.57	32.4	64.6	0.18	0.08
9.89	0.20	0.51	34.6	66.8	0.20	0.09
25.3	0.12	0.51	22.7	57.5	0.27	0.10
45.0	0.10	0.49	26.0	58.3	0.33	0.08

Fractions:

-/+ ratio	f_{diff}^{D}	f_{diff}^{E0}	f_{diff}	f_{free}	f_{D}	f_{E0}	f_{agg}
0.20	0.18	0.00	0.19	0.74	0.06	0.02	0.08
0.41	0.29	0.00	0.29	0.60	0.04	0.07	0.11
0.60	0.36	0.00	0.37	0.51	0.05	0.07	0.12
0.80	0.57	0.01	0.58	0.33	0.00	0.08	0.08
1.02	0.56	0.00	0.56	0.23	0.13	0.08	0.21
1.21	0.69	0.00	0.70	0.03	0.27	0.00	0.27
1.35	0.75	0.01	0.75	0.01	0.23	0.01	0.24
1.50	0.68	0.00	0.68	0.00	0.23	0.08	0.31
2.03	0.71	0.00	0.71	0.00	0.24	0.05	0.29
2.60	0.73	0.00	0.73	0.00	0.23	0.04	0.27
5.40	0.73	0.00	0.73	0.00	0.18	0.08	0.26
9.89	0.71	0.00	0.71	0.01	0.20	0.09	0.28
25.3	0.62	0.00	0.62	0.01	0.26	0.10	0.36
45.0	0.58	0.00	0.58	0.02	0.32	0.08	0.40

References

Chapter 1

1. Watson, J. D.; Crick, F. H. *Nature* **1953**, *171*, 737 – 738.

2. Baxter C. *Nat. Rev. Genet.* **2003**, *4*, 246 – 247.

3. Eley, D. D.; Spivey, D. I. *Trans. Faraday Soc.* **1962**, *58*, 411 – 415.

4. Murphy, C. J.; Arkin, M. R.; Jenkins, Y.; Ghatlia, N. D.; Bossmann, S. H.; Turro, N. J.; Barton, J. K. *Science* **1993**, *262*, 1025 – 1029.

5. Kelley, S. O.; Holmlin, R. E.; Stemp, E. D. A.; Barton, J. K. *J. Am. Chem. Soc.* **1997**, *119*, 9861 – 9870.

6. Barton, J. K. *Pure Appl. Chem.* **1998**, *70*, 873 – 879.

7. Kelley, S. O.; Barton, J. K. *Chem. Biol.* **1998**, *5*, 413 – 425.

8. Chen, J.; Seeman, N., C. *Nature* **1991**, *350*, 631 – 633.

9. Zheng, J.; Birktoft, J. J.; Chen, Y.; Wang, T.; Sha, R.; Constantinou, P. E.; Ginell, S., L.; Mao, C.; Seeman, N. C. *Nature* **2009**, *461*, 74 – 77.

10. Yang, H.; McLaughlin, C. K.; Aldaye, F. A.; Hamblin, G. D.; Rys, A. Z.; Rouiller, I.; Sleiman, H. F. *Nature Chem.* **2009**, *1*, 390 – 396.

11. Aldaye, F. A.; Lo, P. K.; Karam, P.; McLaughlin, C. K.; Cosa, G.; Sleiman, H. F. *Nature Nanotech.* **2009**, *4*, 349 – 352.

12. Lo, P. K.; Altvater, F.; Sleiman, H. F. *J. Am. Chem. Soc.* **2010**, *132*, 10212 – 10214.

13. Seeman, N. C. *Sci. Am.* **2004**, *290*, 64 – 75.

14. Seeman, N. C. *Trends Biotechnol.* **1999**, *17*, 437 – 443.

15. Olby, R. C. *The path to the double helix: the discovery of DNA*; Dover Publications, Inc: New York, 1994; pp 3 – 10.

16. Manning, G. S. *J. Am. Chem. Soc.* **1979**, *12*, 443 – 449.

17. Manning, G. S. *Q. Rev. Biophys.* **1978**, *2*, 179 – 246.

18. Fenley, M. O.; Manning, G. S.; Olson, W. K. *Q. Biopolymers* **1990**, *30*, 1191 – 1203.

19. Calascibetta, F. G.; Dentini, M.; De Santis, P.; Morosetti, S. *Biopolymers* **1975**, *14*, 1667 – 1684.

20. Bloomfield, V. A. *Biopolymers* **1998**, *44*, 269 – 282.

21. Gao, X.; Kim. K; Liu, D. *AAPS J.* **2007**, *9*, 92 – 104.

22. Eichhorn, G. L.; Shin, Y. A. *J. Am. Chem. Soc.* **1968**, *90*, 7323 – 7328.

23. Guay, F.; Beauchamp, A. L. *J. Am. Chem. Soc.* **1979**, *101*, 6260 – 6263.

24. Diguid, J.; Bloomfield, V. A.; Benevides, J.; Thomas, Jr. G. J. *Biophys. J.* **1993**, *65*, 1916 – 1928.

25. Anastassopoulou, J. *J. Mol. Struct.* **2003**, *651*, 19 – 66.

26. Souza, H. K. S. *Thermochim. Acta* **2010**, *501*, 1 – 7.

27. Eichhorn, G. L.; Butzow, J. J.; Shin, Y. A. *J. Biosci.* **1985**, *8*, 527 – 535.

28. Guéron, M.; Demaret, J-P.; Filoche, M. *Biophys. J.* **2000**, *78*, 1070 – 1083.

29. Rich, A.; Zhang, S. *Nature* **2003**, *4*, 566 – 573.

30. Andrushchenko, V.; Tsankov, D.; Wieser, H. *J. Mol. Struct.* **2003**, *661*, 541 – 560.

31. Chan, P. P.; Glazer, P. M. *J. Mol. Med.* **1997**, *75*, 267 – 282.

32. Muñoz, J.; Gelpi, J. L.; Soler-López, M.; Subirana, J. A.; Orozco, M.; Luque, F. J. *J. Phys. Chem. B* **2002**, *106*, 8849 – 8857.

33. Wan, C.; Cui, M.; Song, F.; Liu, Z.; Liu, S. *J. Am. Soc. Mass. Spectrom.* **2009**, *20*, 1281 – 1286.

34. Burge, S.; Parkinson, G. N.; Hazel, P.; Todd, A. K.; Neidle, S. *Nucleic Acids Res.* **2006**, *34*, 5402 – 5415.

35. Hadjiliadis, N. D.; Sletten, E. *Metal complex-DNA interactions*; Wiley-VCH: Weinheim, 2009; pp 59 – 61.

36. Ma, C.; Bloomfield, V. A. *Biophys. J.* **1994**, *67*, 1678 – 1681.

37. Yamasaki, Y.; Yoshikawa, K. *J. Am. Chem. Soc.* **1997**, *119*, 10573 – 10578.

38. Widom, J.; Baldwin, R. L. *J. Mol. Med.* **1980**, *144*, 431 – 453.

39. Venner, H.; Zimmer, C. H. *Biopolymers* **1980**, *19*, 3221 – 3226.

40. Abrescia, N. G. A.; Huynh-Dihn, T.; Subirana, J. A. *J. Biol. Inorg. Chem.* **2002**, *7*, 195 – 199.

41. Sorokin, V. A.; Valeev, V. A.; Gladchenko, G. O.; Sysa, I. V.; Blagoi, Y. P.; Volchok, I.R. *J. Inorg. Biochem.* **1996**, *63*, 79 – 98.

42. Ha, S. C.; Lowenhaupt, K.; Rich, A.; Kim, Y-G.; Kim, K .K. *Nature* **2005**, *437*, 1183 – 1186.

43. Cheng, A.-J.; Van Dyke, M. W. *Nucleic Acids Res.* **1993**, *21*, 5630 – 5635.

44. Yanaka, K.; Yamada, Y.; Shionoya, M. *J. Am. Chem. Soc.* **2002**, *124*, 8802 – 8803.

45. Ohyama, T. *DNA Conformation and Transcription*; Springer-Verlag: New York, 2005; pp 105 – 181.

46. Porschke, D. *Biochemistry* **1984**, *23*, 4821 – 4828.

47. Gosule, L. C.; Schellman, J. A. *Nature* **1976**, *259*, 333 – 355.

48. Chattoraj, D. K.; Gosule, L. C.; Schellman, J. A. *J. Mol. Biol.* **1978**, *121*, 327 – 337.

49. Widom, J.; Baldwin, R. L. *J. Mol. Biol.* **1980**, *144*, 431 – 453.

50. Widom, J.; Baldwin, R. L. *Biopolymers* **1983**, *22*, 1595 – 1620.

51. Dias, R. S.; Lindman, B. *DNA Interactions with Polymers and Surfactans*; Wiley & Sons, Inc.: New Jersey, 2008; pp 59 – 88.

52. Dias, R. S.; Innerlohinger, J.; Glatter, O.; Miguel, M. G.; Lindman, B. *J. Phys. Chem. B* **2005**, *109*, 10458 – 10463.

53. Gorelov, A. V.; Kudryashov, E. D.; Jacquier, J-C.; McLoughlin, D. M.; Dawson, K. A. *Physica A* **1998**, *249*, 216 – 225.

54. Zhou, S.; Liang, D.; Burger, C.; Yeh, F.; Chu, B. *Biomacromolecules* **2004**, *5*, 1256 – 1261.

55. Miyazawa, N.; Sakaue, T.; Yoshikawa, K.; Zana, R. *J. Chem. Phys.* **2005**, *122*, 044902.

56. Wang, X.-L.; Zhang, X.-H.; Cao, M.; Zheng, H.-Z.; Xiao, B.; Wang, Y. *J. Phys. Chem. B* **2009**, *113*, 2328 – 2332.

57. Koltover, I.; Salditt, T.; Rädler, J. O.; Safinya, C. R. *Science* **1998**, *281*, 78 – 81.

58. Menger, F. M.; Littau, C. A. *J. Am. Chem. Soc.* **1991**, *113*, 1451 – 1452.

59. Zana, R. *Curr. Opin. Colloid Interface Sci.* **1996**, *1*, 566 – 571.

60. Rosen, M. J.; Tracy, D. J. *J. Surfactants Deterg.* **1998**, *1*, 547 – 554.

61. Snyder, E. L.; Dwody, S. F. *Pharm. Res.* **2004**, *21*, 389 – 393.

62. Oda, R.; Huc, I.; Candau, S. J. *Chem. Commun.* **1997**, *21*, 2105 – 2106.

63. Karlsson, L.; van Eijk, M. C. P.; Söderman, O. *J. Colloid Interface Sci.* **2002**, *252*, 290 – 296.

64. Bombelli, C.; Borocci, S.; Diociaiuti, M.; Faggiolo, F.; Galantini, L.; Luciani, P.; Mancini, G.; Sacco, M. G. *Langmuir* **2005**, *21*, 10271 – 10274.

65. Garett, R. H.; Grisham, C. M. *Biochemistry, Second Edition*; Saunders College Publishing: Orlando, FL, 1995; pp 378 – 379.

66. Pouton, C. W.; Lucas, P.; Thomas, B. J.; Uduehi, A. N.; Milroy, D. A.; Moss, S. H. *J. Control. Release* **1998**, *53*, 289 – 299.

67. Wagner, E.; Cotton, M.; Foisner, R.; Birnstiel, M. L. *Proc. Natl. Acad. Sci.* **1991**, *88*, 4255 – 4259.

68. Pei, R.; Cui, X.; Yang, X.; Wang, E. *Biomacromolecules* **2001**, *2*, 463 – 468.

69. Lvov, Y.; Decher, G.; Sukhorukov, G. *Macromolecules* **1993**, *26*, 5396 – 5399.

70. Stryer, L.; Haugland, R. P. *Proc. Natl. Acad. Sci.* **1967**, *58*, 719 – 726.

71. Drake, J. M.; Klafter, J.; Levitz, P. *Science* **1991**, *251*, 1574 – 1579.

72. Lakowicz, J. R. *Principles of Fluorescence Spectroscopy*; Plenum Press: New York, 1983; pp 266 – 267.

73. Atherton, S. J.; Beaumont, P. C. *J. Phys. Chem.* **1986**, *90*, 2252–2259.

74. Rupcich, N.; Chiuman, W.; Nutiu, R.; Mei, S.; Flora, K. K.; Li, Y.; Brennan, J. D. *J. Am. Chem. Soc.* **2006**, *128*, 780 – 790.

75. Burns, V. W. F. *Arch. Biochem. Biophys.* **1969**, *133*, 420 – 424.

76. Wu, J.; Du, F.; Zhang, P.; Khan, I. A.; Chen, J.; Liang, Y. *J. Inorg. Biochem.* **2005**, *99*, 1145 – 1154.

77. Zhao, X.; Shang, Y.; Liu, H.; Hu, Y. *J. Colloid Interface Sci.* **2007**, *314*, 478 – 483.

78. Winnik, F. M. *Chem. Rev.* **1993**, *93*, 587 – 614.

79. Zhao, X.; Shang, Y.; Hu, J.; Liu, H.; Hu, Y. *Biophys. Chem.* **2008**, *138*, 144 – 149.

80. Vuorimaa, E.; Urtti, A.; Seppanen, R.; Lemmetyinen, H.; Yliperttula, M. *J. Am. Chem. Soc.* **2008**, *130*, 11695 – 11700.

81. Mathew, A. K.; Siu, H.; Duhamel, J. *Macromolecules* **1999**, *32*, 7100 – 7108.

82. Duhamel, J. *Acc. Chem. Res.* **2006**, *39*, 953 – 960.

83. Kanagalingam, S.; Spartalis, J.; Cao, T.; Duhamel, J. *Macromolecules* **2002**, *35*, 8571 – 8577.

84. Siu, H.; Duhamel, J. *Macromolecules* **2004**, *37*, 9287 – 9289.

85. Ingratta, M.; Duhamel, J. *Macromolecules* **2007**, *40*, 6647 – 6657.

86. Ingratta, M.; Hollinger, J.; Duhamel, J. *J. Am. Chem. Soc.* **2008**, *130*, 9420 – 9428.

87. Ingratta, M.; Duhamel, J. *Macromolecules* **2009**, *42*, 1244 – 1251.

88. Duhamel, J.; Kanagalingam, S.; O'Brien, T. J.; Ingratta, M. W. *J. Am. Chem. Soc.* **2003**, *125*, 12810 – 12822.

89. Ingratta, M.; Duhamel, J. *J. Phys. Chem. B* **2008**, 112, 9209 – 9218.

Chapter 2

1. Eley, D. D.; Spivey, D. I. *Trans. Faraday Soc.* **1962**, *58*, 411 – 415.
2. Prunkl, C.; Berndl, S.; Wanninger-Weiss, C.; Barbaric, J.; Wagenknecht, H.-A. *Phys. Chem. Chem. Phys.* **2010**, *12*, 32 – 43.
3. Genereux, J. C.; Boal, A. K.; Barton, J. K. *J. Am. Chem. Soc.* **2010**, *132*, 891-905.
4. Watson, J. D.; Crick, F. H. *Nature* **1953**, *171*, 737 – 738.
5. Shriver, D. F.; Atkins, P. W. *Inorganic Chemistry, 3rd Ed.;* W. H. Freeman and Company: New York, 1999, p. 352.
6. Barnett, R. N.; Bongiorno, A.; Cleaveland, C. L.; Joy, A.; Landman, U.; Schuster, G. B. *J. Am. Chem. Soc.* **2006**, *128*, 10795 – 10800.
7. Lyras, L.; Cairns, N. J.; Jenner, A.; Jenner, P.; Halliwell, B. *J. Neurochem.* **1997**, *68*, 2061 – 2069.
8. Gabbita, S. P.; Lovell, M. A.; Markesbery, W. R. *J. Neurochem.* **1998**, *71*, 2034 – 2040.
9. Kawanishi, S.; Hiraku, Y, Oikawa, S. *Mutat. Res.* **2001**, *448*, 65 – 76.
10. Lapierre-Devlin, M. A.; Asher, C. L.; Taft, B. J.; Gasparac, R.; Roberts, M. A.; Kelley, S. O. *Nano Lett.* **2005**, *5*, 1051 – 1055.
11. Wong, E. L. S.; Gooding, J. J. *Anal. Chem.* **2006**, *78*, 2138 – 2144.
12. Mascini, M.; Palchetti, I.; Marrazza, G. *Fresenius J. Anal. Chem.* **2001**, *369*, 15 – 22.
13. Fang, Z.; Soleymani, L.; Pampalakis, G.; Yoshimoto, M.; Squire, J. A.; Sargetn, E. H.; Kelley, S. O. *ACS Nano* **2009**, *3*, 3207 – 3213.
14. Gorodetsky, A. A.; Buzzeo, M. C.; Barton, J. K. *Bioconjugate Chem.* **2008**, *19*, 2287 – 2296.
15. Park, S. H.; Yan, H.; Reif, J. H.; LaBean, T. H. *Nanotechnology* **2004**, *15*, 525 – 527.
16. Aldaye, F. A.; Palmer, A. L.; Sleiman, H. F. *Science*, **2008**, *321*, 1795 – 1799.
17. Kershner, R. J.; Bozano, L. D.; Micheel, C. M.; Hung, A. M.; Fornof, A. R.; Cha, J. N.; Rettner, C. T.; Bersani, M.; Frommer, J.; Rothemund, P. W. K.; Wallraff, G. M. *Nat. Nanotechnol*. **2009**, *4*, 557 – 561.
18. Prusik, T.; Geacintov, N. E. *FEBS Lett.* **1976**, *71*, 236 – 240.

19. Atherton, S. J.; Beaumont, P. C. *J. Phys. Chem.* **1986**, *90*, 2252 – 2259.

20. Atherton, S. J.; Beaumont, P. C. *J. Phys. Chem.* **1987**, *91*, 3993 –3 997.

21. Atherton, S. J.; Beaumont, P. C. *J. Phys. Chem.* **1995**, *99*, 12025 – 12029.

22. Baguley, B. C.; Le Bret, M. *Biochemistry* **1984**, *23*, 937 – 943.

23. Fromherz P.; Rieger, B. *J. Am. Chem. Soc.* **1986**, *108*, 5361 – 5362.

24. Brun, A. M.; Harriman, A. *J. Am Chem. Soc.* **1992**, *114*, 3656 – 3660.

25. Harriman, A. *Angew. Chem. Int. Ed.* **1999**, *38*, 945 – 949.

26. Arkin, M. R.; Stemp, E. D. A.; Holmlin, R. E.; Barton, J. K.; Hormann, A.; Olson, E. J. C.; Barbara, P. F. *Science* **1996**, *273*, 475 – 480.

27. Grinstaff, M. W. *Angew. Chem. Int. Ed.* **1999**, *38*, 3629 – 3635.

28. Turro, N.J.; Barton, J. K. *J. Biol. Inorg. Chem.* **1998**, *3*, 201 – 209.

29. Maiya, B. G.; Ramasarma, T. *Curr. Sci*. **2001**, *80*, 1523 – 1530.

30. Lewis, F. D.; Wu, Y. *J. Photochem. Photobiol., C* **2001**, *2*, 1 – 16.

31. Lewis, F. D.; Letsinger, R. L. *J. Biol. Inorg. Chem.* **1998**, *3*, 215 – 221.

32. Lewis, F. D.; Liu, X.; Wu, Y.; Miller, S. E.; Wasielewski, M. R.; Letsinger, R. L.; Sanishvili, R.; Joachimiak, A.; Tereshko, V.; Egli, M. *J. Am. Chem. Soc.* **1999**, *121*, 9905 – 9906.

33. Lewis, F. D.; Taifeng, W.; Zhang, Y.; Letsinger, R. L.; Greenfield, S. R.; Wasielewski, M. R. *Science*, **1997**, *277*, 673 – 676.

34. Siegmund, K.; Daublain, P.; Wang, Q.; Trifonov, A.; Fiebig, T.; Lewis, F. D. *J. Phys. Chem. B* **2009**, *113*, 16276 – 16284.

35. Fukui, K.; Tanaka, K.; Fujitsuka, M.; Watanabe, A.; Ito, O. *J. Photochem. Photobiol., B* **1999**, *50*, 18 – 27.

36. Fukui, K.; Tanaka, K. *Angew. Chem. Int. Ed.* **1998**, *37*, 158 – 161.

37. Wan, C.; Feibig, T.; Kelley, S. O.; Treadway, C. R.; Barton, J. K.; Zewail, A. H.; *Proc. Natl. Acad. Sci.* **1999**, *96*, 6014 – 6019.

38. Kelley, S. O.; Holmin, E.; Stemp, E. D. A.; Barton, J. K. *J. Am. Chem. Soc.* **1997**, *119*, 9861 – 9870.

39. Wagenknecht, H-A. *Charge Transfer in DNA: From Mechanism to Application*; Wiley-VCH Verlag GmbH and Company: Weinheim, Germany, 2005.

40. Murphy, C. J.; Arkin, M. R.; Jenkins, Y.; Ghatlia, N. D.; Bossmann, S. H.; Turro, N. J.; Barton, J. K. *Science* **1993**, *262*, 1025 – 1029.

41. Gorodetsky, A. A.; Buzzeo, M. C.; Barton, J.K. *Bioconjugate Chem.* **2008**, *19*, 2285 – 2296.

42. Augustyn, K. E.; Stemp, E. D. A.; Barton, J.K. *Inorg. Chem.* **2007**, *46*, 9337 – 9350.

43. Valis, L.; Wang, Q.; Raytchev, M.; Buchvarov, I., Wagenknecht, H-A.; Fiebig, T. *Proc. Nat. Acad. Sci. U.S.A.* **2006**, *103*, 10192 – 10195.

44. Hall, D. B.; Kelley, S. O.; Barton, J. K. *Biochemistry* **1998**, *37*, 15933 – 15940.

45. Shao, F.; Barton, J. K. *J. Am. Chem. Soc.* **2007**, *129*, 14733 – 14738.

46. Kelley, S. O.; Barton, J. K. *Science* **1999**, *283*, 375 – 381.

47. Krider, E. S.; Meade, T. J. *J. Biol. Inorg. Chem.* **1998**, *3*, 222 – 225.

48. Mathew, A. K.; Siu, H.; Duhamel, J. *Macromolecules* **1999**, *32*, 7100 – 7108.

49. Duhamel, J. *Acc. Chem. Res.* **2006**, *39*, 953 – 960.

50. Kanagalingam, S.; Spartalis, J.; Cao, T.; Duhamel, J. *Macromolecules* **2002**, *35*, 8571 – 8577.

51. Siu, H.; Duhamel, J. *Macromolecules* **2004**, *37*, 9287 – 9289.

52. Ingratta, M.; Duhamel, J. *Macromolecules* **2007**, *40*, 6647 – 6657.

53. Ingratta, M.; Hollinger, J.; Duhamel, J. *J. Am. Chem. Soc.* **2008**, *130*, 9420 – 9428.

54. Ingratta, M.; Duhamel, J. *Macromolecules* **2009**, *42*, 1244 – 1251.

55. Duhamel, J.; Kanagalingam, S.; O'Brien, T. J.; Ingratta, M. W. *J. Am. Chem. Soc.* **2003**, *125*, 12810 – 12822.

56. Ingratta, M., Duhamel, J. *J. Phys. Chem. B* **2008**, 112, 9209 – 9218.

57. Tachiya, M. *Chem. Phys. Lett.* **1975**, *33*, 289 – 292.

58. Infelta, P. P. *Chem. Phys. Lett.* **1979**, *61*, 88 – 91.

59. Yekta, A.; Aikawa, M.; Turro, N. J. *Chem. Phys. Lett.* **1979**, *63*, 543 – 548.

60. Gaugain, B.; Barbet, J.; Oberlin, R.; Roques, B. P.; Le Pecq, J.-B. *Biochemistry* **1978**, *17*, 5071 – 5078.

61. Le Pecq, J.-B.; Paoletti, C. *J. Mol. Biol.* **1967**, *27*, 87 – 106.

62. Burns, V. W. F. *Arch. Biochem. Biophys.* **1969**, *133*, 420 – 424.

63. Izatt, R. M.; Christensen, J. J.; Rytting, J. H. *Chem. Rev.* **1971**, *71*, 439 – 481.

64. Garland, F.; Graves, D. E.; Yielding, L. W.; Cheung, H. C. *Biochemistry* **1980**, *19*, 3221 – 3226.

65. Cantor, C. R.; Warshaw, M. M. *Biopolymers* **1970**, *9*, 1059 – 1077.

66. Olmsted III, J.; Kearns, D. R. *Biochemistry* **1977**, *16*, 3647 – 3654.

67. McMurray, C. T.; Small, E. W.; van Holde, K. E. *Biochemistry* **1991**, *30*, 5644 – 5652.

68. Chen, F.-M. *Biochemistry* **1991**, *30*, 4427 – 4479.

69. Barton, J. K.; Danishefsky, A. T.; Goldberg, J. M. *J. Am. Chem. Soc.* **1984**, *106*, 2172 – 2176.

70. Purugganan, M. D.; Kumar, C. V.; Turro, N. J.; Barton, J. K. *Science* **1988**, *241*, 1645 – 1649.

71. Turro, N. J.; Yekta, A. *J. Am. Chem. Soc.* **1978**, *100*, 5951 – 5952.

72. Hochstrasser, R. A.; Millar, D. P. *Proc. SPIE* **1992**, *1640*, 599 – 605.

73. Fenley, M. O.; Manning, G. S.; Olson, W. K. *Biopolymers* **1990**, *30*, 1191 – 1203.

74. Manning, G.S.; Mohanty, U. *Physica A* **1997**, *247*, 196 – 204.

75. Hamman, B. D.; Oleinikov, A. V.; Jokhadze, G. G.; Bochkariov, D. E.; Traut, R. R.; Jameson, D. M. *J. Biol. Chem.* **1996**, *271*, 7568 – 7573.

76. Teertstra, S. J.; Lin, W. Y.; Gauthier, M.; Ingratta, M.; Duhamel, J. *Polymer* **2009**, *50*, 5456 – 5466.

77. Duhamel, J.; Jones, A. S.; Dickson, T. J. *Macromolecules* **2000**, *33*, 6344 – 6352.

Chapter 3

1. Watson, J. D.; Crick, F. H. *Nature*, **1953**, *171*, 737 – 738.

2. Chang, S. L.; Chen, S.-H.; Rill, R. L.; Lin, J. S. *J. Phys. Chem.* **1990**, *94*, 8025 – 8028.

3. Stryer, L.; Haugland, R. P. *Proc. Natl. Acad. Sci.* **1967**, *58*, 719 – 726.

4. Drake, J. M.; Klafter, J.; Levitz, P. *Science* **1991**, *251*, 1574 – 1579.

5. Tuschl, T.; Gohlke, C.; Jovin, T. M.; Westhof, E.; Eckstein, F. *Science* **1994**, *266*, 785 – 789.

6. Daoud, M.; Cotton, J. P.; Farnoux, B.; Jannik, G.; Sarma, G.; Benoit, H.; Duplessix, R.; Picot, C.; de Gennes, P.-G. *Macromolecules* **1975**, *8*, 804 – 818.

7. Matsuoka, H.; Ise, N. *Adv. Polym. Sci.* **1994**, *114*, 187 – 231.

8. Rong, G.; Wang, H.; Reinhard, B. M. *Nano Lett.* **2010**, *10*, 230 – 238.

9. Yang, L.; Wang, H.; Yan, B.; Reinhard, B. M. *J. Phys. Chem. C.* **2010**, *114*, 4901 – 4908.

10. Chen, D.; Li, J. *J. Phys. Chem. C* **2007**, *111*, 2351 – 2367.

11. Marcus, R. A.; Sutin, N. *BBA* **1985**, *811*, 265 – 322.

12. Wagenknecht, H-A. *Charge Transfer in DNA: From Mechanism to Application*; Wiley-VCH Verlag GmbH and Company: Weinheim, Germany, 2005.

13. Mathew, A. K.; Siu, H.; Duhamel, J. *Macromolecules* **1999**, *32*, 7100 – 7108.

14. Keyes Baig, C.; Duhamel, J. *J. Phys. Chem. B* **2010**, *114*, 13950 – 13960.

15. Garland, F.; Graves, D. E.; Yielding, L. W.; Cheung, H. C. *Biochemistry* **1980**, *19*, 3221 – 3226.

16. Venner, H.; Zimmer, C. H. *Biopolymers* **1980**, *19*, 3221 – 3226.

17. McMurray, C. T.; Small, E. W.; van Holde, K. E. *Biochemistry* **1991**, *30*, 5644 – 5652.

18. Chen, F.-M. *Biochemistry* **1991**, *30*, 4427 – 4479.

19. Kelley, S. O.; Barton, J. K. *Chem. Biol.* **1998**, *5*, 413 – 425.

20. Siu, H.; Duhamel, J. *Macromolecules* **2004**, *37*, 9287 – 9289.

21. Ingratta, M.; Duhamel, J. *Macromolecules* **2007**, *40*, 6647 – 6657.

22. Turro, N. J.; Yekta, A. *J. Am Chem. Soc.* **1978**, *100*, 5951 – 5952.

23. Morishima, Y.; Ohgi, H.; Kamachi, M. *Macromolecules* **1993**, *26*, 4293 – 4297.

24. Lakowicz, J. R. *Principles of Fluorescence Spectroscopy*; Plenum Press: New York, 1983; pp 266 – 267.

25. Wan, C.; Fiebig, T.; Kelley, S. O.; Treadway, C. R.; Barton, J. K.; Zewail, A. H. *Proc. Natl. Acad. Sci.* **1999**, *96*, 6014 – 6019.

26. Sorokin, V. A.; Valeev, V. A.; Gladchenko, G. O.; Sysa, I. V.; Blagoi, Y. P.; Volchok, I.R. *J. Inorg. Biochem.* **1996**, *63*, 79 – 98.

27. Morawetz, H.; Gordimer, G. *J. Am Chem. Soc.* **1970**, *92*, 7532 – 7536.

28. Manning, G. S. *Q. Rev. Biophys.* **1978**, *2*, 179 – 246.

29. Fenley, M. O.; Manning, G. S.; Olson, W. K. *Biopolymers* **1990**, *30*, 1191 – 1212.

30. Atherton, S. J.; Beaumont, P. C. *J. Phys. Chem.* **1986**, *90*, 2252 – 2259.

Chapter 4

1. Menger, F. M.; Littau, C. A. *J. Am. Chem. Soc.* **1991**, *113*, 1451 – 1452.

2. Menger, F. M.; Littau, C. A. *J. Am. Chem. Soc.* **1993**, *115*, 10083 – 10090.

3. Zana, R. *Curr. Opin. Colloid Interface Sci.* **1996**, *1*, 566 – 571.

4. Rosen, M. J.; Tracy, D. J. *J. Surfactants Deterg.* **1998**, *1*, 547 – 554.

5. Menger, F. M.; Keiper, J. S. *Angew. Chem. Int. Ed.* **2000**, *39*, 1906 – 1920.

6. Shukla, D.; Tyagi, V. K. *J. Oleo Sci.* **2006**, *55*, 381 – 390.

7. Hait, S., K; Moulik, S. P. *Curr. Sci.* **2002**, *82*, 1101 – 1111.

8. Chen, H.; Han, L.; Luo, P.; Ye, Z. *Surf. Sci.* **2004**, *552*, L53 – L57.

9. Han, L.; Ye, Z.; Chen, H.; Luo, P. *J. Surfactants Deterg.* **2009**, *12*, 185 – 190.

10. Alami, E.; Levy, H.; Zana, R. *Langmuir* **1993**, *9*, 940 – 944.

11. Karaborni, S.; Esselink, K.; Hilbers, P. A. J.; Smit, B.; Karthäuser, J.; van Os, N. M.; Zana, R. *J. Science* **1994**, *266*, 254 – 256.

12. Danino, D.; Talmon, Y.; Zana, R. *Langmuir* **1995**, *11*, 1448 – 1456.

13. Oda, R.; Huc, I.; Candau, S. J. *Chem. Commun.* **1997**, *21*, 2105 – 2106.

14. Knaebel, A.; Oda, R.; Mendes, E.; Candau, S. J. *Langmuir* **2000**, *16*, 2489 – 2494.

15. Kirby, A. J.; Camilleri, P.; Engberts, J. B. F. N.; Feiters, M. C.; Nolte, R. J. M.; Söderman, O.; Bergsma, M.; Bell, P.C.; Fielden, M.L.; Rodríguez, C. L. G.; Guédat, P.; Kremer, A.; Mcgregor, C.; Perrin, C.; Ronsin, G.; van Eijk, M. C. P. *Angew. Chem. Int. Ed.* **2003**, *42*, 1448 – 1457.

16. Wettig, S. D.; Verrall, R. E.; Foldvari, M. *Curr. Gene Ther.* **2008**, 8, 9 – 23.

17. McGregor, C.; Perrin, C.; Monck, M.; Camilleri, P.; Kirby, A. J. *J. Am. Chem. Soc.* **2001**, 123, 6215 – 6220.

18. Bell, P. C.; Bergsma, M.; Dolbnya, I. P.; Bras, W.; Stuart, M. C. A.; Rowan, A. E.; Feiters, M. C.; Engberts, J. B. F. N. *J. Am. Chem. Soc.* **2003**, 125, 1551 – 1558.

19. Badea, I.; Verrall, R; Baca-Estrada, M.; Tikoo, S.; Rosenberg, A.; Kumar, P.; Foldvari, M. *J. Gene. Med.* **2005**, 7, 1200 – 1214.

20. Bombelli, C.; Faggioli, F.; Luciani, P.; Mancini, G.; Sacco, M. G.; Kumar, P. *J. Med. Chem.* **2005**, 48, 5378 – 5382.

21. Wang, C.; Li, X.; Wettig, S. D.; Badea, I.; Foldvari, M.; Verall, R. E. *Phys. Chem. Chem. Phys.* **2007**, 9, 1616 – 1628.

22. Wang, C.; Wettig, S. D.; Foldvari, M.; Verrall, R. E. *Langmuir* **2007**, *23*, 8995-9001.

23. Lakowicz, J. R. *Principles of Fluorescence Spectroscopy*; Plenum Press: New York, 1983; p 45.

24. Lakowicz, J. R. *Principles of Fluorescence Spectroscopy: Third Edition*; Plenum Press: New York, 2006; p 290.

25. Bambot, S. B., Rao, G., Carter, G. M., Romauld, M., Sipior, J., Terpetchnig, E., Lakowicz, J. R. *Biosens. Bioelectron.* **1995**, *10*, 643 – 653.

26. Siu, H., Duhamel, J. *J.Phys. Chem. B* **2005**, *109*, 1770 – 1780.

27. Yip, J.; Duhamel, J.; Bahun. G. J.; Adronov, A. *J. Phys. Chem. B.* **2010**, 114, 10254 – 10265.

28. Prazeres, T. J. V.; Beingessner, R.; Duhamel, J.; Olesen, K.; Shay, G.; Bassett, D. R. *Macromolecules* **2001**, *34*, 7876-7884.

29. Siu, H.; Duhamel, J. *Macromolecules* **2004**, *37*, 9287-9289.

30. Chen, S.; Duhamel, J.; Winnik, M. A. submitted to *J. Phys. Chem. B* **2010**.

31. Siu, H.; Duhamel, J., Sasaki, D. Y.; Pincus, J. L. *Langmuir* **2010**, *26*, 10985-10994.

32. Birks, J. B. *Photophysics of Aromatic Molecules*. Wiley: New York, 1970; p 301.

33. Winnik, M. A.; Egan, L. S.; Tencer, M.; Croucher, M. D. *Polymer*, **1987**, *28*, 1553-1560.

34. Zachariasse, K. A.; Vaz, W. L. C.; Sotomayor, C.; Kuhnle, W. *Biochim. Biophys. Acta* **1982**, *688*, 323-332.

35. Lianos, P.; Lux, B.; Gerard, D. *J. Chim. Phys.* **1980**, *77*, 907-912.

36. Winnik, F. M. *Macromolecules* **1987**, *20*, 2745 – 2750.

37. Winnik, F. M. *Chem. Rev.* **1993**, *93*, 587 – 614.

38. Yekta, A.; Turro, N. J. *J. Am. Chem. Soc.* **1978**, *100*, 5951-5952.

39. Winnik, F. M.; Regismond, S. T. A. *Colloids Surf. A: Physicochem. Eng. Asp.* **1996**, *118*, 1-39.

40. Duhamel, J. *Molecular Interfacial Pehnomena of Polymers and Biopolymers*; Chen, P., Ed.; Woodhead: New York, 2005; pp 214 – 248.

41. Tsai, F-J.; Torkelson, J. M. *Polymer* **1988**, *29*, 1004 – 1009.

42. Torkelson, J. M.; Lipsky, S.; Tirrell, M.; Tirrell, D. A. *Macromolecules* **1983**, *16*, 326 – 330.

Chapter 5

1. Wolff, J. A. *Nat. Biotechnol.* **2002**, *20*, 768 – 769.

2. Gao, X.; Kim, K. S.; Liu, D. *AAPS J.* **2007**, *9*, E92 – E104.

3. Li, S.; Huang, L. *Gene Ther.* **2000**, *7*, 31 – 34.

4. Mountain, A. *Trends Biotechnol.* **2000**, *18*, 119 – 128.

5. Graham, F. L. *Trends Immunol. Today* **2000**, *21*, 426 – 428.

6. Wolfgang, W.; Ulrike, S. *Drugs* **2000**, *60*, 249 – 271.

7. Ledford, H. *Nat. Biotechnol.* **2007**, *25*, 1067.

8. Lehn, P.; Fabrega, S.; Oudrhiri, N.; Navarro, J. *Adv. Drug Delivery Rev.* **1998**, *30*, 5 – 11.

9. Mintzer, M. A.; Simanek, E. E. *Chem. Rev.* **2009**, *109*, 259 – 302.

10. Dias, R.S.; Lindman, B. *DNA Interactions with Polymers and Surfactants*; John Wiley & Sons Inc.: New Jersey, 2008; p 89 – 117.

11. Dasgupta, A; Das, P. K.; Dias, R.S.; Miguel, M. G.; Lindman, B.; Jadhav, V. M.; Gnanamani, M.; Maiti, S. *J. Phys. Chem. B* **2007**, *111*, 8502 – 8508.

12. Liu, F.; Yang, J.; Huang, L.; Liu, D. *Pharm. Res.* **1996**, *13*, 1642 – 1646.

13. Wettig, S. D.; Verrall, R. E.; Foldvari, M. *Curr. Gene Ther.* **2008**, *8*, 9 – 23.

14. Bombelli, C.; Giansanti, L.; Luciani, P.; Mancini, G. *Curr. Med. Chem.* **2009**, *16*, 171 – 183.

15. McGregor, C.; Perrin, C.; Monck, M.; Camilleri, P.; Kirby, A. J. *J. Am. Chem. Soc.* **1994**, *123*, 6215 – 6220.

16. Koltover, I.; Salditt, T.; Rädler, J. O.; Safinya, C. R. *Science* **1998**, *281*, 78 – 81.

17. Kennedy, M. T.; Pozharski, E. V.; Rakhmanova, V. A.; MacDonald, R. C. *Biophys. J.* **2000**, *78*, 1620 – 81633.

18. Pedroso de Lima, M. C.; Simões, S.; Pires, P.; Faneca, H.; Düzgüneş, N. *Adv. Drug Delivery Rev.* **2001**, *47*, 277 – 294.

19. De Smedt, S. C.; Demeester, J.; Hennink, W. E. *Pharm. Res.* **2000**, *17*, 113 – 126.

20. Wolfert, M. A.; Dash, P. R.; Nazarova, O.; Oupicky, D.; Seymour, L. W.; Smart, S.; Strohalm, J.; Ulbrich, K. *Bioconjugate Chem.* **1999**, *10*, 993 – 1004.

21. Dufès, C.; Uchegbu, I. F.; Schätzlein, A. G. *Adv. Drug Delivery Rev.* **2005**, *57*, 2177 – 2202.

22. Snyder, E. L.; Dwody, S. F. *Pharm. Res.* **2004**, *21*, 389 – 393.

23. Zorko, M.; Langel, U. *Adv. Drug Delivery Rev.* **2005**, *57*, 259 – 545.

24. Oda, R.; Huc, I.; Candau, S. J. *Chem. Commun.* **1997**, *21*, 2105 – 2106.

25. Hait, S. K.; Moulik, S. P. *Curr. Sci.* **2002**, *82*, 1101 – 1111.

26. Ronsin, G.; Perrin, C.; Guédat, P.; Kremer, A.; Camilleri, P.; Kirby, A. J. *Chem. Commun.* **2001**, 2234 – 2235.

27. Rosenweig, H. S.; Rakhmanova, V. A.; MacDonald, R. C. *Bioconjugate Chem.* **2001**, *12*, 258 – 263.

28. Badea, I.; Verrall, R.; Baca-Estrada, M.; Tikoo, S.; Rosenberg, A.; Kumar, P.; Foldvari, M. *J. Gene Med.* **2005**, *12*, 1200 – 1214.

29. Wang, C.; Li, X.; Wettig, S. D.; Badea, I.; Foldvari, M.; Verrall, R. E. *Phys. Chem. Chem. Phys.* **2007**, *9*, 1616 – 1628.

30. Wang, C.; Wettig, S. D.; Foldvari, M.; Verrall, R. E. *Langmuir* **2007**, *23*, 8995 – 9001.

31. Jiang, N.; Wang, J.; Wang, Y.; Yan, H.; Thomas, R. K. *J. Colloid Interface Sci.* **2005**, *284*, 759 – 764.

32. Rosen, M. J.; Mathias, J. H.; Davenport, L. *Langmuir* **1999**, *15*, 7340 – 7346.

33. Zhao, X.; Shang, Y.; Liu, H.; Hu, Y. *J. Colloid Interface Sci.* **2007**, *314*, 478 – 483.

34. Zhao, X.; Shang, Y.; Hu, J.; Liu, H.; Hu, Y. *Biophys. Chem.* **2008**, *138*, 144 – 149.

35. Dong, D. C.; Winnik, M. A. *Photochem. Photobiol.* **1982**, *35*, 17 – 21.

36. Dong, D. C.; Winnik, M. A. *Can. J. Chem.* **1984**, *62*, 2560 – 2565.

37. Winnik, F. M. *Chem. Rev.* **1993**, *93*, 587 – 614.

38. Siu, H.; Duhamel, J. *J. Phys. Chem. B* **2005**, *109*, 1770 – 1780.

39. Yip, J.; Duhamel, J.; Bahun. G. J.; Adronov, A. *J. Phys. Chem. B.* **2010**, 114, 10254 – 10265.

40. Birks, J. B. *Photophysics of Aromatic Molecules*. Wiley: New York, 1970; p 301.

41. Winnik, M. A.; Egan, L. S.; Tencer, M.; Croucher, M. D. *Polymer* **1987**, *28*, 1553-1560.

42. Li, Z. X.; Dona, C. C.; Thomas, R. K. *Langmuir* **1999**, *15*, 4392 – 4396.

43. Manne, S.; Schäffer, T. E.; Huo, Q.; Hansma, P. K.; Morse, D. E.; Stucky, G. D.; Aksay, I. A. *Langmuir* **1997**, *13*, 6382 – 6387.

44. Vayá, I.; Gustavsson, T.; Miannay, F.-A.; Douki, T.; Markovitsi, D. *J. Am. Chem. Soc.* **2010**, *123*, 11834 – 11835.

45. Vayá, I.; Miannay, F.-A.; Gustavsson, T.; Markovitsi, D. *ChemPhysChem* **2010**, *11*, 987 – 989.

46. Pisarevskii, A. N.; Cherenkevich, S. N.; Andrianov, V. T. *J. Appl. Spectrosc.* **1966**, *5*, 621 – 624.

47. Costa, D.; Hansson, P.; Schneider, S.; Miguel, M. G.; Lindman, B. *Biomacromolecules* **2006**, *7*, 1090 – 1095.

48. Rosen, M. J.; Liu, L. *J. Am. Oil. Chem. Soc.* **1996**, *73*, 885 – 890.

49. Karlsson, L.; van Eijk, M. C. P.; Söderman, O. *J. Colloid Interface Sci.* **2002**, *252*, 290 – 296.

50. Bombelli, C.; Borocci, S.; Diociaiuti, M.; Faggiolo, F.; Galantini, L.; Luciani, P.; Mancini, G.; Sacco, M. G. *Langmuir* **2005**, *21*, 10271 – 10274.

51. Miyazawa, N.; Sakaue, T.; Yoshikawa, K.; Zana, R. *J. Chem. Phys.* **2005**, *122*, 044902.

52. Wang, X.-L.; Zhang, X.-H.; Cao, M.; Zheng, H.-Z.; Xiao, B.; Wang, Y. *J. Phys. Chem. B.* **2009**, *113*, 2328 – 2332.